FLNP

JOINT INSTITUTE FOR NUCLEAR RESEARCH

FRANK LABORATORY OF NEUTRON PHYSICS

ANNUAL REPORT 2009

Dubna

PREFACE

We would like to offer the readers the report on the scientific activity of the Frank Laboratory of Neutron Physics for 2009. The first part presents a brief review of the experimental and theoretical results achieved in the main scientific directions – condensed matter physics, neutron nuclear physics and applied research. The second part includes the reports on the modernization of the IBR-2 pulsed reactor and realization of the IREN project. The third part is concerned with the development and creation of elements of neutron spectrometers for condensed matter investigations. The fourth part presents the experimental reports that cover the main scientific directions in greater detail. The list of publications for 2009 completes the report.

During 2009 the works on the modernization of ***IBR-2*** were mainly focused on:

- Installation of the reactor vessel at its work site and of in-vessel components. Loading of dummy fuel assembly cartridges into the reactor core.
- Installation of the movable reflector MR-3 in the operative position.
- Replacement of a cold trap for purifying sodium coolant in loop "A" of the second reactor cooling circuit.
- Installation of stationary reflectors and water moderators on the trolleys of the rolling shields.
- Installation of executive mechanisms and control units of the reactor.
- Manufacturing and installation of an additional storage facility for the IBR-2 used fuel in the reactor hall.
- Installation of equipment of the cryogenic helium refrigerator KGU-700/15 and helium pipelines between the cryogenic refrigerator and the rolling shields.

The IREN Project. In accordance with the decision of the JINR Directorate to realize the IREN project in several stages, the construction of the electron accelerator and the nonmultiplying neutron-producing target complex has been completed. Since the beginning of 2009 the carrying out of experimental investigations on newly constructed source has been started.

In spite of the IBR-2 reactor shutdown the activities of the Department of Condensed Matter Research and the Department of Spectrometers Complex were focused both on modernization of the spectrometers and scientific research in allied centers in Russia and abroad.

The manufacturing of the head part of the mirror vacuum neutron guide has been completed and its installation on beam 6b of the IBR-2M reactor has been carried out within the framework of realization of the project of construction of the DN-6 diffractometer for microsample investigations. The manufacturing of a vacuum casing for the tail part of the neutron guide has continued. The designing of a gas position-sensitive detector has started.

The manufacturing, vacuum testing and installation of the head part of the GRAINS reflectometer on the reactor have been completed. The manufacturing of the rail support and the casing for the beam-forming system has started. The components of the given system (variable slits, beam-

deflecting mirrors) have been tested. The technical documentation on the manufacturing of a mechanical drum chopper has been prepared.

Work to prepare a working platform for the installation of a mirror neutron guide on the DIN-2PI spectrometer has been carried out. Mirror segments, materials for effective biological shielding of the neutron guide of the first flight path of the spectrometer and mechanical units for positioning the neutron guide have been purchased. The processing of the experimental data on the simulation at the DIN-2PI spectrometer of a model of a cryogenic moderator to be installed at the IBR-2M reactor has been completed.

A schematic design of a new backscattering detector for the HRFD diffractometer has been developed on the basis of ZnS-elements. The solid angle of the new detector is ~10 times that of the available detector, which will make it possible, in case of realization of the project, to significantly improve conditions for conducting structural experiments on HRFD.

Neutron diffraction studies of the atomic and magnetic structure of 314-cobaltites Sr3YCo4O10.5+δ (or Sr0.75R0.25CoO2.625+δ/4) wherein A-positions are perfectly ordered have been continued. In 2009, the compounds with partial substitution of Ca for Sr, namely $Sr_{0.75-x}Ca_xY_{0.25}CoO_{3-y}$ with $x \approx 0.30$ and $y \approx 0.35$ were studied, for which from indirect data some evidence was found for the partial stabilization of ferromagnetism due to the effect of Ca on the charge state of Co. The preliminary analysis showed the presence of magnetic phase transition at $T \approx 260$ K with the appearance of the AFM structure and a possible small FM component.

The studies of high pressure effects on the crystal and magnetic structures of complex anion-deficient cobalt oxides have been continued in a wide temperature range. In the $Sr_{0.7}Y_{0.3}CoO_{2.62}$ compound a pressure-induced change in the spin configuration for Co^{3+} ions has been revealed, which results in a modification of the symmetry of the antiferromagnetic state.

The structural characteristics of optically active nanostructured materials ($0.95GeO_2$-$0.05Eu_2O_3$, $0.949GeO_2$-$0.05Eu_2O_3$-0.001Ag and $0.999GeO_2$-0.001Ag) annealed in air at T = 900°C have been investigated by small-angle neutron scattering and X-ray diffraction. It has been found that a considerable change in the relative intensity of luminescence excitation bands of Eu^{3+} ions by doping with Ag correlates with a decrease in the characteristic sizes of polydisperse clusters formed during annealing.

Complex investigations of the size regulation effect for magnetite nanoparticles in ferrofluids with non-polar organic carriers and stabilization by monocarboxylic acids, have been completed. It has been confirmed that the replacement of non-saturated oleic acid (C_{18}) used in the classical stabilization procedure with saturated acids from a series of lauric (C_{12}), myristic (C_{14}), palmitic (C_{16}), stearic (C_{18}) acids results in a decrease in the effective size of stabilized magnetite.

The structure of the aggregates of nanodiamond particles (detonation) dispersed into polar liquids (water, DMSO) by a special wet milling procedure has been determined with the use of small-angle neutron scattering. The contrast variation with the use of mixtures of protonated and deuterated

solvents allowed us to determine the mean density of the particles composing the cluster, and thus to conclude about the existence of a non-diamond component on the nanodiamond surface.

The micellization of sodium dodecyl(sulfophenoxy)benzene sulfonate and nonyl benzene deca(ethylene oxide) has been investigated in neutral and alkaline electrolyte solutions of different concentrations by small-angle neutron scattering. The correlation of the data obtained with the geometry of track nanopores and the dynamics of their etching in surfactant-containing solutions has been revealed and the model of the influence of surfactants on the formation of pores with specific geometry has been developed.

The experimental investigations concerning the problem of coexistence of ferromagnetism (F) and superconductivity (S) have been continued. The magnetic state of the Fe/V bilayer has been studied using a neutron wave resonator MgO/V/Cu. The behaviour of the bilayer in reality corresponded to the behaviour of a three-layer F/F-S/S structure in which the intermediate F-S layer was a mixture of vanadium and iron atoms. The direct and inverse proximity effects were observed.

The X-ray diffraction technique was applied to study water solutions of multilayer vesicles of multicomponent membranes modeling the mucous membranes of the human oral cavity (Oral Stratum Corneum, OSC) and the membranes comprising the mixture sphingomyelin /dipalmitoylphosphatidylcholine/dipalmitoylphosphatidylethanolamine (SM/DPPC/DPPE).

Using the neutron diffraction data the texture of special steels, graphite, zirconium niobate (various processes of manufacturing) has been determined. It has been shown that the austenitic facing of the VVER-1000 reactor vessel has a sharp radial texture (rotation of grains around the normal to the steel plane (002)), which results in a complex distribution of residual stresses in it, and in this case the minimal values of the Young's modulus are attained in the direction of the normal to the surface of the reactor vessel.

The investigations of texture and internal stresses of rock samples from the Central Alpes (Switzerland) in the region of the Gotthard Base Tunnel have been carried out. The obtained results are important to estimate the influence of the tunnel excavation work on the geomechanical conditions of the mountain ranges surrounding the tunnel.

The inelastic neutron scattering method has been applied to study vibrational spectra of hexane and isomers of hexanol. The theoretical simulation of the vibrational spectra using the density functional theory has been performed. It has been found that to describe the dynamics of hydroxyl groups, the formation of hydrogen bonds between hexanol molecules should be taken into account.

In 2009 a number of experiments were carried out and some interesting results were obtained in the field of nuclear physics.

The physical start-up of the first stage of the IREN facility has been carried out at FLNP JINR. The IREN first stage includes one section of the electron accelerator and a nonmultiplying tungsten target. The achieved parameters (peak electron beam current – 2.0 A; electron energy – 30 MeV; pulse width – 100 ns; repetition rate – 25 Hz; integral neutron yield – (3÷5)·1010 n/s) already make it

possible to carry out experiments, which require high energy resolution in the energy range from fractions of eV to hundreds of eV.

At the IBR-2 pulsed reactor the construction of the "Kolkhida" setup intended for studies of neutron optics phenomena in interactions of polarized neutrons with polarized nuclei has been completed. The computer simulation of an experiment on neutron paramagnetic resonance shift has been performed.

The investigations of P-odd secondary particle emission asymmetry in the reactions of polarized cold neutrons and light nuclei of 6Li and 10B have been continued in ILL (Grenoble). Both obtained values ($f_\pi^{6Li} \leq 1.1 \cdot 10^{-7}$ and $f_\pi^{10B} \leq 2.4 \cdot 10^{-7}$ (at 90 % confidence level)) contradict "the best" DDH value $f_\pi^{DDH} = 4.6 \cdot 10^{-7}$.

In October-November, 2009, a new experiment to measure α^{10B}_{P-odd} was conducted. The 50-day measurement was carried out on the polarized cold neutron beam at ILL. The use of improved geometry made it possible to reduce the background and to improve the precision (1.8×10^{-8} instead of 3.9×10^{-8}). A «zero»-experiment was performed as well.

On the cold neutron beam in ILL the FLNP specialists in collaboration with the French scientists have measured the concentration of hydrogen atoms in diamond nanopowder before and after degassing, total scattering cross-section for hydrogen (not removed by degassing) and its temperature dependence. It has been revealed that the amount of hydrogen in the nanopowder before and after degassing can be expressed by the ratios C_8H and $C_{15}H$, respectively. An increase in the reflection probability from a powder of diamond nanoparticles, which is of interest as a reflector for very cold neutrons, is possible either by removing/replacing hydrogen or by suppressing the channel of inelastic losses by cooling the powder to liquid helium temperatures.

The studies of properties of nuclei in the neutron binding energy range have been continued. It has been demonstrated that the main obstacle in obtaining reliable information on this process is serious methodical errors in the analysis of data from multiparameter experiments by some groups of physicists.

The investigations of the (n,p), (n,α) reactions induced by fast neutrons have been continued. The experiments are carried out at the Van de Graaf accelerator EG-5 in FLNP JINR (Dubna, Russia) and EG-4.5 of the Institute of Heavy Ion Physics of Peking University (Beijing, China) in collaboration with the University of Lodz (Poland), the National University of Mongolia (Ulaanbaatar, Mongolia) and the Oak Ridge National Laboratory (USA).

Data on neutron reactions with emission of charged particles induced by fast neutrons are of much interest both for the creation of constructional materials for nuclear power engineering and for studying mechanisms of nuclear reactions and for determining the parameters of an optical potential. Within the framework of joint investigations at the EG-4.5 accelerator of the Institute of Heavy Ion Physics of Peking University (Beijing, China) the measurements of the parameters of the ^{143}Nd(n,α)^{140}Ce and ^{95}Mo(n, α)^{92}Zr reactions at E_n=4.0, 5.0 and 6.0 MeV and the ^{147}Sm(n, α)^{144}Nd reaction at E_n=5.0

and 6.0 MeV have been carried out. The energy spectra of charged particles have been obtained. The data treatment and theoretical calculations were completed in 2009.

In 2009, in the Neutron Activation Analysis Sector (FLNP JINR) the RFFI-Romania project «Geochronology and retrospective study of pollution of unconsolidated sediments from oxygenated and anoxic territories of the Western Black Sea» was completed. The results of the performed investigations were printed in scientific publications in international peer-reviewed journals of special interest for geology. In 2009, the State Prize of the Government of the Republic of Macedonia was awarded to the research work conducted in the NAA sector in collaboration with the Macedonian specialists on the creation of the geochemical Atlas of one of environmentally unsound areas in Macedonia.

In conclusion, it might be well to point out that great interest is being expressed by the JINR Member States in the work in the field of neutron investigations. It is also significant that in the lastfew years a lot of young people have come to the Laboratory. All these facts confirm that the Laboratory continues to develop successfully and dynamically, carrying out investigations in the interests of the JINR Member States.

A.V.Belushkin
Director

1. SCIENTIFIC RESEARCH

1.1. CONDENSED MATTER PHYSICS

The main objectives of research in the framework of the theme involved the application of neutron scattering techniques and complementary methods to investigate the structure, dynamics and microscopic properties of nanosystems and novel materials, which are of great importance for the development of nanotechnologies in the fields of electronics, pharmacology, medicine, chemistry, modern condensed matter physics and interdisciplinary sciences. In view of the IBR-2 reactor shutdown for modernization, the experimental activities conducted by the personnel of the FLNP Department of Neutron Investigations of Condensed Matter (NICM) were carried out in neutron and synchrotron centers in Russia and abroad. This work was performed in accordance with the Topical Plan for JINR Research and International Cooperation under the existing cooperation agreements and accepted beam time application proposals. The activities on the IBR-2 reactor were carried out in accordance with the modernization program plan for the spectrometers. Most attention was given to the realization of the top priority projects (construction of the new DN-6 diffractometer for studying microsamples, multipurpose GRAINS reflectometer and modernization of the SKAT/EPSILON spectrometers for geophysical research).

Within the framework of investigations under the theme, the employees of the NICM Department maintained broad cooperation with many scientific organizations in Russia and abroad. The cooperation, as a rule, was documented by joint protocols or agreements. In Russia, particularly active collaboration was with the thematically close organizations, such as RRC KI, PNPI, MSU, IMP, ISSP RAS, IC RAS, and others.

A list of main scientific topics studied by the employees of the NICM Department includes:

- Investigation of structure and properties of novel crystal materials and nanosystems by neutron diffraction;
- Investigation of magnetic colloidal systems in bulk and at interfaces;
- Investigation of structure of carbon nanomaterials;
- Magnetism of layered nanostructures;
- Investigation of supermolecular structure and functional characteristics of biological, colloidal and polymeric nanodispersed materials;
- Investigation of nanostructure and properties of lipid membranes and lipid complexes;
- Investigation of atomic dynamics of nanosystems and materials by neutron inelastic scattering;
- Investigation of texture and properties of minerals and rocks;
- Analysis of internal stresses in bulky materials and factory-made goods.

1. Scientific results

1.1. Structure investigations of novel oxide materials

Neutron diffraction studies of the atomic and magnetic structure of 314-cobaltites $Sr_3YCo_4O_{10.5+\delta}$ (or $Sr_{0.75}R_{0.25}CoO_{2.625+\delta/4}$) wherein A-positions are perfectly ordered have been continued. For these compounds it has been revealed that Co atoms occupying different

positions in a unit cell have different magnetic moment magnitudes correlating with the oxygen surrounding of the atom, i.e. for the first time the direct correlation between the charge and spin states of the Co atoms has been revealed for perovskite-like cobaltites. The compounds with different oxygen contents have been found to have AFM structure of G-type without any sign of the presence of the ferromagnetic component of the moment [1]. In 2009, the compounds with partial substitution of Ca for Sr, namely $Sr_{0.75-x}Ca_xY_{0.25}CoO_{3-y}$ with $x \approx 0.30$ and $y \approx 0.35$ were studied, for which from indirect data some evidence was found for the partial stabilization of ferromagnetism due to the effect of Ca on the charge state of Co. To test this model, on the HRPT diffractometer (PSI) neutron diffraction spectra were obtained in the temperature range from 1.5 to 300 K (**Fig. 1**). The preliminary analysis showed the presence of magnetic phase transition at $T \approx 260$ K with the appearance of the AFM structure and a possible small FM component.

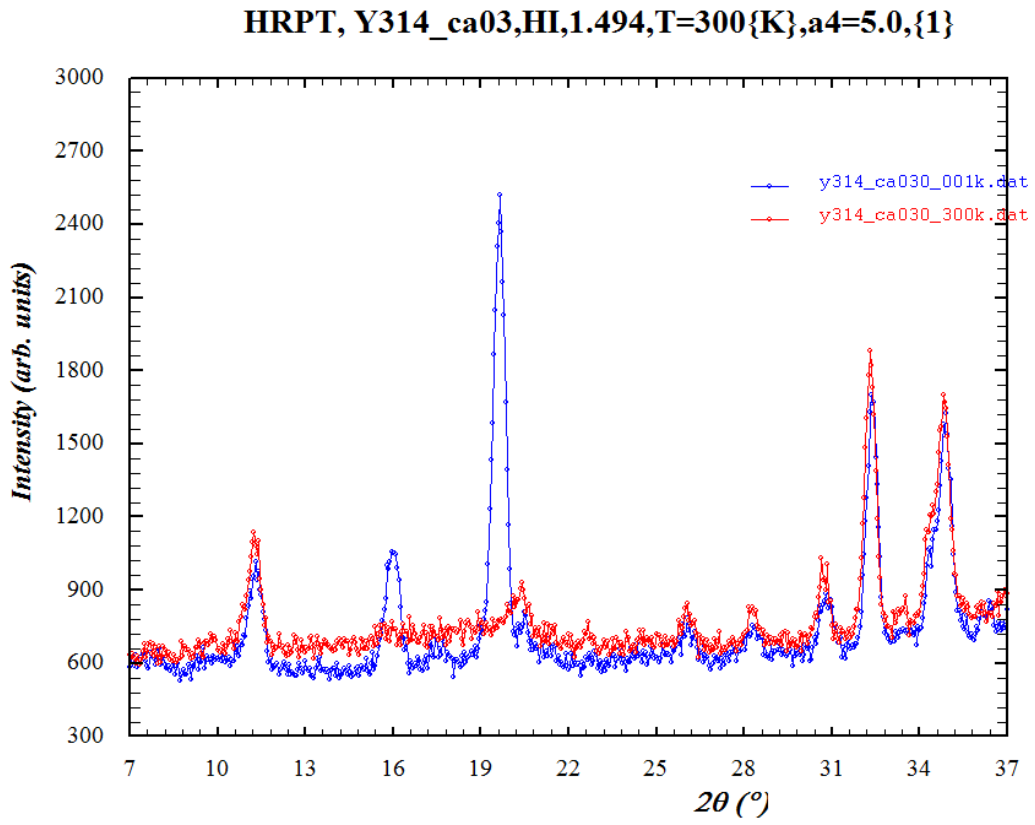

Fig. 1. Diffraction spectra of $Sr_{0.75-x}Ca_xY_{0.25}CoO_{3-y}$ with $x \approx 0.30$ obtained at temperatures of 1.5 and 300 K. The preliminary analysis showed that the difference in the intensity of some peaks is due to the occurrence of long-range magnetic order as the temperature decreases.

The studies of high pressure effects on the crystal and magnetic structures of complex anion-deficient cobalt oxides have been continued in a wide temperature range. In the $Sr_{0.7}Y_{0.3}CoO_{2.62}$ compound a pressure-induced change in the spin configuration for Co^{3+} ions has been revealed, which results in a modification of the symmetry of the antiferromagnetic state [2].

The structural characteristics of optically active nanostructured materials ($0.95GeO_2$-$0.05Eu_2O_3$, $0.949GeO_2$-$0.05Eu_2O_3$-0.001Ag and $0.999GeO_2$-0.001Ag) annealed in air at $T = 900$ °C have been investigated by small-angle neutron scattering and X-ray diffraction. The $0.999GeO_2$-0.001Ag system obtained at $T = 150$ °C forms an amorphous phase and at $T = 200$ °C crystallizes in

the trigonal space group *P3₂21*. The $0.95GeO_2$-$0.05Eu_2O_3$ and $0.949GeO_2$-$0.05Eu_2O_3$-0.01Ag systems obtained at T = 150-800 °C also have trigonal space group symmetry *P3₂21*. The formation of polydisperse clusters in the $0.95GeO_2$-$0.05Eu_2O_3$ and $0.949GeO_2$-$0.05Eu_2O_3$-0.01Ag systems in the annealing temperature range of 350-555 °C has been revealed by the small-angle neutron scattering technique. Cluster size distribution functions have been calculated (**Fig. 2**). At T = 850 °C the disintegration of clusters is observed. It has been found that a considerable change in the relative intensity of luminescence excitation bands of Eu^{3+} ions by doping with Ag correlates with a decrease in the characteristic sizes of polydisperse clusters formed during annealing [3].

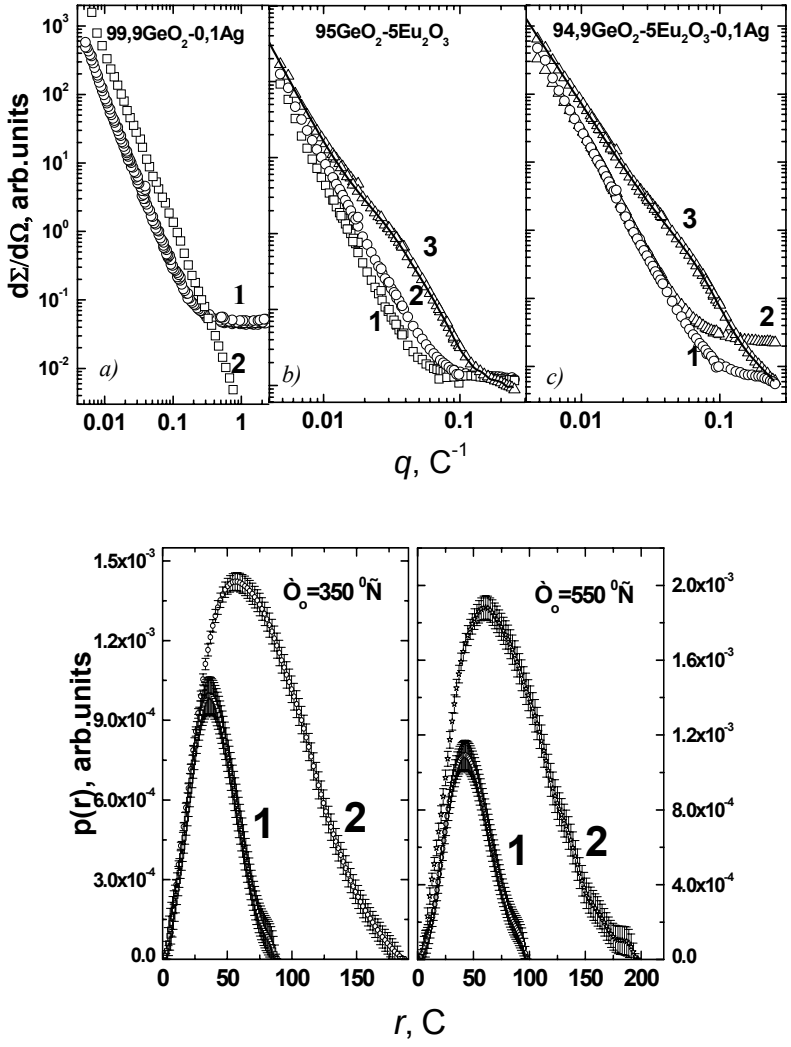

Fig. 2. At the top: small-angle neutron scattering curves of xerogels $99,9GeO_2$-0,1Ag (*a*), 95,0GeO2-5Eu2O3 (*b*) and $94,9GeO2$-$5Eu_2O_3$-0,1Ag (*c*) for annealing temperatures T = 150 (1), 550 (3) and 850 °C (2). For the curves corresponding to T = 550 °C a theoretical curve is presented. At the bottom: intermediate aggregate size distribution function for xerogels $94,9GeO_2$-$5Eu_2O_3$-0,1Ag (1) and 95,0GeO2-$5Eu_2O_3$ (2) for annealing temperatures T = 350 (left) and 550 °C (right).

1.2. Investigations of magnetic fluids

Complex investigations of the size regulation effect for magnetite nanoparticles in

ferrofluids with non-polar organic carriers and stabilization by monocarboxylic acids have been completed. The studies have been performed using the static magnetization analysis, transmission electron microscopy, diffraction and small-angle scattering of synchrotron radiation and small-angle scattering of polarized neutrons. It has been confirmed that the replacement of non-saturated oleic acid (C_{18}) used in the classical stabilization procedure with saturated acids from a series of lauric (C_{12}), myristic (C_{14}), palmitic (C_{16}), stearic (C_{18}) acids results in a decrease in the effective size of stabilized magnetite [4]. In particular, the diffraction and small-angle scattering of synchrotron radiation point to a difference in the size of the coherent scattering region of magnetite between the samples stabilized by oleic acid and saturated fat acids. The combined use of the two methods allows us to conclude reliably that the revealed effect is related to the change in the size of dispersed magnetite and not with the differences in the possible aggregation. As a result, it has been shown that the characteristic magnetite size can be changed within the interval of 5 – 8 nm by using various surfactant mixtures.

A number of water-based biocompatible magnetic fluids have been studied using small-angle neutron scattering. The systems under study have been considered as sources and media for storing magnetic nanoparticles used in biomedical applications. Structural characteristics of particles and their aggregates have been obtained. The structural stability of the fluids under various conditions has been investigated.

1.3 Investigations of carbon nanomaterials

The structure of the aggregates of nanodiamond particles (detonation) dispersed into polar liquids (water, DMSO) by a special wet milling procedure has been determined with the use of small-angle neutron scattering. The size and fractal characteristics of the aggregates, as well as the structural features of the nanodiamond particles (size, surface character) have been obtained. The comparison with the aggregate structure in initial nanodiamond powders has been performed. The analysis of the structure factor as a function of the number of particles points to the cluster interpenetration upon concentrating dispersions. The contrast variation with the use of mixtures of protonated and deuterated solvents allowed us to determine the mean density of the particles composing the cluster, and thus to conclude about the existence of a non-diamond component on the nanodiamond surface. Due to these investigations basing on different complementary methods (transmission electron microscopy, X-ray diffraction, small-angle neutron scattering) the description of all states of the colloidal nanodiamond dispersions (**Fig. 3**) has been completed [5].

Complex investigations of fullerene (C_{60}) cluster formation in low-polar (carbon disulfide, toluene, benzene) and polar (N-methyl-pirrolidone) solvents, as well as their mixtures were continued. Investigations were carried out with application of spectroscopy and extraction, mass-spectroscopy, small-angle neutron scattering. It is confirmed that for low-polar solutions the cluster growth in some cases can be initiated by non-equilibrium conditions of solution preparation (ultrasound, long intensive stirring). For polar solutions, where clusters always appear, changes of absorption spectra and extraction with time (temporal solvatochromic effect) have been analyzed and related to the cluster growth. The effects of water and toluene addition into cluster solution C_{60}-N-methyl-pirrolidone have been compared. It has been shown that in both cases a decrease in apparent cluster size takes place.

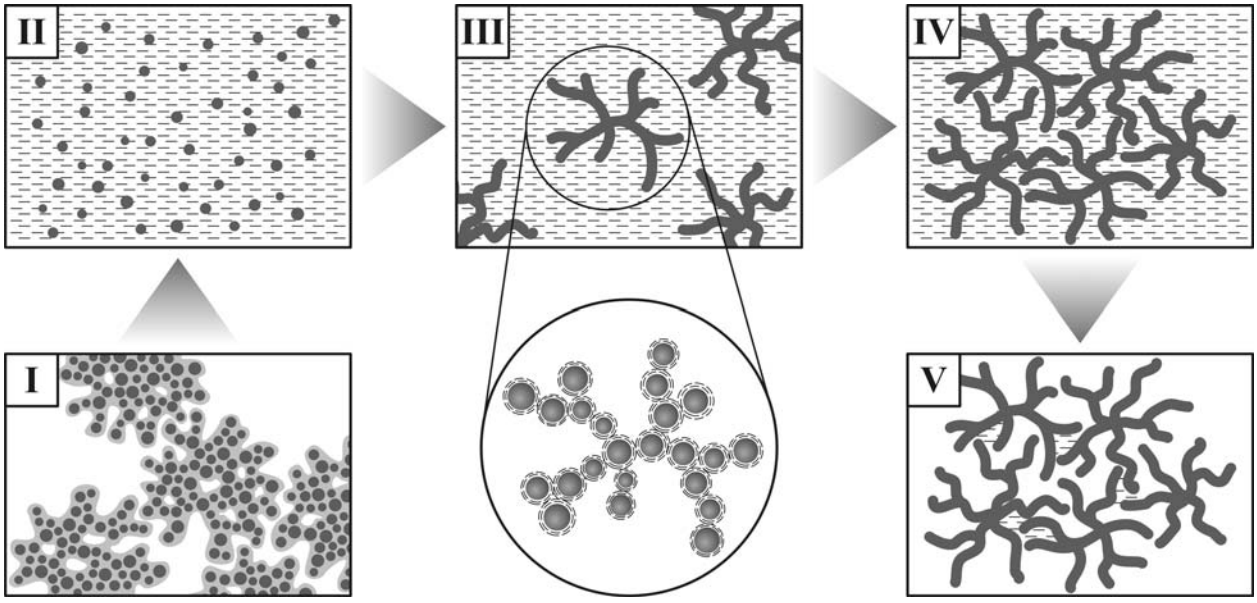

Fig. 3. Conventional representation of various states of colloidal nanodiamond dispersions. **(I)** Initial powders; size of dense (chemically stable) aggregates is more than 40 nm; aggregates have a developed surface with the dimension $D \sim 1.26$; **(II)** Liquid dispersion right after the wet milling procedure; nanodiamond particles are separated; **(III)** Liquid dispersion of low concentration ($C \sim 1$ wt %) after the formation of aggregates with the fractal dimension $D \sim 2.3$ and size of more than 40 nm; characteristic size of diamond crystallite is about 7 nm; thickness of a non-diamond component on the nanoparticle surface is about 0.5 nm; **(IV)** Liquid dispersion after concentrating ($C \sim 10$ wt %); aggregates interpenetrate each other due to the developed structure; **(V)** Dispersion after the evaporation of the bulk solvent; water remains partially in small pores with characteristic size of about 7 nm.

1.4 Investigations of magnetic layered nanostructures

The experimental investigations concerning the problem of coexistence of ferromagnetism (F) and superconductivity (S) have been continued. The magnetic state of the Fe/V bilayer has been studied using a neutron wave resonator MgO/V/Cu [6]. The behaviour of the bilayer in reality corresponded to the behaviour of a three-layer F/F-S/S structure in which the intermediate F-S layer was a mixture of vanadium and iron atoms. The direct and inverse proximity effects were observed. The direct effect consisting in the appearance of the superconducting order in ferromagnetic F-S manifested itself at the transition of the vanadium layer (S) into the superconducting state ($T = T_c$) as a decrease in the magnetization vector and its approach to the direction of the external magnetic field. The inverse proximity effect, i.e. the appearance of ferromagnetic order in the superconductor F-S was observed at a temperature of $0.6T_c$ and involved an increase in the magnetization vector and its deviation from the direction of the magnetic field (**Fig. 4**).

The peculiarities of the passage of polarized and nonpolarized neutrons through two-layer and three-layer magnetic nanostructures have been studied. In particular, it has been found that the passage of nonpolarized neutrons through noncoplanar structures under certain conditions is left-right asymmetric. One of the consequences of this fact is that similar noncoplanar magnetic structures, whether made artificially or of natural origin, can be a filter making it possible to select nonpolarized ensemble of atoms (molecules) depending on the magnitude of their magnetic moment [7].

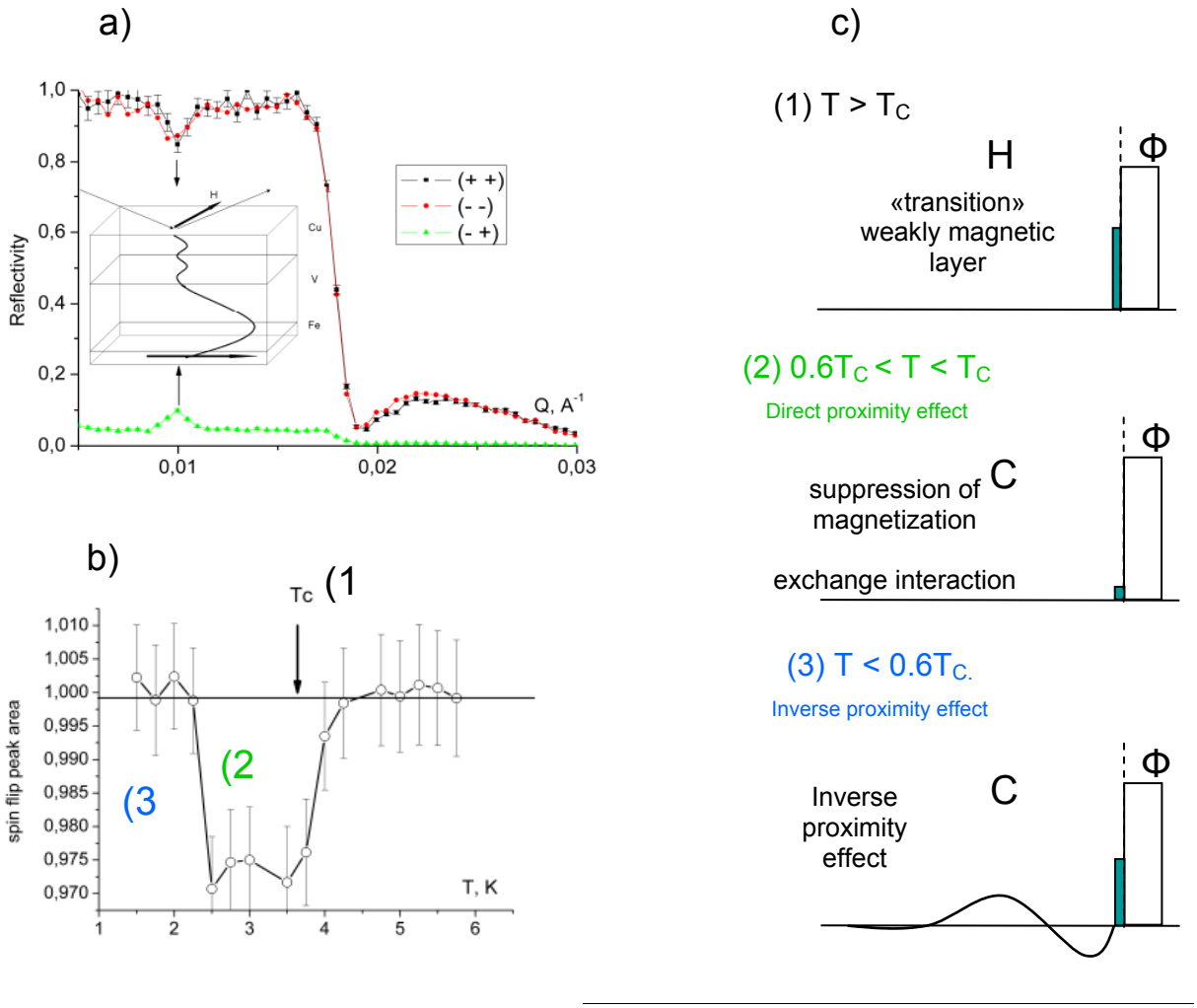

Fig. 4. Polarized neutron reflection coefficient for a superconducting ferromagnetic heterostructure Cu(32nm)/V(40nm)/Fe(1nm)/MgO with a standing neutron wave resonator (a); temperature behaviour of a resonance spin-flip peak (b); changes of magnetic profiles near the interface for various temperature ranges (1)-(3) (c).

1.5 Investigations of biological nanosystems

The surface of mitoplasts (mitochondria devoid of an outer membrane) has been investigated by atomic-force microscopy (AFM). The AFM has revealed folds on the surface of mitoplasts with thicknesses of 30-40 nm (**Fig. 5**), which coincides with that of "dry cristae" in mitochondria measured with small-angle neutron scattering and electron microscopy. These results point to the existence of a specific system maintaining certain configuration of a mitoplast membrane similar to that of the inner membrane of intact mitochondria under their swelling in hypotonic conditions. The prospects of using AFM to study the configuration of the surface of the mitochondrial inner membrane and other biological membrane systems have been demonstrated [8].

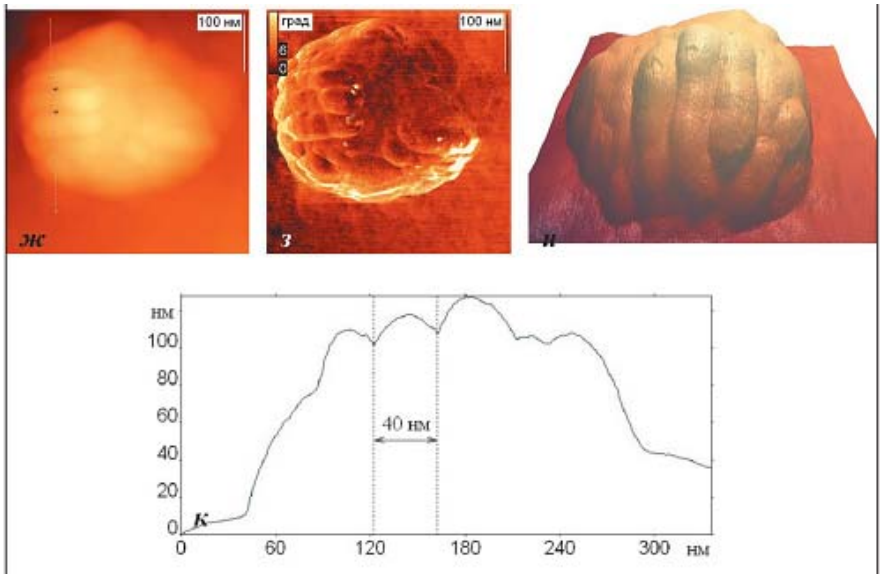

Fig. 5. *ж*)-*и*) AFM-images of rat liver mitoplasts with «dry cristae»; *к*) a cross section made along the dotted line shown in *ж*); *ж*) AFM-images recorded in channel «height»; *з*) in channel «phase»; *и*) 3D representation. A scale line in all insets is 100 nm. The maximum height difference in AFM-image ж) is 172 nm.

The samples containing biogenic ferrihydrite nanoparticles produced by *Klebsiella oxytoca* bacteria have been studied. In particular, by means of optical microscopy, scanning electron microscopy and small-angle X-ray scattering the effect of the bacteria age (the duration of growth) on the nanoparticle properties has been investigated [9].

The X-ray diffraction technique was applied to study water solutions of multilayer vesicles of multicomponent membranes modeling the mucous membranes of the human oral cavity (Oral Stratum Corneum, OSC) and the membranes comprising the mixture sphingomyelin/ dipalmitoylphosphatidylcholine/ dipalmitoylphosphatidylethanolamine (SM/DPPC/DPPE) [10]. The systems of the SM/DPPC/DPPE mixture (mass ratios of 1/1/1, 1/2/1) are characterized by a lamellar structure with a repeat distance of ~ 71 Å. As the mass fraction of DPPE increases, a part of the lipid forms a separate lamellar phase ($d \sim 56$ Å) and a reverse hexogonal phase ($a \sim 56$ Å). The multicomponent OSC membranes based on ceramide 6 and ceramide 3 are complex multiphase systems coming into phase equilibrium in a few days after sample preparation.

1.6 Investigations of polymer and colloidal nanosystems

The structure of silicon-organic dendrimers of the ninth generation with a 4-functional core and butyl end-groups has been investigated with the small-angle neutron scattering method. It has been shown that the dendrimers under study are monodisperse objects of anisometric shape. The partial volume and average scattering density values have been determined using the contrast variation technique. It has been demonstrated that the dendrimers under study are identical in overall dimensions and in the scattering density distribution. It has been found that 20% of the dendrimer overall volume is permeable a solvent. The simulation using the Monte Carlo method has been performed and the spatial distribution of the scattering length density in the dendrimers under study has been determined; a change in the excluded volume for various contrasts has been revealed.

The micellization of sodium dodecyl(sulfophenoxy)benzene sulfonate and nonyl benzene deca(ethylene oxide) has been investigated in neutral and alkaline electrolyte solutions of different concentrations by small-angle neutron scattering. The micelles formed in the solutions have been found to possess a cylindrical (ellipsoid) shape. The characteristic sizes of the micelles have been determined as functions of surfactant and added electrolyte concentrations. The correlation of the data obtained with the geometry of track nanopores and the dynamics of their etching in surfactant-containing solutions has been revealed and the model of the influence of surfactants on the formation of pores with specific geometry has been developed [11].

1.7. Atomic dynamics

The inelastic neutron scattering method has been applied to study vibrational spectra of hexane and isomers of hexanol. The theoretical simulation of the vibrational spectra using the density functional theory has been performed. The frequencies of low-energy torsion modes with respect to C-C bonds and C-C-C bending modes for flat and bent conformations of hexane molecules and isomers of hexanol have been calculated in the range of up to 500 cm^{-1}. On the whole, the calculated spectra of density of vibrational states for isolated molecules are in qualitative agreement with the experimental spectra. However, to describe the dynamics of hydroxyl groups, the formation of hydrogen bonds between hexanol molecules should be taken into account. It has been shown that the calculations of the dynamics of molecules with the formation of hydrogen bonds in dimers allow correct interpretation of the dynamics of hydroxyl groups in the condensed state of these alcohols (**Fig. 6**).

The detailed analysis of the neutron diffraction data on supercritical water that shows much promise as a coolant in the next-generation reactors and is a unique solvent in the oxidation of organic wastes has been performed. A two-structure model suggested earlier for the description of the microdynamics of supercritical water has been verified and substantiated. On the basis of this model a number of neutron-physical characteristics of supercritical water necessary for evaluating parameters of nuclear reactors that use water at ultrahigh parameters as a coolant have been obtained [12].

1.8. Applied research

Among traditional applied investigations in the Department of Neutron Investigations of Condensed Matter are the experimental studies of internal stresses and texture of rocks and minerals, determination of internal stresses in bulk materials and products, including engineering materials and components of machines and devices. For the most part, these investigations are carried out using neutron diffraction.

The investigation of the temperature behaviour of samples of the EK-181 steel has been completed. Temperature dependences of the lattice parameter, internal textural stresses of the third kind and the Debye-Waller factor of this steel have been calculated from the diffraction spectra by the Rietveld method for a temperature range of 15 – 973 K [13]. It has been found that at low temperatures the temperature dependence of the lattice parameter in the EK-181 steel differs from the corresponding dependence in pure iron and binary iron-chromium alloys containing 12 and 16 % Cr. Also, the broadening of the (200) reflection has been observed in the diffraction spectra of the EK-181 steel and the Fe-12Cr alloy, while it is not detected in the spectra of Fe-16Cr and pure iron.

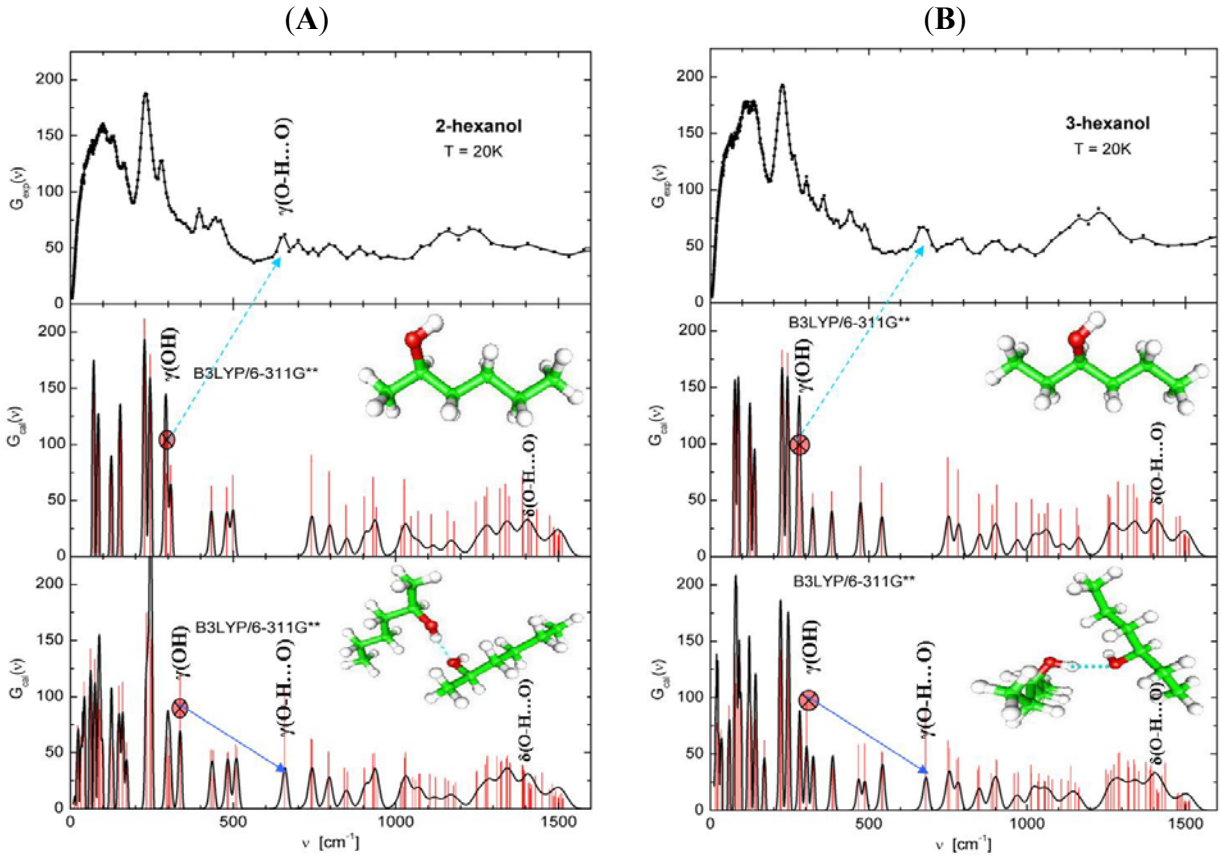

Fig. 6. Comparison of the experimental and calculated IINS spectra of free molecules and their dimmers with hydrogen bonds for 2-hexanol (A) and 3-hexanol (B).

Using the neutron diffraction data the texture of special steels, graphite, zirconium niobate (various processes of manufacturing) has been determined. The crystallite orientation distribution function (ODF) has been determined; the simulation of volume elastic properties of these constructional materials has been performed. It has been shown that the austenitic facing of the VVER-1000 reactor vessel has a sharp radial texture (rotation of grains around the normal to the steel plane (002)), which results in a complex distribution of residual stresses in it, and in this case the minimal values of the Young's modulus are attained in the direction of the normal to the surface of the reactor vessel. For reactor graphite GR-280 it has been shown that the anisotropy of elastic properties is qualitatively connected with the crystallographic texture (**Fig. 7**), which is characterized by the concentration of axes of the 6-th order of graphite perpendicular to the direction of extrusion [14]. And a difference is observed between the real (measured by an ultrasonic method) and simulated (calculated by means of averaging the elasticity tensor using ODF) velocities of longitudinal elastic waves (about 5 times at atmospheric pressure and about 3 times at 150 MPa).

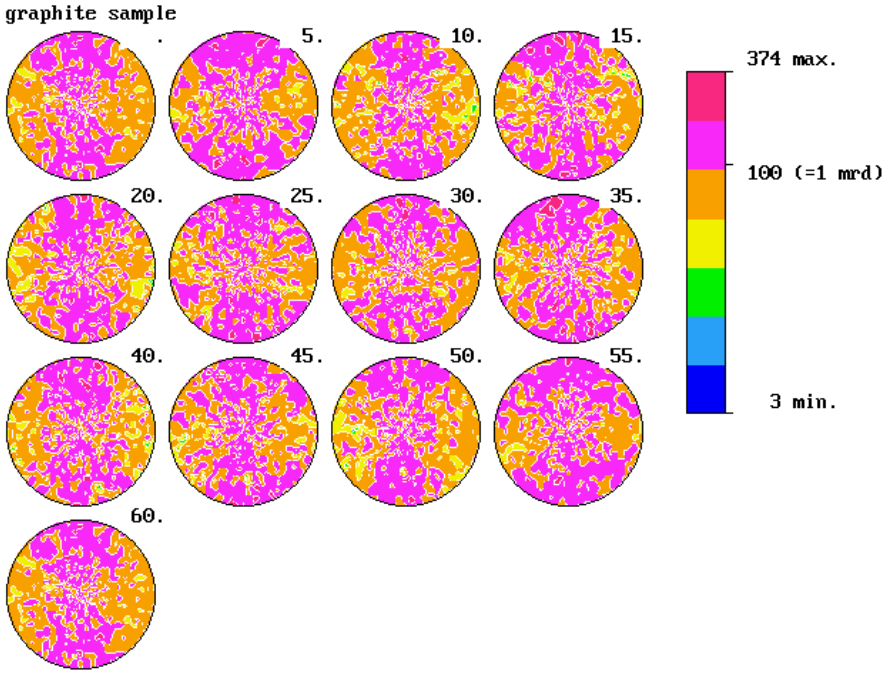

Fig. 7. ODF for graphite sample Gra2, γ-cross-sections (stereographic projection). fmin = 0.03, fmax = 3.74, F2 = 1.21.

In zirconium niobate the process of manufacturing of a rod results in the formation of a sharp radial texture with the rotation of crystallites around the normal to the plane (2-70). Thus the material becomes practically isotropic in its elastic properties. On the basis of the texture measurements the requirements to experiments to study internal stresses in zirconium niobate have been formulated.

The investigations of physical properties and fluid penetrating rate of salts for estimating their barrier properties in the design of radioactive waste repositories have been carried out [15]. The temperature distribution appearing in a saliferous rock in the neighborhood of a heat radiating source has been analytically calculated. At an initial salt temperature of 20°C, radius of cavern with wastes of 5 m, heat emission intensities up to 100 W/m^3 and storage time of up to 100 years the environment temperature does not exceed 90°C, and the maximal gradient is 0.1°C per 1 cm. A theoretical estimate of the maximal speed of the inclusion movement in NaCl monocrystal under the action of the temperature gradient produced by a radioactive source has been obtained. For inclusions with the size of 0.005-0.2 cm located at the distance of the order of 1 m from the repository wall at the radiation intensity of 100 W/m^3 (initial temperature of the inclusion solution is 58.45 °C, constant external thermal gradient is 0.08 °C per 1 cm) speeds of movement lie in the range of (0.2-0.5)∗10^{-10} cm/s. Along with it, the speed of the inclusion movement increases with the growth of the inclusion size. The dynamics of movement has been considered theoretically. Thus, the elongation of the inclusion perpendicular to the temperature gradient is observed together with its fragmentation from the backside, which can cause lattice disturbance in the salt.

The influence of high-current pulsed relativistic electron beams on the mechanism of crater formation in rocks (salts, granites and labradorites) has been studied. For quick estimate of the surface condition of the samples and for determination of the barrier properties of the geomaterials the method of infrared camera monitoring has been probed. It has been shown that such kind of complex experiments is advisable for studying rocks when choosing a place for radioactive waste

storage. A possible mechanism of crater formation in solids under irradiation with high-current electron beams (**Fig. 8**) can be a thermal shock. As a result, thermally stressed places appear and the destruction occurs along the boundary of the melt.

a)

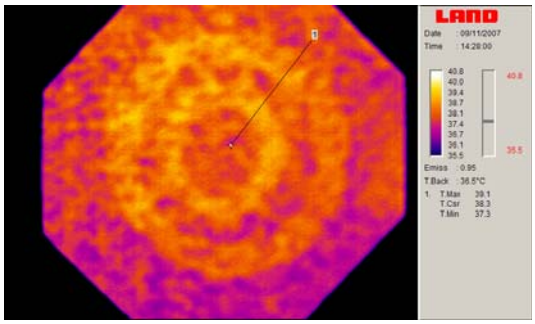

b)

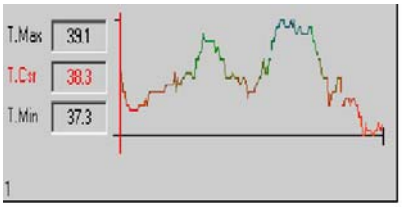

c)

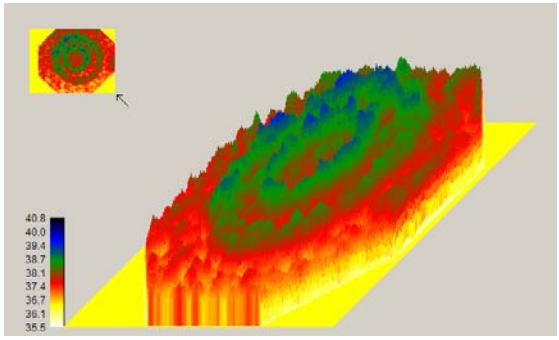

d)

Fig. 8. a) A sample of grey granite irradiated by 20 pulses of high-current relativistic electron beams;
b) frontal IR image of the irradiated sample of grey pink granite exposed to heating;
c) temperature profile of the surface along the line in b);
d) 3D image of the temperature field distribution.

The investigations of texture and internal stresses of rock samples from the Central Alpes (Switzerland) in the region of the Gotthard Base Tunnel have been carried out. The obtained results are important to estimate the influence of the tunnel excavation work on the geomechanical conditions of the mountain ranges surrounding the tunnel.

The studies of anisotropic properties of marble and granite samples and the simulation have been carried out to develop practical recommendations on the optimization of extraction of natural stones in stone quarries [16].

The study of errors in the measurement of pole figures (experimental information on texture obtained with the SKAT spectrometer) has been carried out. The study was conducted with a magnesium alloy sample (Mg+4.5Al+1%Zn). The measurement errors were evaluated for each of 1368 points in a pole figure. It has been found that the diffraction peak half-width determination errors play a major role in the formation of pole figure errors. This conclusion was confirmed by

means of calculation of errors of the pole figures extracted from the simulated individual spectra. A set of 1368 individual neutron diffraction spectra was simulated. The simulation of spectra was performed on the basis of experimental and model pole figures (**Fig. 9**). It has been demonstrated that the pole figure error distribution qualitatively coincides with the peak half-width determination error distribution for both the experimental pole figures and the pole figures extracted from the simulated spectra [17].

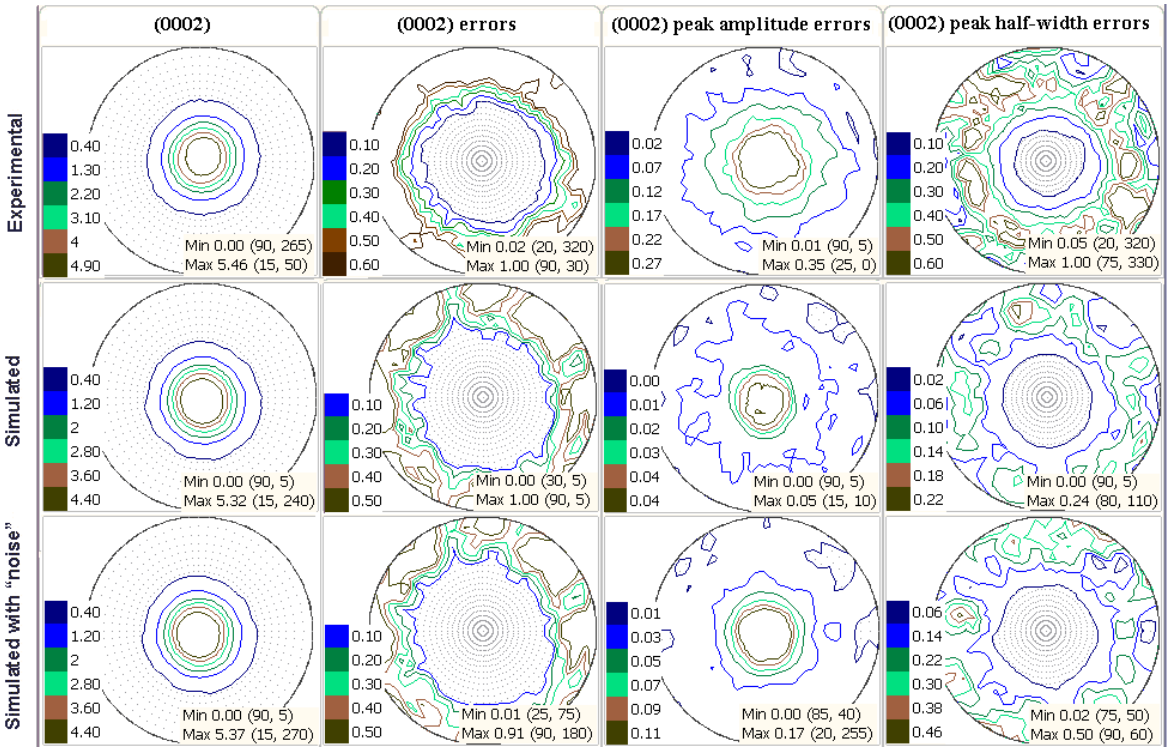

Fig. 9. a) The pole figure (0002) for a Mg+4.5Al+1%Zn sample. The intensities are given in relative units of isotropic distribution. b) The relative pole figure error (0002). c) The peak amplitude determination error. d) The peak half-width determination error. Top row: the experimental pole figure measured on the SKAT texture diffractometer and the errors calculated for the experimental data. Middle row: the pole figure extracted from the simulated spectra and the respective errors. Bottom row: the pole figure extracted from the spectra simulated with an "experimental" error ("noise") and the respective errors.

II. Instrument developments

The manufacturing of the head part of the mirror vacuum neutron guide has been completed and its installation on beam 6b of the IBR-2M reactor has been carried out within the framework of realization of the project of construction of the DN-6 diffractometer for microsample investigations (**Fig. 10**). The manufacturing of a vacuum casing for the tail part of the neutron guide has continued. The designing of a gas position-sensitive detector has started.

Fig. 10. The head part of the mirror vacuum neutron guide installed on beam 6 of the IBR-2 reactor within the framework of realization of the project of construction of the DN-6 diffractometer for microsample investigations.

The manufacturing, vacuum testing and installation of the head part of the GRAINS reflectometer (**Fig. 11**) at the reactor have been completed. The manufacturing of the rail support and the casing for the beam-forming system has started. The components of the given system (variable slits, beam-deflecting mirrors) have been tested. The technical documentation on the manufacturing of a mechanical drum chopper has been prepared.

The work to prepare a working platform for the installation of a mirror neutron guide on the DIN-2PI spectrometer has been carried out. Mirror segments, materials for effective biological shielding of the neutron guide of the first flight path of the spectrometer and mechanical units for positioning the neutron guide have been purchased. The processing of the experimental data on the simulation at the DIN-2PI spectrometer of a model of cryogenic moderator to be installed at the IBR-2M reactor has been completed.

A schematic design of a new backscattering detector for the HRFD diffractometer has been developed on the basis of ZnS-elements (**Fig. 12**). The solid angle of the new detector is ~10 times that of the available detector, which will make it possible, in case of realization of the project, to significantly improve conditions for conducting structural experiments on HRFD.

Fig. 11. The head part of the GRAINS reflectometer.

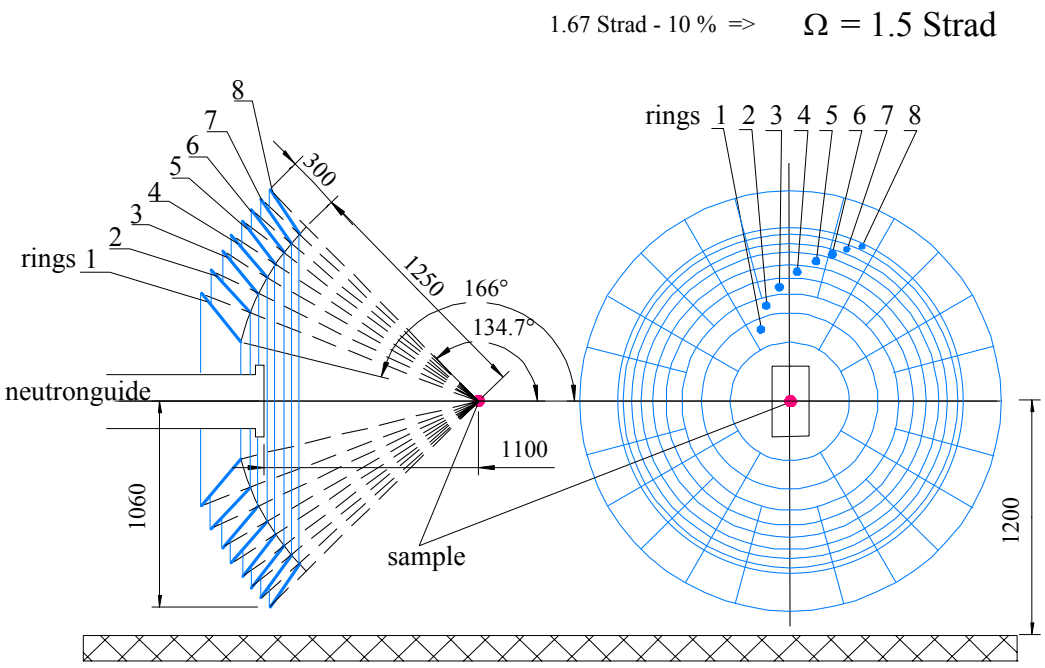

Fig. 12. A conceptual design of a new back-scattering detector on the basis of ZnS-elements for the HRFD diffractometer.

The work to study the possibility of creating supermirrors with a periodic structure has been continued and within the framework of this project the polarized neutron reflectometry experiments with samples with 2, 4, 8 bilayers and float glass substrate (MIRROTRON, Budapest, Hungary) have been carried out.

The investigation of the effect of enhancement of a spin-flip signal in a neutron wave resonator has been performed. It has been demonstrated that in a neutron wave resonator a spin-flip

signal from a magnetically non-collinear layer can be enhanced to the second or even to the third power in relation to the already amplified signal from a nuclear layer. This makes it possible to study subatomic magnetic layers down to 10^{-5} nm thick or nanolayers with extremely small magnetization of 10^{-3} Gs [18].

Within the framework of the project aimed at constructing curved mirror neutron guides for the EPSILON and SKAT spectrometers on beam 7a of the IBR-2 reactor the work to design and manufacture mechanical and optical units of the neutron guides has continued [19]. In particular, the designs of a vacuum system and a background shield of the EPSILON and SKAT spectrometers and of a docking part of the neutron guide of the NERA-PR spectrometer have been developed, the development and manufacturing of the disk background chopper and three drum λ-choppers are nearing completion. The control system of choppers based on electric drives from Toshiba has been developed, manufactured and debugged. The reconstruction of the supporting column of IBR-2 and a biological shield of the head part of beam 7 to accommodate three neutron guides on the channel has been completed. The posts and beam-positioning support pillars of the neutron guide head part have been produced. The manufacturing of 92 vacuum casings for the curved neutron guides for the EPSILON and SKAT spectrometers is in progress.

The main result of activities in 2009 under the project of construction of curved mirror neutron guides for the EPSILON and SKAT spectrometers is the installation of two sections of the head part (splitter) of beam 7 including the assembling of internal sections and beam positioning as well as the installation of vacuum casings (**Fig. 13**).

Fig. 13. The head part of the splitter of beam 7 of the IBR-2M reactor for the neutron guide system of the EPSILON (7A-1), SKAT (7A-2) and NERA (7B) diffractometers. The installation of the splitter is carried out within the framework of the BMBF project on modernization of the neutron guide system of the EPSILON and SKAT diffractometers on beam 7A of the IBR-2M reactor.

References

1. D.V.Sheptyakov, V.Yu.Pomjakushin, O.A.Drozhzhin, S.Ya.Istomin, E.V.Antipov, I.A.Bobrikov, A.M.Balagurov, Correlation of chemical coordination and magnetic ordering in $Sr_3YCo_4O_{10.5+\delta}$, δ=0.02 and 0.26 *Phys. Rev. B*, v.80, pp. 024409 (1-9) (2009)
2. N.O.Golosova, D.P.Kozlenko, L.S.Dubrovinsky, O.A.Drozhzhin, S.Ya.Istomin, B.N.Savenko, Spin State and Magnetic Transformations in $Sr_{0.7}Y_{0.3}CoO_{2.62}$ at High Pressures, *Phys. Rev. B*, v. 79, pp. 104431 (1-5) (2009)
3. A.V.Belushkin, S.Ye.Kichanov, D.P.Kozlenko, Ye.V.Lukin, B.N.Savenko, S.K.Rakhmanov, G.P.Shevchenko, V.S.Gurin, G.E.Malashenko, V.M.Garamus, D.K.Pogoreliy, K.M.Podurets, Study of structural aspects of formation of optical properties of the GeO_2-Eu_2O_3-Ag nanosystem, *Physics of Solid State* (2009) (in Russian) (submitted)
4. M.V.Avdeev, D.Bica, L.Vekas, V.L.Aksenov, A.V.Feoktystov, O.Marinica, L.Rosta, V.M.Garamus, R.Willumeit, Comparative structure analysis of non-polar organic ferrofluids stabilized by saturated mono-carboxylic acids, *J. Colloid Interface Sci*. 334 (2009) 37–41
5. M.V.Avdeev, N.N.Rozhkova, V.L.Aksenov, V.M.Garamus, R.Willumeit, E.Osawa, Aggregate structure in concentrated liquid dispersions of ultrananocrystalline diamond by small-angle neutron scattering, *J. Phys. Chem. C* 113 (2009) 9473–9479
6. V.L.Aksenov, Yu.N.Khaidukov, Yu.V.Nikitenko, Peculiarities of magnetic states in Ferromagnet/Superconductor heterostructures due to proximity effects, *Journal of Physics: Conference Series* (submitted)
7. V.K.Ignatovich, Yu.V.Nikitenko, A.A.Fraerman, Passage of polarized neutrons through magnetic non-coplanar layered systems, *JETP*, v. 138, №1 (2010) (in Russian)
8. E.V.Dubrovin, T.N.Murugova, K.A.Motovilov, L.S.Yaguzhinskii, I.V.Yaminskya, Application of Atomic-Force Microscopy Technology to a Structural Analysis of the Mitochondrial Inner Membrane, *Russian nanotechnologies*, 4, №9-10, 2009, pp. 66-68
9. Yu.L.Raikher, V.I.Stepanov, S.V.Stolyar, V.P.Ladygina, D.A.Balaev, L.A.Ishchenko, M.Balasoiu, Magnetic properties of biomineral nanoparticles produced by Klebsiella oxytoca bacteria, *Physics of Solid State,* Vol.52, №.2 (2010)277-284
10. N.Y.Ryabova, M.A.Kiselev, O.V.Naida, A.V.Zabelin, S.Dante, T.Hauss, A.M.Balagurov, Neutron and synchrotron studies of the structure of *oral stratum corneum* lipid model membranes, RSNE-NBIC 2009 (Book of Abstracts), Moscow, November 16-20, 2009
11. Yu.S.Kovalev, N.V.Levkovich, A.I.Kuklin, P.Yu.Apel', Surfactant aggregation in solutions applied for track etching and its possible effect on the pore shape in track membranes, *Colloid Journal*, 2009, v.71, №5, pp. 634-639
12. Yu.V.Lisichkin, A.G.Novikov, L.A.Sakharova, Structural and dynamical peculiarities of water in the supercritical state, *Preprint IPPE-3148*, Obninsk, 2009, 36 pages (in Russian)
13. V.V.Sumin, V.G.Simkin, S.G.Sheverev, M.V.Leont'eva-Smirnova and V.M.Chernov, Temperature dependence of the lattice parameter and Debye-Waller factor of a high-chromium pressure-vessel steel, *The Physics of Metals and Metallography*. v.108, №6, pp.600-605 (2009)
14. T.Lokajicek, P.Lukas, A.N.Nikitin, I.V.Papushkin, V.V.Sumin, R.N.Vasin, Elastic properties of reactor graphite GR-280 and their anisotropy from neutron diffraction and ultrasonic measurements, 2010. *Carbon* (submitted)
15. A.N.Nikitin, O.A.Pocheptzova, S.Matthies, Account of thermal and transport properties of crystalline salt in the design of radioactive waste storage facilities in halide formations, *Crystallography Reports*, 2009 (accepted)
16. S.Mosch, D.Nikolayev, S.Siegesmund, O.Ewiak, 3D Modelling of quarry block size volumes, *Bulletin of Engineering Geology and the Environment* (submitted)
17. T.A.Lychagina, D.I.Nikolayev, F.Wagner, Using Individual Spectra Simulation for the Study of Pole Figures Errors, *Texture, Stress, and Microstructure*, Hindawi, vol. 2009 (2009), Article ID 237485, 10 pages, 2009. doi:10.1155/2009/237485; www.hindawi.com/journals/tsm/2009/237485.html
18. V.L.Aksenov, Yu.V.Nikitenko, Patent for invention "Method of determination of spatial distribution of magnetic moments in nanolayers", № 2360234 of 27.06.09
19. S.A.Manoshin, A.V.Belushkin, S.A.Kulikov, Ye.P.Shabalin, K.Walther, C.Scheffzuek, V.V.Zhuravlev, Optimization of a moderator-neutron guide system for diffractometers of beam line 7A of the IBR-2M reactor, *Nuclear Instruments and Methods in Physics A*: 608 (3), 447-453 (2009).

1.1. ИССЛЕДОВАНИЯ НАНОСИСТЕМ И НОВЫХ МАТЕРИАЛОВ С ИСПОЛЬЗОВАНИЕМ РАССЕЯНИЯ НЕЙТРОНОВ

Основные цели исследований по теме состояли в изучении структуры, динамики и микроскопических свойств наносистем и новых материалов, имеющих большое значение для развития нанотехнологий в сфере электроники, фармакологии, медицины, химии, современной физики конденсированных сред и смежных областей методами рассеяния нейтронов и комплементарными методами. В связи с продолжающейся остановкой реактора ИБР-2 на модернизацию научная экспериментальная работа сотрудников НЭО НИКС проводилась в нейтронных и синхротронных центрах в России и за рубежом. Она осуществлялась в соответствии с Проблемно-тематическим планом ОИЯИ, на основе существующих соглашений о сотрудничестве и принятых предложений на эксперимент. Работы на реакторе ИБР-2 выполнялись по плану модернизации спектрометров. Основное внимание было уделено реализации первоприоритетных проектов (создание нового дифрактометра для исследования микрообразцов ДН-6, многофункционального рефлектометра ГРЭЙНС, модернизация комплекса спектрометров для геофизических исследований СКАТ/Эпсилон).

В рамках исследований по теме сотрудники отдела НИКС поддерживали широкие связи со многими научными организациями в странах-участницах ОИЯИ, а также других странах. Как правило, сотрудничество оформлялось совместными протоколами или соглашениями. В России наиболее активное сотрудничество велось с близкими по тематике организациями, такими как РНЦ КИ, ПИЯФ, МГУ, ИФМ, ИК РАН, ИЯИ РАН и др.

Главными направлениями научных исследований, реализация которых осуществлялась сотрудниками НЭО НИКС, являются:

- Исследование структуры и свойств новых кристаллических материалов и наносистем методом дифракции нейтронов;
- Исследование магнитных коллоидных систем в объеме и на границах раздела;
- Исследование структуры углеродных наноматериалов;
- Магнетизм слоистых наноструктур;
- Исследование надмолекулярной структуры и функциональных характеристик биологических, коллоидных и полимерных нанодисперсных материалов;
- Исследования наноструктуры и свойств липидных мембран и липидных комплексов;
- Исследование атомной динамики наносистем и материалов методом неупругого рассеяния нейтронов;
- Исследование текстуры и свойств минералов и горных пород;
- Анализ внутренних напряжений в объемных материалах и изделиях.

1. Научные результаты

1.1. Структурные исследования новых оксидных материалов

Продолжалось нейтронное дифракционное исследование атомной и магнитной структуры 314-кобальтитов типа $Sr_3YCo_4O_{10.5+\delta}$ (или $Sr_{0.75}Y_{0.25}CoO_{2.625+\delta/4}$), в которых A-позиции являются идеально упорядоченными. Для этих составов было найдено, что атомы Co, находящиеся в различных позициях элементарной ячейки, имеют различную величину магнитного момента, которая коррелирует с кислородным окружением атома, т.е. впервые для перовскитоподобных кобальтитов была установлена прямая связь между зарядовым и спиновым состояниями атомов Co. В составах с разным содержанием кислорода был установлен G-тип AFM структуры, без признаков наличия ферромагнитной компоненты момента [1]. В 2009 г. изучались составы с частичным замещением Sr на Ca, а именно,

$Sr_{0.75-x}Ca_xY_{0.25}CoO_{3-y}$ с x ≈ 0.30 и y ≈ 0.35, для которых из косвенных данных были получены указания на частичную стабилизацию ферромагнетизма вследствие влияния Ca на зарядовое состояние Co. Для проверки этой модели на дифрактометре HRPT (PSI) были измерены нейтронные дифракционные спектры в интервале температур от 1.5 до 300 K (рис. 1). Предварительный анализ показал наличие магнитного фазового перехода при $T \approx 260$ K с появлением AFM структуры и возможной небольшой FM компонентой.

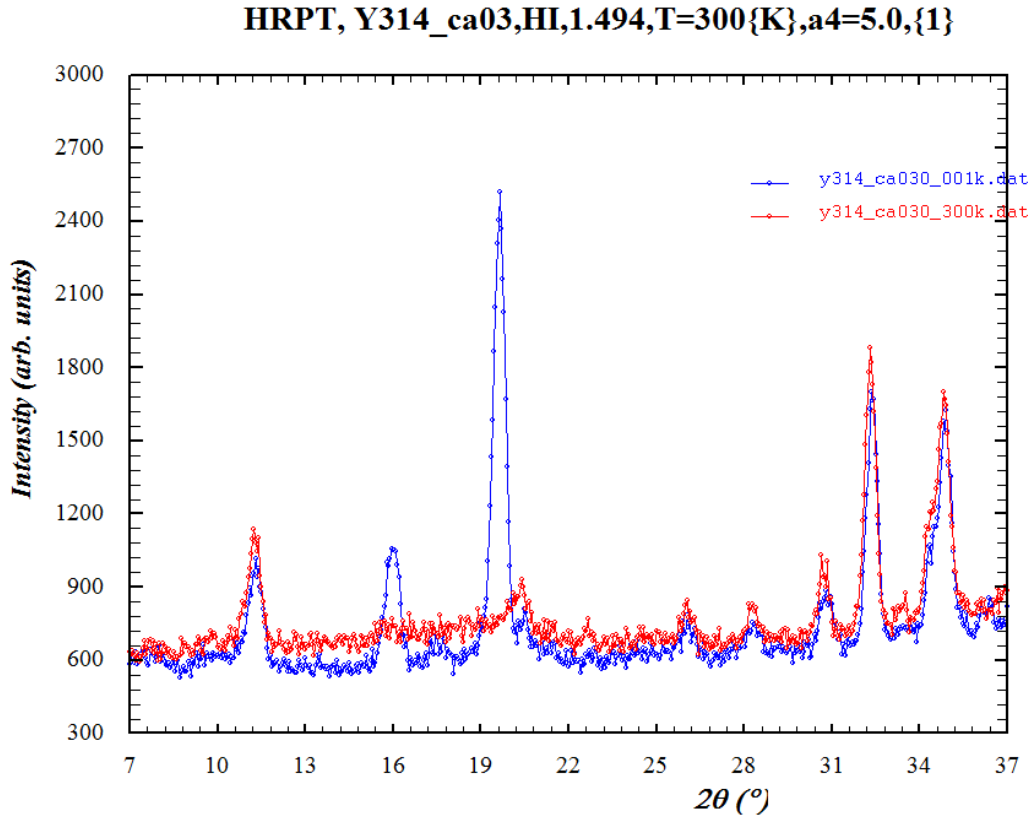

Рис. 1. Дифракционные спектры состава $Sr_{0.75-x}Ca_xY_{0.25}CoO_{3-y}$ с x ≈ 0.30, измеренные при температурах 1.5 и 300 K. Предварительный анализ показал, что различие в интенсивности отдельных пиков обусловлено возникновением дальнего магнитного порядка при понижении температуры.

Продолжались исследования влияния высокого давления на кристаллическую и магнитную структуры сложных анион-дефицитных оксидов кобальта в широком диапазоне температур. В соединении $Sr_{0.7}Y_{0.3}CoO_{2.62}$ обнаружено изменение спиновой конфигурации ионов Co^{3+} при воздействии высокого давления, которое приводит к изменению симметрии антиферромагнитного состояния [2].

Методами рентгеновской дифракции и малоуглового рассеяния нейтронов исследованы структурные характеристики оптически-активных наноструктурированных оксидных материалов состава $0.95GeO_2$-$0.05Eu_2O_3$, $0.949GeO_2$-$0.05Eu_2O_3$-0.001 Ag и $0.999GeO_2$-0.001Ag, отожженных на воздухе до $T = 900°$ C. Система $0.999GeO_2$-0.001Ag, полученная при $T_O = 150\ ^0$C образует аморфную фазу, а при $T_O = 200\ ^0$C – кристаллизуется в тригональной фазе симметрии $P3_221$. Системы $0.95GeO_2$-$0.05Eu_2O_3$ и $0.949GeO_2$-$0.05Eu_2O_3$-0.01Ag, полученные при $T_O = 150$-$800\ ^0$C также имеют тригональную кристаллическую структуру симметрии $P3_221$. Методом малоуглового рассеяния нейтронов обнаружено образование полидисперсных кластеров в системах $0.95GeO_2$-$0.05Eu_2O_3$ и $0.949GeO_2$-$0.05Eu_2O_3$-0.01Ag в диапазоне температур отжига 350-555 ^{0}C. Рассчитаны функции распределения кластеров по

размерам (рис. 2). При T_O =850 ^{0}C наблюдается распад кластеров. Установлено, что значительное изменение относительной интенсивности полос возбуждения люминесценции ионов Eu^{3+} при введении серебра коррелирует с уменьшением характерных размеров полидисперсных кластеров, образующихся при отжиге [3].

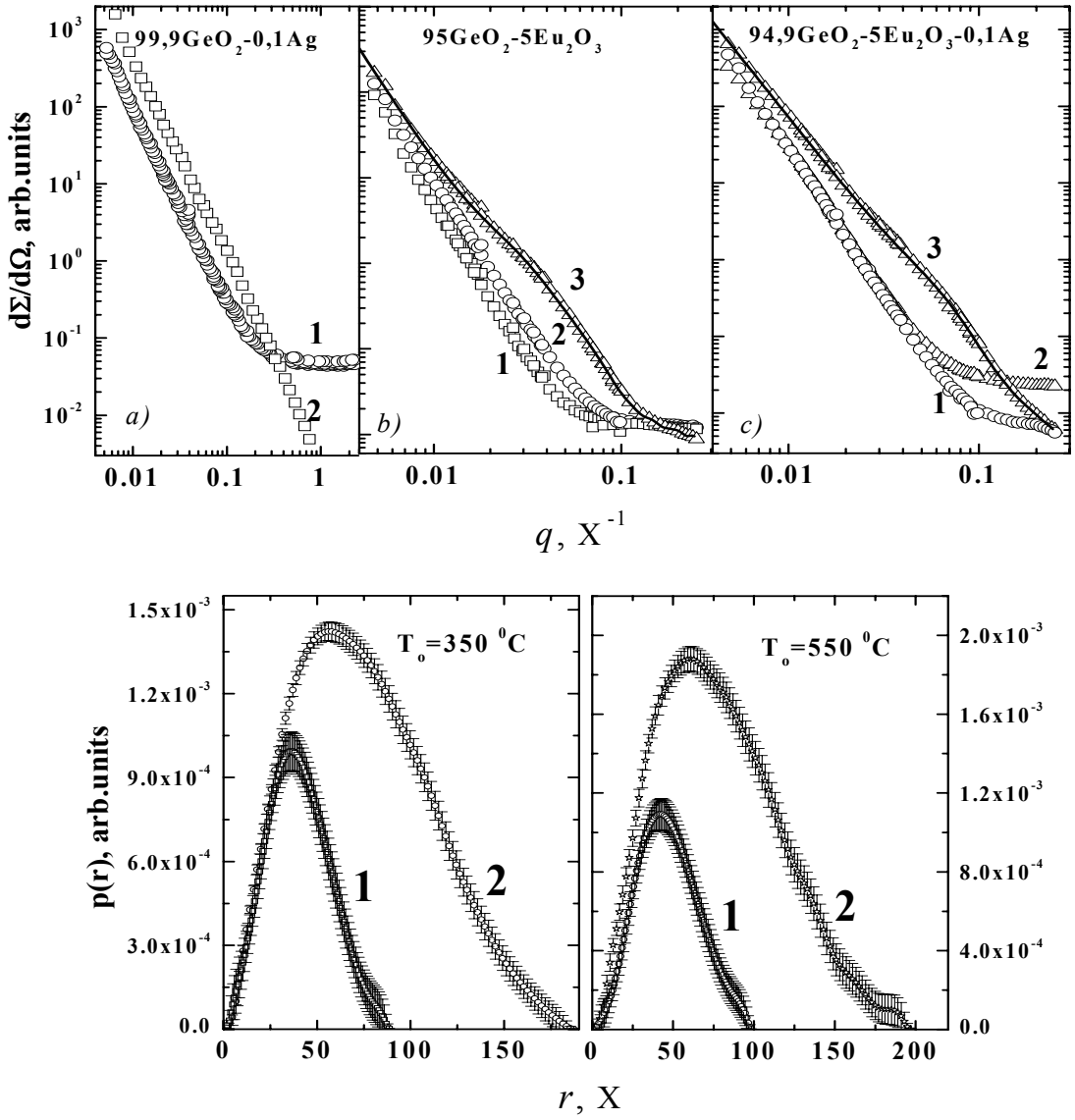

Рис. 2. Вверху: кривые малоуглового рассеяния нейтронов ксерогелей 99,9GeO_2-0,1Ag (*a*), 95,0GeO2-5Eu2O3 (*b*) и 94,9GeO2-5Eu_2O_3-0,1Ag (*c*) для температур отжига T_O=150 (1), 550 (3) и 850 ^{0}C (2). Для кривых, соответствующей T_O=550 ^{0}C, представлена теоретическая кривая, рассчитанная по формуле (2). Внизу: функция распределения размеров промежуточных агрегатов для ксерогелей 94,9GeO_2-5Eu_2O_3-0,1Ag (1) и 95,0GeO2-5Eu_2O_3 (2) для температур отжига 350 (слева) и 550 ^{0}C (справа).

1.2 Исследования магнитных жидкостей

Завершено комплексное исследование эффекта регулирования размера наночастиц магнетита в феррожидкостях с неполярными органическими основами при стабилизации монокарбоновыми кислотами. Исследования проведены с применением анализа статической намагниченности, просвечивающей электронной микроскопии, дифракции и малоуглового

рассеяния синхротронного излучения, малоуглового рассеяния поляризованных нейтронов. Подтверждено, что при замене ненасыщенной олеиновой кислоты (C_{18}), используемой в классической процедуре стабилизации, насыщенными кислотами из ряда лауриновая (C_{12}), миристиновая (C_{14}), пальмитиновая (C_{16}), стеариновая (C_{18}) кислоты происходит уменьшение эффективного размера стабилизированного магнетита [4]. В частности, дифракция и малоугловое рассеяние синхротронного излучения указывают на различия в размере когерентной области рассеяния магнетитом между образцами со стабилизацией олеиновой кислотой и насыщенными жирными кислотами. Совместное использование двух методов позволяет сделать четкий вывод о том, что обнаруженный эффект связан с изменением в размере диспергированного магнетита, а не с различиями в возможной агрегации. В результате исследований показано, что характерный размер магнетита при использовании различных смесей ПАВ можно изменять в диапазоне 5 – 8 нм.

С использованием метода малоуглового рассеяния нейтронов проведены исследования ряда водных биосовместимых магнитных жидкостей. Исследуемые системы рассматривались как источники и среды для хранения магнитных наночастиц, используемых в биомедицинских приложениях. Получены структурные характеристики частиц и их агрегатов. Исследована структурная стабильность жидкостей в различных условиях.

1.3 Исследование углеродных наноматериалов

С помощью малоуглового рассеяния нейтронов определена структура агрегатов наноалмазных частиц (детонация), диспергированных в полярные жидкости (вода, ДМСО) согласно специальной процедуре «мокрого» размалывания. Получены размер и фрактальные характеристики агрегатов, а также структурные особенности наноалмазных частиц (размер, характер поверхности). Проведено сравнение со структурой агрегатов в изначальных наноалмазных порошках. Анализ зависимости структурного фактора от числа частиц в растворе указывает на перекрытие разветвленных кластеров при концентрировании дисперсий. Вариация контраста с использование смесей протонированных и дейтерированных растворителей позволила определить среднюю плотность частиц, составляющих кластер, и сделать вывод о существовании неалмазной компоненты на поверхности наноалмазов. Благодаря данным исследованиям завершено описание всех состояний коллоидных наноалмазных дисперсий (рис. 3) на основе различных дополняющих методов (просвечивающая электронная микроскопия, рентгеновская дифракция, малоугловое рассеяние нейтронов) [5].

Продолжены комплексные исследования кластерообразования фуллеренов (C_{60}) в слабополярных (сероуглерод, толуол, бензол) и полярных (N-метил-2-пирролидон) растворителях, а также их смесях. Исследования проводились с применением спектроскопии и экстракции, масс-спектрометрии, малоуглового рассеяния нейтронов. Подтверждено, что для слабополярных растворов рост кластеров в ряде случаев можно инициировать неравновесными условиями приготовления раствора (ультразвук, интенсивное долгое перемешивание). Для полярных растворов, где кластеры появляются всегда, проанализированы изменения во времени спектров поглощения (временной сольватохромный эффект) и экстракции, которые связаны в той или иной степенью с ростом кластеров. Проведено сравнение влияния добавки воды или толуола в кластерный раствор C_{60}- N-метил-2-пирролидон. Показано, что в обоих случаях наблюдается уменьшение видимого размера кластеров.

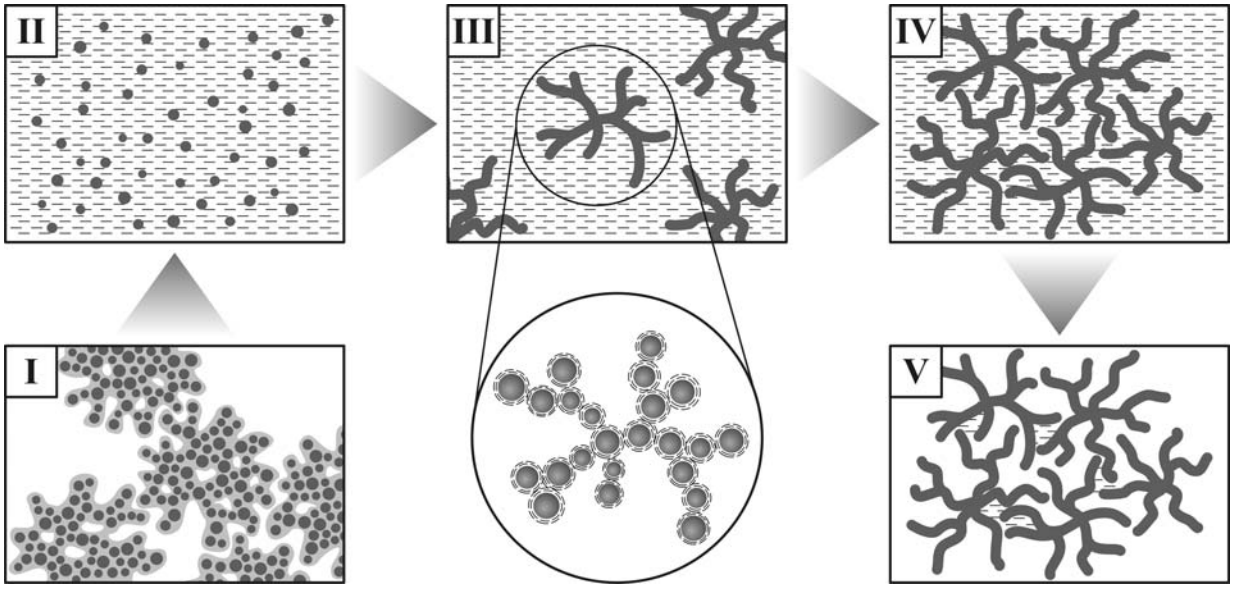

Рис. 3. Условное представление о различных состояниях коллоидных наноалмазных дисперсий. **(I)** изначальные порошки; размер плотных (химически стабильных) агрегатов составляет более 40 нм; агрегаты имеют развитую поверхность с характерной размерностью D_s ~ 2.5; закрытее поры организуют фрактальную структуру с размерностью D ~ 1.26; **(II)** жидкая дисперсия сразу после процедуры жидкого размола; наноалмазные частицы разделены; **(III)** жидкая дисперсия низкой концентрации (C ~ 1 вес. %) после образования агрегатов с фрактальной размерностью D ~ 2.3 и размером более 40 нм; характерный размер кристаллита алмаза составляет ~7 nm; толщина неалмазной компоненты на поверхности наночастиц ~ 0.5 нм; **(IV)** жидкая дисперсия после коцентрирования (C ~ 10 вес. %); агрегаты проникают друг в друга благодаря разветвленной структуре; **(V)** дисперсия при испарении объемного растворителя; вода частично удерживается в мелких порах с характерным размером ~7 nm.

1.4 Исследование магнитных слоистых наноструктур

Продолжались экспериментальные исследования по проблеме сосуществования ферромагнетизма (F) и сверхпроводимости(S). Магнитное состояние бислоя Fe/V было исследовано с помощью нейтронного волнового резонатора MgO/V/Cu [6]. Поведение бислоя в действительности соответствовало поведению трёхслойной структуры F/F-S/S, в которой промежуточный слой F-S представлял собой смесь атомов ванадия и железа. Наблюдались прямой и обратный эффект близости. Прямой эффект, заключающийся в установлении сверхпроводящего параметра порядка в ферромагнетике F-S, проявился при переходе слоя ванадия (S) в сверхпроводящее состояние ($T=T_c$) в виде уменьшения и поворота вектора намагниченности к направлению внешнего магнитного поля. Обратный эффект близости, заключающийся в установлении ферромагнитного порядка в сверхпроводнике F-S, наблюдался при температуре 0.6 T_c и состоял в увеличении вектора намагниченности и его повороте от направления магнитного поля (**рис. 4**).

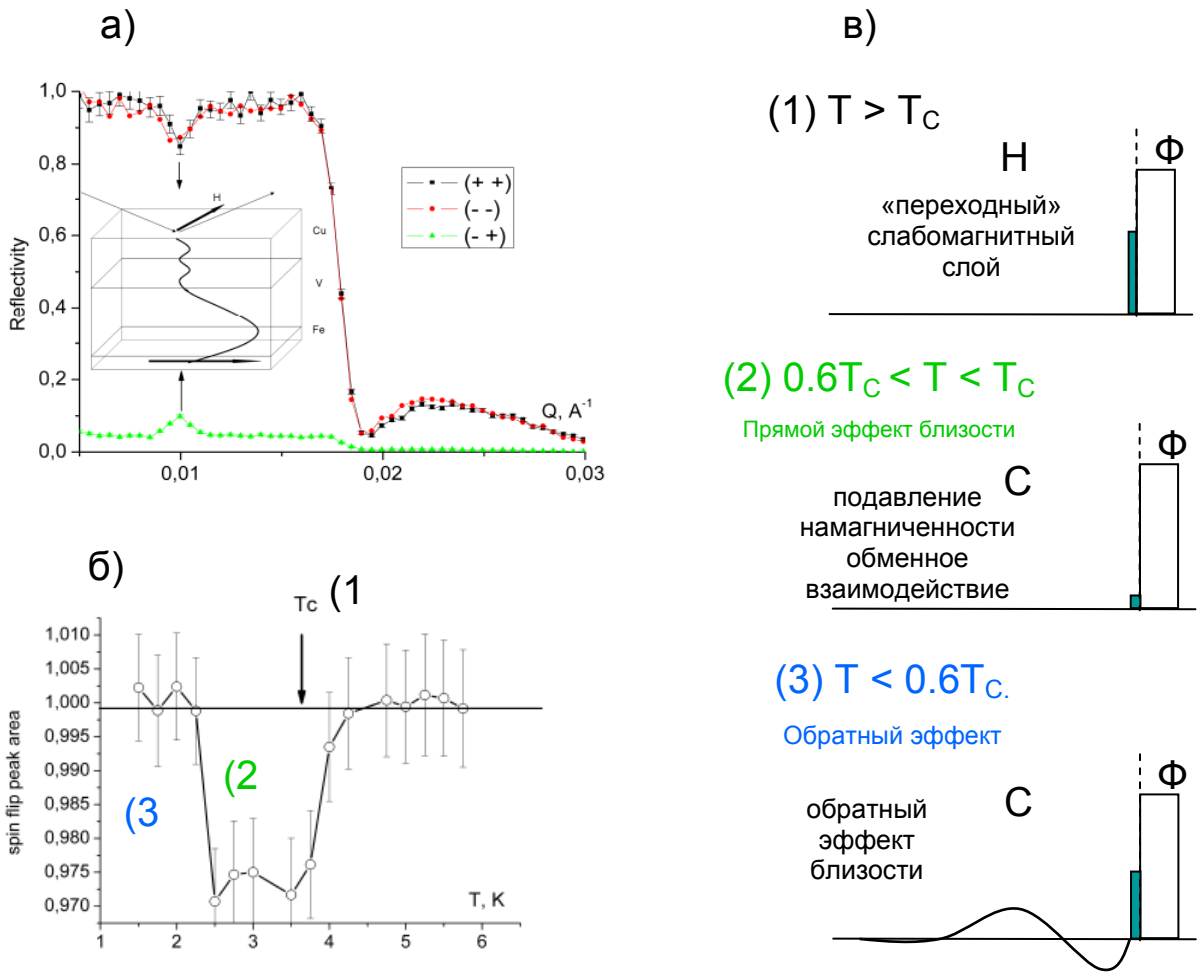

Рис.4. Коэффициент отражения поляризованных нейтронов от сверхпроводяще-ферромагнитной гетероструктуры Cu(32нм)/V(40нм)/Fe(1нм)/MgO с резонатором стоячих нейтронных волн (а); температурное поведение резонансного спин-флоп пика (б); изменение магнитного профиля вблизи границы раздела для различных температурных областей (1)-(3) (в).

Изучены особенности прохождения поляризованных и неполяризованных нейтронов через двухслойные и трёхслойные магнитные наноструктуры. При этом, в частности, обнаружено, что прохождение неполяризованных нейтронов через некомпланарные структуры при некоторых условиях является лево-право асимметричным. Одним из следствий этого является то, что подобные некомпланарные магнитные структуры, созданные искусственно или существующие в природе, могут быть фильтром, позволяющим селектировать неполяризованный ансамбль атомов (молекул) в зависимости от величины их магнитного момента [7].

1.5 Исследование биологических наносистем

Методом атомно-силовой микроскопии (АСМ) была исследована поверхность митопластов (митохондрий, лишенных внешней мембраны). С помощью АСМ на поверхности митопластов были обнаружены складки, толщина которых равна 30-40 нм (рис. 5) и совпадает с толщиной "сухих крист" митохондрий, измеренной с помощью малоуглового рассеяния нейтронов и электронной микроскопии. Полученные результаты свидетельствуют о существовании специальной системы, поддерживающей определенную конфигурацию мембраны митопластов, сходную с конфигурацией, которую приобретает

внутренняя мембрана интактных митохондрий в условиях их набухания в гипотонических средах. В работе показана перспективность использования АСМ для изучения конфигурации поверхности внутренней мембраны митохондрий и соответственно других биологических мембранных систем [8].

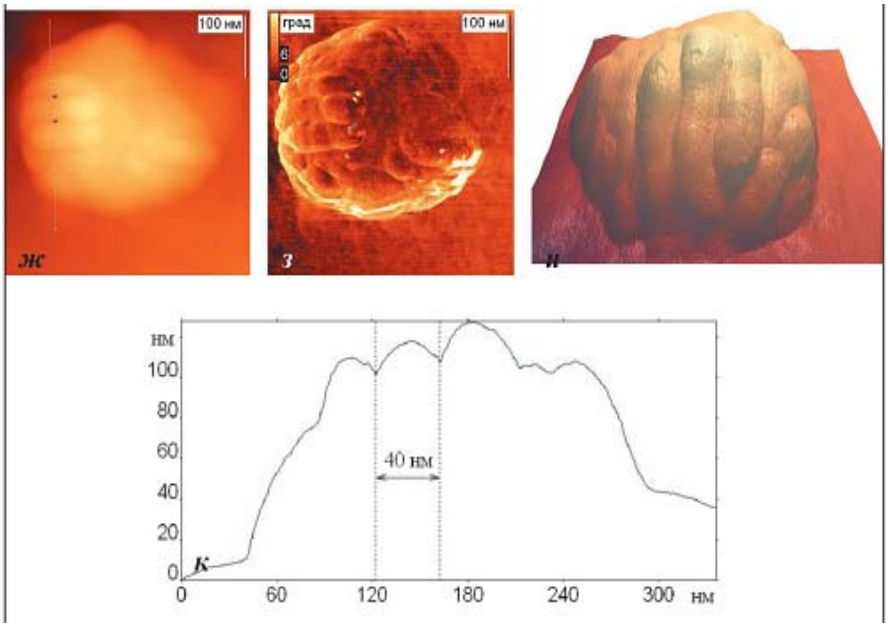

Рис. 5. *ж*)-*и*) – АСМ-изображения митопластов печени крысы с наличием «сухих крист»; *к*) – сечение, проведенное вдоль пунктирной линии, показанной на *ж*). ж - АСМ-изображения, записанные по каналу «высота»; з – по каналу «фаза», и – трехмерное представление. Размер масштабного отрезка на всех изображениях составляет 100 нм. Максимальный перепад высоты на АСМ-изображении ж) составляет 172 нм.

Были изучены образцы, содержащие биогенные наночастицы ферригидрита, полученные с помощью бактерий *Klebsiella oxytoca.* В частности, с помощью оптической микроскопии, сканирующей электронной микроскопии и малоуглового рентгеновского рассеяния исследовался эффект возраста бактерий (продолжительность роста), влияющий на свойства наночастиц [9].

Методом рентгеновской дифракции исследованы водные растворы мультислойных везикул многокомпонентных мембран, моделирующих слизистую оболочку ротовой полости человека (Oral Stratum Corneum, OSC) и мембран входящих в их состав смеси сфингомиелен/дипальмитоилфосфатидилхолин/дипальмитоилфосфатидилэтаноламин (SM/DPPC/DPPE) [10]. Системы смеси SM/DPPC/DPPE (при массовом соотношении 1/1/1, 1/2/1) характеризуется ламеллярной структурой с периодом повторяемости ~ 71 Å. При увеличении массовой доли DPPE часть липида образует отдельную ламеллярную фазу (d ~ 56 Å) и обратную гексагональную фазу (a ~ 56 Å). Многокомпонентные мембраны OSC на основе церамида 6 и церамида 3 являются сложными многофазными системами, приходящими в фазовое равновесие после приготовления образцов несколько дней.

1.6 Исследование полимерных и коллоидных наносистем

Методом малоуглового рассеяния нейтронов исследована структура кремнийорганических дендримеров девятой генерации с четырехфункциональным ядром и бутильными концевыми группами. Показано, что исследуемые дендримеры являются монодисперсными объектами анизометричной формы. С помощью метода вариации контраста определены значения парциального объема и значение средней рассеивающей

плотности. Демонстрируется идентичность между собой исследуемых дендримеров по габаритным размерам и распределению рассеивающей плотности. Установлено, что 20% габаритного объема дендримера доступно для проникновения растворителя. Выполнено моделирование с использованием метода Монте-Карло и восстановлено пространственное распределение плотности длины рассеяния в исследуемых дендримерах, обнаружено изменение исключенного объема для разных контрастов.

Методом малоуглового рассеяния нейтронов исследованы мицеллообразование додецил(сульфофеокси)бензолсульфоната натрия и нонилбензолдекаэтиленоксида в нейтральных и щелочных растворах электролитов различной концентрации. Показано, что образующиеся в растворах мицеллы имеют цилиндрическую (эллипсоидальную) форму. Определены характерные размеры мицелл в функции концентраций ПАВ и добавляемого электролита. Получена корреляция структурных данных с геометрией и динамикой травления “трековых” нанопор в растворах, содержащих ПАВ и разработана модель влияния ПАВ на получение пор специфической геометрии [11].

1.7. Атомная динамика

Методом неупругого рассеяния нейтронов исследованы колебательные спектры гексана и изомеров гексанола. Проведено теоретическое моделирование колебательных спектров с использованием теории функционала плотности. Рассчитаны частоты низкоэнергетических торсионных мод относительно С-С связей и С-С-С изгибающих мод для плоских и изогнутых конформаций молекул гексана и изомеров гексанола в диапазоне до 500 $см^{-1}$. В целом, расчетные спектры плотности колебательных состояний для изолированных молекул имеют качественное согласие с экспериментальными спектрами. Однако для описания динамики гидроксильных групп необходимо учитывать формирование водородных связей между молекулами гексанола. Показано, что расчеты динамики молекул с образованием водородной свиязи в димере позволяют правильно интерпретировать динамику гидроксильных групп в конденсированном состоянии этих спиртов (**рис. 6**).

Проведен подробный анализ нейтронографических данных сверхкритической воды, имеющей перспективы для использования в качестве теплоносителя в реакторах следующего поколения и являющейся уникальным растворителем при окислении органических отходов. Была подтверждена и уточнена двухструктурная модель, предложенная ранее для описания микродинамики сверхкритической воды. На основе этой модели был получен ряд нейтронно-физических характеристик сверхкритической воды, необходимых при оценках параметров ядерных реакторов, использующих в качестве теплоносителя воду при сверхвысоких параметрах [12].

1.8. Прикладные работы

К прикладным работам в отделе НИКС ЛНФ традиционно относятся экспериментальные исследования текстуры горных пород и минералов, внутренних напряжений в них и определение внутренних напряжений в объемных материалах и изделиях, включая инженерные материалы и детали машин и устройств. В основном, эти исследования ведутся с помощью дифракции нейтронов.

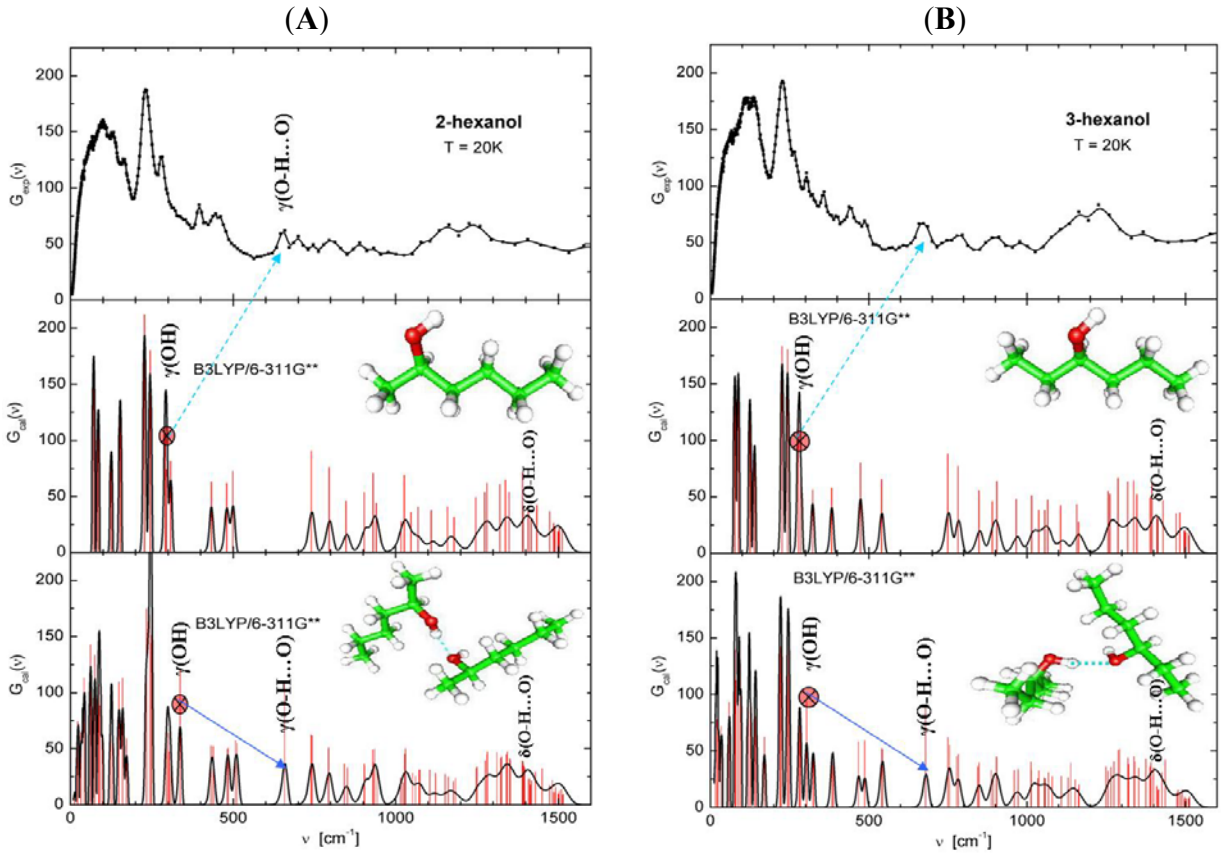

Рис. 6. Сравнение экспериментальных и расчетных спектров HHPH свободных молекул и их димеров с водородной связью для 2-гексонола (A) и 3-гексонола (B).

Завершена работа по изучению температурного поведения образцов стали ЭК-181. Из дифракционных спектров, обработанных по методу Ритвельда, для интервала температур 15 – 973 К определены температурные зависимости параметра кристаллической решетки, внутренних напряжений 3-го рода и фактора Дебая-Валлера этой стали [13]. Оказалось, что в области низких температур ход температурной зависимости параметра решетки в стали ЭК-181 не соответствует таковому в чистом железе и бинарных железо-хромистых сплавах с 12 и 16% Cr. Наряду с этим замечено уширение рефлекса (200) в дифракционных спектрах стали ЭК-181 и сплава Fe-12Cr, не наблюдаемое на спектрах Fe-16Cr и чистого железа.

По данным нейтронографии определена структура специальных сталей, графита, ниобата циркония (различные процессы изготовления). Восстановлена функция распределения кристаллитов по ориентациям (ФРО), проведено моделирование объемных упругих свойств этих конструкционных материалов. Показано, что аустенитная наплавка корпуса реактора ВВЭР-1000 имеет острую радиальную текстуру (вращение зерен вокруг нормали к плоскости (002) стали), что приводит к сложному распределению остаточных напряжений в ней, при этом минимальные значения модуля Юнга достигаются в направлении нормали к поверхности корпуса реактора. Для реакторного графита ГР-280 показано, что анизотропия упругих свойств качественно связана с кристаллографической текстурой (рис.7), которая характеризуется концентрацией осей 6-го порядка графита перпендикулярно направлению экструзии [14]. При этом наблюдается различие между реальными (измеренными ультразвуковым методом) и модельными (рассчитанными с помощью усреднения упругого тензора по ФРО) скоростями продольных упругих волн (около 5 раз при атмосферном давлении и около 3-х – при 150 МПа).

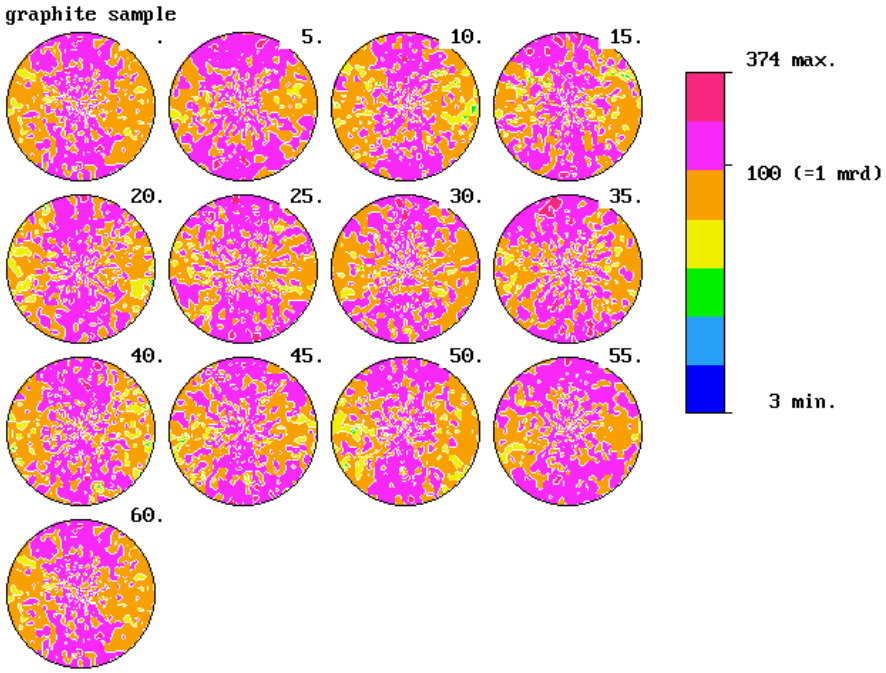

Рис. 7. ФРО графита в образце Gra2, γ-сечения (стереогра-фические проекции). fmin=0.03, fmax=3.74, F2=1.21.

В ниобате циркония процесс изготовления стержня приводит к формированию острой радиальной текстуры с вращением кристаллитов вокруг нормали к плоскости (2-70). При этом материал становится практически изотропным по своим упругим свойствам. На основании текстурных измерений были сформулированы требования к эксперименту по исследованию внутренних напряжений в ниобате циркония.

Проведены исследования физических свойств и флюидопроницаемости соли для оценки ее барьерных свойств при проектировании хранилищ радиоактивных отходов [15]. Аналитически рассчитано температурное распределение, возникающее в соляной породе вблизи размещенного в ней теплоизлучающего источника. При начальной температуре соли 20°С, радиусе каверны с отходами 5 м, интенсивностях тепловыделения до 100 Вт/м^3 и временах хранения до 100 лет температура среды не превышает 90°С, а максимальный градиент составляет 0.1°С на 1 см. Получена теоретическая оценка максимальных скоростей движения включений в монокристалле NaCl под действием градиента температур, создаваемого радиоактивным источником. Для включений размерами 0.005-0.2 см, находящихся на расстоянии порядка 1 м от стенки хранилища при интенсивности излучения 100 Вт/м^3 (начальная температура раствора включения при этом составляет 58.45°С, постоянный внешний тепловой градиент 0.08 °С на 1 см) скорости движения лежат в диапазоне (0.2-0.5)$*10^{-10}$ см/с. При этом, скорость перемещения включения увеличивается с возрастанием его размеров. Теоретически рассмотрена динамика движения, наблюдается вытягивание включения в направлении перпендикулярном градиенту температуры, а также его распад с тыльной стороны на более мелкие части, что может вызывать нарушение кристаллической решетки соли.

Изучено воздействие сильноточных импульсных пучков релятивистских электронов на механизм кратерообразования в образцах горных пород (солей, гранитов и лабродаритов). Для экспресс-оценки состояния поверхности образцов и для установления барьерных свойств геоматериала проведена апробация метода тепловизорного мониторинга. Показано, что проведение подобного рода комплексных экспериментов целесообразно для изучения свойств горных пород, имеющих определяющее значение при выборе мест для захоронения

радиоактивных отходов. Возможным механизмом кратерообразования при облучении твердых тел пучками сильноточных электронов (**рис. 8**) может быть термоудар, в результате которого образуются термонапряженные участки, а разрушение происходит по границе расплава.

а)

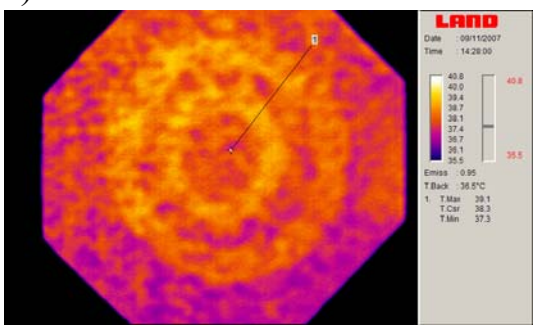

б) в)

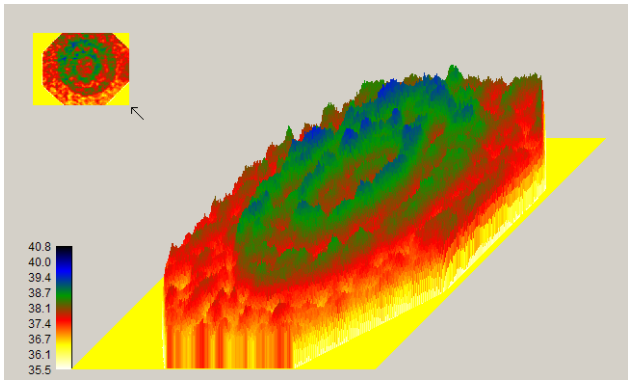

г)

Рис. 8. а) Образец серого гранита, облученного 20 импульсами сильноточных импульсных пучков релятивистских электронов (СИПРЭ); б) фронтальное ИК-изображение облученного образца серовато розового гранита, подвергнутого тепловому воздействию; в) температурный профиль поверхности вдоль линии на рис. б; г) трехмерное изображение распределения температурного поля.

Проведены исследования текстуры и внутренних напряжений образцов горных пород из Центральных Альп (Швейцария) в районе туннеля Gotthard-Base-Tunnel. Полученные результаты важны для оценки влияния работ по устройству туннеля на геомеханическое состояние горных массивов его окружения туннеля.

Проведено исследование анизотропных свойств образцов мрамора и гранита, а также моделирование с целью выработки практических рекомендаций по оптимизации добычи природного камня в каменоломнях [16].

Проведено исследование ошибок измерения полюсных фигур – экспериментальной информации о текстуре, получаемой на спектрометре СКАТ. Исследование проводилось на примере магниевого сплава Mg+4.5Al+1%Zn. Ошибки измерений оценены в каждой из 1368 точек на полюсной фигуре. Выявлено, что на формирование ошибок на полюсной фигуре главным образом влияют ошибки оценки полуширины дифракционного пика. Полученный вывод подтвержден путем расчета ошибок полюсных фигур, извлеченных из модельных индивидуальных спектров. Моделировался набор из 1368 индивидуальных нейтронных дифракционных спектра. Моделирование спектров проводилось на основе экспериментальных и модельных полюсных фигур (рис.9). Показано, что распределение ошибок полюсных фигур качественно совпадает с распределением ошибок вычисления полуширины пика, причем это верно как для экспериментальных полюсных фигур, так и для полюсных фигур, полученных из модельных спектров [17].

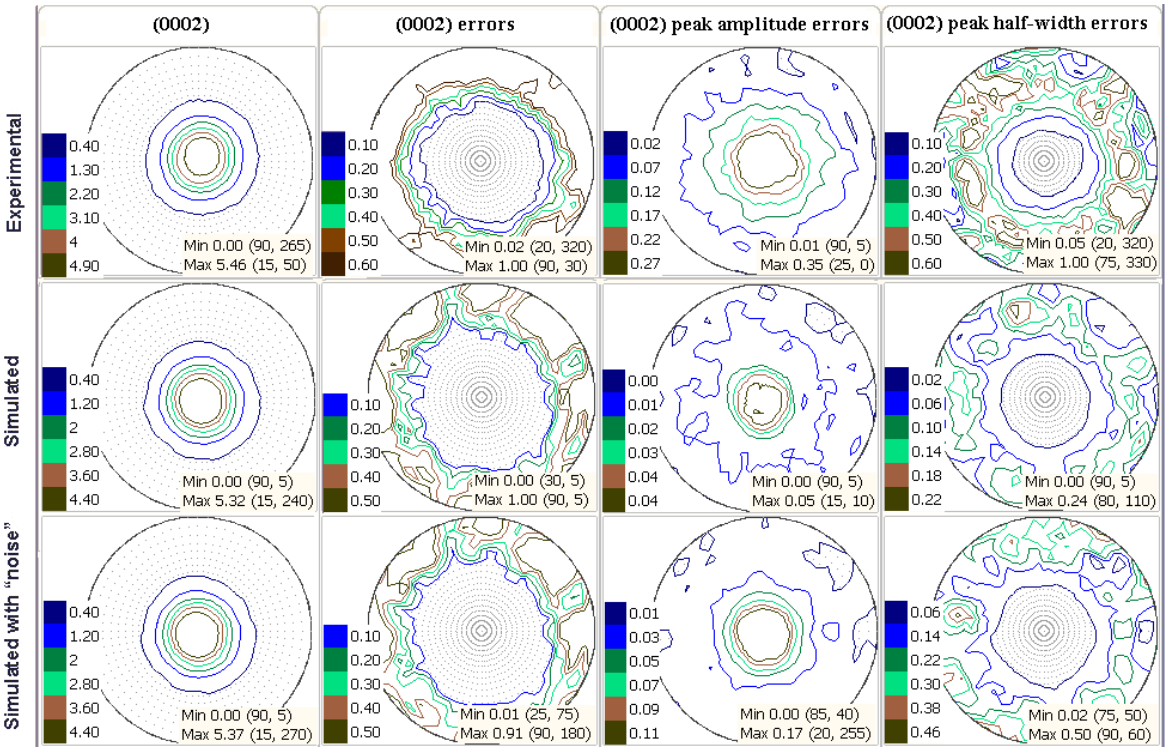

а) б) в) г)

Рис. 9. а) Полюсная фигура (0002) для образца из сплава Mg+4.5Al+1%Zn. Интенсивности даны в единицах изотропного распределения б) Относительная ошибка полюсной фигуры (0002). в) Ошибка определения амплитуды пика. г) Ошибка определения полуширины пика. В верхнем ряду представлены экспериментальная полюсная фигура, измеренная на текстурном дифрактометре СКАТ, и ошибки, рассчитанные для экспериментальных данных; во втором ряду – полюсная фигура, извлеченная из модельных спектров, и соответствующие ошибки; в третьем ряду – полюсная фигура, извлеченная из спектров, смоделированных с "экспериментальной" ошибкой ("шумом") и также соответствующие ошибки.

2. Методические результаты

Завершено изготовление головной части зеркального вакуумного нейтроновода и проведена ее установка на 6 канале реактора ИБР-2М в рамках реализации проекта создания дифрактометра для исследования микрообразцов ДН-6 (рис. 10). Продолжено изготовление

вакуумного кожуха для хвостовой части нейтроновода. Начато проектирование газового ПЧД детектора.

Рис. 10. Головная часть зеркального вакуумного нейтроновода, установленная на 6-м канале реактора ИБР-2 в рамках реализации проекта по созданию нового дифраткометра для исследования микрообразцов ДН-6.

Завершено изготовление, проведены вакуумное тестирование и установка головной части рефлектометра ГРЭЙНС на реакторе (рис. 11). Начато изготовление рельсового основания и кожуха системы формирования пучка. Проведено тестирование элементов данной системы (изменяемые щели, отклоняющие зеркала). Подготовлена рабочая документация на изготовление механического прерывателя барабанного типа.

Проведены работы по подготовке рабочей площадки для установки зеркального нейтроновода на спектрометре ДИН 2ПИ. Закуплены зеркальные сегменты, материалы эффективной биологической защиты нейтроновода первой пролетной базы спектрометра и механические узлы для юстировки нейтроновода. Завершена обработка экспериментальных данных по моделированию на спектрометре ДИН 2ПИ макета криогенного замедлителя, планируемого к постановке на реакторе ИБР–2М.

Подготовлен эскизный проект нового детектора обратного рассеяния для дифрактометра ФДВР на основе ZnS-элементов (рис. 12). Телесный угол нового детектора в ~10 раз превышает телесный угол существующего детектора, что позволит, в случае реализации проекта, значительно улучшить условия проведения структурных экспериментов на ФДВР.

Рис. 11. Головная часть многофункционального рефлектометра GRAINS.

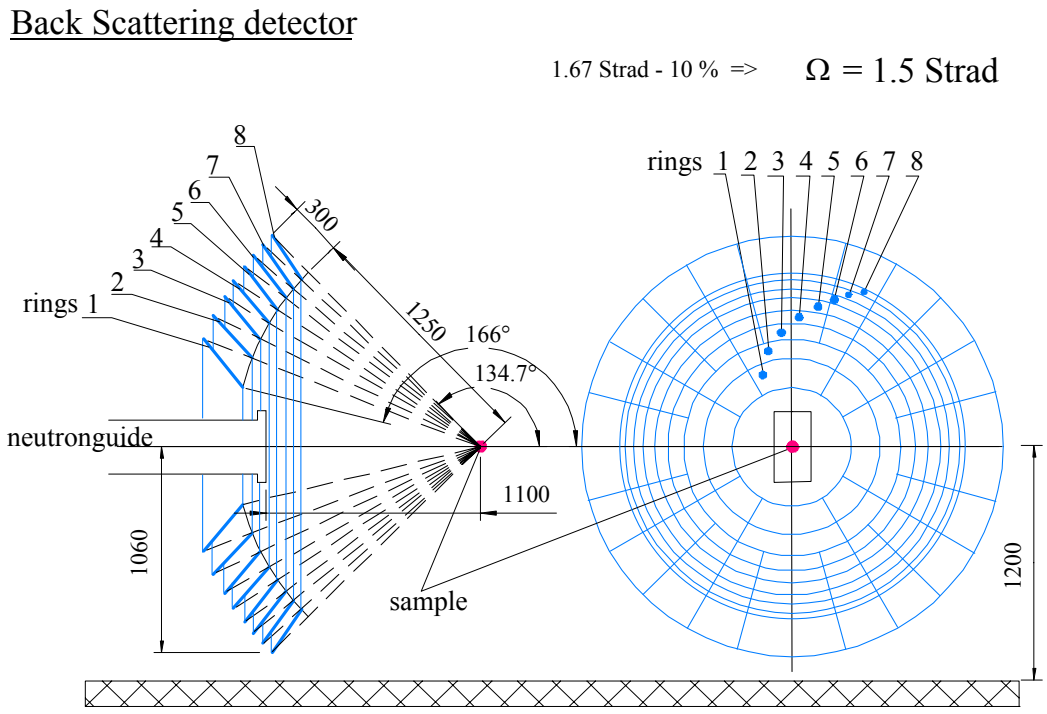

Рис. 12. Проект нового детектора обратного рассеяния для дифрактометра ФДВР на основе ZnS-элементов

Продолжена работа по изучению возможности создания суперзеркал с периодической структурой, в рамках которой были проведены эксперименты по рефлектометрии поляризованных нейтронов на образцах с 2, 4, 8 бислоями NiTi и подложкой floatglass (MIRROTRON, Будапешт, Венгрия).

Проведено исследование эффекта усиления спин-флип сигнала в нейтронном волновом резонаторе. Показано, что в нейтронном волновом резонаторе спин-флип сигнал от

магнитно-неколлинеарного слоя может быть усилен во второй или даже третьей степени по отношению к уже усиленному сигналу от ядерного слоя. Это делает возможным проведение исследований субатомных магнитных слоёв толщиной до 10^{-5} нм или нанослоёв со сверхмалой намагниченностью величиной 10^{-3} Гс [18].

В рамках проекта создания изогнутых зеркальных нейтроноводов спектрометров ЭПСИЛОН и СКАТ на канале 7а реактора ИБР-2 продолжались работы по проектированию и изготовлению механических и оптических узлов нейтроноводов [19]. В частности, разработаны проекты вакуумной системы и фоновой защиты спектрометров Эпсилон и Скат и участка стыковочного нейтроновода спектрометра НЕРА-ПР, разработаны и заканчивается изготовление дискового фонового прерывателя и 3-х барабанных λ-прерывателей. Разработана, изготовлена и отлажена система управления прерывателями на базе электроприводов фирмы Toshiba. Завершена реконструкция несущей колонны ИБР-2 и биологической защиты головной части 7 канала для размещения на канале трех нейтроноводов. Изготовлены стойки и юстировочные опоры головной части нейтроновода. Продолжается изготовление 92 вакуумных кожухов изогнутых нейтроноводов для спектрометров ЭПСИЛОН и СКАТ.

Главным результатом работ по проекту создания изогнутых зеркальных нейтроноводов спектрометров ЭПСИЛОН и СКАТ в 2009 году является монтаж двух секций головной части (сплиттера) 7 канала, включающий установку внутренних секций и юстировку, а также установку вакуумных кожухов (**рис. 13**).

Рис. 13. Головная часть сплиттера 7-ого канала реактора ИБР-2М для нейтроноводной системы дифрактометров ЭПСИЛОН (7А-1), СКАТ (7А-2) и НЕРА (7В). Установка сплиттера производится в рамках проекта BMBF по модернизации нейтроноводной системы дифрактометров ЭПСИЛОН и СКАТ на канале 7А реактора ИБР-2М.

Литература

1. D.V. Sheptyakov, V.Yu. Pomjakushin, O.A. Drozhzhin, S.Ya. Istomin, E.V. Antipov, I.A. Bobrikov, A.M. Balagurov “Correlation of chemical coordination and magnetic ordering in $Sr_3YCo_4O_{10.5+\delta}$, δ=0.02 and 0.26” Phys. Rev. B, v.80, pp. 024409 (1-9) (2009).

2. N.O.Golosova, D.P.Kozlenko, L.S. Dubrovinsky, O.A. Drozhzhin, S.Ya. Istomin, and B.N. Savenko "Spin State and Magnetic Transformations in $Sr_{0.7}Y_{0.3}CoO_{2.62}$ at High Pressures", Phys. Rev. B, v. 79, pp. 104431 (1-5) (2009).
3. А.В. Белушкин, С.Е. Кичанов, Д.П. Козленко, Е.В. Лукин, Б.Н. Савенко, С.К. Рахманов, Г.П. Шевченко, В.С.Гурин, Г.Е.Малашенко, В. Гарамус, Д.К. Погорелый, К.М. Подурец "Исследование структурных аспектов формирования оптических свойств наносистемы GeO_2-Eu_2O_3-Ag", направлено в ФТТ (2009).
4. M.V.Avdeev, D.Bica, L.Vekas, V.L.Aksenov, A.V.Feoktystov, O.Marinica, L.Rosta, V.M.Garamus, R.Willumeit. Comparative structure analysis of non-polar organic ferrofluids stabilized by saturated mono-carboxylic acids. *J. Colloid Interface Sci*. 334 (2009) 37–41.
5. M.V.Avdeev, N.N.Rozhkova, V.L.Aksenov, V.M.Garamus, R.Willumeit, E.Osawa, Aggregate structure in concentrated liquid dispersions of ultrananocrystalline diamond by small-angle neutron scattering, *J. Phys. Chem. C* 113 (2009) 9473–9479.
6. V.L.Aksenov, Yu.N.Khaidukov, Yu.V.Nikitenko, "Peculiarities of magnetic states in Ferromagnet/Superconductor heterostructures due to proximity effects", subm. to Journal of Physics: Conference Series.
7. В.К. Игнатович, Ю.В. Никитенко, А.А. Фраерман, Прохождение поляризованных нейтронов через магнитные некомпланарные слоистые системы, ЖЭТФ, т. 138, вып. 1 (2010).
8. Е.В. Дубровин, Т.Н. Муругова, К.А. Мотовилов, Л.С. Ягужинский, И.В. Яминский. Применение технологии атомно-силовой микроскопии для структурного анализа внутренней мембраны митохондрий. Российские нанотехнологии, 4, №9-10, 2009, с. 66-68.
9. Yu. L. Raikher, V.I.Stepanov, S.V.Stolyar, V.P.Ladygina, D.A.Balaev, L.A. Ishchenko, M.Balasoiu, „Magnetic properties of biomineral nanoparticles produced by Klebsiella oxytoca bacteria", *Physics of Solid State,* Vol.52, No.2 (2010)277-284.
10. Н.Ю.Рябова, М.А.Киселёв, О.В.Найда, А.В.Забелин, С.Данте, Т.Хаусс, А.М.Балагуров "Нейтронное и синхротронное исследование структуры модельных липидных мембран *oral stratum corneum*", РСНЭ-НБИК (сборник тезисов), Москва, 16-20 ноября, 2009.
11. Ю. С. Ковалев, Н. В. Левкович, А. И. Куклин, П. Ю. Апель. Агрегация поверхностно-активных веществ в растворах, применяемых для травления треков, и ее возможное влияние на форму пор в трековых мембранах. Коллоидный журнал, 2009, том 71, №5, с. 616-622.
12. Ю.В.Лисичкин, А.Г.Новиков, Л.А.Сахарова, Структурно-динамические особенности воды в сверхкритическом состоянии. Препринт ФЭИ-3148, Обнинск, 2009, 36с.
13. В.В.Сумин, В.Г.Симкин, С.Г.Шеверев, М.В.Леонтиева-Смирнова, В.М.Чернов. Температурная зависимость параметра кристаллической решетки и фактора Дебая-Валлера стали ЭК-181. ФММ 2009, т. 108, с. 1-6.
14. Lokajicek T., Lukas P., Nikitin A.N., Papushkin I.V., Sumin V.V., Vasin R.N. Elastic properties of reactor graphite GR-280 and their anisotropy from neutron diffraction and ultrasonic measurements. 2010. Carbon, submitted.
15. Никитин А.Н., Почепцова О.А., Маттис З. Учет тепловых и транспортных свойств кристаллической соли при проектировании хранилищ радиоактивных отходов в галоидных формациях. Кристаллография, 2009, принята в печать.
16. Mosch, S.Nikolayev, D., Siegesmund, S. & O. Ewiak. 3D Modelling of quarry block size volumes. Bulletin of Engineering Geology and the Environment (submitted).
17. T. A. Lychagina, D.I. Nikolayev, F. Wagner "Using Individual Spectra Simulation for the Study of Pole Figures Errors," Texture, Stress, and Microstructure, Hindawi, vol. 2009 (2009), Article ID 237485, 10 pages, 2009. doi:10.1155/2009/237485; www.hindawi.com/journals/tsm/2009/237485.html.
18. В.Л. Аксёнов, Ю.В. Никитенко, патент на изобретение "Способ определения пространственного распределения магнитного момента в нанослое, № 2360234 от 27.06.09
19. Manoshin, S.A., Belushkin, A.V., Kulikov, S.A., Shabalin, E.P., Walther, K., Scheffzuek, C. & Zhuravlev, V.V. (2009): Optimization of a moderator-neutron guide system for diffractometers of beam line 7A of the IBR-2M reactor. *Nuclear Instruments and Methods in Physics A*: 608 (3), 447-453.

1.2. NEUTRON NUCLEAR PHYSICS

Introduction

In 2009, at the Frank Laboratory of Neutron Physics the first stage of the pulsed resonance neutron source IREN was put into operation. The parameters of this facility in the current configuration were determined; work to prepare and carry out experiments at IREN started. Also, instrument development activities on the preparation of experiments at the IBR-2M reactor were continued; investigations at the EG-5 accelerator were carried out. The greater part of fundamental and applied investigations in the field of neutron nuclear physics was carried out on neutron beams of nuclear research centers in Russia, Germany, Republic of Korea, China and France. The studies were conducted in the following traditional directions: investigations of time and spatial parity violation processes in neutron-nuclear interactions; studies of fission process; experimental and theoretical investigations of electromagnetic properties of the neutron and of its beta-decay; gamma-spectroscopy of neutron-nuclear interactions, atomic nucleus structure, obtaining of new data for reactor applications and for nuclear astrophysics; experiments with ultracold neutrons; applied research.

1. Development of the first stage of the IREN facility

In January 2009, the installation of the last section of the electron guide in the IREN target hall was completed and an accelerated electron beam was transported to the nonmultiplying neutron-producing target. During the year the work to adjust and develop various systems of the accelerator and target complex, to optimize operating modes of magnetic optical elements of the beam transportation system was carried out. Concurrently the accelerator operated for experiments on the extracted neutron beam and for applied research. By the end of 2009 the following parameters were achieved:

- average accelerated electron energy – 30 MeV;
- pulse current at the target – 3 A;
- pulse repetition rate – 50 Hz;
- integral neutron yield – $7.7 \cdot 10^{10}$ n/s.

Figure 1 presents experimentally measured neutron spectra on a 10 m flight path of the third experimental channel.

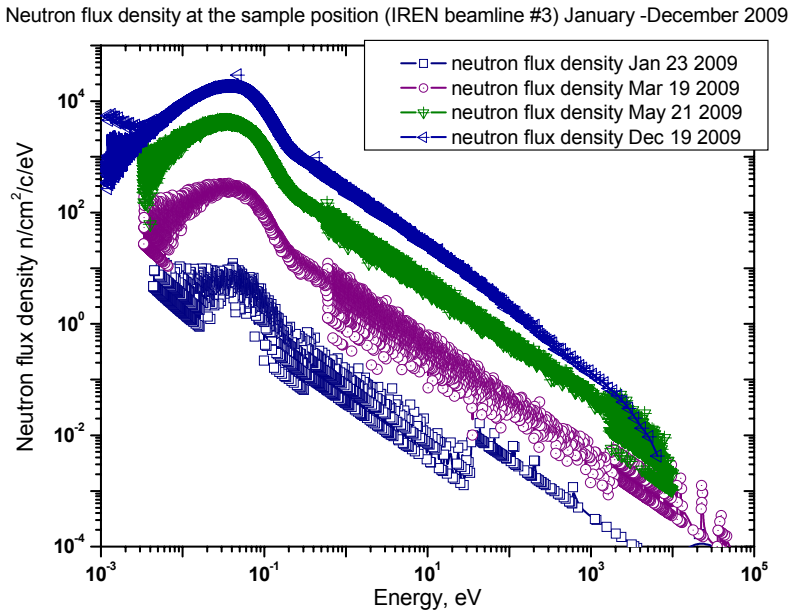

Fig. 1. Neutron flux density (measurements from January to December 2009)

In the process of development of the nonmultiplying target in 2007-2008 the calculations of the duration of a neutron pulse on the moderator surface were made for various ranges of neutron energies and the IREN energy resolution for the 10 m flight path (**Figs. 2** and **3**).

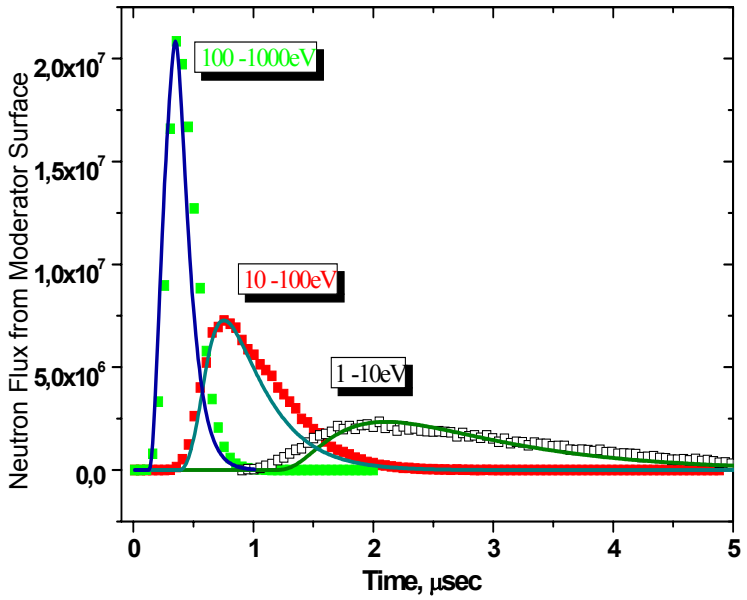

Fig. 2. The duration of a neutron pulse on the 5 cm-thick moderator surface for neutron energy ranges of 1-10 eV, 10-100 eV and 100-1000 eV. The electron pulse duration is 200 ns. Solid curves – analytical calculations, dots – MCNP calculations.

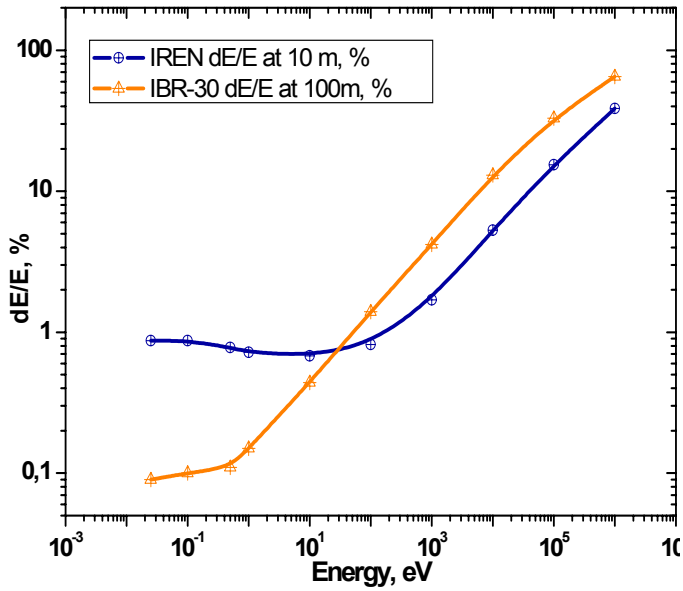

Fig. 3. The comparison of energy resolution of IBR-30 on the 100 m flight path and that of IREN on the 10 m flight path. Only energy resolution related to the fast neutron pulse duration and the influence of the moderator was taken into account.

An experimental estimate of the energy resolution was made in the experiments at IREN (see section "Experiments at IREN") and can be illustrated by comparing the time-of-flight spectra of gamma-quanta after neutron capture by ^{181}Ta nuclei.

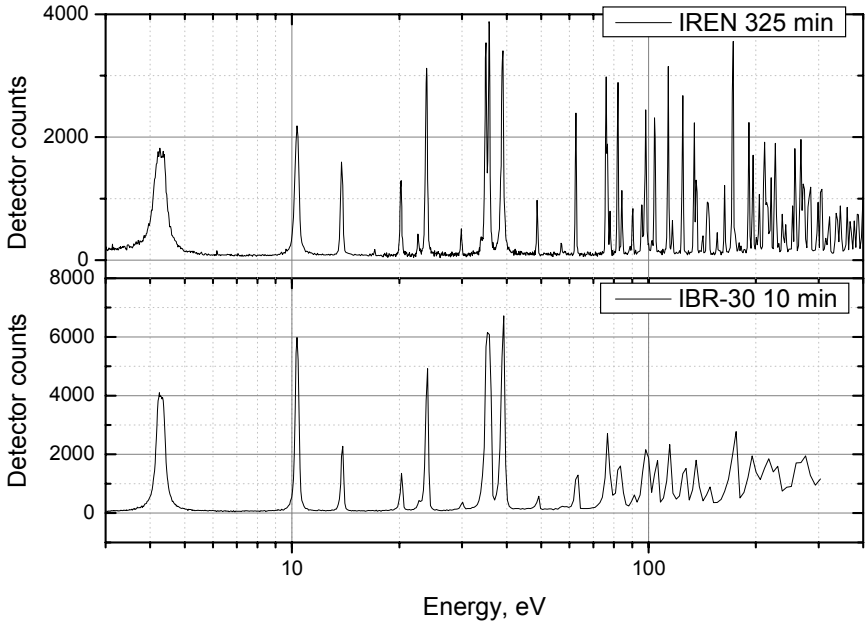

Fig. 4.

2. Experimental investigations

2.1 ***Experiments at IREN***

On the neutron beam of the IREN facility the measurements of the radiative neutron capture have been carried out. A liquid scintillator (n,γ)-detector with a volume of 250 l containing six independent sections served as a detector. The electronics makes it possible to organize a

coincidence mode of any multiplicity. Tantalum, silver and copper were used as targets in the first measurements. One of the tasks was to determine the neutron flux density in the experimental hall № 52 where the detector was located. **Figure 5** shows a part of the time-of-flight spectrum obtained using the (n,γ)-detector with a silver foil as a target. To determine the flux, we used the relation

$$\sum N = F(E)\varepsilon_\gamma \frac{\Gamma_\gamma}{\Gamma} \mathrm{A},$$

where $\sum N$ is the number of counts within the resonance area during the measurement, $F(E)$ is the number of neutrons incident on the whole target area during the measurement, ε_γ is the efficiency of detection of (n,γ)-reaction, Γ_γ and Γ are the radiative and total resonance width, respectively, A is the proportion of captured neutrons, which is determined as a function of resonance parameters, Γ_γ, Γ, A are the tabular parameters. The known resonance parameters and the measured resonance peak areas allowed us to determine the values

$$F(E)\varepsilon_\gamma = \frac{\sum N \cdot \Gamma}{\Gamma_\gamma \mathrm{A}}$$

for a number of resonances. Hence the values for the neutron flux density in bldg. 52 (L = 58 m) were obtained.

$$\phi(E) = \frac{0{,}22}{E^{0{,}9}} \text{ n/cm}^2\cdot\text{s}\cdot\text{eV}$$

The energy dependence of the flux of the form $E^{-0.9}$ is in good agreement with the calculations and similar measurements at IBR-30.

To make a more detailed evaluation of resolution in experiments at IREN at higher energies, the measurements with a copper target have been carried out. The measurements were performed with two time channel widths (1 μs and 259 ns) in the high energy neutron range. Good resolution of resonances can be seen in the energy range up to several keV (see **Fig. 6**).

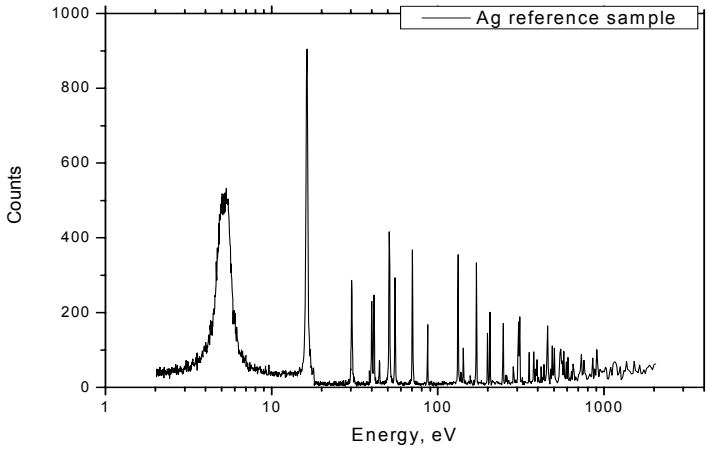

Fig. 5.

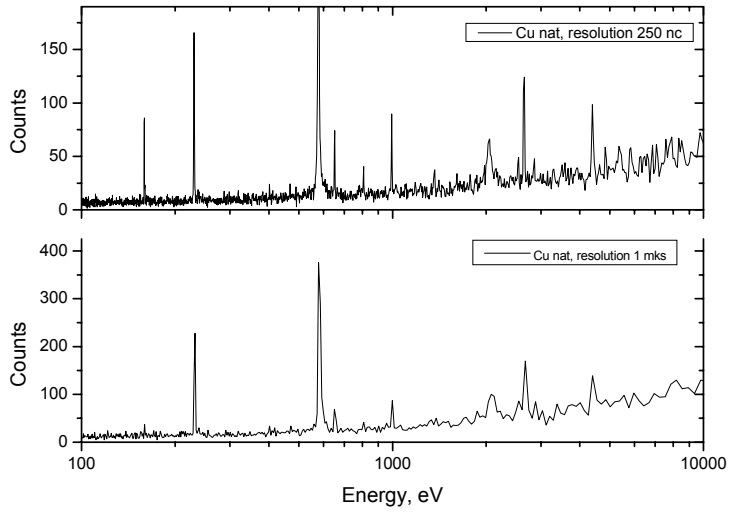

Fig. 6.

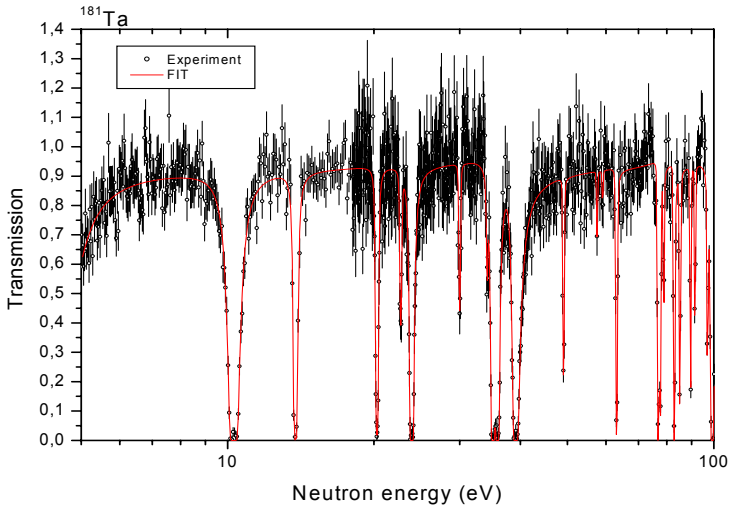

Fig. 7.

To comprehensively test the operation of the neutron source and the scintillation detector with γ-converter on a 60 m time-of-flight path, the measurement of neutron transmission through a ^{181}Ta 2 mm-thick sample has been conducted. Then the neutron transmission spectra in the range up to 450 eV were fitted using the R-matrix formalism to obtain the parameters of neutron resonances. The obtained values of the parameters for the known resonances are in good agreement with the tabular values. A part of the transmission spectrum from 5 up to 100 eV is presented in **Fig. 7**.

Thus, the possibility to significantly extend the energy range of neutron cross-section measurements as compared to IBR-30 has been experimentally demonstrated.

2.2 Measurement of P-odd asymmetry of γ-quantum emission in the $^{10}B(n,\alpha_1)^7Li^* \rightarrow ^7Li+\gamma$ reaction

The investigations of P-odd secondary particle emission asymmetry in the reactions of polarized cold neutrons and light nuclei of ^{6}Li and ^{10}B have been continued in an effort to study neutral weak currents in nucleon-nucleon interactions. At present, the results are as follows: the triton emission asymmetry in the $^6Li(n,\alpha)^3H$ reaction is $\alpha^{6Li}_{P-odd} = -(8.8 \pm 2.1)\cdot 10^{-8}$; the γ-ray emission asymmetry in the nuclear reaction $^{10}B(n,\alpha)^7Li^* \rightarrow \gamma \rightarrow ^7Li(g.s.)$ is $\alpha^{10B}_{P-odd} = +(0.8 \pm 3.9)\cdot 10^{-8}$. Using these values in the framework of the cluster model the weak neutral current constant was estimated to be $f_\pi^{6Li} \leq 1.1 \cdot 10^{-7}$ and $f_\pi^{10B} \leq 2.4 \cdot 10^{-7}$ (at 90 % confidence level). Both these values contradict "the best" DDH value $f_\pi^{DDH} = 4.6 \cdot 10^{-7}$.

In October-November, 2009, a new experiment to measure α^{10B}_{P-odd} was conducted. The 50-day measurement was carried out on the polarized cold neutron beam at ILL, Grenoble. The main difference between this experiment and the previous ones was the improved geometry: earlier a boron target had been right in the air in the neutron beam in front of the detectors, in the last experiment it was placed in the helium-filled neutron guide, which made it possible to reduce the background by 20% and allowed a two-fold accuracy improvement. A preliminary result of the basic experiment (without corrections for beam polarization and average cosine of emission angle) is $-(1.60\pm2.01)\cdot 10^{-8}$. A «zero»-experiment was performed as well: $-(1.01\pm1.25)\cdot 10^{-8}$. The treatment of the results is in progress.

2.3 Investigations of (n,p), (n,α) reactions

The investigations of the (n,p), (n,α) reactions induced by fast neutrons have been continued. The experiments are carried out at the Van de Graaf accelerator EG-5 in FLNP JINR (Dubna, Russia) and EG-4.5 of the Institute of Heavy Ion Physics at Peking University (Beijing, China) in collaboration with the University of Lodz (Poland), the National University of Mongolia (Ulaanbaatar, Mongolia) and the Oak Ridge National Laboratory (USA).

Data on neutron reactions with emission of charged particles induced by fast neutrons are of much interest both for creation of constructional materials for nuclear power engineering and for studying mechanisms of nuclear reactions and for determining the optical potential parameters.

The analysis of the available experimental data for ^{147}Sm, ^{143}Nd, ^{95}Mo isotopes shows that the greater part is given for thermal and resonance neutron energies, as well as for the range of E_n~14 MeV. At the same time there are scarcely any experimental data for the 1-7 MeV neutron energy range. As a result, there are significant discrepancies between the cross section estimates given by different nuclear data libraries.

Within the framework of joint investigations at the EG-4.5 accelerator of the Institute of Heavy Ion Physics of Peking University (Beijing, China) the measurements of the parameters of the ^{143}Nd(n,α)^{140}Ce and ^{95}Mo(n, α)^{92}Zr reactions at E_n=4.0, 5.0 and 6.0 MeV and the ^{147}Sm(n, α)^{144}Nd reaction at E_n=5.0 and 6.0 MeV have been carried out.

The energy spectra of charged particles have been obtained. The data treatment and theoretical calculations were completed in 2009. Our experimental data were compared with the available data, evaluations and model calculations (**Fig. 8, 9**). It should be pointed out that the analysis of new data on fast neutron cross sections was performed along with the analysis of the available data on these reactions induced by resonance neutrons.

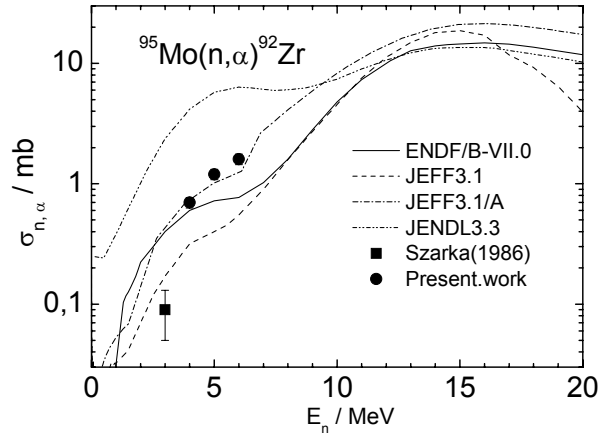

Fig. 8. Cross sections of ^{95}Mo(n, α)^{92}Zr reaction in comparison with the available data and calculations.

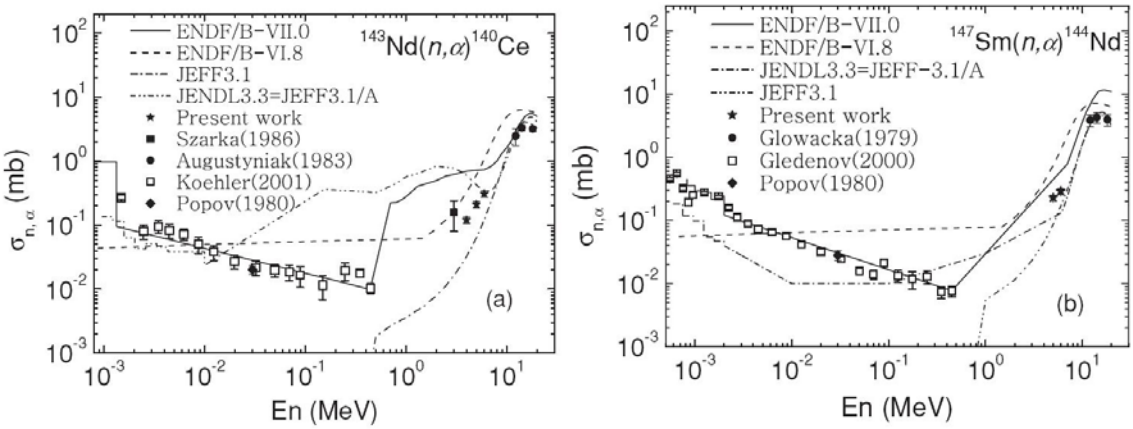

Fig. 9. Cross sections of ^{143}Nd(n, α)^{140}Ce and ^{147}Sm(n, α)^{144}Nd reactions in comparison with the available present-day data and calculations.

The measurement of the total cross section of the ^{67}Zn(n,α)^{64}Ni reaction at E_n = 6.0 MeV has been performed as well, which is a continuation of the studies of Zn isotopes (^{64}Zn(n,α)^{61}Ni reaction had been investigated earlier in the energy range of E_n=2.5÷6.0 MeV). The measurements are planned to be continued at other neutron energies. The cross section value is $\sigma_{n,\alpha}$ = 7.3±1.1 mb.

In October-November, 2009 the measurements of total cross sections and "forward/backward" ratios for the ^{149}Sm(n, α)^{146}Nd reaction started using ionization chambers.

2.4 A new experiment to observe the accelerating matter effect in neutron optics

An optical phenomenon consisting in a change in the wave frequency when it passes through a refractive sample moving with acceleration is referred to as the accelerating matter effect (AME). In accordance with the general principles, the energy of a quantum of radiation or the energy of a massive particle if we are dealing with the latter, also undergoes changes.

The existence of AME in neutron optics was demonstrated for the first time in 2005-2007 in the experiments made by the group from FLNP and the Institute of Laue Langevin (Grenoble, France). In these experiments a change in the energy of ultracold neutrons (UCN) passing through a sample moving with acceleration of several tens of m/s^2 was registered using the precision spectrometry methods. The change in energy was of the order of 10^{-10} eV.

Since up to the present AME has been observed only in one experiment, it was of fundamental importance to detect it by any other method. Such an experiment was carried out in 2009. Ultracold neutrons traversed a thin (2 mm) silicon sample undergoing harmonious spatial vibrations with a frequency of several tens of vibrations per second. The instantaneous acceleration

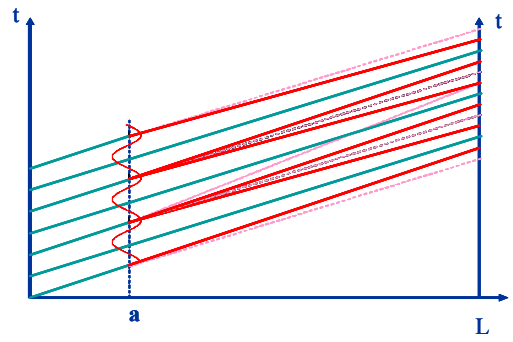

Fig. 10. A coordinate-time diagram illustrating a principle of weak focusing of neutrons in time. *A sample moving with acceleration, which is periodically dependent on time is positioned at point* ***a****. It changes the velocity of initially monochromatic neutrons in such a way that at point* ***L*** *(detector position) the neutron density changes periodically.*

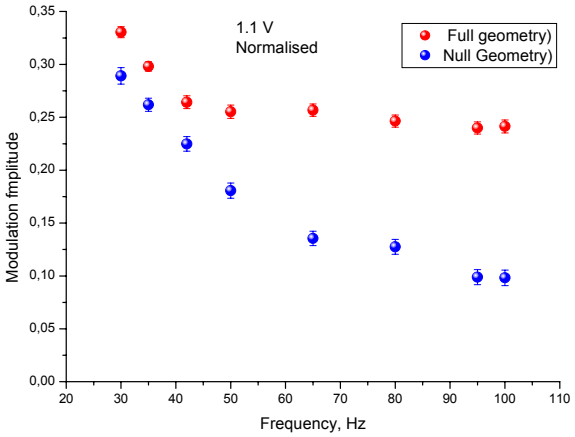

Fig. 11. The amplitude of counting-rate modulation with regard to the calibration of modulation depth depending on the frequency of sample vibrations. Red circles - 1 (AME effect + velocity effect). Blue circles - geometry 2 (only velocity effect).

of the sample amounted to 70 m/s^2. Owing to the accelerated-matter effect, the neutrons that passed through the moving sample periodically changed their energy and velocity. The neutron time of flight from the sample to the detector changed correspondingly.

Such periodic change in the time of flight resulted in the modulation of neutron counting rate as a consequence of weak time focusing of neutrons, which is illustrated in **Fig. 10**.

The problem, however, lay in the fact that at periodic vibrations of a sample not only its acceleration, but also its velocity underwent a change. A variation in the relative velocity of neutrons and the sample led to a change in the transparency of the latter, thereby modulating the flux.

Therefore the measurements were conducted in two geometries. In the first geometry the amplitude of counting-rate modulation was determined by two effects – the sought-for accelerated-matter effect and the systematic velocity effect. In the second geometry the flux was modulated only by the velocity effect. The measurements were carried out for a set of sample vibration frequencies, and the magnitude of the maximum acceleration $\mathbf{a}_{max} = \mathbf{A}\Omega^2$ remained constant ($\Omega = 2\pi\mathbf{f}$, $\mathbf{f}$ – vibration frequency). In addition, special experiments for calibration of modulation depth were performed for quantitative treatment of the results.

The results of the experiment are illustrated in **Fig. 11**. As can be seen, in the absence of AME (blue circles) the modulation amplitude is significantly less than that of the case when the modulation of the flux is determined by both effects. The difference in two geometries (see **Fig. 12**) characterizes the accelerated-matter effect. The quantitative treatment of the results of several measurements points to the agreement of the measured magnitude of the effect with the calculated value within the accuracy of 15 %.

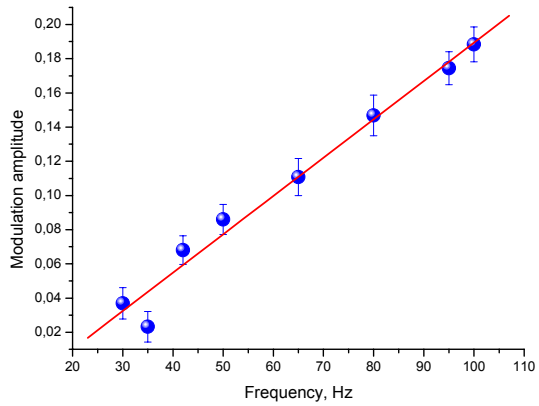

Fig. 12. Accelerated-matter effect as a function of sample oscillation frequency. Circles and a red line are the difference in measurements in two geometries and their linear fit.

Thus, the effect of accelerated matter has been detected by the new method sensitive to a change in the time of flight of UCN after their passage through an accelerated sample.

2.5 Investigations of nuclear structure

The work has been continued to accumulate and analyze the information on the parameters of different nuclei at excitation energies below their neutron binding energy.

The analysis of the published data on the intensities of two-quantum cascades following slow neutron capture within the framework of the technique developed in Dubna of model-free determination of excited level density and radiative strength functions of gamma-transitions has been made. The sources of errors are revealed and their possible values in the data on nuclear parameters of other groups are evaluated.

The re-analysis of the data on two-quantum cascades of thermal neutron capture in ^{95}Mo performed in FLNP has shown that also in this nucleus the level density has a pronounced step-like structure and the sum of radiative strength functions of dipole electric and magnetic transitions has a very clear-cut maximum in the region of levels of mainly collective type.

The parameters of approximation of the level density by the V.M. Strutinsky model and of strength functions by the semiphenomenological model proposed in Dubna do not contradict the analogous data for neighbouring even-even spherical nuclei. The difference in the nuclear parameters presented by the Prague group and the Norwegian collaboration has been completely explained by the errors in the used techniques of the analysis of experimental data.

The results of the re-analysis of the experimental data accumulated all over the world on the intensities of primary gamma-transitions with their averaging over many of the neutron resonances have been published. In all nuclei a step-like structure in the level density is observed. The comparison of its magnitude with the analogous data extracted from the intensities of cascades suggests possible overestimation of the level density from the (n,2γ) reaction. A part of this overestimation can be attributed to the scarcity of the experimental data obtained in FLNP on the dependence of strength functions of dipole gamma-transitions on the nuclear excitation energy (structure of wave functions of the levels connected by gamma-transition).

The necessity to obtain more precise information on the average distance between neutron resonances from the data available in the world (one of the sources of systematic errors in the determination of the level density in any technique existing in the world for determining this nuclear-physical parameter) has been revealed. And what is more important, the evidence for/against a significant change in the structure of neutron resonances with varying neutron energy or their neutron width is required. For this purpose a technique for determination of the most probable average value of neutron amplitude $A = \sqrt{\Gamma_n^o}$ and its most probable dispersion has been developed and is being tested. The results of such analysis are necessary for preliminary selection of targets and subsequent interpretation of results of the planned experiment at IREN to search for a

dependence of the intensity of total gamma-spectra on the structure of neutron resonances. The need for a test of this hypothesis follows from the results of the analysis of intensities of two-quantum cascades.

2.6 Work to prepare and carry out an experiment on the direct measurement of the neutron-neutron scattering cross section at the YAGUAR reactor (RFNC-VNIITF, Snezhinsk)

In 2009, studies of the possibilities to reduce the desorption of atoms from the surface of the nn-scattering chamber during the reactor pulse were carried out. An experimental stand comprising an evacuation system and a vacuum measurement system with the requisite electronics has been constructed. The stand makes it possible to produce a vacuum at a level of $\sim 7 \cdot 10^{-7}$ mbar, to model a pulsed change of vacuum in bulk (for a time less than milliseconds) in a range of $(10^{-7} \div 10^{-3})$ mbar and to detect this change. A great amount of work to study the possibilities of attaining an ultimate vacuum and the capabilities of the vacuum measurement system has been done. In 2010 it is planned to conduct measurements with the vacuum measurement system at the JAGUAR reactor.

A facility to study surface degassing processes under exposure to a proton beam has been designed. Studies of various types of surfaces at EG-5 are scheduled for the end of 2009 - 2010.

2.7 Work within the framework of investigations of interaction of neutrons with nanoparticles

On the cold neutron beam the concentration of hydrogen atoms in a diamond nanopowder before and after degassing, the total scattering cross-section for hydrogen (not removed by degassing) and its temperature dependence have been measured. The concentration was found using the measurement of relative flux intensity of characteristic γ-quanta in the n(p,d)γ reaction from the samples under study and a polyethylene sample.

It has been revealed that the amount of hydrogen in the nanopowder before and after degassing can be expressed by the ratios C_8H and $C_{15}H$, respectively. The total scattering cross-section for a hydrogen atom in this case is ~120 barn. The variation of this cross-section as the temperature changes from 500 K to 80 K does not exceed 3 %.

In addition, excitation spectra of hydrogen atoms in degassed and nondegassed samples have been obtained. The obtained results suggest that hydrogen removed from the powder by pumping and heating is in the form of water adsorbed on the surface of a sample. The hydrogen atoms, which are not removed from the powder by pumping and heating up to 150ºC, are chemically bonded to the sp3-hybridized carbon atom.

Thus, the cooling of a VCN trap with walls containing powder of diamond nanoparticles down to liquid nitrogen temperatures in order to suppress the channel of losses is inadvisable and unpractical. To increase the reflection probability it is necessary either to remove/replace hydrogen chemically bound to carbon or to cool the powder deeply down to liquid helium temperatures.

3. Theoretical investigations

3.1 On neutron surface waves

Earlier in the literature an assumption has been made that neutrons can exist as surface waves at interfaces between different media and this can explain the known anomaly in the UCN loss factor. For example, it has been stated that a surface neutron wave can exist on the surface of a film with a finite optical potential, which is deposited on a substrate with an infinite potential as shown in **Fig. 13**. However, from the usual Schrödinger equation

$$\left[\Delta + k_0^2 - u(\mathbf{r})\right]\psi(\mathbf{r}) = 0$$

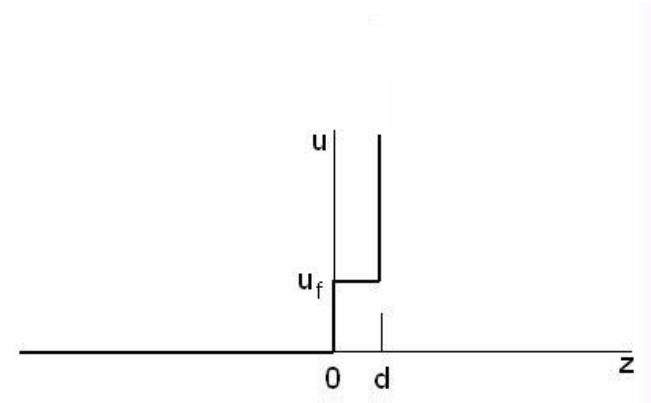

Fig. 13.

follows that a surface wave cannot satisfy the boundary conditions of the continuity of the wave function and its derivative so that the law of conservation of energy holds true. From the latter it follows that with no absorption (and it is absent in a vacuum) the wave vector of a particle must be strictly real. In the case of the potential shown in **Fig. 13**, there is a solution to the equation, but it does not satisfy the law of conservation of energy. The states similar to surface states can exist in films with a negative potential. In this case, however, the wave function of a neutron describes not a surface state but a bound one, which exponentially decreases with increasing distance from a film along the normal and corresponds to a free movement along the film.

The question has been investigated of how elastic and electromagnetic waves differ from neutron waves and why surface states can exist in the case of elastic and electromagnetic waves. The main difference is in the formulation of boundary conditions. In the case of neutron waves the boundary conditions follow from the Schrödinger equation, and for elastic and electromagnetic waves the boundary conditions are formulated basing on additional requirements: from the continuity of normal components of the stress tensor for elastic waves and from the necessity to satisfy the Maxwell equations for fields in the case of electromagnetic waves.

3.2 Limits on a nucleon-nucleon monopole-dipole coupling from spin relaxation of polarized ultracold neutrons in traps

In elementary particle physics a search has been on for a long time for a hypothetical pseudoscalar particle axion, which gives rise to a P- and T-odd monopole-dipole interaction $(\boldsymbol{\sigma}\mathbf{n})gV(r)$ between spinor particles and matter. Here $\boldsymbol{\sigma}$ is the vector of Pauli matrices, $\mathbf{n}=\mathbf{r}/r$ is the unit vector along the radius of the vector between a material particle and the axion, g is the dimensionless coupling constant, and $V(r)\propto\exp(-r/\lambda)$ is the function exponentially descending at a distance Λ. The search for axions have not met with success yet, and limits for g and λ values are set in laboratory experiments. The present work studies how an axion interaction affects the depolarization of ultracold neutrons at their reflection from the walls of storage traps under a weak external field. The results of the calculations have led to a new curve characterizing the limits of coexistence of g and λ.

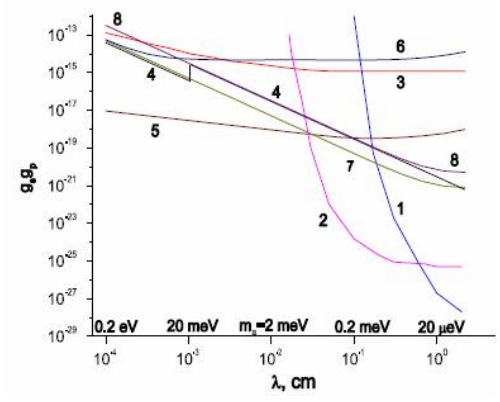

Fig. 14

This curve in **Fig. 14** is denoted by number 6 if the probability of neutron spin-flip is estimated to be 10^{-6} at an external field of 50 G and by number 7 when the probability of neutron spin-flip is 4×10^{-5} and the external field is 0.01 G. In both cases it was assumed that neutrons are stored in a trap with 1cm-thick walls and their velocity is 3 m/s. The parameter designated here as g is laid off on the vertical axis. The curves denoted by other numbers show the constraints obtained in other studies.

3.3 Investigation of neutron refraction and reflection effects in the medium with polarized nuclei

The effects of refraction and reflection of initially nonpolarized slow neutrons in the medium with polarized nuclei have been studied. In this medium a neutron beam is characterized by two refraction indices corresponding to neutron spin projections onto the nuclear polarization vector, which are (+1/2) and (-1/2). It has been shown that having regard to this fact at a nonzero angle of incidence on the interface between the medium with polarized nuclei and vacuum, a nonpolarized neutron beam is spatially split into two neutron beams completely polarized in opposite directions. The angle between the refracted polarized beams increases with decreasing neutron energy and when approaching grazing incidence. It has been demonstrated that under conditions of total internal reflection for one of the refraction indices the reflected and refracted neutrons are completely polarized in opposite directions along and against the nuclear polarization vector.

Numerical estimations for a liquid-hydrogen completely-polarized target have been performed. At an angle of incidence of 85° and neutron energy of 10^{-4} eV the angle between the refracted neutron beams completely polarized in opposite directions is of the order of 1.5° and in principle, the corresponding beams can be spatially split.

4. Applied research

4.1 Applied research at IREN

At the IREN facility the measurements of the flux of thermal, resonance and fast neutrons were carried out using the activation technique. Activated samples (Au, Cu, In, etc.) were placed on the moderator surface. Upon irradiation gamma-quantum spectra were obtained with the help of a semiconductor high-resolution detector.

The resulting values were as follows: resonance neutron flux — $2.5 \cdot 10^6$ n·cm^{-2}s^{-1}; thermal neutron flux $\Phi_{th} = 2.0 \cdot 10^7$ n·cm^{-2}s^{-1}; fast neutron flux $\Phi_{fast} = 2.0 \cdot 10^7$ n·cm^{-2}s^{-1}. These values are in reasonably good agreement with the results obtained on the extracted neutron beam.

In addition, irradiation of geological samples from Mongolia was done to determine rare metal content in the ore. The results of the measurements were forwarded to the Mongolian Academy of Sciences. These investigations will be continued.

In 2009, works using IREN as a bremsstrahlung source were started. The FLNP specialists have performed the calculations of gamma-quantum intensity and estimated the yield of ^{99}Mo and ^{117m}Sn isotopes that can be used for medical purposes (G.G.Bunatyan, V.N.Nikolenko, A.B.Popov, JINR Communications E6-2009-182). The results of the calculations are supported by the data obtained at the microtron. The prospect of enhancing the isotope yield with an increase in electron energy has been shown.

An experiment on irradiation of a number of elements by gamma-quanta has been carried out. In this experiment an electron beam struck a 2mm-thick tungsten target. Gamma-quanta produced as a result of electron deceleration hit Sn, Au, Cu, Zr samples. The aim of the experiment was to determine the gamma-quantum flux. The obtained data are in qualitative agreement with the data gained at the FLNR microtron. In addition, an attempt has been made to determine the yield of the isomeric state ^{117m}Sn ($T_{1/2}$=14 days), which is of interest for use in medicine. This work has been performed in cooperation with an employee of the research center NECSA of South Africa. The obtained data call for more thorough investigation.

4.2 Nuclear-physical analytical techniques based on charged particle beams

In 2009, nuclear-physical analytical techniques on the basis of charged particle beams of the EG-5 accelerator were used for important applied studies. In modern microelectronic and semiconductor devices rectifying and nonrectifying (ohmic) junctions are formed using metal films deposited on the surface of a semiconductor. After depositing a metal film on single-crystal silicon, thermal annealing is usually applied in the course of which both heterodiffusion processes and chemical reactions of interaction of metal atoms with silicon atoms resulting in the formation of chemical compounds (silicides, intermetallides) are possible in the film-semiconductor system. The physical and chemical structure of the phase interface formed in the process of annealing in many respects determines electric properties of metal-semiconductor junctions. It is suggested that refractory metals Nb and Ti be used for junctions of semiconductor devices.

As a result of the conducted investigation the phase formation processes and redistribution of components in the Nb-film – single-crystal-silicon system have been studied.

Thus, nondestructive nuclear-physical analytical techniques make it possible to gain rather important information on the chemical content and structure of nano-sized layers of the materials used in modern technological processes for production of semiconductor and microelectronic devices.

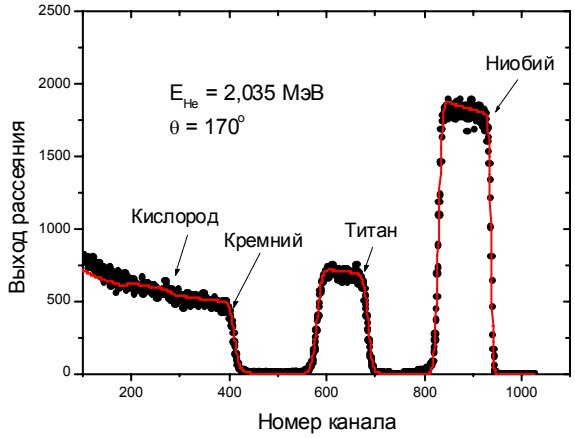

Fig. 15. *Rutherford backscattering spectrum of helium ions from a sample containing a niobium layer (170 nm) and a titanium layer (263 nm) on a silicon substrate.*

4.3 Analytical research at the IBR-2 reactor

Preparation for accreditation of the NAA Sector

In 2009, within the framework of the project for technical cooperation with IAEA «Harmonization of quality control systems according to ISO-17025 and international standards in nuclear analytical laboratories of the Russian Federation» in the NAA Sector the preparation for accreditation scheduled for 2011 after the IBR-2M reactor startup continued. The basic documentation package was prepared, major repairs of the chemical laboratory were made, a part of the equipment for the chemical laboratory and the radioanalytical complex REGATA at the IBR-2 reactor was purchased with IAEA financial support.

Development of the NAA Sector experimental base

IBR-2M Work to improve the spectrometric and service equipment of the REGATA facility and chemical laboratory continued. Natural radiation background measurements in different rooms of the Laboratory building including a bomb-proof shelter were conducted with the aim of finding a place for carrying out measurements of natural and anthropogenic radioactivity of samples.

IREN A design of pneumatic transport system for NAA studies at the IREN facility was developed by the FLNP Design Department in cooperation with «Development and Application Base in Physics (DAB-Physics)», Sofia, Bulgaria.

Biomonitoring

In 2009 a series of studies and publications in the framework of the international program «Heavy metal atmospheric deposition in Europe – estimations based on moss analysis» was completed. These studies cover some regions in Central Russia (Vergel et al., 2009) and South Urals (Pankratova et al., 2009), Belarus (Frontasyeva, Aleksiayenak et al., 2009), Bulgaria (Marinova et al., 2009), Slovakia (Meresova et al., 2009), Serbia (Krmar et al., 2009), Croatia (Spiric et al., 2009) as well as Mongolia (Baljinnyam et al., 2009) and Vietnam (Nguyen Viet et al., 2009). A large methodical study on calibration measurements of element content in atmospheric deposition and moss-transplants used for assessment of atmospheric deposition of heavy metals and other elements has been completed and published. The work has been performed in cooperation with the Institute of Physics in Belgrade, Serbia and the Norwegian University of Science and Technology in Trondheim (Anicic et al., 2009).

Ecosystem condition assessment

In 2009 the two-year RFBR-Romania project «Geochronology and retrospective study of pollution of unconsolidated sediments from oxygenated and anoxic territories of the Western Black Sea» was successfully completed. The results of the performed investigations were printed in seven publications in international peer-reviewed journals. A series of studies was submitted to the 2009 JINR Annual Competition in the category «Scientific-and-Technical and Applied Research» (Duliu, Frontasyeva, Culicov et al., 2009). The cooperation with Mongolian scientists was continued within the framework of the RFBR-Mongolia project «Development of a system of complex monitoring of heavy metals and radionuclides in Mongolia using nuclear-physical analytical techniques». The results were reported at several international conferences (e.g., N.Baljinnyam, Sh.Gerbish et al., 2009). N.Baljinnyam's study won the First Prize at the Young Scientist Contest for Best Research at the Central European International Conference ECOpole'09 in Piechowice, Poland. In 2009, the State Prize of the Government of the Republic of Macedonia was awarded to the research work conducted in the NAA sector in collaboration with the Macedonian and Slovenian specialists on the creation of the geochemical Atlas of one of environmentally unsound areas in Macedonia. In 2009 the data of the Atlas were published as an article in «Journal of Hazardous Materials» (Stafilov et al., 2009). In the framework of the joint study in cooperation with the Chair of Ecology of Dubna University the effect of motor transport on the chemical composition of soils in territories adjacent to highways has been investigated by the example of Dubna and Moscow (Sudnizyn et al., 2009).

Food products and human health

In 2009 at the reactor of the Moscow Engineering Physics Institute (Moscow) the analysis of food products in the framework of the NAA Sector-NESCA (South Africa) project «Comparative Nuclear Physics Analytical Studies of Consumption Effect of Food Products Grown in Some Industrial Regions of Russia and South Africa on Children's Health" continued. The results of bioaccumulation of chemical elements by vegetables on technogenically polluted territories of the Tula Region (Gorelov et al., 2009) are presented in the *Agrochemistry* journal. In 2009 in the framework of the IAEA coordination program «Impact of Toxic and Potentially Toxic Elements on Women of Reproductive Age in Developing Countries» work on multielement analysis of blood samples of specially selected patients from one of the industrial districts in Moscow carried out in cooperation with the RF State Medical University (Moscow), Analytical Center of Geological Institute, RAS and the I.M.Sechenov Moscow Medical Academy was completed and published in the journal «Public Health and Disease Prevention» (Ilchenko et al., 2009). These studies supported

the hypothesis of a correlation between concentrations of such toxic elements as lead, zinc and stibium with the body mass index of examined patients.

Biotechnologies

Work in the field of biotechnological methods of removing toxic elements (mercury, chromium, etc.) from the environment is carried out by the NAA Sector in collaboration with E.Andronikashvili Institute of Physics (Tbilisi, Georgia) and I.Chavchavadze State University (Tbilisi, Georgia). New results on the use of natural bacterial strains extracted from basalt rock to reduce toxic chromium (VI) to nontoxic chromium (III) were published in 2009. The element composition of a series of *Arthrobacter oxidans* samples under the complex action of chromium and mercury was determined by neutron activation at the research reactor at the Delft University of Technology (Netherlands). The preliminary results were reported in December, 2009 at the International Conference BioMicroWorld'2009 (Lisbon, Portugal). In 2009 work to master the techniques of production and detection of nanoparticles of gold, silver and cadmium sulfide in biomaterials started.

Materials science

Synthesis of fine-crystalline diamonds

In cooperation with the specialists from the Institute of Solid State and Semiconductor Physics of NASB (Minsk, Belarus) a chapter of the book «Diamond and Related Materials» (USA) devoted to the investigation of the behavior of defects in fine-crystalline diamonds under neutron irradiation in the presence of catalysts (Dutov et al., 2009) has been prepared and submitted for publication. A preparatory stage of work within the framework of the project of 2009-2010 to study the role of trace impurities in the process of synthesis of boron nitride crystals has been carried out.

Radioecology

The method of moss-biomonitors was applied in Belarus for the first time to estimate atmospheric deposition of radioactive nuclides 20 years after the Chernobyl accident. The measurements of long-lived radioactive nuclides – nuclear fuel fission products – were performed together with Slovakian specialists in the Low Background Laboratory of Bratislava University in 2008-2009. A part of the collected samples was analyzed by NECSA (South Africa) specialists. It has been shown that ^{137}Cs activity levels in mosses collected in the territory of the Gomel Region are 4 times higher than the background level. An increased content of ^{210}Pb was also noted. The results were presented at the 5th International Workshop on Biomonitoring of Atmospheric Pollution (BioMAP-5) in Argentine (Frontasyeva, Aleksiayenak et al., 2009).

Training

On the basis of the REGATA facility, training courses were organized for senior-year students of the University of Dubna and for students of International Summer Schools held by the JINR University Center (from Bulgaria, Czech Republic, Slovakia in July and from the Republic of South Africa in September-October, from Egypt in October-November). During the reported period two term papers, one bachelor's degree paper and one master's degree paper were performed in the NAA Sector. A Reference Manual on NAA for training courses at the REGATA facility (Frontasyeva, 2009) has been prepared.

1.2. НЕЙТРОННАЯ ЯДЕРНАЯ ФИЗИКА

Введение

В 2009 в ЛНФ ОИЯИ была введена в строй первая очередь импульсного источника резонансных нейтронов ИРЕН. Определены параметры этой установки в текущей конфигурации, начались работы по подготовке и проведению экспериментов на ИРЕН. Также продолжились методические работы по подготовке экспериментов на реакторе ИБР-2М, велись исследования на ускорителе ЭГ-5. Основная часть фундаментальных и прикладных исследований в области нейтронной ядерной физики проводилась на нейтронных пучках ядерных центров России, Германии, Республики Корея, Китая, Франции. Работы велись в традиционных направлениях: изучение процессов нарушения пространственной и временной четности при взаимодействии нейтронов с ядрами; изучение процесса деления; экспериментальное и теоретическое исследование электромагнитных свойств нейтрона и его бета-распада; гамма-спектроскопия нейтронно-ядерных взаимодействий; структура атомного ядра; получение новых данных для реакторных приложений и для ядерной астрофизики; эксперименты с ультрахолодными нейтронами; прикладные исследования.

1. Развитие первой очереди установки ИРЕН

В январе 2009 года был завершен монтаж последнего участка электроновода в мишенном зале установки ИРЕН и осуществлена проводка пучка ускоренных электронов до неразмножающей нейтронопроизводящей мишени. В течение года проводились работы по наладке и развитию отдельных систем ускорителя и мишенного комплекса, оптимизации режимов работы магнитооптических элементов системы транспортировки пучка. Параллельно осуществлялась работа ускорителя на нейтронную мишень для экспериментов на выведенном нейтронном пучке и прикладных исследований. К концу 2009 года были достигнуты следующие параметры:

- Средняя энергия ускоренных электронов – 30 МэВ;
- Импульсный ток на мишени – 3 А;
- Частота повторения импульсов – 50 Гц;
- Интегральный выход нейтронов – $7{,}7 \cdot 10^{10}$ н/с;

На рисунке 1 показаны экспериментально измеренные спектры нейтронов на пролетной базе 10 метров третьего экспериментального канала.

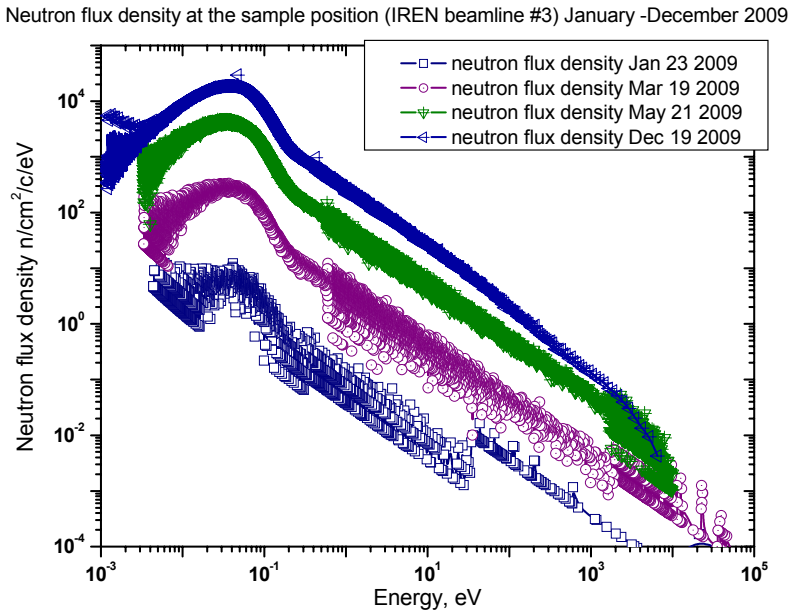

Рис. 1: спектральная плотность потока нейтронов (измерения в период январь – декабрь 2009г.)

При разработке нейтронопроизводящей неразмножающей мишени в 2007-2008 г.г. были выполнены расчеты длительности нейтронного импульса на поверхности замедлителя для разных диапазонов энергий нейтронов и энергетического разрешения ИРЕН для пролетной базы 10 метров (рисунки 2 и 3).

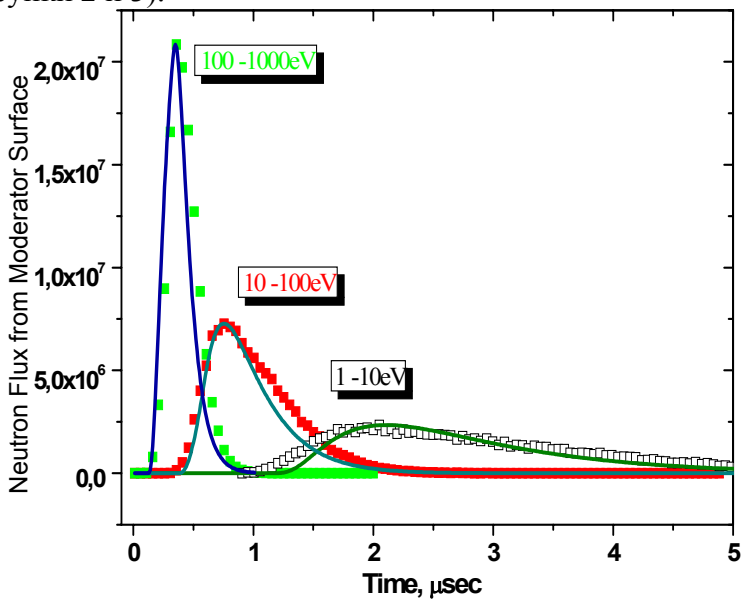

Рис. 2: Длительность импульса нейтронов на поверхности замедлителя толщиной 5 см для диапазонов энергии нейтронов 1-10 эВ, 10-100 эВ и 100-1000 эВ. Длительность импульса электронов 200 нс. Сплошные кривые – аналитический расчет, точки – расчет MCNP.

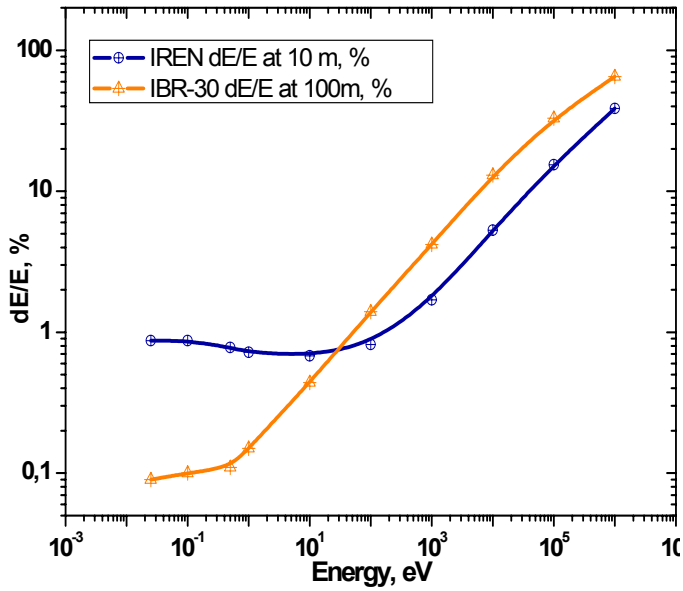

Рис. 3: Сравнение энергетического разрешения ИБР-30 на пролетной базе 100 метров и ИРЕН на пролетной базе 10 метров. Учтено только энергетическое разрешение, связанное с длительностью импульса быстрых нейтронов и влиянием замедлителя.

Экспериментальная оценка энергетического разрешения была выполнена в экспериментах на ИРЕН (см. раздел «Эксперименты на ИРЕН») и может быть проиллюстрирована сравнением времяпролетных спектров гамма-квантов после захвата нейтронов ядрами ^{181}Ta (рисунок 4).

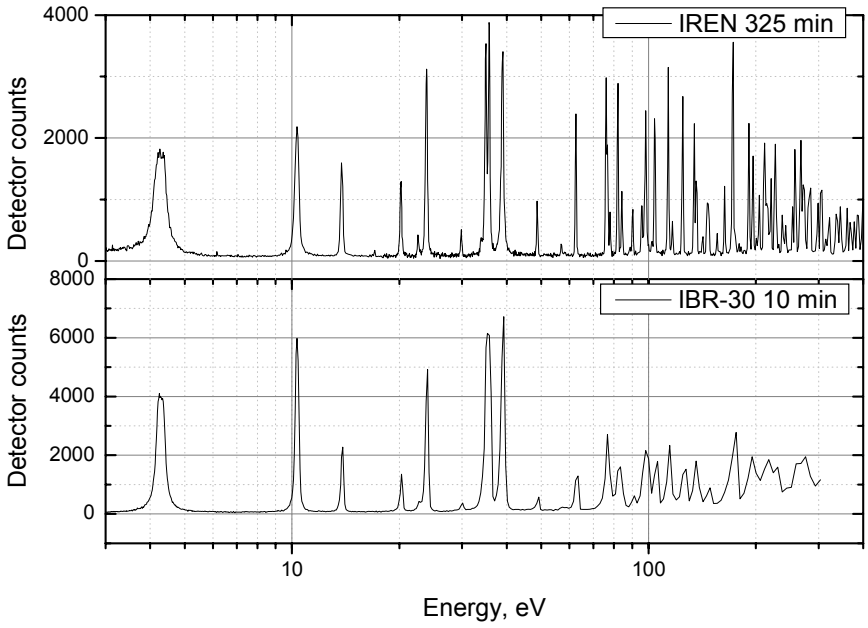

Рис. 4

2. Экспериментальные исследования

2.1 Эксперименты на ИРЕН.

На пучке нейтронов источника ИРЕН проведены измерения радиационного захвата нейтронов. Детектором служил жидкостный сцинтиллятор (n,γ) – детектор объемом 250 литров, содержащий шесть независимых секций. Регистрирующая электроника позволяет организовывать режим совпадений любой кратности. В качестве мишеней в первых измерениях были использованы тантал, серебро и медь. Одной из задач было определение плотности потока нейтронов в экспериментальном павильоне № 52, где располагался детектор. На Рис. 5 показан участок спектра по времени пролета, снятый (n,γ) - детектором с серебряной фольгой в качестве мишени. Для определения потока использовалось соотношение

$$\sum N = F(E)\varepsilon_\gamma \frac{\Gamma_\gamma}{\Gamma} \mathrm{A}$$

Здесь $\sum N$ -число отсчетов по площади резонанса за время измерения, $F(E)$- число нейтронов, падавших на всю площадь мишени за время измерения, ε_γ - эффективность регистрации (n,γ) – реакции, Γ_γ и Г - радиационная и полная ширина резонанса, А – доля захваченных нейтронов, определяемая как функция параметров резонанса, Γ_γ, Г, А – табл. параметры.

Известные параметры резонансов и полученные в измерении площади резонансных пиков позволили определить величины

$$F(E)\varepsilon_\gamma = \frac{\sum N \cdot \Gamma}{\Gamma_\gamma \mathrm{A}}$$

Для ряда резонансов. Отсюда были получены значения плотности потока нейтронов в зд. 52 (L=58м).

$$\phi(E) = \frac{0{,}22}{E^{0{,}9}} \text{ н/см}^2\cdot\text{сек}\cdot\text{эВ}$$

Энергетическая зависимость потока вида $E^{-0,9}$ хорошо согласуется с расчетами и аналогичными измерениями на ИБР-30.

Для более детальной оценки разрешающей способности в экспериментах на ИРЕН при более высокой энергии были проведены измерения с медной мишенью. Измерения были выполнены с двумя ширинами временных каналов в области высоких энергий нейтронов(1 мкс и 250 нс). Видно хорошее разрешение резонансов в области энергии до нескольких кэВ (см. Рис. 6).

Для комплексной проверки работы нейтронного источника и сцинтилляционного детектора с γ-конвертером на времяпролетной базе 60 м, было выполнено измерение пропускания нейтронов через образец ^{181}Ta толщиной 2 мм. Затем спектры нейтронной трансмисси в диапазоне до 450 эВ были профитированы с помощью R-матричного формализма с целью получения параметров нейтронных резонансов. Полученные значения параметров известных резонансов хорошо соответствуют табличным значениям. Участок трансмиссионного спектра от 5 до 100 эВ представлен на Рис. 7. Таким образом, экспериментально продемонстрирована возможность значительного расширения энергетического диапазона измерений нейтронных сечений по сравнению с ИБР-30.

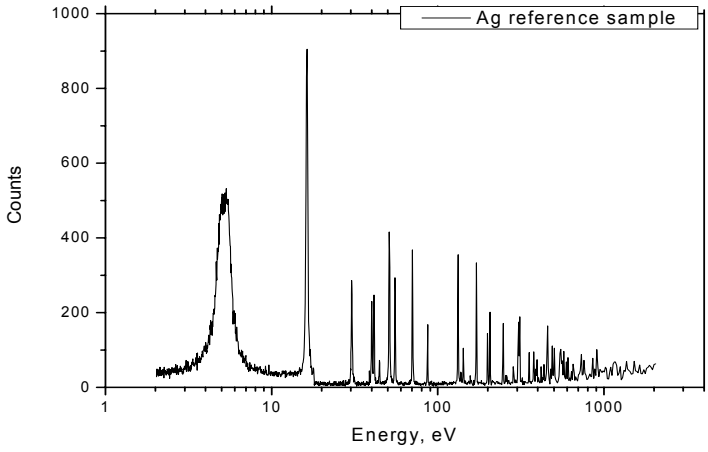

Рис. 5

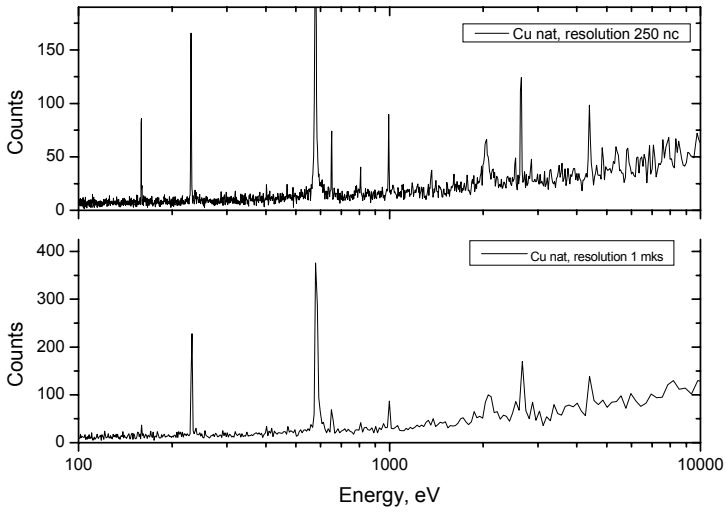

Рис. 6

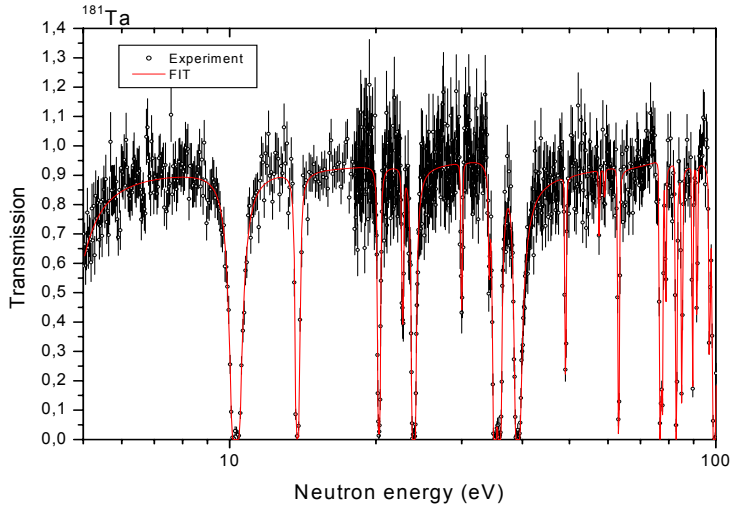

Рис. 7

2.2 Измерение P-нечетной асимметрии вылета γ-квантов реакции $^{10}B(n,\alpha_1)^7Li^* \rightarrow ^7Li+\gamma$

Были продолжены исследования P-нечетной асимметрии эмиссии вторичных частиц в реакциях с поляризованными холодными нейтронами на легких ядрах ^{6}Li и ^{10}B с целью изучения нейтрального слабого тока в нуклон-нуклонном взаимодействии. Результаты на текущий: Асимметрия вылета тритонов в реакции $^6Li(n,\alpha)^3H$ $\alpha^{6Li}_{P-odd} = -(8.8 \pm 2.1) \cdot 10^{-8}$; асимметрия вылета гамма-квантов в ядерной реакции $^{10}B(n,\alpha)^7Li^* \rightarrow \gamma \rightarrow ^7Li(g.s.)$ $\alpha^{10B}_{P-odd} =$

+(0.8±3.9)·10^{-8}. С использованием этих величин в рамках кластерной модели была извлечена константа слабого нейтрального тока: $f_\pi^{6Li} \leq 1.1 \cdot 10^{-7}$ and $f_\pi^{10B} \leq 2.4 \cdot 10^{-7}$ (90% ур.достоверности). Оба этих результата противоречат «лучшему» значению DDH $f_\pi^{DDH} = 4.6 \cdot 10^{-7}$.

В октябре-ноябре 2009 г. был проведен новый эксперимент по измерению α^{10B}_{P-odd}. 50-суточное измерение выполнено на пучке холодных поляризованных нейтронов реактора ИЛЛ, Гренобль. Основным отличием этого эксперимента от предыдущих было улучшение геометрии: если ранее борная мишень устанавливалась на нейтронном пучке перед детекторами прямо в воздухе, сейчас помещалась в заполненный гелием нейтроновод. Это позволило на 20 процентов снизить общий фон и улучшить вдвое точность. Предварительные результаты основного эксперимента (без поправок на поляризацию пучка и средний косинус угла вылета): −(1.60±2.01)·10^{-8}. Проведен также «нуль»-эксперимент: −(1.01±1.25)·10^{-8}. Результаты обрабатываются.

2.3 Исследования реакций (n,p), (n,альфа)

Продолжено изучение реакций (n,p), (n,альфа) на быстрых нейтронах. Эксперименты проводятся на ускорителях Ван-де-Граафа ЭГ-5 в Лаборатории нейтронной физики ОИЯИ и ЭГ-4,5 Института физики тяжелых ионов Пекинского университета совместно с Пекинским университетом при участии сотрудников Лодзинского (Польша) и Монгольского национального университетов и Ок-Риджской национальной лаборатории, США.

Данные о реакциях с вылетом заряженных частиц, вызванных быстрыми нейтронами, представляют значительный интерес как при создании конструкционных материалов для ядерной энергетики, так и при изучении механизмов ядерных реакций и определении параметров оптического потенциала.

Анализ существующих экспериментальных данных для изотопов ^{147}Sm, ^{143}Nd, ^{95}Mo показывает, что большая часть представлена для тепловых и резонансных энергий нейтронов, а так же в области E_n~14 МэВ. В то же время в области энергий нейтронов 1-7 МэВ данных практически нет. Результатом этого факта является большое расхождение между оценками сечений, приводимыми различными библиотеками ядерных данных.

В рамках программы совместных исследований на ускорителе ЭГ-4.5 Института физики тяжелых ионов при Пекинском университете (Китай) были проведены измерения реакций ^{143}Nd(n,α)^{140}Ce и ^{95}Mo(n, α)^{92}Zr при энергиях нейтронов E_n=4.0, 5.0 и 6.0 МэВ, реакции ^{147}Sm(n, α)^{144}Nd при E_n=5.0 и 6.0 МэВ. Получены энергетические спектры заряженных частиц. Обработка данных и теоретические расчеты были закончены в 2009 г. Были проведены сравнения полученных нами экспериментальных данных с существующими данными, оценками и модельными расчетами (**Рис. 8, 9**). Необходимо отметить, что анализ новых данных о сечениях на быстрых нейтронах проводился совместно с имеющимися данными по этим реакциям на резонансных нейтронах.

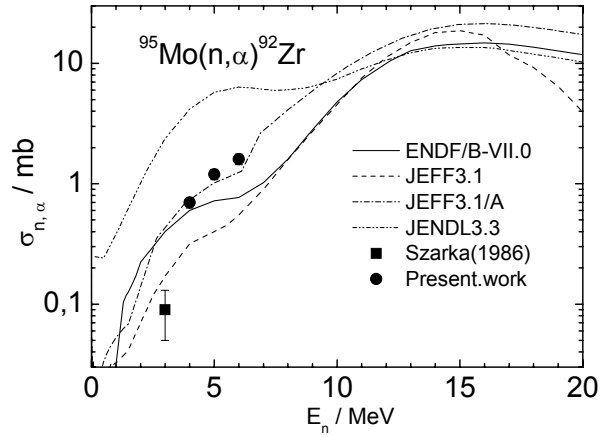

Рис. 8 Сечения реакции ^{95}Mo(n, α)^{92}Zr в сравнении с существующими данными и оценками

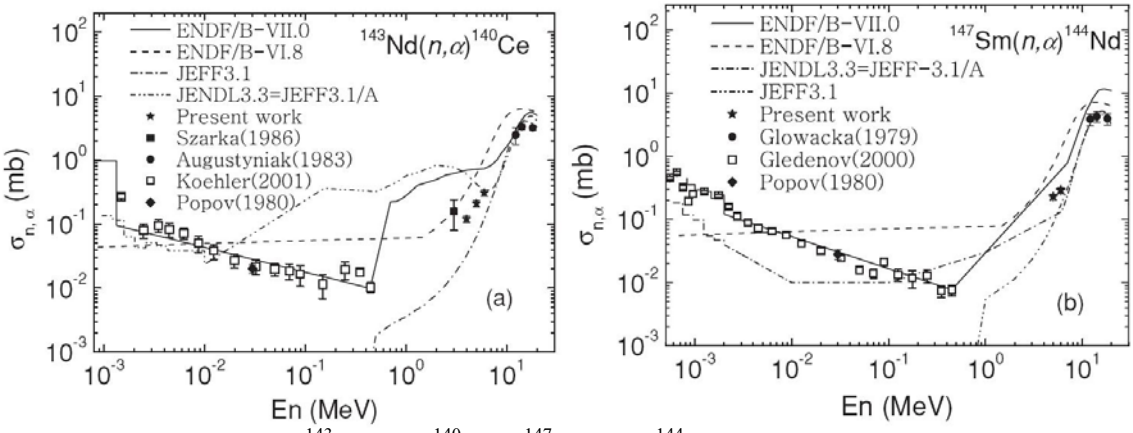

Рис. 9. Сечения реакций ^{143}Nd(n, α)^{140}Ce и ^{147}Sm(n, α)^{144}Nd в сравнении с существующими на сегодняшний день данными и оценками

Также было проведено измерение полного сечения реакции ^{67}Zn(n,α)^{64}Ni при E_n =6.0 МэВ, что является продолжением работ по исследованию изотопов Zn (исследования реакции ^{64}Zn(n,α)^{61}Ni проведены ранее в области энергий E_n=2.5÷6.0 МэВ). Измерения планируется продолжить при других энергиях нейтронов. Значение сечения $\sigma_{n,\alpha}$ = 7.3±1.1 мб.

В октябре-ноябре 2009 г. с использованием ионизационных камер начаты измерения полных сечений и соотношения «вперед/назад» для реакции ^{149}Sm(n, α)^{146}Nd.

2.4 Новый эксперимент по наблюдению эффекта ускоряющегося вещества в нейтронной оптике.

Эффектом ускоряющегося вещества (ЭУВ) называют оптическое явление, состоящее в изменении частоты волны при прохождении через преломляющий образец, движущийся с ускорением. В соответствии с общими принципами при этом изменяется и энергия кванта излучения или энергия массивной частицы, если речь идет о последней.

Существование ЭУВ в нейтронной оптике было впервые продемонстрировано в 2005-2077гг. в экспериментах группы ЛНФ и Института Лауэ-Ланжевена (Гренобль, Франция) В этих работах методами прецизионной спектрометрии регистрировалось изменение энергии ультрахолодных нейтронов (УХН) прошедших через образец, движущийся с ускорением несколько десятков м/с^2. Изменение энергии составляло при этом величину порядка 10^{-10} эВ.

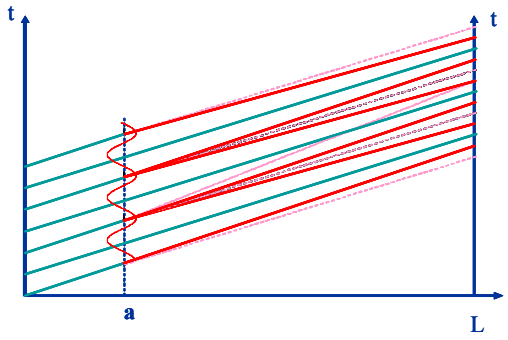

Рис. 10. Координатно-временная схема, иллюстрирующая принцип слабой фокусировки нейтронов во времени**.** *В точке а расположено образец, движущийся с ускорением, периодически зависящим от времени. Он, изменяет скорость изначально монохроматических нейтронов таким образом, что в точке расположения детектора L, плотность нейтронов периодически изменяется.*

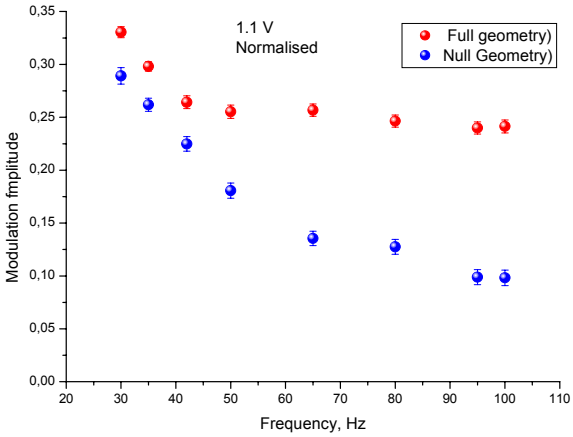

Рис. 11. Амплитуда модуляции скорости счета после учета калибровки глубины модуляции в зависимости от частоты колебания образца. Красные точки - 1 (эффект ЭУВ + скоростной эффект). Синие точки – геометрия 2 (только скоростной эффект)

Поскольку ЭУВ наблюдался до настоящего времени только в одном эксперименте, то представлялось принципиально важным зарегистрировать его каким-либо иным методом. Такой новый эксперимент и был поставлен в 2009г. Ультрахолодные нейтроны проходили через тонкий (2мм) кремниевый образец, совершавший гармоническое колебание в пространстве с частотой несколько десятков колебаний в секунду. Мгновенное ускорение образца достигало величины 70 м/с^2. Вследствие эффекта ускоряющегося вещества, нейтроны, прошедшие через движущийся таким образом образец периодически меняли свою энергию и скорость. Соответственно, изменялось и время пролета нейтронов от образца до детектора.

Такое периодическое изменение времени пролета приводило к модуляции скорости счета нейтронов вследствие слабой временной фокусировки нейтронов, что иллюстрируется рисунком 10.

Проблема, однако, состояла в том, что при периодическом колебании образца менялось не только его ускорение, но и скорость. Вследствие изменения относительной скорости нейтронов и образца прозрачность последнего менялась, что также приводило к модуляции потока.

Поэтому измерения велись в двух геометриях. В первой, амплитуда модуляции скорости счета определялась двумя эффектами – искомым эффектом ускоряющегося вещества и систематическим скоростным эффектом. Во второй геометрии поток модулировался только скоростным эффектом. Измерения проводились для набора частот колебания образца, причем величина максимального ускорения $\mathbf{a_{max}} = \mathbf{A}\Omega^2$ оставалась постоянной ($\Omega = 2\pi\mathbf{f}$, $\mathbf{f}$ – частота колебания). Кроме того, для количественной обработки результатов проводилась специальные эксперименты для калибровки глубины модуляции.

Результаты эксперимента иллюстрируются рисунком 11. Видно, что в отсутствии ЭУВ (синие точки) амплитуда модуляции существенно меньше, чем в случае, когда модуляция потока определяется обоими эффектами. Разность измерений в двух геометриях (см. рис.12) характеризует сам эффект ускоряющегося вещества. Количественная обработка результатов

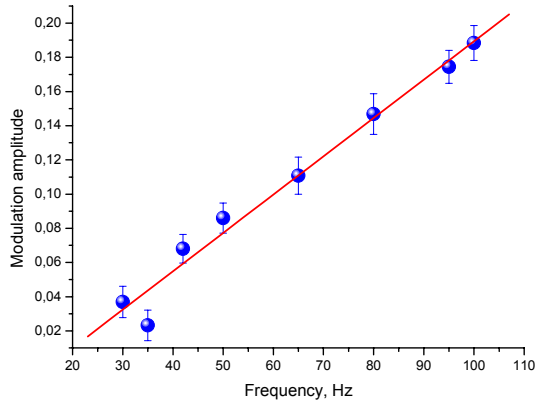

Рис. 12. Эффект ускоряющегося вещества в зависимости от частоты осцилляции образца. Точки и красная прямая – разность измерений в двух геометриях и их линейный фит.

нескольких измерений свидетельствует о согласии измеренной величины эффекта с расчетной в пределах точности 15%.

Таким образом, эффект ускоряющегося вещества был зарегистрирован новым методом, чувствительным к изменению времени пролета УХН после их прохождения через ускоряющийся образец.

2.5 Исследования структуры ядра.

Продолжается работа по накоплению и анализу информации о параметрах различных ядер при энергиях возбуждения ниже энергии связи нейтрона в них.

Выполняется анализ опубликованных данных по интенсивностям двухквантовых каскадов при захвате медленных нейтронов в рамках разработанной в Дубне методики безмодельного определения плотности возбужденных уровней и радиационных силовых функций связывающих их гамма-переходов. При этом выявляются источники ошибок и оценивается их возможная величина в данных по ядерным параметрам других групп.

Выполненный в ЛНФ реанализ данных по двухквантовым каскадам при захвате тепловых нейтронов в ^{95}Mo показал, что и в этом ядре плотность уровней имеет ярко выраженную ступенчатую структуру, а сумма радиационных силовых функций дипольных электрических и магнитных переходов имеет очень ярко выраженный максимум в области уровней преимущественно коллективного типа.

Параметры аппроксимации плотности уровней моделью В М Струтинского и силовых функций - предложенной в Дубне полуфеноменологической моделью не противоречат аналогичным данным для соседних четно-четных сферических ядер. Различие параметров ядра, представляемых пражской группой и норвежской коллаборацией полностью объяснено ошибками в используемых ими методиках анализа данных эксперимента.

Опубликованы результаты реанализа накопленных во всем мире экспериментальных данных по интенсивностям первичных гамма-переходов с их усреднением по многим нейтронным резонансам. Во всех ядрах наблюдается ступенчатая структура в плотности уровней. При этом сопоставление ее величины с аналогичными данными, извлеченными из интенсивностей каскадов, указывает на возможное завышение плотности уровней из реакции (n,2γ). Часть этого завышения может быть отнесена на недостаточность полученных в ЛНФ экспериментальных данных о зависимости силовых функций дипольных гамма-переходов от энергии возбуждения ядра (структуры волновых функций уровней, связываемых гамма-переходом).

Выявлена необходимость в получении из имеющихся в мире данных по параметрам нейтронных резонансов более точной информации о среднем расстоянии между ними (один из источников систематической ошибки определения плотности уровней в любой

существующей в мире методике определения этого ядерно-физического параметра). И, что более существенно, требуется доказательство наличия/отсутствия существенного изменения структуры нейтронных резонансов с изменением энергии нейтронов или их нейтронной ширины. Для этой цели разработана и тестируется методика определения наиболее вероятного среднего значения нейтронной амплитуды $A = \sqrt{\Gamma_n^o}$ и ее наиболее вероятной дисперсии. Результаты такого анализа необходимы для предварительного выбора мишеней и последующей интерпретации результатов предполагаемого эксперимента на ИРЕН по поиску зависимости интенсивности полных гамма-спектров от структуры нейтронных резонансов. Необходимость проверки и такой гипотезы следует из результатов анализа интенсивностей двухквантовых каскадов.

2.6 Работы в рамках подготовки и проведения эксперимента по прямому измерению сечения рассеяния нейтрона на нейтроне на реакторе ЯГУАР (РФЯЦ-ВНИИТФ, г.Снежинск)

В 2009 году были проведены работы связанные с исследованием возможности уменьшения десорбции атомов с поверхности камеры nn-рассеяния в момент импульса реактора. Был изготовлен экспериментальный стенд, включающий систему откачки и систему измерения вакуума с необходимой электроникой. Стенд позволяет получать вакуум на уровне $\sim 7 \cdot 10^{-7}$ мбар, моделировать импульсное изменение вакуума в объёме (за времена менее миллисекунды) в диапазоне ($10^{-7} \div 10^{-3}$) мбар и регистрировать это изменение вакуума. Проведём большой объём работы по изучению возможностей достижения предельного вакуума и возможностей системы регистрации изменения давления. В 2010 году планируется провести измерения с созданной системой регистрации вакуума на реакторе ЯГУАР.

Разработана установка для исследования процессов дегазации поверхности под действием пучка протонов. Исследования различных типов поверхностей планируется провести на ЭГ-5 в конце 2009 – 2010 году.

2.7 Работы в рамках исследования взаимодействия нейтронов с наночастицами.

На пучке холодных нейтронов были измерены измерены концентрация атомов водорода в алмазном нанопорошке до и после обезгаживания, полное сечение рассеяния на водороде, оставшемся после обезгаживания и его температурная зависимость. Концентрация измерялась по измерению относительной интенсивности потока характеристических гамма квантов n(p,d)γ реакции от исследуемых образцов и образца полиэтилена.

Получено, что количество водорода в нанопорошке до и после обезгаживания может быть выражено отношениями C_8H и $C_{15}H$ соответственно. Полное сечение рассеяния атома водорода составляет в этом случае ~120 барн. Изменение этого сечения при изменении температуры от 500K до 80K не превышает 3%.

Дополнительно были измерены спектры возбуждения атомов водорода в обезгаженном и необезгаженом образцах. Полученные результаты указывают на то, что водород, удаляемый из порошка путём откачки и прогрева, находится в виде воды адсорбированной на поверхности образца. Атомы водорода, не удаляющиеся из порошка откачкой и прогревом до 150ºC находятся в химической связи с атомом углерода, находящимся в состоянии sp^3 гибридизации.

Таким образом, охлаждение до температуры жидкого азота ловушки для очень холодных нейтронов из алмазного нанопорошка с целью подавления канала потерь представляется нецелесообразным. Для увеличения вероятности отражения необходимо либо удалять/замещать химически связанный с углеродом водород либо вести глубокое охлаждение порошка до температуры жидкого гелия.

3. Теоретические исследования

3.1 О нейтронных поверхностных волнах

Ранее в литературе было высказано предположение, что нейтроны могут существовать в виде поверхностных волн на границах раздела различных сред, и это может объяснить известную аномалию в коэффициенте потерь ультрахолодных нейтронов. Например, утверждалось, что поверхностная нейтронная волна может существовать на поверхности пленки с конечным оптическим потенциалом, которая напылена на подложку с бесконечным потенциалом, как показано на рисунке. Однако из обычного уравнения Шредингера

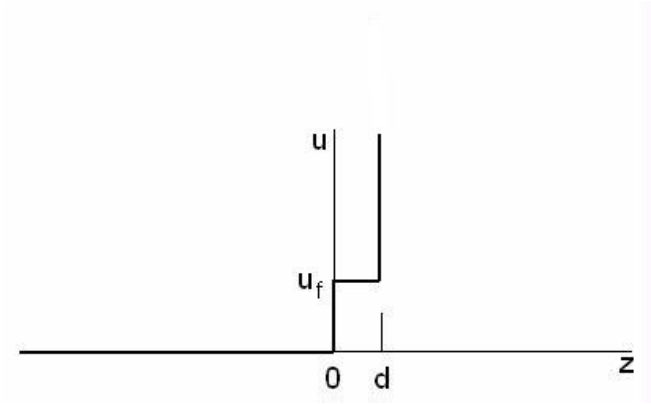

$$\left[\Delta + k_0^2 - u(\mathbf{r})\right]\psi(\mathbf{r}) = 0$$

следует, что поверхностная волна не может удовлетворить граничным условиям непрерывности волновой функции и ее производной так, чтобы при этом выполнялся закон сохранения энергии. Из последнего следует, что при отсутствии поглощения (а в вакууме оно отсутствует) волновой вектор частицы обязан быть строго вещественным.

Рис. 12.

В случае потенциала, показанного на рисунке, решение уравнения существует, но оно не удовлетворяет закону сохранения энергии. Состояния, похожие на поверхностные могут существовать в пленках с отрицательным потенциалом. Однако волновая функция нейтрона в этом случае описывает не поверхностное, а связанное состояние, которое экспоненциально убывает при удалении от пленки в доль нормали и соответствует свободному движению вдоль пленки.

Был исследован вопрос, чем отличаются упругие и электромагнитные волны от нейтронных волн, и почему в случае упругих и электромагнитных волн поверхностные состояния могут существовать. Главное различие состоит в формулировке граничных условий. Если в случае нейтронных волн граничные условия следуют из самого уравнения Шредингера, то в случае упругих и электромагнитных волн граничные условия формулируются из дополниткльных требований: из непрерывности нормальных компонент тензора напряжений для упругих волн и из необходимости удовлетворить уравнениям Максвеела для полей в случае электромагнитных волн.

3.2 Пределы нуклон-нуклонного монопольно-дипольного взаимодействия, извлеченные из деполяризации ультрахолодных нейтронов в ловушках

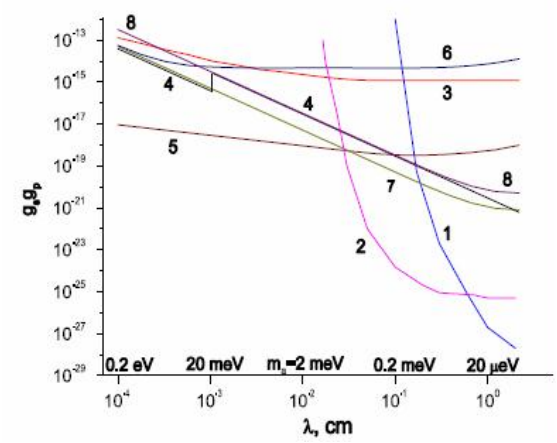

Рис. 13

В физике элементарных частиц давно ведутся поиски гипотетической псевдоскалярной частицы аксиона, которая порождает P- и T-нечетное монополь-дипольное взаимодействие $(\boldsymbol{\sigma}\mathbf{n})gV(r)$ между спинорными частицами и веществом . Здесь $\boldsymbol{\sigma}$ -- вектор матриц Паули, $\mathbf{n}=\mathbf{r}/r$ -- единичны вектор вдоль радиуса вектора между материальной частицей и аксионом, g -- безоазмерная константа взаимодействия, и $V(r)\propto\exp(-r/\lambda)$ -- функция, экспоненциально спадающая на расстоянии Λ. Поиски аксиона пока не увенчались успехом, и в лабораторных экспериментах устанавливают границу на величины g и λ. В настоящей работе исследовано как влияет аксионное взаимодействие на деполяризацию ультрахолодных нейтронов от стенок сосудов хранения при наличии слабого внешнего поля. Результаты расчета привели к новой кривой, характеризующей границу сосуществования g и λ. Эта кривая на указанном рисунке обозначена цифрой 6 в случае если вероятность переворота спина нейтрона оценена величиной 10^{-6} при внешнем поле 50 Гс и цифрой 7 когда вероятность переворота равна $4\text{x}10^{-5}$ и внешнее поле равно 0.01 Гс. При этом в обоих случаях принималось, что нейтроны хранятся в сосуде со стенками толщиной 1 см и их скорость равна 3 м/с. По вертикальной оси отложен параметр, который обозначен здесь g.[6]. Кривые, отмеченные другими цифрами, показывают ограничения, полученные в других работах.

3.3 Исследование эффектов преломления и отражения нейтронов в среде с поляризованными ядрами.

Исследованы эффекты преломления и отражения первоначально не поляризованных медленных нейтронов в среде с поляризованными ядрами. В такой среде пучок нейтронов характеризуется двумя показателями преломления, соответствующими проекциям спина нейтрона на вектор поляризации ядер, равными (+1/2) и (–1/2). Показано, что с учетом этого факта, при ненулевом угле падения на границу между средой с поляризованными ядрами и вакуумом, пучок не поляризованных нейтронов пространственно расщепляется на два пучка нейтронов, полностью поляризованных в противоположных направлениях. Угол между преломленными поляризованными пучками растет с уменьшением энергии нейтронов и при приближении к касательному падению. Показано, что в условиях полного внутреннего отражения для одного из показателей преломления отраженные и преломленные нейтроны полностью поляризованы в противоположных направлениях вдоль и против вектора поляризации ядер.

Проведены численные оценки для случая жидководородной полностью поляризованной мишени. При угле падения 85^0 и энергии нейтронов 10^{-4} эВ угол между пучками преломленных нейтронов, полностью поляризованных в противоположных направлениях, составляет порядка $1{,}5^0$, и соответствующие пучки могут быть в принципе пространственно разделены.

4. Прикладные исследования

4.1 Прикладные исследования на установке ИРЕН

На установке ИРЕН проводились измерения потока тепловых, резонансных и быстрых нейтронов с помощью активационной методики. Активируемые образцы (Au, Cu, In и др.) помещались на поверхности замедлителя. После облучения измерялись спектры гамма-квантов с помощью полупроводникового детектора с высоким разрешением.

В результате были получены следующие значения: поток резонансных нейтронов - $2.5\cdot10^{6}$ н·см$^{-2}$сек$^{-1}$; поток тепловых нейтронов $\Phi_{th}=2.0\cdot10^{7}$ н·см$^{-2}$сек$^{-1}$; поток быстрых нейтронов $\Phi_{fast}=2.0\cdot10^{7}$ н·см$^{-2}$сек$^{-1}$. Эти значения находятся в неплохом согласии с результатами, полученными на выведенном пучке нейтронов.

Кроме, того, было проведено облучение геологических образцов из Монголии с целью определения содержания редких металлов в руде. Результаты измерений переданы в Академию наук Монголии. Эти исследования будут продолжаться.

В 2009 году были начаты работы с использованием ИРЕН как источника тормозного излучения. Сотрудниками ЛНФ были проведены расчеты интенсивности гамма-квантов и получены оценки выхода изотопов ^{99}Mo и ^{117m}Sn, которые могут использоваться в медицинских целях (Г.Г. Бунатян, В.Н. Николенко, А.Б. Попов, Сообщения ОИЯИ Е6-2009-182). Результаты расчетов подтверждаются данными, полученными на микротроне. Показана перспективность увеличения выхода изотопов с увеличением энергии электронов.

Был проведен эксперимент по облучению ряда элементов гамма-квантами. В этом эксперименте электронный пучок попадал на мишень из вольфрама толщиной 2 мм. Полученные в результате торможения электронов гамма-кванты попадали на образцы Sn, Au, Cu, Zr. Целью эксперимента было определение потока гамма-квантов. Полученные данные находятся в качественном согласии с данными, полученными на микротроне ЛЯР. Кроме того, была сделана попытка определения выхода изомера ^{117m}Sn ($T_{1/2}$=14 дн.), представляющим интерес для использования в медицине. Эта работа была проведена вместе с сотрудником исследовательского центра NECSA из ЮАР. Полученные данные требуют более тщательного исследования.

4.2 Ядерно – физические аналитические методики на базе пучков заряженных частиц.

Ядерно – физические аналитические методики на базе пучков заряженных частиц от ускорителя ЭГ – 5 в 2009 году использовались для решения важных прикладных задач. В современных микроэлектронных и полупроводниковых приборах выпрямляющие и невыпрямляющие (омические) контакты формируются с использованием пленок металлов, нанесенных на поверхность полупроводника. После осаждения металлической пленки на

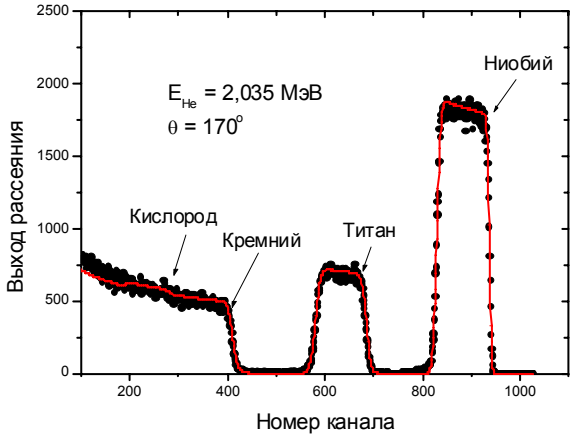

Рис.14. *Спектр резерфордовского обратного рассеяния ионов гелия на образце, содержащем слой ниобия (170 нм) и слой титана (263 нм) на кремниевой подложке.*

монокристаллический кремний обычно производят термический отжиг, в ходе которого в системе пленка – полупроводник возможны, как процессы гетеродиффузии, так и химические реакции взаимодействия атомов металла с атомами кремния, приводящие к образованию химических соединений (силицидов, интерметаллидов). Сформированная в ходе отжига физико - химическая структура межфазной границы во многом определяет электрические свойства контактов металл – полупроводник. В контактах полупроводниковых приборов предлагается использовать тугоплавкие металлы Nb и Ti.

В результате проведенного исследования были изучены процессы фазообразования и перераспределения компонентов в системе пленка Nb – монокристаллический кремний.

Таким образом, неразрушающие ядерно – физические аналитические методики позволяют получить весьма важную информацию о химическом составе и структуре наноразмерных слоёв материалов, используемых в современных технологических процессах производства полупроводниковых и микроэлектронных приборов.

4.3 Аналитические исследования на реакторе ИБР-2

Подготовка к аккредитации сектора НАА

В рамках проекта Технической кооперации с МАГАТЭ «Гармонизация системы контроля качества в соответствии с ISO-17025 и международными стандартами в лабораториях Российской Федерации, использующих ядерно-физические аналитические методы» в 2009 г. в секторе НАА продолжалась подготовка к аккредитации, планируемой на 2011 год после пуска реактора ИБР-2М. Подготовлен основной пакет документов, сделан капитальный ремонт химической лаборатории, при финансовой поддержке МАГАТЭ приобретена часть оборудования для химической лаборатории и радиоаналитического комплекса РЕГАТА на реакторе ИБР-2.

Развитие экспериментальной базы сектора НАА

ИБР-2М Были продолжены работы по усовершенствованию спектрометрического и сервисного оборудования установки РЕГАТА и химической лаборатории. Проведены измерения значений фона естественной радиоактивности в различных помещениях лабораторного корпуса, в том числе в бомбоубежище ЛНФ, с целью выбора места для проведения измерений природной и антропогенной радиоактивности образцов.

ИРЕН Совместно с «Базой развития и внедрения по физике (БРВ-физика)», София, Болгария, и КБ ЛНФ разработан технический проект на изготовление пневмотранспорта для проведения НАА на установке ИРЕН.

Биомониторинг

В 2009 году завершен цикл работ и публикаций, выполненных в рамках международной программы «Атмосферные выпадения тяжелых металлов в Европе – оценки на основе анализа мхов-биомониторов». Эти работы охватывают некоторые регионы Центральной России (Вергель и др., 2009) и Южного Урала (Панкратова и др., 2009), Белоруссии (Frontasyeva, Aleksiayenak et al., 2009;), Болгарии (Marinova et al., 2009), Словакии (Meresova et al., 2009), Сербии (Krmar et al., 2009), Хорватии (Spiric et al., 2009), а также Монголии (Балжинням и др., 2009) и Вьетнама (Nguyen Viet et al., 2009). Заверешена и опубликована большая методическая работа по калибровочным измерениям содержания элементов в атмосферных осадках и мхах-трансплантах, используемых для оценки атмосферных выпадений тяжелых металлов и других элементов, которая была выполнена совместно с Институтом физики в Белграде, Сербия, и Норвежским Университетом науки и технологии в Трондхейме (Anicic et al., 2009).

Оценка состояния экосистем

В 2009 году успешно завершен двухлетний проект РФФИ – Румынская Академия наук «Геохронология и изучение ретроспективных загрязнений незатвердевших донных

отложений из кислородосодержащих и бескислородных акваторий западной части Черного моря», результатом которого явилась публикация 7 работ в международных реферируемых журналах. Цикл работ подан на Конкурс ОИЯИ 2009 года по разделу «Научно-технические и прикладные работы» (Duliu, Frontasyeva, Culicov et al, 2009). Продолжено сотрудничество с монгольскими учеными в рамках проекта РФФИ-Монголия «Разработка системы комплексного мониторинга тяжелых металлов и радионуклидов в Монголии с использованием ядерно-физических аналитических методов». Результаты докладывались на нескольких международных конференциях (напр., N. Baljinnyam, Sh. Gerbish et al., 2009). Работа Н. Балжинням была отмечена первой премией на конкурсе работ молодых ученых на Центрально-европейской международной конференции в Пьеховице, Польша. В 2009 году работа сектора НАА в сотрудничестве с Македонией и Словенией по созданию Атласа загрязнения почв тяжелыми металлами одного из экологически проблемных регионов Македонии была удостоена Государственной премии Правительства Республики Македония. В 2009 году материалы атласа опубликованы в виде статьи в международном журнале «Journal of Hazardous Materials» (Stafilov et al., 2009). В совместной работе с кафедрой экологии Университета Дубна изучено влияние автотранспорта на химический состав почв на территориях, прилегающих к автомагистралям на примере Дубны и Москвы (Судницын и др., 2009).

Продукты питания и здоровье человека

В 2009 году на реакторе МИФИ (Москва) продолжены работы по анализу продуктов питания в связи с проектом сектора НАА с NECSA, ЮАР: «Сравнительное изучение воздействия на здоровье детей потребления продуктов питания, выращенных в некоторых промышленных районах России и Южной Африки, с использованием ядерно-физических аналитических методов». В журнале *Агрохимия* представлены результаты биоаккумуляции химических элементов овощными культурами на техногено загрязненных территориях Тульской области (Горелова и др., 2009). В рамках координационной программы МАГАТЭ «Воздействие токсичных и потенциально токсичных элементов на женщин репродуктивного возраста в развивающихся странах» совместно с Российским государственным медицинским университетом (Москва), Аналитическим центром Геологического института РАН и Медицинской Академией им. И.П. Сеченова в 2009 году завершена и опубликована в журнале «Общественное здоровье и профилактика» работа по определению многоэлементного анализа образцов крови специально подобранных пациентов из одного из промышленных районов Москвы (Ильченко и др., 2009). Эти исследования подтвердили гипотезу о корреляции концентраций таких токсичных элементов, как свинец, цинк и сурьма, с индексом массы тела обследуемых пациентов.

Биотехнологии

Работы по биотехнологии очистки окружающей среды от токсичных элементов (ртуть, хром и др.) ведутся в секторе НАА совместно со специалистами Института физики им. Э. Андроникашвили и Университета им. И. Чавчавадзе (Тбилиси, Грузия). В 2009 г. опубликованы новые результаты по использованию природных штаммов бактерий, выделяемых из базальтов, для восстановления токсичного хрома (VI) в нетоксичную форму хром (III). Элементный состав серии образцов бактерий *Arthrobacter oxidans* при комплексном воздействии хрома и ртути был определен методом нейтронной активации на исследовательском реакторе Университета в Дельфте, Нидерланды. Предварительные результаты доложены в декабре 2009 г. на международной конференции BioMicroWorld’2009 (Лиссабон, Португалия). В 2009 году начаты работы по освоению методик получения и обнаружения наночастиц золота, серебра и сульфида кадмия в биоматериалах.

Материаловедение

Синтез мелкокристаллических алмазов

Совместно со специалистами Института твердого тела и полупроводников Беларуси подготовлена и сдана в печать глава книги «Diamond and Related Materials» (США), посвященная изучению поведения дефектов в мелкокристаллических алмазах под воздействием нейтронного облучения в присутствии катализаторов (Дутов и др., 2009). Выполнен подготовительный этап работ в рамках проекта 2009-2010 гг. по изучению роли микропримесей в процессе синтеза кристаллов нитрида бора.

Радиоэкология

Впервые на территории Беларуси был применен метод мхов-биомониторов для оценки атмосферных выпадений радионуклидов спустя 20 лет после Чернобыльской аварии. Измерения долгоживущих радионуклидов – продуктов деления ядерного топлива – были проведены в 2008-2009 гг. совместно со словацкими специалистами в низкофоновой лаборатории Братиславского Университета. Часть проб была проанализирована специалистами NECSA в ЮАР. Показано, что уровни активности ^{137}Cs в образцах мха, собранных на территории Гомельской области, в 4 раза превышают фоновые. Отмечено также повышенное содержание ^{210}Pb. Эти результаты были доложены в сентябре 2009 г. на 5-ом международном совещании по биомониторингу воздушных загрязнений (BioMAP-5) в Аргентине (Frontasyeva, Aleksiayenak et al., 2009).

Учебный процесс

На базе установки РЕГАТА в 2009 году проводился Практикум для студентов старших курсов Университета «Дубна» и студентов Международных Летних Школ, организуемых УНЦ ОИЯИ (июль – Болгария, Чехия, Словакия; сентябрь-октябрь ЮАР, октябрь-ноябрь – Египет). За отчетный период на базе сектора НАА были выполнены две курсовых, одна бакалаврская и одна магистерская работа. Подготовлено Учебное пособие по НАА для Практикума на установке РЕГАТА (Фронтасьева, 2009).

2. NEUTRON SOURCES

2.1. THE IBR-2 PULSED REACTOR

Starting in December 2006 after the reactor shutdown the modernization of IBR-2 was conducted in accordance with the "Program of activities on the IBR-2 reactor during its temporary shutdown (2007-2010)" in compliance with the quarterly plans approved by the FLNP chief engineer.

Activities completed in 2009

1. Installation of the reactor vessel at its work site and of in-vessel components. Loading of dummy fuel assembly cartridges into the reactor core.
2. Installation of the movable reflector MR-3 in the operative position.
3. Replacement of a cold trap for purifying sodium coolant in loop "A" of the second reactor cooling circuit.
4. Installation of stationary reflectors and water moderators on the trolleys of the rolling shields.
5. Installation of executive mechanisms and control units of the reactor.
6. Manufacturing and installation of an additional storage facility for the IBR-2 used fuel in the reactor hall.
7. Installation of equipment of the cryogenic helium refrigerator KGU-700/15 and helium pipelines between the cryogenic refrigerator and the rolling shields.

Activities still in progress according to the plan

1. Installation and stage-by-stage adjustment of the operator console on the main control panel of the reactor.
2. Installation and adjustment of communications and power electrical equipment of the reliable power supply system, of the power supply system of the standby control board and the heaters of the IBR-2M cooling circuits from the standby power supply system.
3. Installation of equipment and switching lines of the technological parameters control system (TPCS) and the automatic safety and control system (ASCS-12R).
4. Preparation to the filling of the reactor cooling circuits with a liquid sodium coolant.
5. Manufacturing of a cryogenic moderator for beams 7-11 (CM 202).
6. Installation of an experimental stand for testing transportation modes of mesitylene balls to the cryogenic moderator.

Problems

There was an unforeseen delay in the delivery of electronic equipment of the automatic safety and control system (ASCS-12R). The designer and manufacturer of the given equipment failed to fulfill contractual obligations to deliver the equipment by September 01, 2009 and postponed the final delivery of the certified complex ASCS-12R by 9 months, until the end of June, 2010. For this reason the beginning of work on the physical start-up of IBR-2M is scheduled for September, 2010.

Building and construction activities to ensure safe operation of the reactor

1. The greater part of the work to prepare the territory in the immediate vicinity of IBR-2 to make a local protected zone for physical protection of the reactor has been fulfilled.
2. The repairs of the rooms and the roof of the reactor cryogenic area have been completed.
3. Construction works in the rooms for a reliable power supply system have been completed.
4. The repairs to the rooms for the primary and standby control panels of the reactor as well as to

the rooms for the measuring equipment of the reactor diagnostics system have been finished.

Financing in 2009

In 2009 the financial plan allowed for 1380 k$ on the reactor modernization. The real financing of works on the modernization project corresponded to the approved plan.

In 2010 the planned expenses on modernization will be 960 k$. In addition, a total of 1246 k$ is planned to be allocated on the creation of the system of physical protection of IBR-2M.

2.2. IREN FACILITY

In accordance with the decision of the JINR Directorate to realize the IREN project in several stages, the construction of the electron accelerator and the nonmultiplying neutron-producing target complex has been completed. Since the beginning of 2009 the carrying out of experimental investigations on newly constructed source has been started.

2. ИСТОЧНИКИ НЕЙТРОНОВ

2.1. ИМПУЛЬСНЫЙ РЕАКТОР ИБР-2

Работы по модернизации ИБР-2, начиная с декабря 2006 г. после остановки реактора, ведутся в соответствии с «Программой работ на реакторе ИБР-2 в режиме временного останова (2007-2010 г.г.)» по квартальным планам, утверждаемым главным инженером ЛНФ.

Работы, завершенные в 2009 г.

1. Закончен монтаж корпуса реактора на рабочее место и внутрикорпусных устройств. Проведена загрузка в активную зону кассет-иммитаторов ТВС.
2. Установка подвижного отражателя ПО-3 в рабочее положение.
3. Замена холодной ловушки для очистки натриевого теплоносителя петли «А» 2-го контура охлаждения реактора.
4. Монтаж стационарных отражателей и водяных замедлителей на тележках откатных защит.
5. Монтаж исполнительных механизмов и органов регулирования реактора.
6. Изготовление и монтаж в реакторном зале дополнительного хранилища для отработанного топлива ИБР-2.
7. Монтаж оборудования холодильной установки КГУ 700/15 и гелиевых трубопроводов на участке между криогенной машиной и откатными защитами.

Работы, продолжающиеся по плану

1. Монтаж и поэтапная наладка пульта оператора на основном пульте управления реактором.
2. Монтаж и наладка коммуникаций и силового электрооборудования системы надежного питания, системы электроснабжения резервного щита управления и нагревателей контуров охлаждения ИБР-2М от системы резервного электропитания.
3. Монтаж оборудования и коммутационных линий системы контроля технологических параметров реактора (СКТП) и автоматизированной системы контроля и защиты (АСУЗ-12Р).
4. Подготовка к заполнению контуров охлаждения реактора жидким натриевым теплоносителем.
5. Изготовление криогенного замедлителя для пучков 7-11 (КЗ 202).
6. Монтаж экспериментального стенда для отработки режимов транспортировки мезитиленовых шариков в криогенный замедлитель.

Проблемы

Возникла непредвиденная задержка с поставкой электронного оборудования автоматизированной системы управления и защиты реактора ИБР-2М (АСУЗ-12Р). Разработчик и производитель данного оборудования не смог выполнить контрактные обязательства по поставке аппаратуры к 01 сентября 2009 г. и перенес срок окончательной поставки сертифицированного комплекса АСУЗ-12Р на 9 месяцев, на конец июня 2010 г. По этой причине начало работ по физическому пуску ИБР-2М планируется на сентябрь 2010 г.

Строительные работы для обеспечения безопасной эксплуатации реактора

1. Выполнена основная часть работ по подготовке территории, прилегающей к комплексу ИБР-2 для устройства локальной защищенной зоны для обеспечения физической защиты реактора.
2. Завершен ремонт помещений и кровли криогенного участка реактора.
3. Закончены строительные работы в помещениях для системы надежного питания.
4. Закончены работы по ремонту помещений основного и резервного пультов управления реактором, а также помещения для размещения измерительного оборудования системы диагностики состояния реактора.

План работ на 2010 г.

1. Завершение монтажа, испытания, наладка и приемка в эксплуатацию автоматизированной системы управления и защиты ИБР-2М (АСУЗ 12Р), основного резервного пультов управления реактором.
2. Наладка и испытания экспериментального стенда для отработки режимов транспортировки мезитиленовых шариков.
3. Изготовление криогенного замедлителя для нейтронных пучков 2-3 (КЗ 203). Монтаж трубопроводов подачи мезитилена для криогенного замедлителя пучков 7-11 (КЗ 202) и для криогенного замедлителя пучков 2-3 (при положительных результатах испытаний на экспериментальном стенде).
4. Подготовка к физическому пуску реактора:
   - наладка и комплексные испытания вновь смонтированного технологического и электрического оборудования и электроники;
   - подготовка необходимой организационной и технической документации;
   - комиссионная приемка реактора ИБР о готовности к физпуску.
5. Физический пуск ИБР-2М.
6. Создание системы физической защиты ИБР-2М в соответствии с современными правилами.

Финансирование работ по модернизации

Финансовым планом на работы по модернизации реактора в 2009 г. предусматривались расходы в размере 1380 k$. Реальное финансирование работ соответствовало утвержденному плану.

В 2010 г. плановые расходы на модернизацию составят 960 k$. Дополнительно планируется выделение 1246 k$ на создание системы физической защиты ИБР-2М.

2.2. УСТАНОВКА ИРЕН

В соответствие с решением дирекции ОИЯИ по реализации ИРЕН в нескольких этапов, были завершены конструкция электронного ускорителя и комплекс неразмножающей мешень. С началам 2009 г. проводится эксперименты на новом установке.

3. NOVEL DEVELOPMENT AND CONSTRUCTION OF EQUIPMENT FOR IBR-2M SPECTROMETERS COMPLEX

In 2009, work in the framework of the theme was focused on several activities connected with the construction and modernization of the equipment, electronic data acquisition and accumulation systems as well as the information-computation infrastructure of the IBR-2M spectrometers complex.

Cryogenic moderators

The conceptual design, development of technical documentation, manufacturing and mounting of the main parts of a full-scale stand of the technological system of the cryogenic moderator (CM) have been accomplished. The stand is a full-scale model of the future CM system with a copy of the CM camera, technological system and the system for delivery of mesitylene beads (**Figs. 1-4**). The stand cooling system comprises two coolant loops connected by a heat exchanger. In the first coolant loop, helium is driven by a helium blower through the heat exchanger and the CM chamber. In the second coolant loop, helium is forced through the heat exchanger by a helium refrigerator (500 W, 15 K). As a result of simultaneous operation of the helium refrigerator and the helium blower in the CM chamber the required temperature is achieved and mesitylene beads are transported by the flow of gaseous helium from the charging device to the CM chamber.

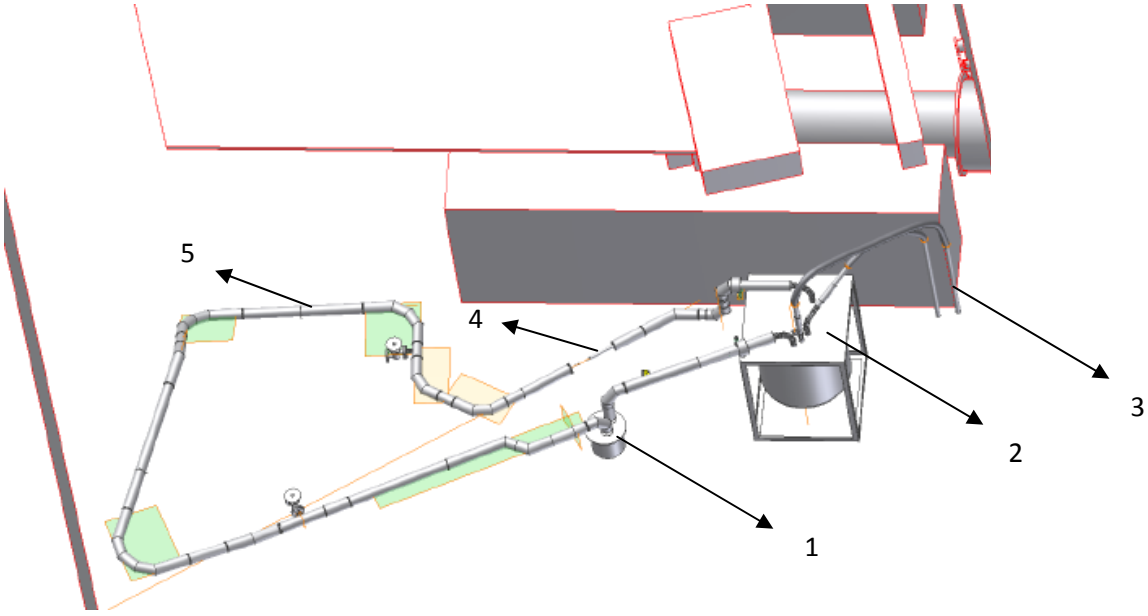

Fig. 1. The main elements of the full-scale model of the technological system of cryogenic moderators (1 – chamber of a cryogenic moderator with vacuum shielding, 2 – heat exchanger with a helium blower, 3 – cryogenic pipes from/to a helium cooler, 4 – place for a charging device, 5 – cryogenic transport tube).

In the FLNP Department of Spectrometers Complex a special integrated control system for monitoring different parameters of the stand and the respective software complex have been developed. The system includes various sensors (15 pieces altogether), a gas blower motor drive controller and a controller of the step motor of the dispenser of balls into the system. The system makes it possible to control the main parameters of the moderator stand:

- transport of balls through a pneumatic conveying pipe (controlled by an original method based on gas-dynamic effects);

- filling of the moderator chamber with beads (monitored with a web-camera through quartz glasses);
- gas flow rate;
- pressure and temperature of helium.

Fig. 2. Mounting of the cryogenic transport tube.

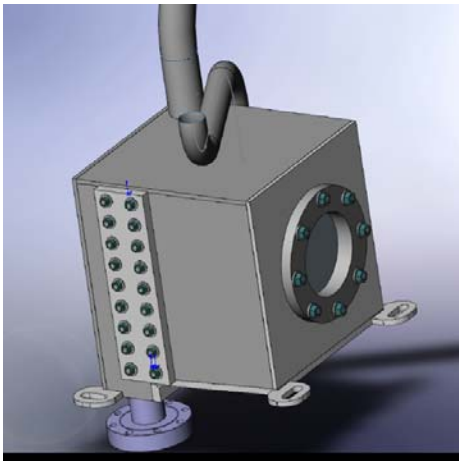

Fig. 3. Model of the cold moderator chamber.

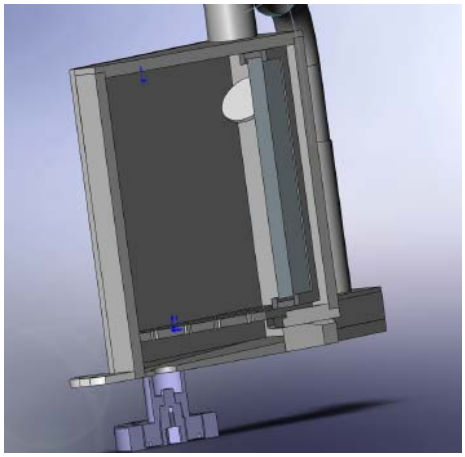

Fig. 4. The inner part of the cryogenic moderator chamber model.

At present, the manufacturing of the elements of the stand has been completed and the process of assembling and testing has started.

Test beam

A technical project for construction of a test beam on channel 13 of the IBR-2M reactor has been developed; the assignments to develop equipment units for the channel have been given to the Design Department. The requirements specification for a biological shield (**Fig. 5** illustrates the suggested location of the shield) has been prepared as well. In October 2009, PNPI (Gatchina) came up with a suggestion to install the FSS Fourier diffractometer (which will be turned over to PNPI by GKSS in view of the FRG-1 reactor shutdown) on channel 13 of the IBR-2M reactor. This suggestion will most likely be accepted. This means that beam 13 will be used both for testing

various elements of spectrometers and for carrying out a limited number of experiments on the FSS diffractometer. From a practical point of view the gained benefit, in case the suggestion is accepted, is quite appreciable, since this will make it possible to considerably save on the equipment of the channel and possible "expenses" (experiments on FSS) will be insignificant, because FSS will not be included in the IBR-2 user program. Besides, the expected workload of the channel with testing experiments will hardly exceed 50%. Thus, one or the other decision of the question on installation of FSS will significantly affect the cost and time of realization of the project.

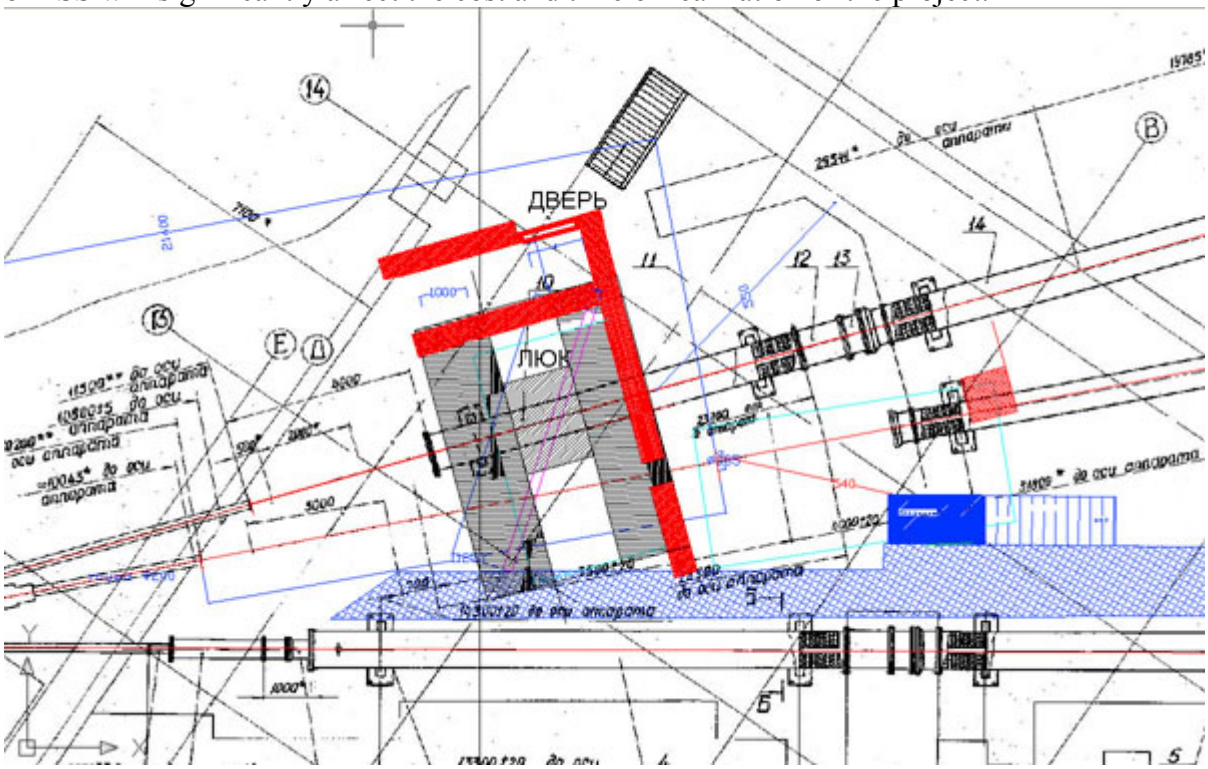

Fig. 5. Suggested location of the biological shield.

Neutron beam-forming systems

In cooperation with the German Institutes and PNPI (Gatchina) within the framework of the project aimed at constructing curved mirror neutron guides for the EPSILON and SKAT spectrometers on beam 7a of the IBR-2 reactor the work to design and manufacture mechanical and optical units of the neutron guides has continued. In particular, the designs of a vacuum system and a background shield of the EPSILON and SKAT spectrometers and of a docking part of the neutron guide of the NERA-PR spectrometer have been developed, the documentation has been worked out and the manufacturing of the disk background chopper and three drum λ-choppers is nearing completion.

The reconstruction of the supporting column of IBR-2 (**Fig. 6**) and a biological shield of the head part of beam 7 to accommodate three neutron guides on the channel has been completed. The equipment from the embedded pipe of the ring corridor wall has been dismantled. In NPO «Atom» the posts and beam-positioning support pillars of the neutron guide head part (**Fig. 7**) have been produced. In JSC «Komtrast» the manufacturing of 92 vacuum casings for the curved neutron guides for the EPSILON and SKAT spectrometers is in progress.

Fig. 6. Reconstruction of the supporting column in bldg.117 for laying curved neutron guides for the EPSILON and SKAT spectrometers.

Fig. 7. The beam-positioning support pillars of the neutron guide head part of beam 7.

At present, the assembly of the head part (splitter) of beam 7 and the adjustment of mechanical units of the choppers have started.

Cryogenic stand

A test cryostat (**Fig. 8**) for working with closed cycle cryocoolers has been developed. The manufacturing of a control panel of the helium circulation system for additional refrigerators that can be placed in this cryostat is in progress.

The cryogenic stand is used to test and adjust cryogenic systems. At present, the modernization of the cryostat for the inelastic neutron scattering spectrometer (beam 7b, IBR-2) is under way. The cryostat shaft (70 mm in diameter) allows for fast cold sample change. The expected final temperature is 4.5 K.

Fig. 8. A test cryostat of the cryogenic stand (1 – cryostat, 2 – cryostat trestle, 3 – cold head, 4 – control panel of the gas circulation system, 5 – He-3 storage tank).

Development of control systems of choppers

In FLNP the control system of choppers based on the VFAS1-series variable-frequency electric drives from Toshiba (**Fig. 10**) has been developed, manufactured and debugged for the disk background chopper (**Fig. 11**) and three drum λ-choppers of the EPSILON, SKAT and NERA-PR spectrometers. The electric drive has a built-in microprocessor, which realizes the control algorithm according to the speed of rotation and the moment of rotation on the motor shaft. An incremental magnetic coding sensor for measuring speed, accelerating the disk and forming signals carrying information on an opened state of the chopper is installed on the motor axis. A phase controller CC-07 enables a chopper disk (drum) window position phase to be regulated with respect to the reactor start. The brief characteristics of control parameters are given in **Table 1**.

Table 1

№	Parameter	Background chopper	λ-chopper	
1	*Motor power (kW)*	*22*	*2.2*	
2	*Rotational speed (rev/min)*	*300*	*150*	*75*
3	*Starting current (A)*	*12*	*5*	*5*
4	*Rated current (A)*	*10*	*3*	*4*
5	*Accuracy of phase equalization (μs)*	*50*	*50*	*100*
6	*Start-up and equalization time (min)*	*10*	*10*	*10*

Fig. 10. An electric drive from Toshiba (22 kW) for a background chopper (left) and two electric drives (2.2 kW) for λ-choppers (right).

Fig. 11. A disk background chopper of beam 7 of IBR-2M.

A control system of choppers based on microcontrollers with CAN interface has been developed. As a result, control over each chopper is exerted by a computer of the respective spectrometer. A chopper controller is connected to the CAN bus and to a PC (via a "USB-to-CAN compact" converter).

The performed development work and tests have demonstrated the possibility of using variable-frequency VFAS1 drives and control systems to replace outdated EKT2 on the choppers of other IBR-2M spectrometers.

Calculations of spectrometers

Calculations of neutron spectra and optimization of beam geometry from moderator to sample for the EPSILON-SKAT spectrometer (beam 7a) have been completed. This will allow the neutron flux at the sample position to be increased by 20-30%. Preliminary calculations for beam 10 (GRAINS) have been made as well. The simulation of the instrument and its elements has been performed and recommendations to increase the neutron flux have been given. New modules for the VITESS software package have been developed:

● module for simulating the attenuation of a neutron beam passing through various elements of the medium (including gases) or combinations of elements (alloys, air);
● module for simulating moving slits and gratings (work has been performed in cooperation with JCNS-Munich, Germany).

Detectors

The anode and cathode electrodes have been manufactured, the position-sensitive detector for the GRAINS spectrometer has been assembled and filled with a gas mixture. The tests of the detector and the measurement of its characteristics have been carried out on beam 5 of the IR-8 reactor in the RRC «Kurchatov Institute» (tests were conducted with the available De-Li-DAQ board).

The detectors were filled with a test mixture 70 mbar ^{3}He + 2000 mbar CF_4 + 2400 mbar ^{4}He. A series of measurements with pin-hole and slit cadmium masks has been made at various values of anode voltage and different levels of discrimination of input signals. The PSD counting characteristics were measured with the pin-hole and slit exposure of the detector. Optimum operating modes of the detector were chosen and the coordinate resolution (no more than 2 mm for both coordinates), inhomogeneity of the gain factor (no more than 10%) and the detector efficiency were measured. Also, using the detector the profiles of beam 5 of the IR-8 reactor (**Fig. 12**) and of the IREN facility (**Fig. 13**) were obtained.

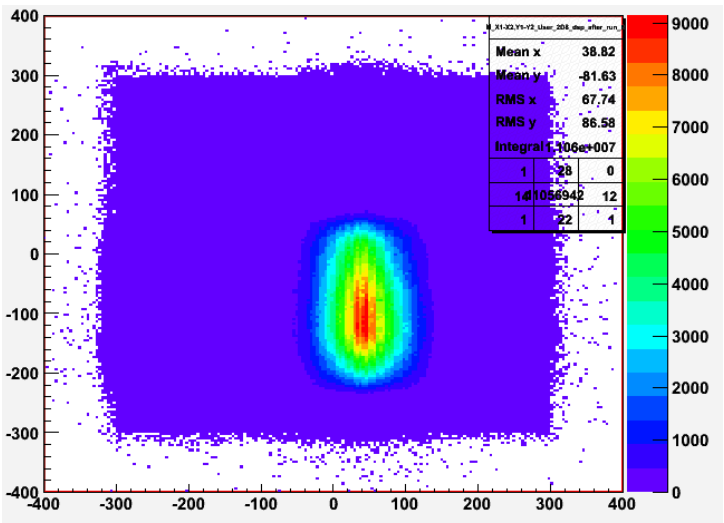

Fig. 12. A profile of direct beam 5 of the IR-8 reactor.

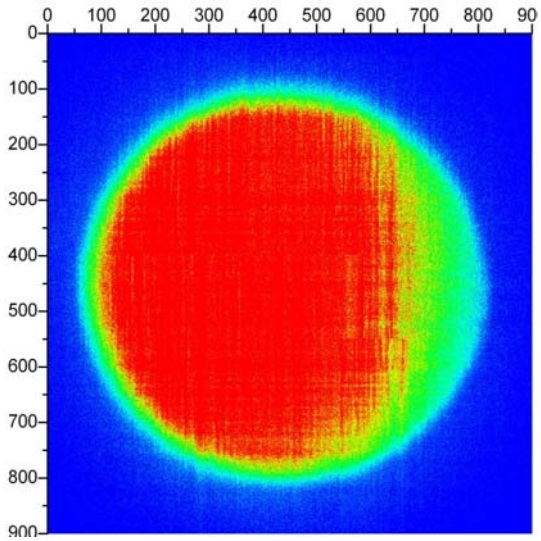

Fig. 13. A profile of the IREN facility beam in the thermal spectrum range.

A new high-speed neutron counter with a peak load of up to $3 \cdot 10^6$ n/s (see Fig. 14) has been developed. The counter is a rectangular parallelepiped made of duraluminium of dimensions 250×80×40 mm^3 and with internal working volume of 150×30×20 mm^3. The anode is a multi-wire frame coupled to the common electrode brought out through a vacuum connector outside. A pressure-optimized mixture of ^{3}He и CF_4 is used as a working gas. DAQ electronics, PC interface and software for the counter have been developed as well. The counter has been tested on the SuperADAM reflectometer (ILL, Grenoble, France).

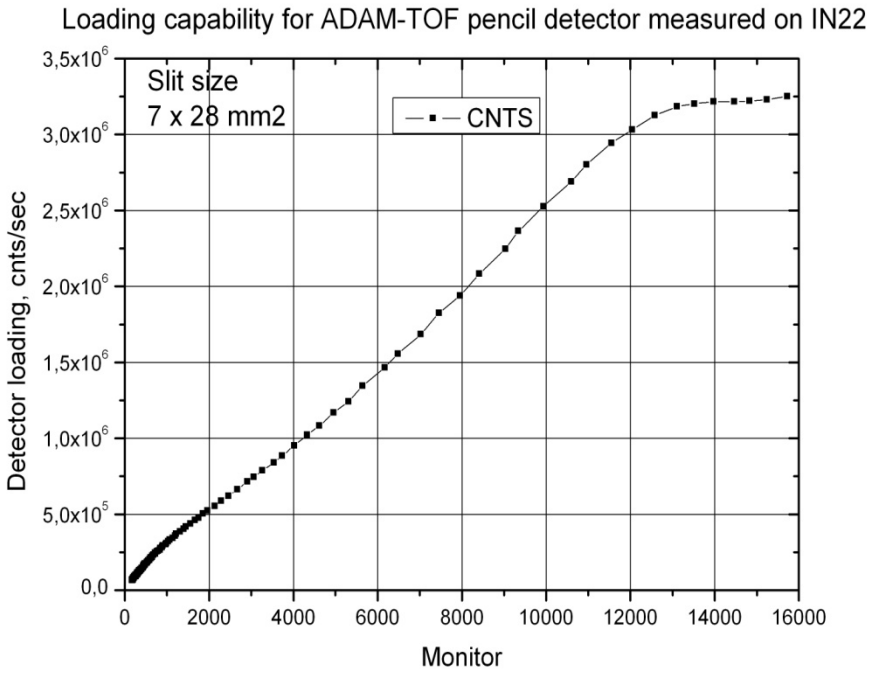

Fig. 14. Loading capability of the counter.

The development of a new ring-shaped multi-section MWPC-based detector for the DN-6 diffractometer has started. At the first stage it is proposed that one ring-shaped detector be constructed and installed at a scattering angle of 90°. The advantages of the new ring-shaped gas multi-section detector as compared to the previously used ring-shaped detector based on SNM-17 gas counters are:

- large size of the detector working volume will allow the count rate of scattered neutrons to be increased several times;
- shared working volume makes it possible to have practically the same efficiency for all sections;
- rectangular geometry of counting sections should improve the homogeneity of detection efficiency;
- smaller sizes of "dead zones" of the detector.

The detector is a ring, which is divided into 32 sections. Each section accommodates an electrode system consisting of a wire anode and two cathodes, which limit the sensitive area of the detector. The entrance window for neutrons will be the surface of the inner ring of the detector. Thin insulated drift electrodes are glued to the entrance window and the rear wall. At the center there is an anode plane with six thin (10-20 μm) tungsten wires wound around it, which are oriented along the chords of the detector ring. This makes it possible to obtain coordinate resolution along the beam. Anode wires are spaced ~10 mm apart. The total number of measuring channels is 36×6=192. Negative high voltage ~ –3–4 kV is fed to the drift planes. Signals are picked up directly from the anode. This scheme allows us to discard the use of coupling capacitor, thus, saving space inside the hermetically sealed volume of the detector and improving its reliability. The working gas mixture consists of a neutron converter (^{3}He) and a quenching gas (CF_4).

The design parameters of the detector are presented in **Table 2** and its external view is shown in **Fig. 15**.

Table 2. Basic design parameters of the detector.

№	Parameter	Value
1.	Width of entrance window, mm	~70
2.	Number of anode wires in a section	6
3.	Covered angle, deg.	360
4.	Number of sections	32
5.	Number of measuring channels	Up to 192
6.	Efficiency, % (λ=4Å)	~70
7.	Radius of inner ring, mm	>300
8.	Radius of outer ring, mm	~400
9.	Thickness of entrance window, mm	~7
10.	Material of the detector case	Al-Mg alloy
11.	Thickness of sensitive volume, mm	~40

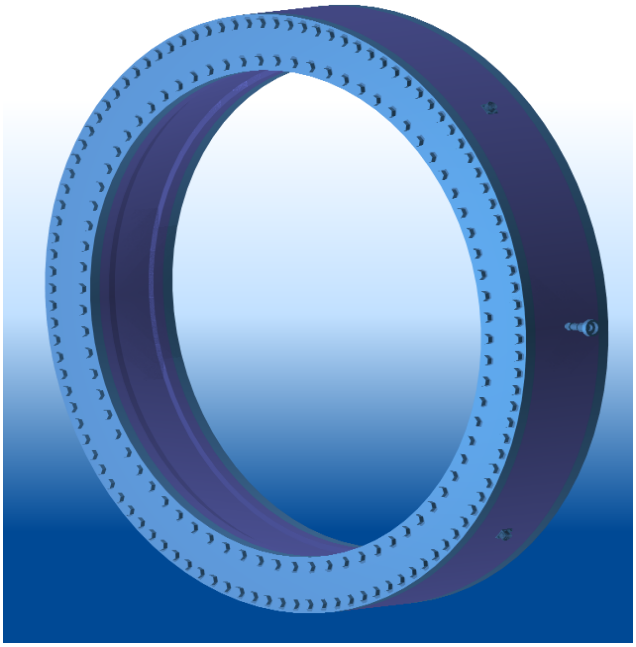

Fig. 15. Sketch drawing of the ring-shaped multi-section detector (external view).

Electronics and computing

Requirements specifications have been approved and the development of electronic blocks for acquisition and accumulation of raw data on the EPSILON, HRFD and DN-6 diffractometers has been started. These diffractometers will employ different detector systems (EPSILON – up to 128 helium neutron counters, HRFD – up to 200 scintillator plates with ZnS/6LiF coating and light collection using wavelength shifting fibers, DN-6 – ring-shaped multi-section MWPC-based detector with 32 sections and up to 192 measuring channels) but the common feature, which all of them share, is that all these systems can be considered as a set of point detectors with fixed spatial geometry. This makes it possible to apply a common approach to the design of data acquisition systems for the above-mentioned spectrometers, i.e. to design identical (from the viewpoint of hardware) electronic blocks, in which all functions, both common (encoding of the detector number, registration of time of flight) and specific to each concrete diffractometer, are realized on the level of microprograms, which are executed in FPGA of respective block.

A new test program has been developed and a high-speed DAQ block for 1D and 2D MWPC detectors with delay line readout has been tested. According to the results of the tests, all FPGA microprograms were optimized for operation in various data accumulation modes, redesign of printed boards was performed and the order for their production was placed. The above-mentioned test program is a basis for creation of a standard interface to the Sonix+ software package.

A schedule for conducting maintenance work on the IBR-2 spectrometers according to which the modernization and repair of electronic equipment and the preparation of spectrometers to the reactor start-up will be carried out. This work is already in progress on four spectrometers.

In 2009, new equipment of external communication channels for 10 Gbit/s operation was installed in the JINR local area network. This, in its turn, requires partial replacement of the existing switching equipment in the central and peripheral segments of the FLNP network. The analysis of possible changes in the network architecture and of characteristics of the equipment available in the market has been made with due regard for prospects of further evolution of the network. In view of limited financing it has been decided to purchase one intellectual multilevel router of WS-3560 series, which can operate in different configurations of Fast Ethernet and Gigabit Ethernet and provide high level of accessibility, scalability, safety and control. A limited set of communication modules for this router will be purchased as well. The corresponding contract is in the realization stage. After this equipment is tested, it will be installed in one of the IBR-2M experimental halls. During the reported year a large amount of work to support and modernize the FLNP network infrastructure has been performed.

3. ПЕРСПЕКТИВНЫЕ РАЗРАБОТКИ И СОЗДАНИЕ ОБОРУДОВАНИЯ ДЛЯ СПЕКТРОМЕТРОВ ИБР-2М

В 2009 г. работы по теме велись в нескольких направлениях, связанных с созданием и модернизацией оборудования, электронных систем сбора и накопления данных, а также информационно-вычислительной инфраструктуры комплекса спектрометров ИБР-2М.

Холодные замедлители

Выполнено концептуальное проектирование, разработана техническая документация, изготовлены и смонтированы основные узлы полномасштабного стенда технологической системы криогенного замедлителя (КЗ). Стенд является полномасштабной моделью будущей системы криогенного замедлителя с копией камеры КЗ, технологической системы и системы транспортировки мезитиленовых шариков (**Рис. 1-4**). Система охлаждения стенда включает в себя два контура криогенных труб, объединенных посредством теплообменника. В первом контуре, гелий циркулирует посредством побудителя движения холодного гелия (газодувки) через теплообменник и камеру замедлителя. Во втором контуре, гелий циркулирует через теплообменник посредством холодильной гелиевой установки (ХГУ-500, 500 Вт,15 К).

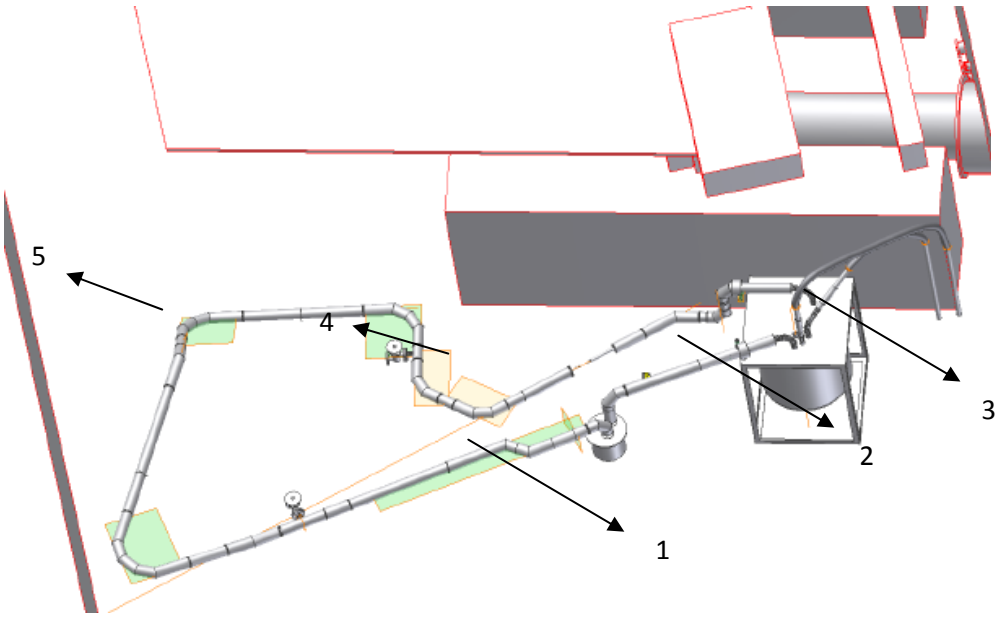

Рис.1. Главные элементы полномасштабной модели технологической системы холодного замедлителя (1- камера холодного замедлителя с вакуумной защитой, 2- теплообменник с гелиевой газодувкой, 3- криогенный трубопровод из/в гелиевого охладителя, 4- место для зарядного устройства, 5- криогенная транспортная труба).

В результате одновременной работы ХГУ и газодувки достигается необходимая температура в камере замедлителя и происходит транспортировка мезитиленовых шариков газообразным гелием от загрузочного устройства в камеру замедлителя.

В отделе НЭОКС разработана специальная интегрированная система контроля различных параметров стенда с комплексом соответствующего программного обеспечения. В состав системы входят различные датчики (всего 15 шт.), контроллер привода управления двигателем газодувки и контроллер управления шаговым двигателем дозатора поступления «шариков» в систему. Система позволяет контролировать основные параметры стенда замедлителя:

- прохождение шариков через пневмотранспортную магистраль (регистрируется оригинальным методом, основанным на газодинамических эффектах);
- заполнение шариками камеры замедлителя (наблюдается при помощи веб-камеры через кварцевые стекла);
- скорость газового потока;
- давление и температуру гелия.

Рис. 2 Монтаж криогенной транспортной трубы)

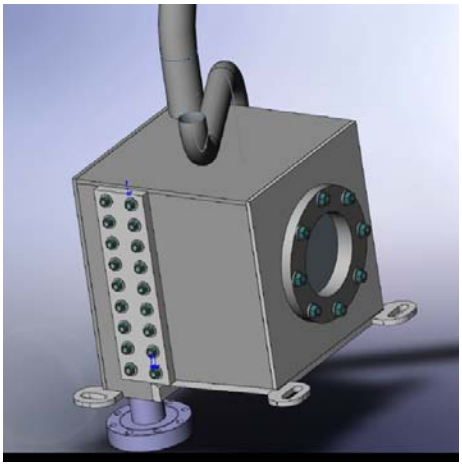

Рис.3 Макет камеры холодного замедлителя

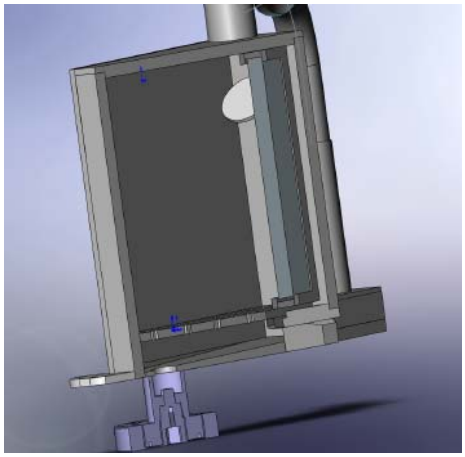

Рис. 4 Внутренняя часть макета камеры холодного замедлителя.

В настоящее время завершено изготовление элементов стенда и начаты работы по его сборке и проверке.

Тестовый пучок

Разработан технический проект создания тестового пучка на 13 канале ИБР-2М, в конструкторское бюро даны задания на разработку узлов оборудования канала. Подготовлено также техническое задание на проектирование биологической защиты (на **Рис. 5** показано предлагаемое размещение защиты). В октябре 2009 г. из ПИЯФ (Гатчина) поступило предложение об установке на 13 канале ИБР-2М Фурье-дифрактометра FSS, который будет передан ПИЯФ из GKSS в связи с остановкой там реактора FRG-1. Вероятно, это предложение будет принято.

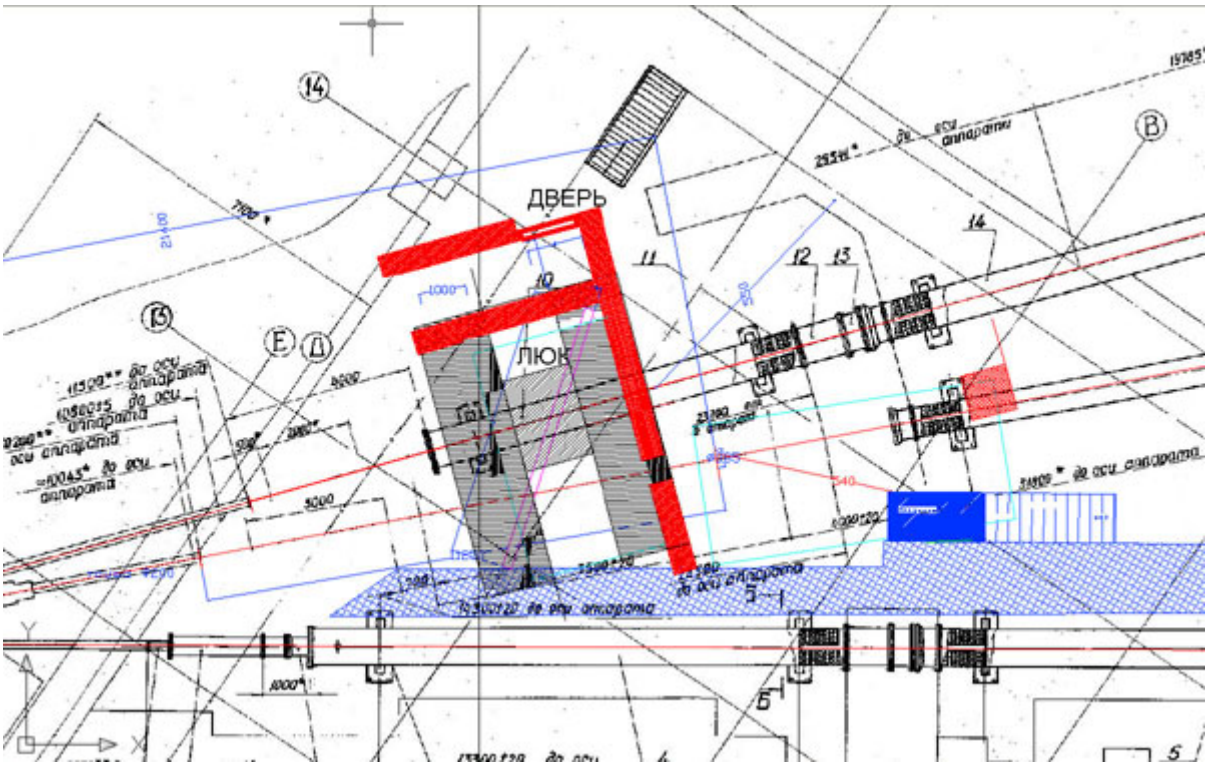

Рис. 5. Предлагаемое место размещения биологической защиты.

Это означает, что 13 пучок будет использоваться как для испытания различных элементов спектрометров, так и для проведения ограниченного числа экспериментов на дифрактометре FSS. В практическом плане выгода от принятия данного предложения состоит в том, что можно существенно сэкономить на оборудовании канала, а возможные «издержки» (эксперименты на FSS) невелики, т.к. FSS не будет включен в программу пользователей ИБР-2, к тому же ожидаемая загрузка канала работами по тестированию вряд ли превысит 50%. Таким образом, то или иное решение вопроса о размещении FSS существенно повлияет на стоимость и сроки реализации проекта.

Системы формирования нейтронных пучков

В рамках проекта создания изогнутых зеркальных нейтроноводов спектрометров ЭПСИЛОН и СКАТ на канале 7а реактора ИБР-2 совместно с институтами ФРГ и ПИЯФ г. Гатчина продолжались работы по проектированию и изготовлению механических и оптических узлов нейтроноводов. В частности, разработаны проекты вакуумной системы и фоновой защиты спектрометров ЭПСИЛОН и СКАТ и участка стыковочного нейтроновода спектрометра НЕРА-ПР, разработана документация и заканчивается изготовление дискового фонового прерывателя и трех барабанных λ-прерывателей.

Завершена реконструкция несущей колонны ИБР-2 **(Рис.6)** и биологической защиты головной части 7-го канала для размещения на канале трех нейтроноводов. Демонтировано

оборудование из закладной трубы стены кольцевого коридора. В ООО «НПО «Атом» изготовлены стойки и юстировочные опоры головной части нейтроновода **(Рис.7)**. В ЗАО «Комтраст» продолжается изготовление 92 вакуумных кожухов изогнутых нейтроноводов для спектрометров ЭПСИЛОН и СКАТ.

Рис. 6. Реконструкция несущей колонны здания 117 для проводки изогнутых нейтроноводов спектрометров Эпсилон и Скат.

Рис. 7. Стойки и юстировочные опоры головной части нейтроновода 7 канала.

В настоящее время начинается монтаж головной части (сплиттера) 7 канала и наладка механических узлов прерывателей.

Криостенд

Разработан тестовый криостат для работы с криокулерами замкнутого цикла (**Рис.8)**. В стадии изготовления находится пульт управления системой циркуляции гелия для дополнительных рефрижераторов, которые могут размещаться в этом криостате.

Рис. 8. Тестовый криостат криостенда (1 – криостат , 2 – стойка криостата, 3 – холодная головка, 4 – пульт управления системой циркуляции газа. 5– бак хранения гелия-3).

На криостенде ведутся работы по наладке криогенных систем. В настоящее время проходит модернизацию криостат для неупругого рассеяния нейтронов 7-б канала реактора ИБР-2 (**Рис. 9).** Криостат содержит шахту диаметром 70мм для оперативной холодной перезагрузки образцов. Ожидаемая конечная температура - 4.5 К.

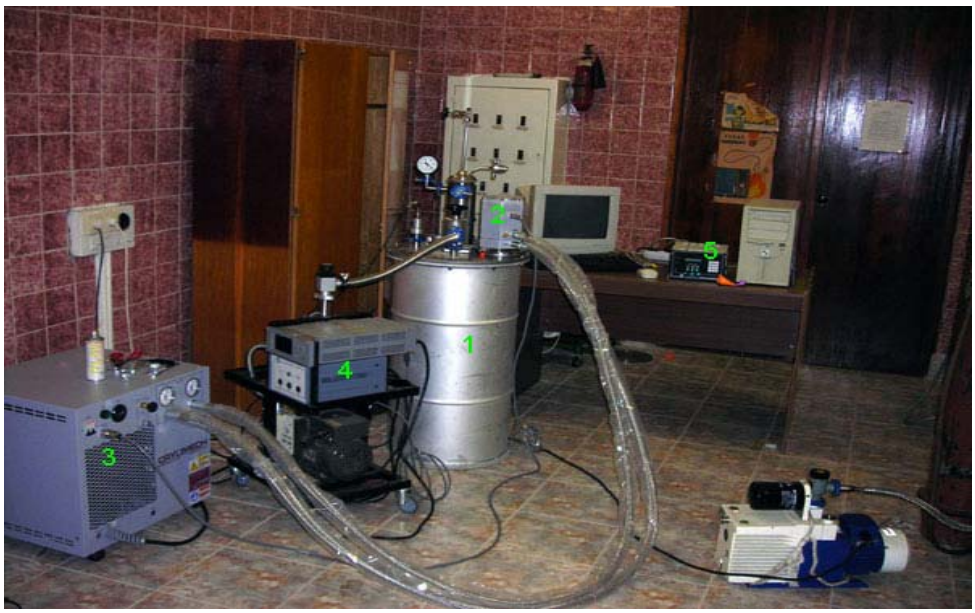

Рис. 9. Шахтный криостат (1 – криостат, 2 – холодная головка, 3 – компрессор, 4 – вакуумный пост, 5 - система контроля и управления температурой).

Развитие систем контроля и управления прерывателями.

В ЛНФ разработана, изготовлена и отлажена система управления прерывателями на базе частотных электроприводов серии VFAS1 фирмы Toshiba (**Рис. 10**) для дискового фонового прерывателя (**Рис. 11**) и трех барабанных λ-прерывателей спектрометров ЭПСИЛОН, СКАТ и НЕРА-ПР. Электропривод имеет встроенный микропроцессор, который реализует алгоритм управления по скорости вращения и по моменту на валу двигателя. На оси двигателя устанавливается инкрементный магнитный кодирующий датчик для измерения скорости и ускорения диска и формирования сигнала, несущего информацию об открытом состоянии прерывателя. Контроллер фазировки СС-07 позволяет регулировать

фазу положения окна диска (барабана) прерывателя относительно старта реактора. Краткие характеристики параметров управления приведены в **Табл. 1**.

Табл. 1

№	Параметр	Фоновый прерыватель	λ-прерыватель	
1	*Мощность двигателя (кВт)*	*22*	*2,2*	
2	*Частота вращения (об/мин)*	*300*	*150*	*75*
3	*Пусковой ток (А)*	*12*	*5*	*5*
4	*Номинальный ток (А)*	*10*	*3*	*4*
5	*Точность стабилизации фазы (мкс)*	*50*	*50*	*100*
6	*Время запуска и стабилизации (мин)*	*10*	*10*	*10*

Рис.10. Электропривод фирмы Toshiba 22 кВт для фонового прерывателя (слева) и два электропривода 2,2 кВт для λ-прерывателей (справа).

Рис.11. Дисковый фоновый прерыватель 7 канала ИБР-2М.

Выполнена разработка системы контроля прерывателей, основанной на микроконтроллерах с CAN интерфейсом. В результате, контроль каждого прерывателя осуществляется компьютером соответствующего спектрометра. Контроллер управления

прерывателем подключается к шине CAN и к ПК (через преобразователь «USB-to-CAN compact»).

Проведенные испытания показали возможность использования частотных приводов VFAS1 и систем управления для замены устаревших ЭКТ2 на прерывателях других спектрометров ИБР-2М.

Расчеты спектрометров

Завершены расчеты спектра нейтронов и оптимизация геометрии пучков от замедлителя до образца для спектрометров EPSILON-SCAT (канал 7а). Это позволит увеличить поток нейтронов на образце на 20-30%. Выполнены также предварительные расчеты для канала 10 (GRAINS). Проведено моделирование установки и ее отдельных элементов, даны рекомендации по увеличению потока нейтронов. Разработаны новые модули программного обеспечения для пакета VITESS:

- модуль для моделирования затухания нейтронного пучка при прохождении через различные элементы среды (включая газы) или комбинации элементов (сплавы, воздух);
- модуль для моделирования движущихся щелей и решеток (работа выполнена совместно с JCNS- Muenchen, Germany).

Детекторы

Изготовлены анодный и катодные электроды, произведены сборка и заполнение газовой смесью позиционно-чувствительного детектора для спектрометра GRAINS. Испытание детектора и измерение его характеристик было проведено на 5 пучке реактора ИР-8 в РНЦ «Курчатовский институт» (испытания проводились с существующей платой De-Li-DAQ).

Детекторы были заполнены тестовой смесью 70 мбар ^{3}He + 2000мбар CF_4 + 2400 мбар ^{4}He. Был выполнен цикл измерений с точечными и щелевыми кадмиевыми масками при различных значениях анодного напряжения и различных уровнях дискриминации входных сигналов. Сняты счетные характеристики ПЧД при точечной и щелевой засветке детектора. Выбраны оптимальные режимы работы детектора и измерены координатное разрешение (не более 2 мм по обеим координатам), неоднородность коэффициента усиления (не более 10%), эффективность детектора и др. С помощью детектора был также измерен профиль 5-го пучка реактора ИР-8 (**Рис. 12**) и установки ИРЕН (**Рис .13**).

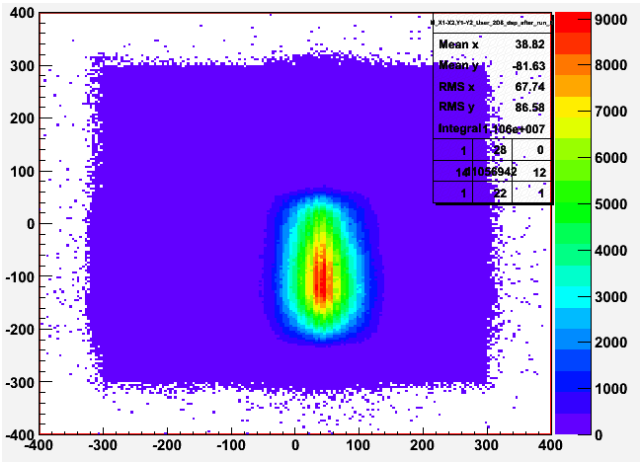

Рис.12. Профиль прямого пучка №5 реактора ИР-8.

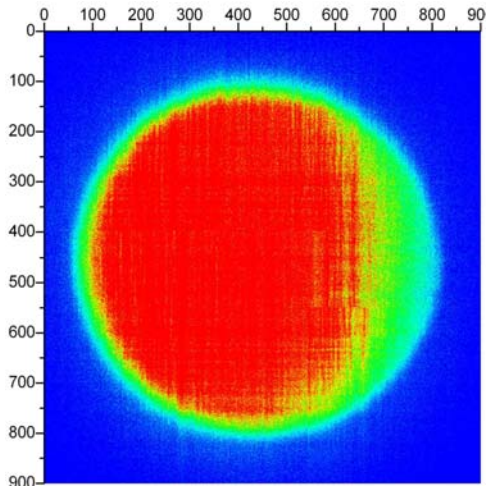

Рис.13. Профиль пучка ИРЕН в тепловой области спектра.

Разработан новый высокоскоростной счетчик нейтронов с предельной загрузкой до $3 \cdot 10^6$ нейтронов/сек (см. **Рис. 14**). Конструктивно счетчик представляет собой прямоугольник из дюралюминия с габаритами 250x80x40мм^3 и с внутренним рабочим объемом 150x30x20мм^3. Анодом служит многонитевая рамка, объединенная в общий электрод, выведенный через вакуумный разъем наружу. В качестве рабочего газа использовалась оптимизированная по давлению смесь ^{3}He и CF_4. Разработана также электроника съема и регистрации данных от счетчика, интерфейс к PC и программное обеспечение. Испытания счетчика были проведены на рефлектометре SuperADAM (ILL, Grenoble, France).

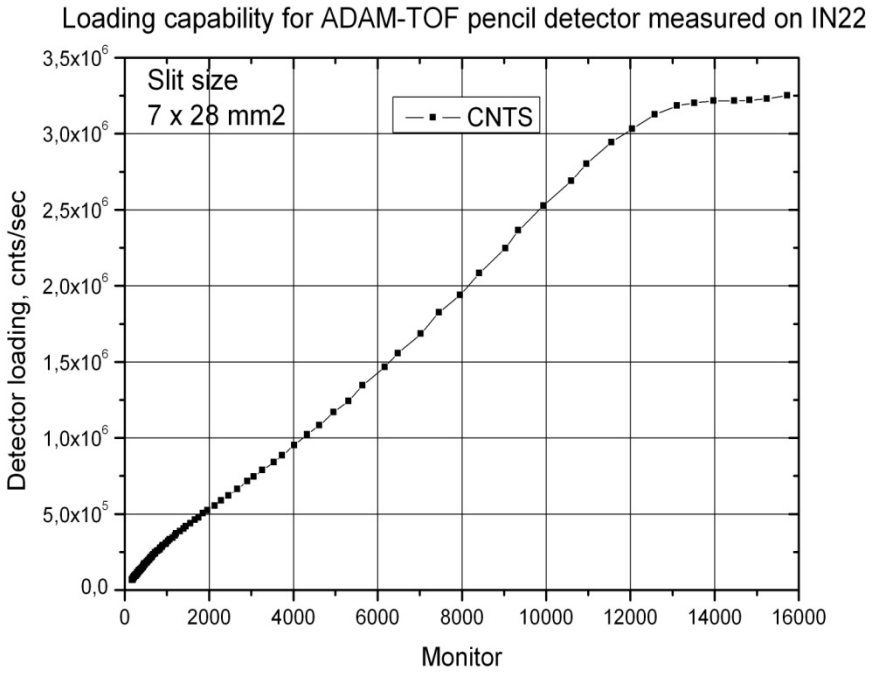

Рис. 14. Загрузочная способность счетчика.

Начата разработка нового кольцевого секционированного детектора на основе MWPC для дифрактометра ДН-6. На первом этапе предлагается создание одного кольцевого детектора для установки под углом рассеяния 90°. Преимущества кольцевого газового секционированного детектора по сравнению с ранее применявшимся на ДН-12 кольцевым детектором на основе газовых счетчиков СНМ-17:

- большие размеры рабочего объема детектора позволят в несколько раз увеличить скорость счета рассеянных нейтронов;
- общий рабочий объем позволяет иметь практически одинаковую эффективность для всех секций;
- прямоугольная геометрия счетных секций должна улучшить однородность эффективности детектора;
- меньшие размеры “мертвых зон” детектора.

Конструктивно детектор представляет собой кольцо, которое разбито на 32 секции. В каждой секции расположена электродная система, состоящая из проволочного анода и двух катодов, ограничивающих чувствительную область детектора. Входным окном для нейтронов будет являться поверхность внутреннего кольца детектора. На входное окно и заднюю стенку наклеиваются тонкие изолированные дрейфовые электроды. В центре находится анодная плоскость, с намотанными на нее 6 тонкими (10-20 мкм) вольфрамовыми проволочками, которые сориентированы по хордам детекторного кольца. Это позволяет

получить координатное разрешение вдоль пучка. Расстояние между анодными нитями ~10 мм. Общее количество измерительных каналов = 32x6=192. На дрейфовые плоскости подается отрицательное высокое напряжение ~ -3-4 кВ. Съем сигнала осуществляется напрямую с анода. Подобная схема позволяет отказаться от использования разделительных емкостей, тем самым, экономя место внутри герметичного объема детектора и повышая надежность. Рабочая газовая смесь состоит из конвертера нейтронов (^{3}He) и гасящего газа (CF_4).

Проектные параметры детектора приведены в **Табл. 2**, внешний вид детектора показан на **Рис. 15**.

Таб. 2. Основные проектные параметры детектора:

№	Параметр	Значение
1.	Ширина входного окна, мм	~70
2.	Количество анодных проволочек в секции	6
3.	Перекрываемый угол, градусов	360
4.	Число секций	32
5.	Число измерительных каналов	192
6.	Эффективность, % (λ=4Å)	~70
7.	Радиус внутреннего кольца, мм	>300
8.	Радиус внешнего кольца, мм	~400
9.	Толщина входного окна, мм	~7
10	Материал корпуса	сплав Al-Mg
11	Толщина чувствительного объема, мм	~40

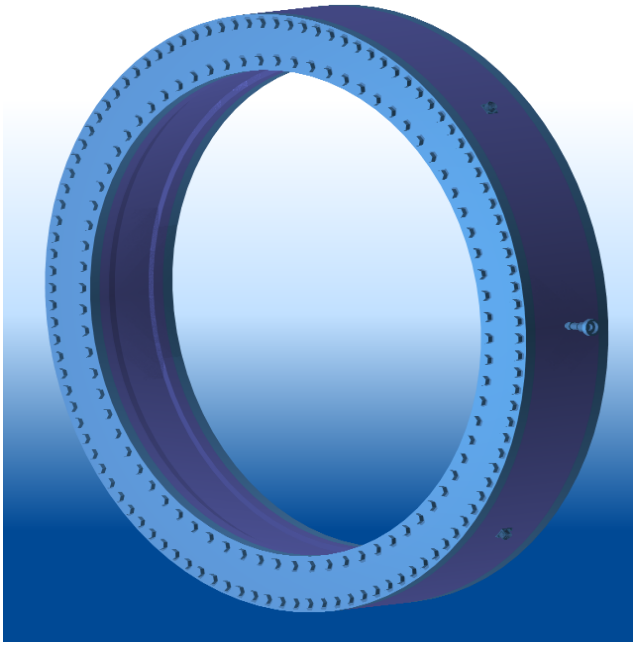

Рис. 15. Эскизный проект кольцевого секционированного детектора (внешний вид).

Электроника, компьютинг

Согласованы технические задания и начата разработка электронных блоков для сбора и накопления сырых данных на дифрактометрах EPSILON,HRFD и DN-6. На этих дифрактометрах будут использоваться различные детекторные системы (EPSILON – до 128 гелиевых нейтронных счетчиков, HRFD – до 200 сцинтилляционных пластин с покрытием ZnS/^{6}LiF и сбором света с помощью спектросмещающих волокон, DN-6 – кольцевой

секционированный детектор на основе многопроволочной пропорциональной камеры с числом секций – 32 и числом измерительных каналов – до 192), но общим для них является то, что все эти системы могут рассматриваться как некий массив точечных детекторов с фиксированной пространственной геометрией. Это позволяет применить единый подход к созданию систем сбора данных для указанных дифрактометров, т.е. проектировать одинаковые с точки зрения hardware электронные блоки, в которых все функции, как общие (кодирование номера детектора, регистрация времени пролета), так и специфические для конкретного дифрактометра, реализуются на уровне микропрограмм, выполняемых в FPGA соответствующего блока.

Разработана новая тестовая программа и завершено тестирование быстродействующего DAQ блока для 1D и 2D MWPC детекторов со съемом информации с линий задержки. По результатам тестирования оптимизированы все микропрограммы FPGA для работы в различных режимах накопления данных, выполнена перетрассировка печатных плат и размещен заказ на их изготовление. Указанная тестовая программа является основой для создания стандартного интерфейса к пакету Sonix+.

Разработан план-график проведения профилактических работ на спектрометрах ИБР-2, в соответствии с которым будут осуществляться модернизация и ремонт электронного оборудования и подготовка спектрометров к пуску реактора. Эти работы уже ведутся на четырех спектрометрах.

В 2009 г. в локальной вычислительной сети ОИЯИ установлено новое оборудование внешних каналов связи для работы на скоростях до 10 Гбит/с. Это в свою очередь требует частичной замены существующего коммутационного оборудования в центральном и периферийных сегментах сети ЛНФ. Проведен анализ возможных изменений в архитектуре сети и характеристик доступного на рынке оборудования с учетом перспектив дальнейшего развития сети. В условиях ограниченного финансирования принято решение приобрести в текущем году один интеллектуальный многоуровневый маршрутизатор серии WS-3560, способный работать в разных конфигурациях Fast Ethernet и Gigabit Ethernet и обеспечивающий высокий уровень доступности, масштабирования, безопасности и управления. Будет приобретен также ограниченный набор коммуникационных модулей для этого маршрутизатора. Соответствующий контракт находится в стадии реализации. После испытаний указанное оборудование будет установлено в одном из экспериментальных залов ИБР-2М. В течение года выполнен большой объем работ по поддержке и модернизации сетевой инфраструктуры ЛНФ.

4. EXPERIMENTAL REPORTS

4.1. CONDENSED MATTER PHYSICS

1. Combined Investigations of Ferrofluids with Neutron and Synchrotron Radiation Scattering.
   M.V. Avdeev, A.V. Feoktystov, V.L. Aksenov, L. Vekas, A.V. Porokhova, Y.V. Zubavichus, A.A. Veligzhanin, L. Rosta, V.M. Garamus, R. Willumeit
2. Mass Spectrometry Study of Fullerene C60 Solutions.
   M.V. Avdeev, O.A. Kyzyma, T.V. Tropin, S.V. Snegir
3. Small Angle Neutron Scattering Investigations of Ferrofluid – Elastomer Composites.
   M. Balasoiu, I. Bica, A.V. Rogachev , A.I. Ivankov , J. Plestil, L. Almasy, B. Vatzulik, A.I. Kuklin
4. The Study of Structure Aspects of Optical Properties in the Nanosystem GeO_2-Eu_2O_3-Ag.
   A.V. Belushkin, S.E. Kichanov, D.P. Kozlenko, E.V. Lukin, B.N. Savenko, S.K. Rakhmanov, G.P. Shevchenko, V.S. Gurin, G.E. Malashkevich, V. Haramus, D.K. Pogoreliy, K.M. Podurets
5. Investigation of Liquid Lithium Relaxation Time by Means of the Memory Function Formalism.
   N. Blagoveshchenskii, A. Novikov
6. SANS and SAXS Study of Laser Pyrolysis Carbon Nanostructures.
   R. V. Erhan, M. Balasoiu, E. Barna, I. Morjan, E. Anitas, J. Plestil, Yu.S. Kovalev and A. I. Kuklin
7. Pressure Induced Changes in Magnetic Structure of $BiMnO_3$.
   S.E. Kichanov, D.P. Kozlenko, B.N. Savenko, I. Mirebeau, O.L.Makarova
8. Extraction and Mass Spectroscopy of Aggregates in C_{60}/N-Metyl-2-Pyrrolidone and Its Mixture With Water.
   O.A. Kyzyma, M.V. Avdeev, V.L. Aksenov, L.A. Bulavin, M.V. Korobov, S.V. Snegir
9. Is Solvatochromism Related to Fullerene Cluster Formation in C_{60}/N-Methyl-2-Pyrrolidone?
   O.A. Kyzyma, M.V. Avdeev, V.I. Petrenko, V.L. Aksenov, L.A. Bulavin, M.V. Korobov, V.M. Garamus
10. Elastic Properties of Reactor Graphite GR-280 and Their Anisotropy from Neutron Diffraction and Ultrasonic Measurements.
    T. Lokajicek, P. Lukas , A.N. Nikitin, I.V. Papushkin, V.V. Sumin, R.N. Vasin
11. Структура гидридов $CeNi_3$ после десорбции водорода.
    С.А. Лушников, И.А. Бобриков, А.М. Балагуров, В.П. Глазков, В.А. Соменков
12. Using Individual Spectra Simulation for Study of Pole Figures Errors.
    T.A. Lychagina, D.I. Nikolayev, F. Wagner, C. Scheffzuek
13. Neutron Reflectometry Mode at Mond Diffractometer of IR–8 Reactor.
    N.F. Miron, A.B. Rubtsov, V.A. Somenkov, V.I. Bodnarchuk, S.P. Yaradaikin
14. Small-Angle Neutron Scattering From Very Diluted Magnetic Fluids.
    A.V. Nagornyi, V.I. Petrenko, M.V. Avdeev, V.L. Aksenov, L.A. Bulavin
15. SAS Study of the Structure and Properties of Carbosilane Dendrimers.
    A.V. Rogachev, A.Yu. Cherny, A.N. Ozerin, A.M. Muzafarov, E. Atatarinova, V.I. Gordeliy, A.I. Kuklin
16. Результаты первого синхротронного исследования структуры многослойных везикул смеси сфингомиелен/фосфолипиды.
    Н.Ю. Рябова, М.А. Киселёв, О.В. Найда, А.В. Забелин, А.М. Балагуров

17. The Upgrade of Package for Preliminary Treatment of Small-Angle Scattering Spectra.
A.G. Soloviev, T.M. Solovieva, S.A.Kutuzov, A I. Kuklin

4.2. NEUTRON NUCLEAR PHYSICS

1. Heavy Metals in the Environmental Objects of Non-Ferrous Industrial Region of Mongolia, the Town of Erdenet.
N. Baljinnyam, Sh. Gerbish, G. Ganbold, S. Lodoysamba, M.V. Frontasyeva, S.S. Pavlov
2. Investigation of Periodic Multilayers.
V. Bodnarchuck, V. Ignatovich, S. Yaradaykin, L. Cser, T. Veres
3. INAA for Studying Hg (II) Accumulation by Arthrobacter Globiformis.
M.V. Frontasyeva, S.S. Pavlov, I.I. Zinicovscaia, N. Tsibakhahsvili, L. Mosulishvili, E. Kirkesali, I. Murusidze, P. Bode, and Th.G. van Meerten
4. Cross Section Measurement for the ^{95}Mo(n, α)^{92}Zr Reaction at 4.0, 5.0 and 6.0 meV.
Zhang Guohui, Zhang Jiaguo, Wu Hao, Liu Jiaming, and Chen Jinxiang, Yu.M. Gledenov, M. V. Sedysheva, G. Khuukhenkhuu, P. E. Koehler, P. J. Szalanski
5. Level Density, Radiative Strength Functions from the $(n_{th},2\gamma)$ Reaction and Main Properties of the ^{96}Mo Nucleus.
V.A. Khitrov, A.M. Sukhovoj
6. Investigation of Light Element Contents in Subsurface Layers of Silicon.
A.P. Kobzev, J. Huran, D. Maczka, M.Turek
7. Extraction of the Neutron-Electron Scattering Length from the Neutron Diffraction Data Measured on Noble Gases.
L,V. Mitsyna, V.G. Nikolenko, S.S. Parzhitski, A.B. Popov, G.S. Samosvat
8. An Influence of Hypothetical Extra-Short-Range Interaction on the Scattering Anisotropy of Cold Neutrons by Noble Gases.
A.B. Popov
9. Measurement of Neutron Total Cross-Section and Resonance Parameters of Xenon.
V.R. Skoy, T.F. Wang, G.N. Kim, Y.D. Oh, M.H. Cho, I.S. Ko, W. Namkung
10. Multicrystal Scintillation Detector for Investigation of Angular Correlations in (n,γ) Reactions.
V.R. Skoy, Guinyun Kim, Manwoo Lee, and Kyung Sook Kim
11. Neutron Activation Analysis for Air Pollution Study in Croatia.
Z. Spiric, M.V.Frontasyeva, S.S. Pavlov, S.F. Gundorina, T.M. Ostrovnaya
12. Neutron Emission in Fission of ^{252}Cf(SF).
Sh. Zeynalov, F.-J. Hambsch, S. Oberstedt, I. Fabry
13. DSP Algorithms for Fission Fragment and Prompt Fission Neutron Spectroscopy
O. Zeynalova, Sh. Zeynalov, F.-J. Hambsch, S. Oberstedt, I. Fabry

COMBINED INVESTIGATIONS OF FERROFLUIDS WITH NEUTRON AND SYNCHROTRON RADIATION SCATTERING

M.V.Avdeev[a], A.V.Feoktystov[a,b], V.L.Aksenov[c,a,d], L.Vekas[e], A.V.Porokhova[d,c], Y.V.Zubavichus[c], A.A.Veligzhanin[c], L.Rosta[f], V.M. Garamus[g], R. Willumeit[g]

[a]*Frank Laboratory of Neutron Physics, Joint Institute for Nuclear Research, Dubna, Russia*

[b]*Taras Shevchenko Kyiv National University, Kyiv, Ukraine*

[c]*Russian Research Center "Kurchatov Institute", Moscow, Russia*

[d]*Physical Faculty, Moscow State University, Moscow, Russia*

[e]*Center for Fundamental and Advanced Technical Research, Romanian Academy, Timisoara Division, Romania*

[f]*Research Institute for Solid State Physics and Optics, Hungarian Academy, Budapest, Hungary*

[g]*GKSS Research Centre, Geesthacht, Germany*

Complex investigations of the size regulation effect for magnetite nanoparticles in ferrofluids with non-polar organic carriers and stabilization by monocarboxylic acids, have been completed. They included diffraction and small-angle scattering of synchrotron radiation (Kurchatov Center of Synchrotron Radiation and Nanotechnology), as well as small-angle scattering of non-polarized (RISSPO HAS, Hungary) and polarized neutrons (GKSS, Germany). It is confirmed that replacing of non-saturated oleic acid (C_{18}) used in the classical stabilization procedure with saturated acids from a series of lauric (C_{12}), myristic (C_{14}), palmitic (C_{16}), stearic (C_{18}) acids results in a decrease in the effective size of stabilized magnetite [1]. In particular, diffraction and small-angle scattering of synchrotron radiation (Fig.1*a*,*b*) show a difference in the size of the coherent scattering region of magnetite between samples stabilized by oleic acid and saturated fat acids. The combined use of the two methods allows us to conclude reliably that the revealed effect is related to the change in the size of the dispersed magnetite, but not with the differences in the possible aggregation. The small-angle neutron scattering data (Fig.1*c*) obtained for the samples in the deuterated solvent again show a great difference in the curves for oleic acid and saturated acids. Also, a modulation of the scattering over the length of the used surfactanf is observed. In addition to the parameters of the particle size distribution the thickness of the surfactant stabilizing shell is obtained. The numerecal data of the fits are gathered in Table 1. The principle scheme of the found effect is presented in Fig.3. As a result, it has been shown that the characteristic magnetite size can be changed within interval of 5 – 8 nm by using various surfactant mixtures.

Table 1. Results of the synchrotron and neutron analysis of the magnetic particle structure in the studied MFs including the mean magnetite size from the widening of diffraction peaks (D_{diffr}), parameters of the log-normal size distribution of magnetite (D, σ), effective thickness of the surfactant shell (h).

Sample	D_{diffr}, nm	D, nm	σ, nm	h, nm
OA	8.6	7.31	2.88	1.40
LA	5,7	5.30	1.51	1.85
MA	5,0	5.16	1.47	1.55
PA	5,1	5.51	1.57	1.35
SA	4,9	5.22	1.49	1.25

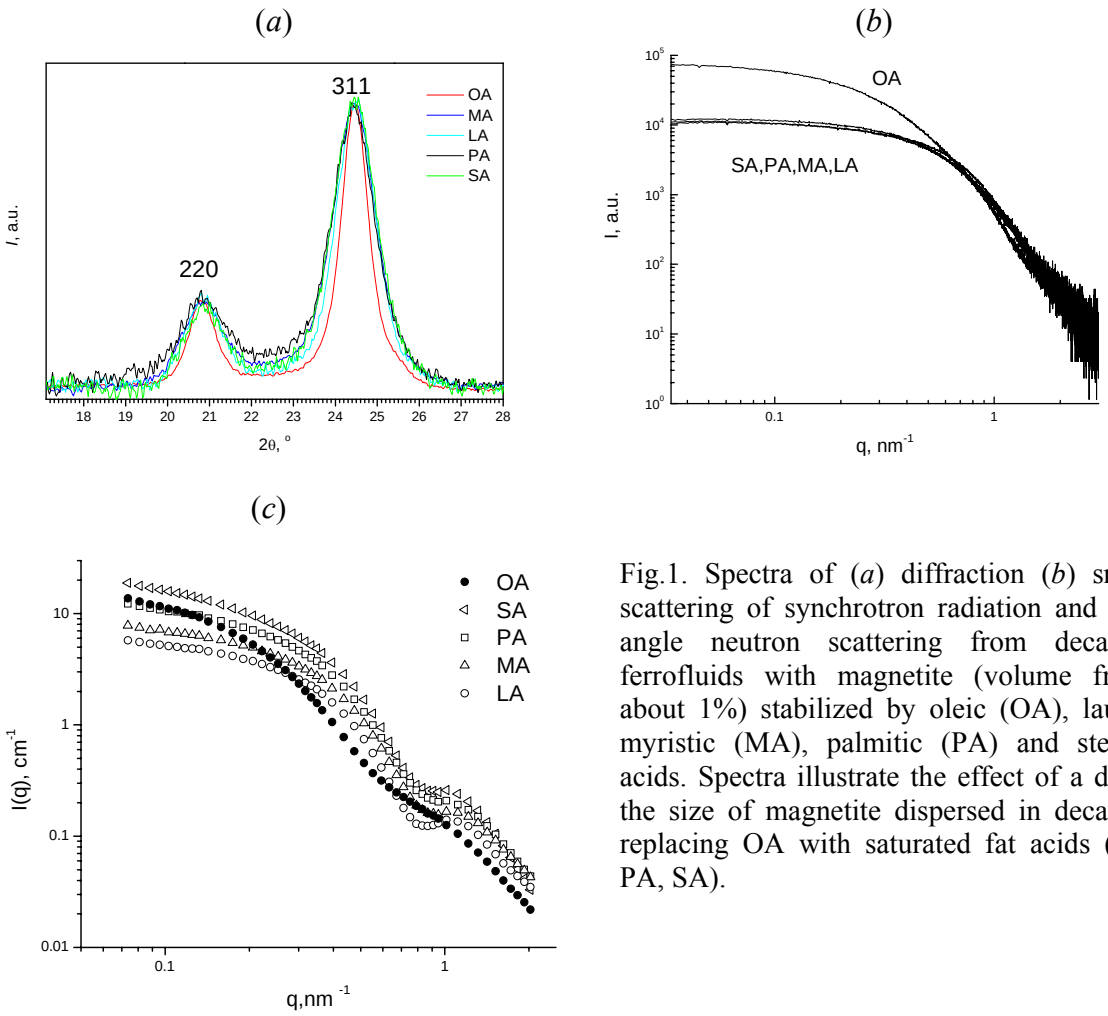

Fig.1. Spectra of (*a*) diffraction (*b*) small-angle scattering of synchrotron radiation and (*c*) small-angle neutron scattering from decaline-based ferrofluids with magnetite (volume fraction of about 1%) stabilized by oleic (OA), lauric (LA), myristic (MA), palmitic (PA) and stearic (SA) acids. Spectra illustrate the effect of a decrease in the size of magnetite dispersed in decaline when replacing OA with saturated fat acids (LA, MA, PA, SA).

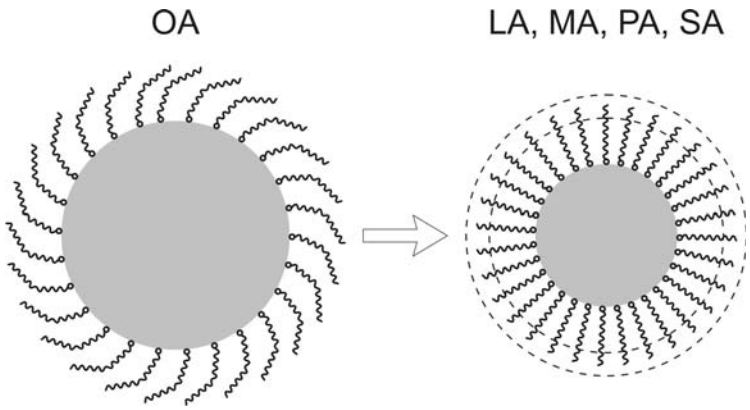

Fig.2. Schematic representation of the effect of the change in the magnetite size in ferrofluids when replacing oleic acid (OA) with saturated fat acids (LA, MA, PA, SA). Dashed lines in the right image denote the boundaries of the surfactant shell depending on the used acid.

The work has been performed with the support of the Helmholtz (Germany) –RFBR grant, Joint Research Groups (HRJRG-016).

[1] M.V.Avdeev, D.Bica, L.Vekas, V.L.Aksenov, A.V.Feoktystov, O.Marinica, L.Rosta, V.M.Garamus, R.Willumeit. Comparative structure analysis of non-polar organic ferrofluids stabilized by saturated mono-carboxylic acids. *J. Colloid Interface Sci*. 334 (2009) 37–41.

MASS SPECTROMETRY STUDY OF FULLERENE C60 SOLUTIONS

M.V.Avdeev[a], O.A.Kyzyma[a,b], T.V.Tropin[a], S.V.Snegir[c]

[a]*Frank Laboratory of Neutron Physics, Joint Institute for Nuclear Research, Dubna, Russia*

[b]*Taras Shevchenko Kyiv National University, Kyiv, Ukraine*

[c]*Institute of surface chemistry, NAS of Ukraine, Kiev, Ukraine*

The laser desorption/ionization mass spectrometry (LDI MS) and its variations is a well-proven method for detecting molecule types in different systems including biomolecules (proteins, peptides, sugars), large organic molecules (polymers, dendrimers), as well as synthetic structures and nanomaterials [1]. Mass spectrometry is often used in studies of fullerenes and their derivatives [2,3]. In the given paper we apply LDI MS to fullerene C_{60} dissolved in different solvents and then dried. Here, we find that in addition to this typical mass spectrum of C_{60} in molecular state for the precipitated fullerene some features exist depending on the initially used solvent. They correlate to some extent with a tendency of C_{60} towards the formation of aggregates in the solutions, which is determined by the solvent polarity [4]. The aggregates (size 10-100 nm) can appear in these solutions under non-equilibrium conditions. The examples based on the results of dynamic light scattering, electron microscopy and small-angle neutron scattering are the solutions of C_{60} in carbon disulfide [5], toluene [6], benzene [4]. The aggregation effect is more pronounced in polar solvents like pyridine [7], N-methyl-pyrrolidone [8], benzonitrile [4]. The larger aggregates (size up to 500 nm) appeared within about one month after the dissolution of C_{60} are rather stable with respect to shaking and ultrasonication indicating that the binding in them is quite strong. In the current study the solutions of C_{60} are based on the solvents with various polarity including carbon disulfide (CS_2, $\varepsilon = 1.6$), toluene (TL, $\varepsilon = 2.4$), benzene (BZ, $\varepsilon = 2.7$) and N-methyl-pyrrolidone (NMP, $\varepsilon = 32$).

Saturated solutions of fullerene C_{60} (Fullerene Technologies, purity > 99.5%) in benzene, toluene, carbon disulfide and NMP (all from Merck, purity > 99.5%) are prepared by stirring for four days at room temperature. The UV-Vis spectra repeat well the standard dependences for these solutions. Laser desorption/ionization time-of-flight mass spectrometry is performed on the Bruker Daltonics Autoflex II instrument. Both the positive and negative ion extraction modes are used. LDI MS experiments are performed on fresh (right after the preparation) and old (one month after the preparation) solutions. Between these experiments the solutions are kept in dark at room temperature.

The spectra for the samples prepared from all solutions are compared in Fig. 1. Mass spectrum of C_{60} in the molecular state contains the only peak at m/z = 720.6 Da [9]. Here, one can see that besides this pronounced peak the spectra have additional peculiarities, which depend on the initially used solvent. In the case of C_{60}/CS_2 (Fig. 1 (a)) there is also a small peak at m/z = 736.6 Da, which we relate to ions $[C_{60}O]^+$. The signals from other possible fragments are of the order of the background level. The spectra from the samples C_{60}/BZ (Fig. 1(b)), C_{60}/TL (Fig. 1(c)) and C_{60}/NMP (Fig. 1 (d)) represent the sets of peaks differing by 24 Da due to the fact that the excited fullerene loses even number of carbon atoms under laser desorption/ionization. In all these samples the lower masses are identified as ion fragments C_{58}, C_{56},…C_{48}, which are a result of decomposition of the excited molecular ions stabilized by the detachment of C_{2n} with n = 1,2,…6.

The significant difference between C_{60}/CS_2 (non-polar), C_{60}/BZ, C_{60}/TL (low polarity) and C_{60}/NMP (polar) can be seen for higher masses. In C_{60}/BZ (Fig. 1 (b)) and C_{60}/TL (Fig. 1(c)) there is a group of peaks close to m/z = 1440 Da, which can be described by desorption/ionization of the C_{60} dimer. These signals are less intensive than the $[C_{60}]^+$ signal by about three orders of magnitude, but are still well distinguished against the background. In the case of C_{60}/NMP (Fig. 1 (d)) several

peak groups corresponding to multiples (up to 10) of the C_{60} mass are determined. Now, the signals from dimers are only three times smaller than the signals from $[C_{60}]^+$.

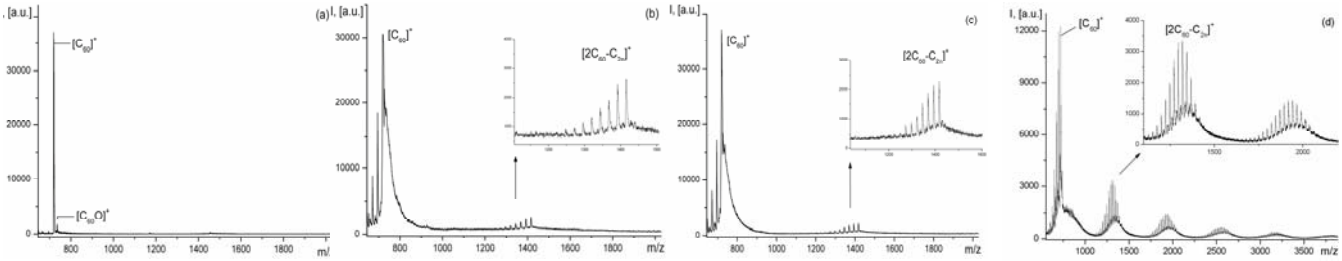

Fig. 1. Mass spectra of fullerene C_{60} for different solutions: (a) – CS_2; (b) – BZ; (c) – TL; (d) – NMP.

In fact, the clear dependence of the signals from aggregates on the used solvent type indicates that these aggregates exist in the samples before the laser desorption/ionization. The similar asymmetry of the peak distribution in the observed groups points to their common origin for the three solvents. If one takes into account that the solutions C_{60}/NMP reveal quite intensive aggregation right after the dissolution, the discussed peak groups can be well associated with the aggregates appeared in the initial solutions. In this connection, the difference in the ion formation between dimer of C_{60}/TL and C_{60}/NMP for the mass range of 1000–1600 Da (Fig. 2) can be well explained in terms of the aggregate decomposition. It can be described by the formula $[2C_{60}\text{-}C_{2n}]^+$, where n is the number of atoms emitted by the exited ion under stabilization. For C_{60}/BZ, C_{60}/TL and C_{60}/NMP n is equal to 1, 2, …, 7 and 1, 2,…, 12, respectively. It means that the stabilization of the desorbed and exited dimer ions goes via the detachment of carbon pairs with the possibility of further decomposition into two parts $2C_{60}\text{-}C_{2n} = (C_{60}\text{-}C_{2j}) + (C_{60}\text{-}C_{2k})$, where $j + k \geq 7$ for C_{60}/BZ and C_{60}/TL. In contrast, the aggregate fragmentation in C_{60}/NMP (Fig. 2 (*a*)) is much deeper with $j + k \geq 12$. The most abundant ion signals for C_{60}/NMP and C_{60}/TL are related to the ions $[2C_{60}\text{-}C_{10}]^+$ and $[2C_{60}\text{-}C_2]^+$, respectively. It is possible that the ablation of the molecules in C_{60}/BZ, C_{60}/TL goes via desorption of intact exited monomers, dimers and trimers. The next step is the ionization and stabilization by emitting C_{2n} ($n < 7$). As for the C_{60}/NMP system desorption/ionization processes are differing from the other systems and might be connected with intermolecular interactions that have strong impact on the signal formation (Fig. 2).

The effect of the solution age on the mass spectra also supports the relation of the obtained mass spectra with the aggregates in the initial solutions. If the spectra for C_{60}/CS_2, C_{60}/TL, C_{60}/BZ do not show any change with respect to the fresh and old (one month) solutions, the spectrum for the sample C_{60}/NMP prepared from the old solution (Fig. 3) is totally different as compared to the sample prepared from the fresh solution. The characteristic groups of peaks for small aggregates disappear, and the only pronounced signals with low intensity again correspond to single C_{60} ions and its fragments in the low mass range. This correlates well with the time increase in the aggregate size in C_{60}/NMP revealed by dynamic light scattering and small-angle neutron scattering [10].

It is interesting to follow how the peak groups corresponding to the aggregates change with increasing laser fluence (Fig. 4). The character of the spectrum for C_{60}/CS_2 solution does not depend on the laser fluence. For the systems C_{60}/BZ and C_{60}/TL we can clearly see an increase in the peak intensity of the group corresponding to dimers. In the case of C_{60}/NMP the effect of the fluence increase is the most pronounced. In addition to a clear increase in the initial groups of peaks in Fig. 2 (d), new groups corresponding to higher aggregates (containing up to 10 molecules of C_{60}) appear. This shows that the laser energy is now enough for desorption of quite large molecules.

As it was mentioned in the Introduction part, the fullerene crystals (fullerites) are characterized by comparatively weak Van-der-Waals bonds between C_{60} molecules. This means

that the fullerene aggregation in solutions is more complicated process in comparison with crystallization. The chemical interaction with the solvent should be involved to explain the formation of new type of bonds, which, in fact, transforms in some cases initially molecular solutions of C_{60} to colloidal systems. The development of the specific fullerene-solvent interaction is supported by solvatochromic effects in these solutions, as well as by characteristic IR and Raman spectra.

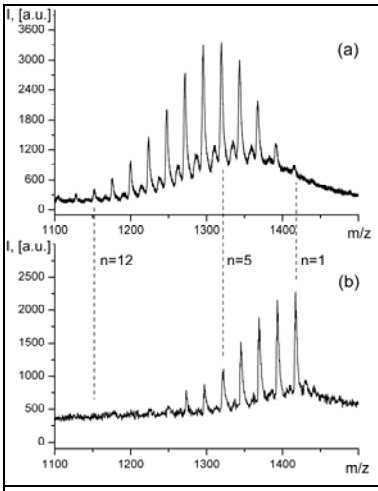

Fig.2. Mass spectra of positive ions of fullerene C_{60} for (*a*) – C_{60}/NMP (*n* =1,2,…12); (*b*) – C_{60}/TL (*n* = 1,2,…7).

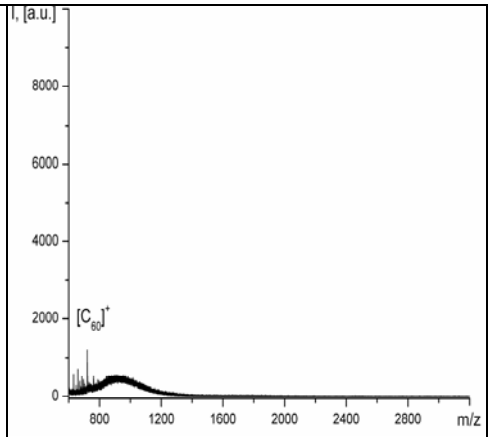

Fig.3. Mass spectrum of positive ions of fullerene C_{60} for C_{60}/NMP one month after solution preparation.

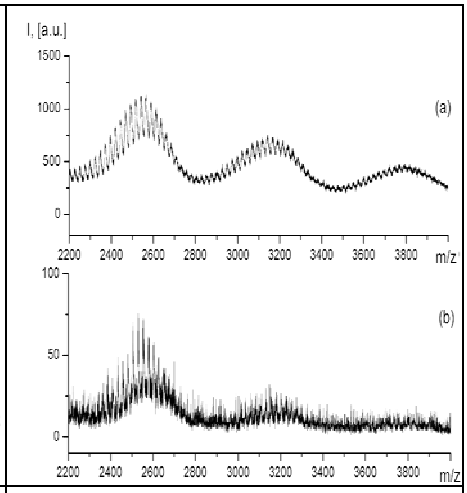

Fig.4. Mass spectra of positive ions of fullerene C_{60} for C_{60}/NMP obtained under laser fluence: (a) – 110 mj/cm^2; (b) – 70 mj/cm^2.

The correlation between aggregation in solutions of C_{60} and mass spectra from dried samples is observed. It is concluded from (i) the comparison of solutions with different polarities; (ii) the ageing effect for the solution, where the aggregates certainly form and develop with time. This suggests the binding of C_{60} molecules into the aggregates, which is weakly affected by laser desorption/ionization parameters. It takes place not only in large aggregates (aggregate numbers above 10000), but also in small associates (aggregate numbers below 10). We suppose that the found effect has prospects for developing mass spectrometry research of liquid-containing systems.

References

[1] Khitrov GA, Strouse GF. J. Am. Chem. Soc. 2003; 125 (34): 10469.
[2] Fati D, Vasil'ev YV, Wachter NK, Taylor R, Drewello T. Int. J. Mass Spectrom. 2003; 229: 3.
[3] Manil B, Maunoury L, Huber BA, Jensen J, Schmidt HT, Zettergren H, Ceberquist H, Tomita S, Hvelplund P. Phys. Rev. Lett. 2003; 91: 215504.
[4] Nath S, Pal H, Sapre AV. Chem. Phys. Lett. 2000; 327: 143.
[5] Tropin TV, Avdeev MV, Aksenov VL. Fullerenes Nanotubes Carbon Nanostruct. 2008; 16: 616.
[6] Torok G, Lebedev VT, Cser L. Phys. Solid State. 2002; 44: 572.
[7] Mrzel A, Mertelj A, Omerzu A, et al. J. Phys. Chem. 1999; 103: 11256.
[8] Alfe M, Apicella B, Barbarella R, et al. Chem. Phys. Lett. 2005; 405: 193.
[9] Yeretzian Ch, Beck RD, Whetten RL. Int. J. Mass Spectrom. Ion Proc. 1994; 135: 79.
[10] Aksenov VL, Avdeev MV, Tropin TV, Kozhemyakina NV, Avramenko NV, Rosta L. Physica B. 2006; 385: 795.

Small angle neutron scattering investigations of ferrofluid – elastomer composites

M.Balasoiu[1,2], I.Bica[3], A.V. Rogachev[1] , A.I. Ivankov[1] , J.Plestil[4], L.Almasy[5], B.Vatzulik[3], A.I.Kuklin[2]

.[1]National Institute of Physics and Nuclear Engineering, Bucharest, Romania
[2]Joint Institute of Nuclear Research, Dubna, Russia
[3]West University of Timisoara, Department of Electricity and Magnetism, Timisoara, Romania
[4]Institute of Macromolecular Chemistry, Academy of Sciences of the Czech Republic, Prague
[5]Paul Sherrer Institute, Villigen, Switzerland
email balasoiumaria@yahoo.com

The interest in rubber-like smart active material devices in recent years stimulates an increasing number of efforts on both basic and applied research aspects for new elastomer technology. Magnetic elastomers belong to a specific class of so-called smart materials because they can respond to changes in their environment. They are composed of magnetic particles and a low-permeability matrix. Applying an external magnetic field, a structure will be formed inside the material or the structure embedded in the material will be changed [3-5].

In this work, the variation of the ferrofluid-elastomer microscopic properties due to particle concentration variation and application of a magnetic field during the polymerization process is investigated by means of SAXS and SANS methods.

The magnetic elastomer (ME) is produced by using the procedure described in Ref.[1]. It is composed from (in vol. %): 60%-70% silicone rubber (SR) (RTV 3325PC-Bluestar Silicones SAS); 1% silicone oil (SO), Merk type, with viscosity of ~200 mPas and density of ~ 1040 kg $\cdot$ m^{-3} ; 5% catalyst (C), 60R (Rhone-Poulenc) type; 34%-24% Fe_3O_4 ferrofluid [2] based on transformer oil (Fig.1).

A small angle X-ray scattering (SAXS) experiment on magnetic elastomers samples was performed on the Rigaku SAXS spectrometer at IMC, Prague, in the Q, momentum transfer value range of 0.004 - 1.1 A^{-1} (Fig.2).

Fig.1 Example of magnetic elastomer samples.

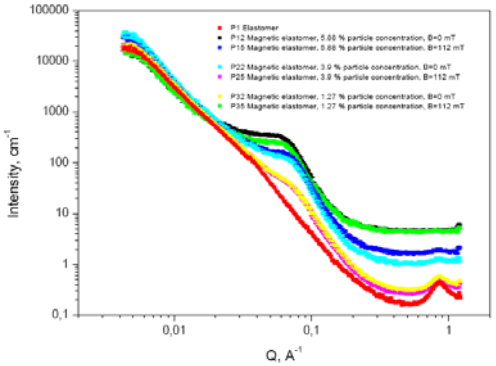

Fig. 2 SAXS experimental curves from sample P12, P15, P22, P25, P32, P35 and a simple elastomer P1, obtained at Rigaku spectrometer at IMC, Prague.

A small angle neutron scattering (SANS) experiment on magnetic elastomers samples was performed on the SINQ time-of-flight spectrometer SANS II, in the Q, momentum transfer value range of 0.015 - 1.8 nm^{-1} (Fig.3)

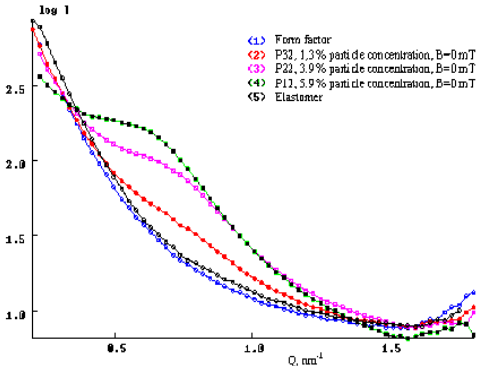

Fig. 3 SANS experimental curves for the magnetic elastomer samples with 5.88% (P12), 3.9% (P22), 1.27% particle volume concentrations (P32), for the elastomer matrix (P1) and the form factor curve.

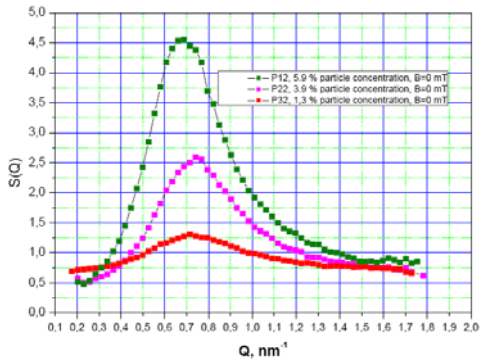

Fig. 4 Representation of the structure factor of the magnetic elastomer samples with 5.88% (P12), 3.9% (P22) and 1.27% particle volume concentrations (P32) polymerized in ZF.

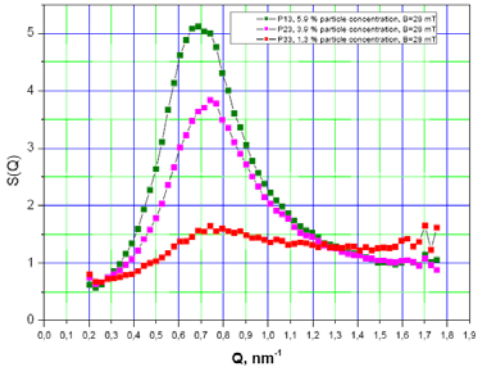

Fig. 5 Representation of the structure factor of the magnetic elastomer samples with 5.88% (P13), 3.9% (P23) and 1.27% particle volume concentrations (P33) polymerized in magnetic field of 28 mT.

From structure factor functions, ***S(Q)*** (Fig.4 and Fig.5), the particle correlation lengths are obtained (Table 1).

Table1

Samples	Particle volume concentration [%]	Polymerization field [mT]	Correlation length [nm]
P12	5.88	0	9.17
P22	3.9	0	8.49
P32	1.27	0	8.16
P13	5.88	28	8.97
P23	3.9	28	8.49
P33	1.27	28	8.49

As preliminary results the following are remarked: (i) with the particle concentration, the correlation length in the composite is slightly increasing; (ii) the application of a transversal magnetic field (28 mT) during the polymerization process induces smaller modification than the particle concentration variation on the ferrofluid-elastomer XY microstructure.

Further data analyses are in progress.

References

[1] I.Bica, Mater. Lett. 63 (2009)2230
[2] D.Bica, RO Patent 90078(1985)
[3] M .Balasoiu, M.L.Craus, A.I.Kuklin, et al, JOAM, Vol.10 Issue 11 (2008)2932
[4] M .Balasoiu, E.M.Anitas, I.Bica, et al., OAM-RC, Vol.3 No.6 (2009) 621-624
[5] M .Balasoiu, M.L.Craus,E.M.Anitas, et al, FTT, Vol52 Issue 5(2010)861-865

THE STUDY OF STRUCTURE ASPECTS OF OPTICAL PROPERTIES IN THE NANOSYSTEM GeO_2-Eu_2O_3-Ag

A.V.Belushkin, S.E.Kichanov*, D.P.Kozlenko, E.V.Lukin, B.N.Savenko
Frank Laboratory of Neutron Physics, JINR, Russia
* e-mail: ekich@nf.jinr.ru

S.K.Rakhmanov, G.P.Shevchenko, V.S.Gurin
Research Institute for Physical Chemical Problems of the BSU, 220080, Minsk, Belarus

G.E.Malashkevich
B.I.Stepanov Institute of Physics NASB, 220072 Minsk, Belarus

V.Haramus
GKSS, D-21502, Geesthacht, Germany

D.K.Pogoreliy, K.M. Podurets
Russian Research Center "Kurchatov Institute", 123182, Moscow, Russia

Introduction

At the present time one of the topical problems in optoelectronics is a search for nanosystems, which under excitation with light could efficiently radiate energy in a given spectrum range with minimal losses [1]. The promising materials are nanostructured oxide systems synthesized by colloidal chemical methods and containing rare-earth and noble metal ions [2-4]. Their physical and functional properties depend on both the chemical composition of oxide matrixes and nanosystem active components and the structure parameters of all nanosystem constituents. In our work most attention is focused on the research of crystal structure and structure aspects of cluster formation in GeO_2 xerogels containing europium and silver. The xerogels with compositions of $95GeO_2–5Eu_2O_3$, $94.9GeO_2–5Eu_2O_3–0.1Ag$ and $99.9GeO_2–0.1Ag$ were annealed in air up to T_O = 850°C and investigated by means of X-ray diffraction and small-angle neutron scattering.

Experimental

The small-angle neutron scattering experiments were carried out with the spectrometer SANS-1 [5] on the research reactor FRG-1 (GKSS, Germany). The X-rays diffraction experiments were performed with the powder diffractometer at the experimental station "Mediana" (synchrotron radiation source "Siberia-2", RRC "Kurchatov Institute") [6].

Results and discussions

It was determined that the $99.9GeO_2–0.1Ag$ system synthesized at T_O = 150°C is amorphous and at T_O > 200°C is crystallized into hexagonal phase with $P3_221$ symmetry. The $95GeO_2–5Eu_2O_3$ and

94.9GeO_2–5Eu_2O_3–0.1Ag systems obtained at T_O = 150-800°C also have hexagonal structure with $P3_221$ symmetry.

The formation of polydisperse clusters in the 95GeO_2–5Eu_2O_3 and 94.9GeO_2–5Eu_2O_3–0.1Ag systems was revealed in the annealing temperature range of 350-550°C (Fig.1). The cluster size distribution functions were calculated and it was found that silver doping results in an approximately twofold decrease in their average size. This fact can be explained by the breakage of clusters because of the formation of Eu–O–Ag chemical bonds. An increase in the relative intensity of luminescence excitation lines ${}^7F_0 \rightarrow {}^5L_6$ and ${}^7F_0 \rightarrow {}^5H_6$ of Eu^{3+} ions confirms this fact. At a high annealing temperature T_O = 850°C the dissociation of the formed clusters was observed, which may be connected with the formation of a new phase of europium germanate.

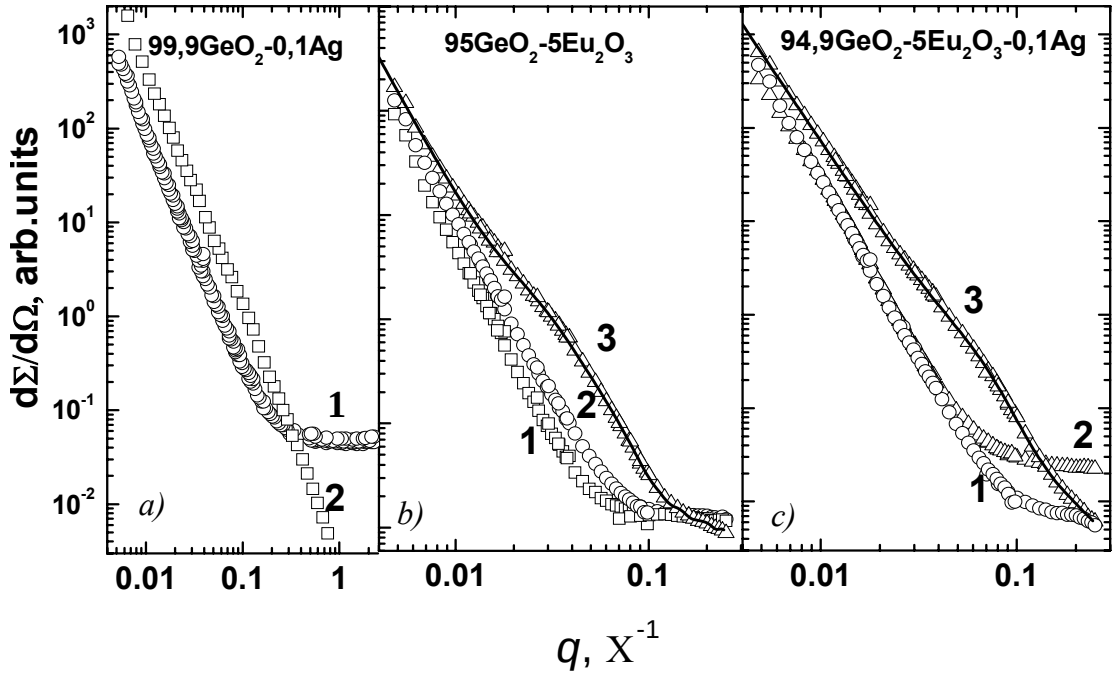

Fig.1. The neutron scattering curves xerogels with compositions 99.9GeO_2-0.1Ag (*a*), 95.0GeO2-5Eu2O3 (*b*) и 94.9GeO2-5Eu_2O_3-0.1Ag (*c*) and annealing temperature T_{an}=150 (1), 550 (3) и 850 ^{0}C (2).

References

[1] H.Chandler, *Mater.Sci.Eng.R.*, V.49 P.113-155 (2005).

[2] B.Long, Z.Lide, W.Xiaoping, *Solid State Commun.,* 104(9), 553 (1997).

[3] S.T.Selvan, T.Hayakawa, M.Nagami, *J. Phys. Chem. B.,* V. 103, P. 7064 (1999).

[4] H.Nabika, S.Deki, *Eur. Phys. J. D.*, V. 24, P. 363 (2003).

[5] H.B.Stuhrmann, N.Burkhardt, G.Dietrich, R.Jünemann, W.Meerwinck, M.Schmitt, J.Wadzack, R.Willumeit, J.Zhao, K.H.Nierhaus, *Nucl. Instr. & Meth., A*, 356, 133 (1995).

[6] V.L.Aksenov, V.P.Glazkov, S.E.Kichanov, D.K.Pogoreliy, K.M.Podurets, V.A.Somenkov, B.N.Savenko, *Nucl. Instr. & Meth. A*, 575, 266-268 (2007).

INVESTIGATION OF LIQUID LITHIUM RELAXATION TIME BY MEANS OF THE MEMORY FUNCTION FORMALISM

N.Blagoveshchenskii, A.Novikov

SSC RF - Institute for Physics and Power Engineering, 249033, Obninsk, Russia

Previously [1], our experimental data on quasielastic neutron scattering by liquid lithium were analyzed with use of the diffusion phenomenological model. The average resident lifetime τ_0 describing the atom relaxation in existing neighboring has been estimated.
However, it is interesting to illuminate the relaxation processes in liquid lithium by the memory function (MF) formalism [2,3] exploiting.
The equation of an atomic movement in liquid (*Langevin* equation) generalization,

$$mdV / dt = -m\Gamma V(t) + R(t) \qquad (1)$$

can be held by means of memory function *Γ(t)* formalism, the latter being introduced as time-dependent friction coefficient analog through the expression of mean force by the integral taking into account the memory on last particle dynamics as the *Γ(t)* and *V(t)* convolution:

$$mdV / dt = -m\int_0^t \Gamma(t-\tau)V(\tau)d\tau + R(t) \qquad (2)$$

Here *R(t)* – random force component, with zero average value, non correlated with a velocity *V(t)* of particle (mass *m*).
Note that the equation (2) corresponds to the description of the real atom movement better than the equation (1) does, where the friction is established only by up-to-moment value of the particle velocity. In such the way liquid having the atom velocity V(t), must restore its equilibrium corresponding to this value of the velocity, the memory effect with respect to previous dynamics being destroyed.
For the velocity autocorrelation function (VACF), *Ψ(t)* = < *V(0)V(t)* >/ < *V(0)V(0)* > we have:

$$d\Psi / dt = -\int_0^t \Gamma(t-\tau)\Psi(\tau)d\tau, \quad \text{or} \quad d\Psi / dt = -\int_0^t \Gamma(\tau)\Psi(t-\tau)d\tau \qquad (3)$$

As far as relaxation is possible as inner interatomic one, and as neighboring (cluster) relaxation, the model of MF becomes two-component:

$$\Gamma(Q,t) = \Gamma(Q,0) * [\alpha_Q * \exp(-t/\tau_\mu) + (1-\alpha_Q) * \exp(-t/\tau_\alpha)] \qquad (4)$$

Here τ_μ – fast relaxation time (μ – process); τ_α – slow relaxation time (α – process); α_Q and $(1-\alpha_Q)$ – their weights; $\Gamma(Q,0) = \Omega^2$ (Squared Einstein energy) [2,3].
Firstly, we shall execute the numerical solution of Volterra equation (3) for VACF by the method developed in [2,3] based on recurrent relations for memory function, and try to estimate the relaxation times for liquid lithium with use of VACF obtained in experiment [4].
Secondly, we shall use the computative design developed in [5,6] for the analysis of experimental data on quasielastic neutron scattering in supercooled water. In this case

$$\Gamma(Q,0) = {\Omega_0}^2 + 2\left(\frac{k_B T}{m}\right)Q^2, \qquad (5)$$

$$\Omega_0^{\,2} = \frac{4\pi n}{3m}\int_0^{\infty} r^2 dr\left[\phi''(r) + 2\left(\frac{\phi'(r)}{r}\right)\right]g(r) \quad , \tag{6}$$

where n – atomic density, $g(r)$ – radial atom-atom pair distributive function, $\phi'(r)$ and $\phi''(r)$ – first and second derivatives of the interatomic potential, correspondingly.
Resulting expression for the scattering function S(Q,ω), corresponding to the lineshape of the quasielastic peak,which one can derive directly [5,6] has the simple but somewhat tedious form:

$$S(Q,\omega) = \frac{A_0\Gamma(Q,0)A_2}{A_3\left[\dfrac{A_0^{\,2}\Gamma^2(Q,0)A_2^{\,2}}{A_3^{\,2}} + \left(\omega - \dfrac{A_0A_1}{A_3}\right)^2\right]} \quad , \text{ where} \tag{7}$$

$$A_0 = \left(\frac{k_BT}{m}\right)Q^2 \quad , \qquad A_1 = \Gamma(Q,0)\left[-\frac{\alpha_Q\omega}{\omega^2 + \tau_\mu^{\,-2}} - \frac{(1-\alpha_Q)\omega}{\omega^2 + \tau_\alpha^{\,-2}}\right] + \omega \quad ,$$

$$A_2 = \frac{\alpha_Q\tau_\mu^{\,-1}}{\omega^2 + \tau_\mu^{\,-2}} + \frac{(1-\alpha_Q)\tau_\alpha^{\,-1}}{\omega^2 + \tau_\alpha^{\,-2}} \quad , \qquad A_3 = \Gamma^2(Q,0)A_2^{\,2} + A_1^{\,2}$$

Note that fitting of VACF by damping cosine expression [7], $\Psi(t) = \mathrm{sech}(t/\tau)*\cos(\omega t)$ gives the value of $\tau = 0.035$ ps. It is the orientational value of fast relaxation time.
For the numerical solution of Volterra equation (3) the model description [4] yields $\Omega_0 = 21.85$ meV and accurately corresponds to the Einstein energy $E_E = 22.4$ meV estimated from the elementary excitation spectrum of liquid lithium analysis [8]. As a result of memory function analysis, the value of the fast relaxation time, $\tau_\mu = 0.023$ ps has been estimated. The attempt to infer the second, slow component (τ_α) of relaxation time failed (α_Q=1). Fig.1 demonstrates a good description of model VACF with respect to the experimental data. The absence of τ_α in the description of memory function we connect with omitting of quasielastic component during the VACF extraction from experimental frequency spectrum [4].
Situation differs when we deal with memory function concerning the quasielastic scattering itself, that *a priory* contains the slow component τ_α . Keeping the parameter $\Omega_0^{\,2}$ (6) fixed equal $\Omega_0^{\,2} = E_E^{\,2} = [22.4\ \mathrm{meV}]^2 = (1152\ \mathrm{ps}^{-2})$ (from the dispersion curve of liquid lithium analysis [8]), we steadily get fitting by use of the expression (7). Fig.2 demonstrates the fitting result for some values of Q. The average values at the interval Q = 0.65 – 1.87A^{o-1} of weight α_Q and relaxation times are:

$$<\alpha_Q> = 0.974 \pm 0.005; <\tau_\alpha> = (0.59 \pm 0.08)\,pS; <\tau_\mu> = 0.033\,pS \tag{8}$$

As expected, the diffusion component weight became ~ 3%. The main contribution to MF is due to the fast binary term. At the time, one can mark the proximity between estimated value of $<\tau_\alpha> = 0.59$ ps, time $\tau_0 = (0.6 \pm 0.1)$ ps estimated in [1], and qualitative accordance with $\tau_\alpha \sim$ 0.3 ps from the paper [9].
At the next step of fitting $\alpha_Q = 0.974$ and $\Omega_0^{\,2} = 1152\ \mathrm{ps}^{-2}$ were fixed, while τ_μ and τ_α were kept free. The average fast relaxation time became $<\tau_\mu> = 0.032$ ps (fig.4) and well coincides with the start value of primary fitting value, $\tau_\mu = 0.033$ ps. The average slow relaxation time became $<\tau_\alpha> = 0.53$ ps (fig.5).
Despite estimation of τ_μ and τ_α is in good accordance with results of other authors [9], we hadn't reveal the Q – dependence of τ_μ and τ_α. Perhaps it is connected with our experimental data restrictions.

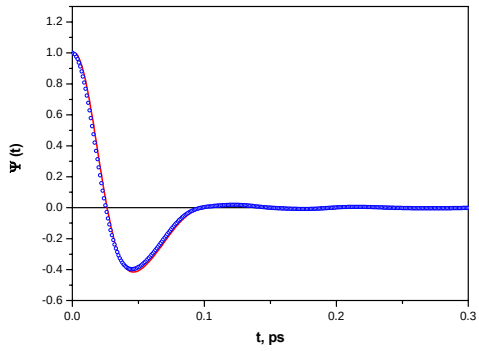

Fig. 1 Experimental VACF(dot) in comparison with calculated one (curve) obtained by (3)

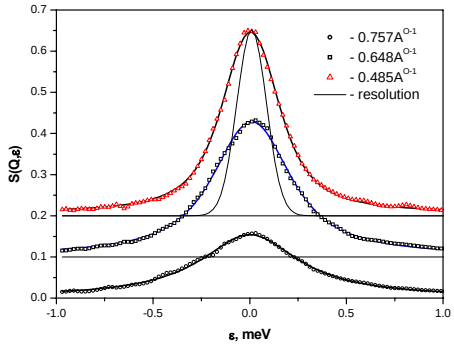

Fig. 2 A quality of scattering function S(Q, ω) description by formula (6)

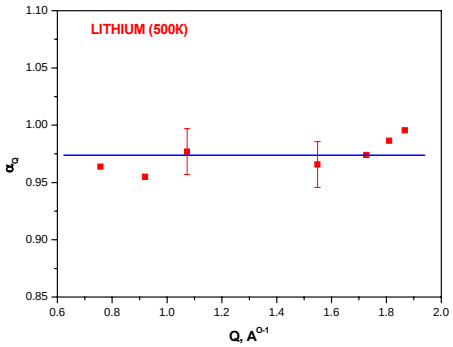

Fig. 3 The weight of fast relaxation component in content of MF. $< \alpha_Q > = 0.974$

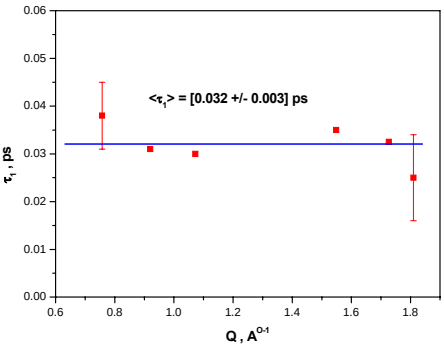

Fig. 4 Q – dependence of the fast relaxation time in liquid lithium

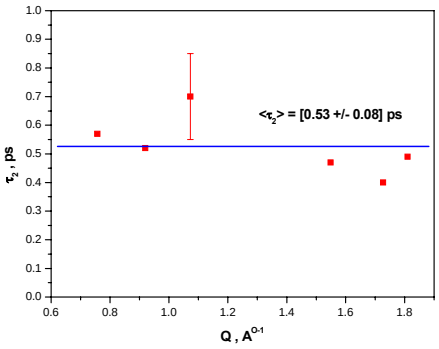

Fig. 5 Q – dependence of the slow relaxation time in liquid lithium

REFERENCES

[1] Sobolev O.V., Blagoveshchenskii N.M., Morozov V.A., Novikov A.G., Pashnev M.A., Savostin V.V., Shimkevich A.L. J.Phys.: Cond.Matter. 20 (2008) 104211
[2] Hoheisel C. Computer Physics Reports 12 (1990) 29
[3] Berne B.J. and Harp G.D. Advances in Chemical Physics 17 (1970) 63
[4] Blagoveshchenskii N., Novikov A., Savostin V. Annual Report of FLNP 2008, JINR, Dubna
[5] Di Cola D., Deriu A., Sampoli M. Physica B226 (1996) 46
[6] Di Bari M., Deriu A., Sampoli M. Physica B266 (1999) 92
[7] Sharma S.K. and Tankeshwar K. J.Phys.: Cond. Matter. 8 (1966) 10839
[8] Blagoveshchenskii N.M. et al. Annual Report of FLNP 2007, JINR, Dubna
[9] Scopigno T. et al. arXiv:cond-mat/0001190v3, 30 aug.2000

SANS and SAXS study of laser pyrolysis carbon nanostructures

R. V. Erhan[1,3,*], M. Balasoiu[1,3], E. Barna[2], I. Morjan[4], E. Anitas[1], J. Plestil[5],

Yu.S. Kovalev[1] and A. I. Kuklin[1]

[1] Frank Laboratory of Neutron Physics, Joint Institute for Nuclear Research, Joliot-Curie str., Dubna, Moscow reg., 141980, Russia;
[2] Faculty of Physics, University of Bucharest, Str. Atomistilor, nr. 405, Magurele, Jud. Ilfov, Romania;
[3] Horia Hulubei National Institute of Physics and Nuclear Engineering, Str. Atomistilor, nr.407, P.O.BOX MG-6, Bucharest - Magurele, Romania;
[4] National Institute for Laser, Plasma and Radiation Physics, Str. Atomistilor, Nr. 409, PO BOX MG-36, 077125, Magurele, Bucharest, Romania;
[5] Institute of Macromolecular Chemistry, Academy of Sciences of the Czech Republic, Heyrovského nám. 2, CZ-162 06, Praha 6, Czech Republic;

The latest research advances of physical and chemical properties of carbon nanostructures show that these could be the basis of notable advances in nanoscale electronic devices [1], environmental pollution control [2], electro-magnetic interference shielding [3], reinforcement of light-weight materials, energy storage [4], catalysts / catalysts supports [5] and field emission [6]. Nanostructured carbon powders can be produced using different techniques like: resistive heating of graphite [7], ablation of carbon-containing materials [8], graphite vaporization [9] and pyrolysis of hydrocarbons.
Carbon soot synthesis by laser pyrolysis of hydrocarbons has the background into the resonance between the laser radiation and at least one of the reactant composing gas mixture [10].
Due to the fact that nanosized soot particles scatter at low angles, we have chosen small-angle neutron scattering [12] like an appropriate additional method to analyze the bulk information from the soot samples.
The purpose of this article is to obtain a correlation between the parameters of synthesis process and the phase composition of carbon nanopowders investigated.

The studied samples were synthesized at National Institute for Laser, Plasma and Radiation Physics, Bucharest, Romania by the laser induced pyrolysis of ethylene [13]; the soot samples containing carbon nanostructures were: C_2H_2/C_2H_4 and C_2H_2/SF_6.
The small-angle scattering experiments were carried out on YuMO small-angle time-of-flight spectrometer [14] at the IBR-2 pulsed reactor, Joint Institute for Nuclear Research, Dubna, Russia in two detector system [15,16] with PSD detector in second position [17].
The small-angle X-ray scattering measurement was performed at Institute of Macromolecular Chemistry, Prague, Czech Republic on Rigaku 2D multi-wire proportional counter [20].
For the measurements the soot was introduced in quartz 2 mm Helma cells, the experiment was performed at room temperature (~ 20 ºC) controlled by a Lauda thermostat within 0.5 ºC.

The hydrocarbons laser pyrolysis leads to carbon nanodisperse powders in which is revealed the presence of three types of carbon: amorphous carbon, carbon with small graphitic sheets or fullerene-like structures. The transmission electron micrograph (TEM) investigation showed that curved structures (spherical shape nanoparticles) are general feature of the morphology of carbons [11].

The graphics (Fig.1, Fig.2, Fig.3) showed are in log/log scale with absolute intensity on Y direction.

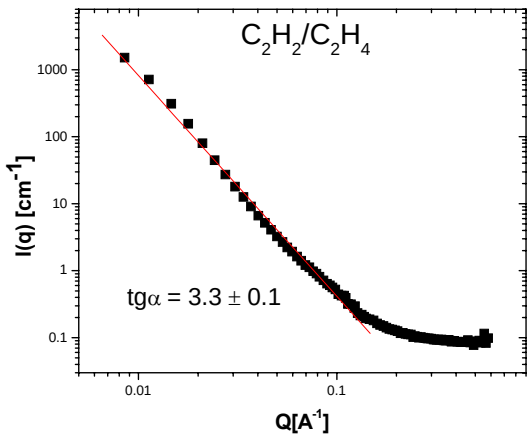

Figure 1. Scattering curve for C_2H_2/C_2H_4 (solid square) and linear fit.

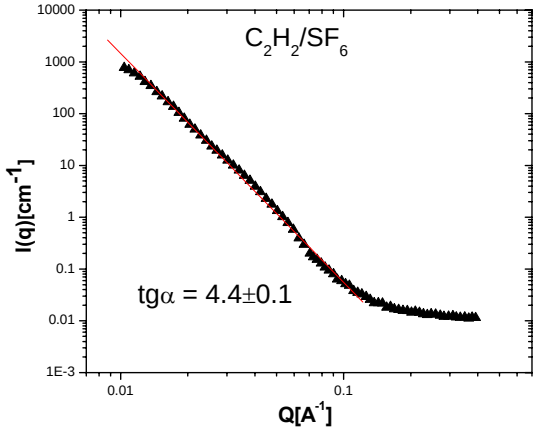

Figure 2. Scattering curve for C_2H_2/SF_6 (solid triangle) and linear fit.

We observe the straight line in Q-range at least Q_{max}/Q_{min} one order. It means we can describe the result for the 3.3 ± 0.1 slope in terms of surface fractal model [18].
In Fig. 1 are presented covers for the C_2H_2/C_2H_4 samples obtained by laser pyrolysis technique described above. A part of the cover shows that the straight line is in 0.12 Å up to 8×10^{-3} Å (Q range). The small deviation near straight line is within statistical errors.
The same behavior of covers can be observed in Fig. 2 for C_2H_2/SF_6 and in small Q-range the start at 0.1 Å corresponds to a particle size about 63 Å. For first sample the size is about 60 Å also.

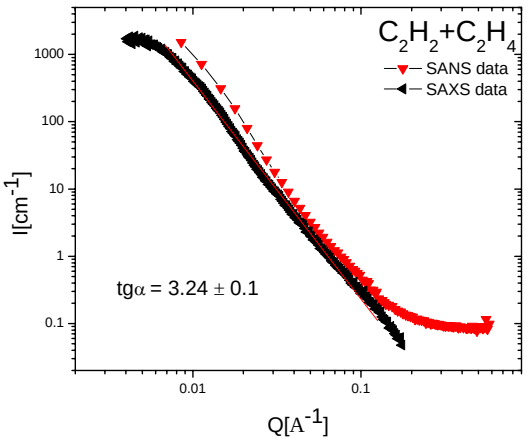

Figure 3. Comparison between SANS and SAXS data for C_2H_2/C_2H_4 sample and linear fit for SAXS data.

Differences of fractal dimension are observed for the studied samples.
The slope coefficient is 3.3 ± 0.1 for C_2H_2/C_2H_4 sample and 4.4 ± 0.1 for the C_2H_2/SF_6 sample; the comparison between them shows different structure organization of samples.

The 3.3 ± 0.1 coefficient of the slope show surface fractal model-like with fractal dimension D = 2.7 ± 0.1, in agreement with HREM measurements [13] where it is revealed the non-smoothly surface of the aggregates.
One of the approaches for the next coefficient 4.4 from Fig.2 could be described in terms of porosity samples [19]. This result requests further investigation including TEM or HREM analysis.
From Fig. 1 we can see the point on Q-scale where exists a deviation of scattering curve from the straight line. The position of this point, which corresponds to ~ 60 Å, could be explained by the size of particles which construct the whole fractal system.
This size determined could be used like estimation.

Acknowledgements.

The authors are indebted to the plenipotentiary of Romania at Joint Institute for Nuclear Research, Dubna for the approval of a grant for this research.

The authors are thankful to A. Kh. Islamov for the valuable advices during the measurements.

References

1. L. Chico, V. H. Crespi., L. H. Benedict , S. G. Louie, M. L. Cohen, *Phys Rev Lett* **76**, 1996, 971.
2. K. Knoblauch, E. Richter , H. Juntgen, *Fuel 1981*, **60**, 832-8.
3. B. D. Mottahed, S. Manoocheheri, *Polym. Plast. Technol. Eng. 1995*, **34** , 2, 271.
4. W. A. de Heer, A. Chatelain, D. Ugarte, *Science 1995*, **270**, 1179–80.
5. J. W. Geus, A. J. Van Dillen, M. S. Hoogenraad, *Mater. Res. Soc. Symp. Proc. 1995*, 368 - 387.
6. R. H. Baughman, C. Cui, A. Zachidov, Z. Iqbal, G. M. Spinks, G. G. Wallace et al., *Science 1999*, **284**, 1340 – 1344.
7. W. Kratschmer, L. D. Lamb, K. Fostiropoulos, D. R. Huffman, *Nature 1990*, 347:354–8.
8. E. A. Rohlfing, D. M. Cox, A. Kaldor, *J. Chem. Phys. 1984*, **81**(7):3322–30.
9. D. E. Powers, S. G. Hansen, M. E. Geusic, A. C. Pulu, J. B. Hopkins, T. G. Dietz et al., *J Phys Chem 1982*, **86**:2556– 2560.
10. J. S. Haggerty, W. R. Cannon, In: *Laser induced chemical 284 processes*, edited by Steinfeld JI, vol. **165**, 1981.
11. I. Morjan et al., *Carbon*, **42**, Issue 7, 2004, 1269-1273
12. J. Teixeira, *J. Apll. Cryst.* (1988), **21**, 781-785
13. I. Morjan, I. Voicu et al., *Carbon*, **41**, Issue 15, 2003, 2913-2921
14. Yu. M. Ostanevich, *Macromol Chem Macromol Symposia*, **15**, 91–103, 1988.
15. A. I. Kuklin, A. Kh. Islamov, V. I. Gordeliy, *Neutron News*, **16**, Issue 3, 2005
16. A. I. Kuklin, A. Kh. Islamov, Yu. S. Kovalev, P. K. Utrobin and V. I. Gordeliy, *Surface*, **6**, 74-83 (in russian).
17. A. Kuklin, G. Eckold , V. Gordeliy, S. Kutuzov, A. Islamov, A. Smirnov, P. Utrobin, A. Bogdzel, N. Alekseev, V. Comparat, A. Pelissier, J. Ballon, J. Teixeira , G. Koskas, A. Gabriel, *LLB Scientific Report 2003-2004*
18. P. W. Schmidt, *J. Appl. Cryst.* (1991), 24, 414 - 435
19. P. W. Schmidt, *J. Chem. Phys.* 94 (2), 1991
13. *www.rigaku.com/saxs*

PRESSURE INDUCED CHANGES IN MAGNETIC STRUCTURE OF $BiMnO_3$

S.E.Kichanov*, D.P.Kozlenko, B.N.Savenko
Frank Laboratory of Neutron Physics, JINR, Russia
* e-mail: ekich@nf.jinr.ru

I.Mirebeau,
Laboratoire Léon Brillouin, CEA Saclay, 91191 Gif-sur-Yvette Cedex, France

O.L.Makarova
Russian Research Center "Kurchatov Institute", 123182, Moscow, Russia

Introduction

$RMnO_3$ compounds are intensively studied due to the coupling of electric and magnetic properties (multiferroic materials). $BiMnO_3$ is one of the most studied multiferroic materials among perovskite-type oxides at ambient pressure [1]. Below 500 K, its structure is a highly distorted perovskite type monoclinic one with space group *C*2/c resulting in the off-centering Bi $6s^2$ lone pairs. The ferroelectric (FE) phase transition temperature T_{FE} = 500 K of $BiMnO_3$ is coincident with the structural phase transition temperature to this monoclinic phase. Below T_C = 100 K, a ferromagnetic state is realized in $BiMnO_3$. An observation of magnetodielectric anomaly implies a strong coupling of FE and magnetic properties [2]. Some recent reports have shown the orbital ordering and superexchange interaction responsible for the FM state in this system, which is in contrast difference with the A-type AFM state of relevant $LaMnO_3$ compound. The recent magnetic susceptibility measurements demonstrated that FM ground state in $BiMnO_3$ is extremely unstable with respect to application of high pressure, and it is fully suppressed above P = 1 GPa [3], while above this pressure a new magnetic phase appears below T_{C1} = 90 K. In order to clarify the nature of the pressure-induced magnetic state of $BiMnO_3$, we performed neutron diffraction experiments.

Experimental

Neutron powder-diffraction measurements were performed with the G6.1 diffractometer using a setup for high-pressure experiments at the Orphée reactor. An incident neutron wavelength was 4.74 Å. Sample with a volume of ~1mm^3 was loaded into a sapphire anvil high-pressure cell. As a pressure transmitting medium, NaCl was admixed to the sample. The pressure was measured by the ruby fluorescence technique. All our experiments were carried out in the pressure range of 0–2.7 GPa and the temperature range of 1.5–300 K.

Results and discussions

For additional background removal the low temperature spectra were subtracted to high temperature spectra. The subtracted diffraction patterns measured at T=2 K in pressure range 0-2.7

GPa were presented at Fig. 1. At ambient pressure the ferromagnetic phase FM are exist in $BiMnO_3$ as were observed at previous experiments [4].

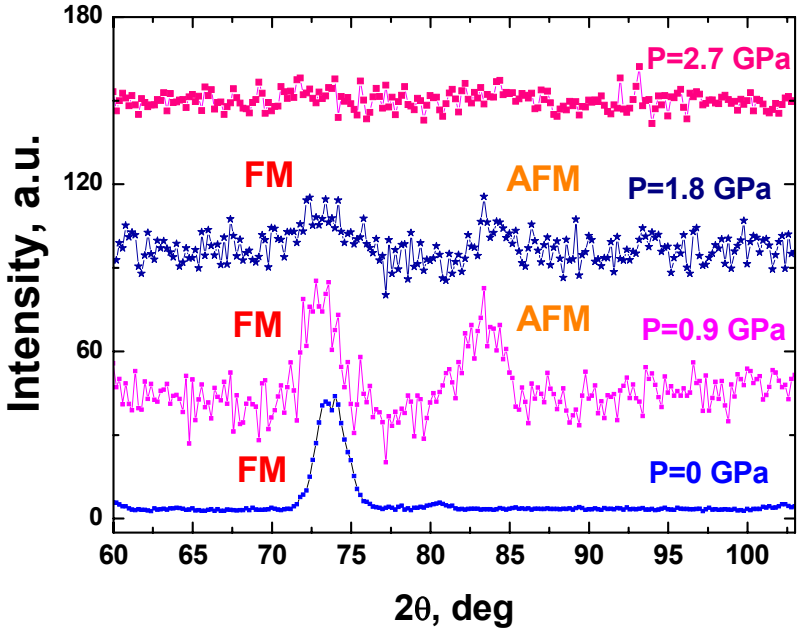

Fig. 1. The background subtracted neutron diffraction patterns of $BiMnO_3$ at different pressures at low temperature T=2 K.

At high pressure *P*=1.2 GPa the additional magnetic peaks at 2θ ~ 26 and 83^0 were appearing. This fact is clear shown the existing of additional antiferromagnetic AFM phase in $BiMnO_3$ at high pressure. The calculated propagation vector of this AFM phase is described as ***k***=[-1 0 1].

References

[1] T. Yokosawa et al., Phys. Rev. B **77** (2008) 124111

[2] T. Kimura *et al*, Phys. Rev. B **67** (2003) 080401

[3] C.C. Chou *et al*, Phys. Rev. B **78** (2008) 092404

[4]A.M. dos Santos et al, Phys. Rev. B **66** (2002) 064425

[5] D.P.Kozlenko, I. Mirebeau, J.-G.Park, I.N.Goncharenko et al., Phys. Rev. B **78** (2008) 054401

EXTRACTION AND MASS SPECTROSCOPY OF AGGREGATES IN C_{60}/N-METYL-2-PYRROLIDONE AND ITS MIXTURE WITH WATER

O.A.Kyzyma[a,b], M.V.Avdeev[b], V.L.Aksenov[c,a,d], L.A.Bulavin[b], M.V.Korobov[d], S.V.Snegir[e]

[a]*Frank Laboratory of Neutron Physics, Joint Institute for Nuclear Research, Dubna, Russia*

[b]*Taras Shevchenko Kyiv National University, Kyiv, Ukraine*

[c]*Russian Research Center "Kurchatov Institute", Moscow, Russia*

[d]*Moscow State University, Moscow, Russia*

[e]*Institute of surface chemistry, NAS of Ukraine, Kiev, Ukraine*

The specific behavior of fullerenes dissolved in polar solvents is of current interest [1,2]. The important feature of this type of fullerene solutions is the aggregate formation in neat solvents and their mixtures, which besides the fundamental viewpoint also has prospects for practical applications [3]. In this work we study aggregates appeared in the solution of fullerene C_{60} in N-methyl-2-pyrrolidone (NMP) [4,5]. Previously, it has been shown that quite large (size up to 500 nm) and polydisperse stable aggregates are formed during about 1 month after the solution preparation. It is worth mentioning that the growth of the aggregates is accompanied by smearing of the UV-Vis spectrum with time (time-dependent solvatochromism), although the connection between the two effects is not clear. Some reorganization of the aggregates with respect to the size distribution function is concluded from small-angle neutron scattering (SANS) after water (miscible with NMP in any proportion) is added to the system [6]. Namely, the disaggregation takes place [7]. Again the sharp solvatochromism is observed as well; still, its reason is also an open question. Similar effects characterize solutions of C_{60} in pyridine [6]. Here, we follow the aggregation changes in the system C_{60}/NMP and its mixture with water using the combination of the solvent extraction and mass spectroscopy performed at different time stages. As the second phase (extraction medium), hexane is used. We use it for structure diagnostics of the first phase. In particular, we show that the extraction is sensitive to the aggregate development, so it can be used in the analysis of the aggregation processes in the studied systems. Additionally, some correlation between the formation/change in the aggregates and mass spectroscopy data is established. It supports the results of the extraction analysis.

Fullerite C_{60} (Fullerene Tekhnologies, purity > 99.5%) is added to NMP (Merck, purity > 99.5%) and stirred for one hour at room temperature in dark place. The extraction of C_{60} is performed during one month after the dissolution with the time step of about one day. Hexane (Merck, purity > 99.5%) is added to C_{60}/NMP with hand shaking; then the system is left as it is for ten minutes in a vertical quartz cell, which results in the separation into two phases (C_{60}/NMP plus C_{60}/hexane) with a distinct interface. The UV-Vis spectrum of the C_{60}/hexane solution is obtained using Helios UV-Visible spectrophotometer (wavelength range 200-1000 nm, 10 mm path length). Water is added in one-month-old solution C_{60}/NMP with volume fraction of 50% in the final mixture. The hexane extraction is repeated for the new system during one day after the mixing with the time step of 1 h.

Laser desorption/ionization time-of-flight mass spectroscopy (LDI TOF MS) is performed on the Bruker Daltonics Autoflex II instrument. All kinds of fullerene solutions are deposited onto a standard steel target; then the solvent is evaporated.

Spectra of C_{60} extracted by hexane from C_{60}/NMP solution (Fig.1) repeat those reported [8] for C_{60} dissolved directly in hexane. To follow the influence of the age of the initial C_{60}/NMP solution on the extraction, the corresponding changes in the absorbance at $\lambda = 253$ nm are shown in the inset to Fig.1. One can see that the fullerene extraction drops and almost stops after one month. Taking into account that this time coincides with the characteristic period of the aggregate

formation in the initial C_{60}/NMP solution, it is reasonable to conclude that the observed decrease in the extraction is related to the aggregation process, i.e. the fullerene is transformed to the hexane phase only as separate molecules (monomers), whose number finally reduces to zero with the cluster growth in time. The final stop of the extraction indicates that all fullerene dissolved in NMP comes to the aggregated state in the sufficiently old solution. The extraction resumes and increases after water is added to one-month-old solution C_{60}/NMP (Fig.2). It strongly evidences that the disaggregation in the system C_{60}/NMP/water [9] is a result of detachment of individual fullerene molecules from large aggregates, which initiates the extraction. In fact, we observe the dissolution of the aggregated fullerene in the mixture NMP/water.

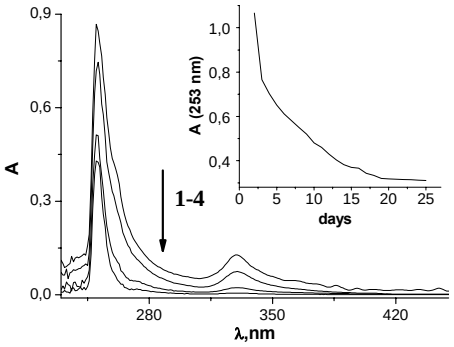

Fig.1. UV-Vis absorption spectra of extracted C_{60} in hexane added to C_{60}/NMP solution at different time (7 (1), 10 (2), 19 (3) and 25 (4) days) after preparation of solution. Inset shows variation of absorbance at wavelength of 253 nm with time.

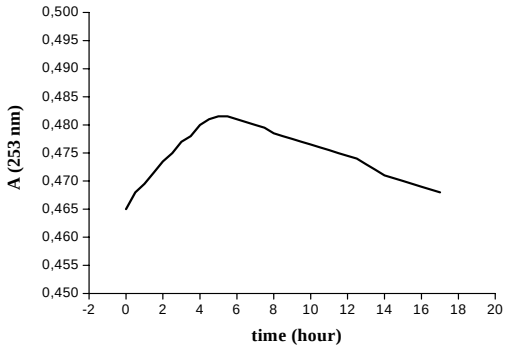

Fig.2. Time variation (starting in 10 min after preparation) in absorbance of extracted C_{60} in hexane added to C_{60}/NMP/water solution.

By comparing the absolute values in Figs.1,2 one can see that the maximal value of C_{60} adsorption in hexane after water addition is almost twice less than that in fresh NMP. This is consistent with the fact that the direct extraction constant should decreases for the mixture NMP/water as compared to the fresh NMP solution. Really, let us denote the cases "fresh NMP" and "NMP/water" by indexes *I* and *II*, respectively. Then, in the linear approximation one can write:

$$c_{1,I} = k_I\, c_{2,I}, \qquad (1a)$$

$$c_{1,II} = k_{II}\, c_{2,II}, \qquad (1b)$$

where c_1, c_2 are the concentrations of free C_{60} monomers in the first and second phases at the extraction, respectively; and k is the extraction constant, which is determined by the saturation concentrations of free monomers in both phases, $c_1^{\max}$ and $c_2^{\max}$, as

$$k = c_1^{\max} / c_2^{\max}. \qquad (2)$$

In case *I* the concentration $c_{1,I}$ coincides with the total fullerene concentration, $c_{1,I}^{\text{tot}}$, of C_{60} in the first phase (NMP):

$$c_{1,I} = c_{1,I}^{\text{tot}}. \qquad (3)$$

In case *II* the concentration $c_{1,II}$ takes a part, $x_{II} < 1$, of the total concentration in the first phase (NMP/water), $c_{1,II}^{\text{tot}}$, which is followed from the existing of aggregates in NMP/water observed in SANS experiments [17,18]. Then,

$$c_{1,II} = x_{II} c_{1,II}^{\text{tot}} = x c_{1,I}^{\text{tot}} / 2. \qquad (4)$$

Here, we use the fact that the initial system is dissolved twice by water, so the total fullerene concentration is divided by 2. Substituting (3), (4) in (1) and taking into account the observed above ratio $c_{2,I} = 2c_{2,II}$ one obtains:

$$x = k_{II} / k_I < 1 \quad (5)$$

or

$$k_{II} < k_I \quad (6)$$

From the k definition (2) we see that the concentration distribution in case *II* shifts towards the hexane phase (decrease in the extraction constant) as a result of the worse solubility of C_{60} in the mixture NMP/water in comparison with neat NMP.

Mass-spectra of the samples from various stages of the studied system are given in Fig.3. For fresh C_{60}/NMP (Fig.3a) the spectrum is a set of peaks differing by 24 Da due to the fact that excited fullerene loses even number of carbon atoms under the laser irradiation. The peaks are grouped around mass values, which are multiples of the molecular weight of C_{60} (720 Da). Thus, besides single fullerene, the clusters of two, three, four, etc. fullerene molecules are detected. One can see that the observed spectrum correlates with the cluster formation in the solution at the beginning stage of the aggregation process. Furthermore, the influence of the aggregation on the mass spectra is clearly confirmed by the spectrum from old C_{60}/NMP (Fig.3b) where such peak groups disappear, and significant decrease of the peak corresponding to single C_{60} is observed. Both changes in the mass-spectrum reflect well the formation of large tight aggregates accompanied by a decrease in the number of C_{60} monomers in the solution. The addition of water to old C_{60}/NMP results in a significant increase of the peak corresponding to single C_{60} (Fig.3c). At the same time, small clusters like in fresh C_{60}/NMP are not observed. So, one can conclude that single fullerene molecules from the aggregates are really dissolved in the mixture NMP/water, as was supposed above.

The explanation for the found dissolution C_{60} in NMP/water is that fullerene molecules at the interface of the aggregates in NMP interact with the solvent and form donor-acceptor complexes, which exhibit higher solubility in the mixture NMP/water than in pure NMP. Still, their solubility is less than the solubility of free C_{60} in fresh NMP solutions. Such complexes were assumed [4] to be responsible for the time solvatochromism in C_{60}/NMP. Another evidence of the formation of these complexes is that fullerene itself is not dissolved when added to the same NMP/water mixture. It can be noted that the time behavior of the system C_{60}/NMP/water reflected in the extraction analysis (Fig.2) is somewhat similar to that for C_{60}/NMP (Fig.1), but at a different time scale. In the given case the monomer concentration grows only for several hours after the water addition showing that the new dissolution process (disaggregation of the initial clusters) takes some time. Then we can observe its decrease, which suggests that the clusterization starts again in the solution C_{60}/NMP/water.

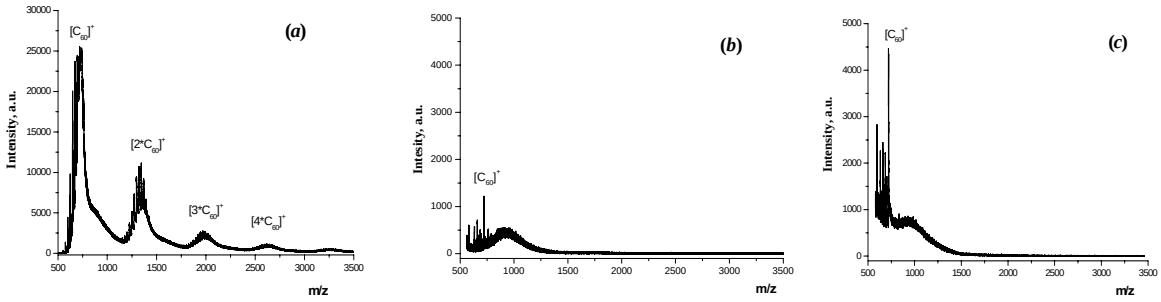

Fig. 3. Mass-spectra of fresh C_{60}/NMP (*a*), old C_{60}/NMP (*b*) and C_{60}/NMP/water (*c*).

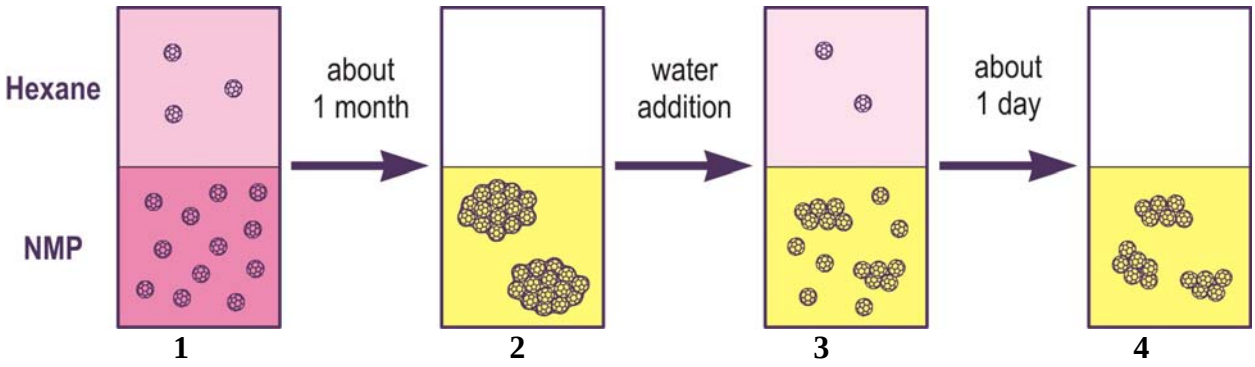

Fig. 4. Schematic view of various stages of fullerene extraction to hexane. **1.** Molecular C_{60} is extracted to hexane from molecular solution C_{60}/NMP; both solutions turn to mauve of different intensity. **2.** C_{60} is not extracted to hexane; all C_{60} in C_{60}/NMP (brownish yellow) is in aggregated state. **3.** Molecular C_{60} is extracted to hexane (which turns to mauve) from solution C_{60}/NMP/water (which remains brownish yellow). **4.** C_{60} is not extracted to hexane; all C_{60} in C_{60}/NMP/water (brownish yellow) is in aggregated state.

The proposed extraction method allows us to conclude about the relative change in the concentration of non-aggregated fullerene molecules during the aggregate growth and reorganization in the system C_{60}/NMP and C_{60}/NMP/water, respectively. The prospects for using this method in the study of the cluster growth kinetics in various solutions should be mentioned. The impact of the aggregation in the studied systems on the mass-spectra of the dried samples is observed. The mass-spectrometry measurements fully support the conclusions based on the extraction data.

References

[1] T. Malaspina, E.E. Fileti, R. Rivelino, J. Phys. Chem. B 111 (2007) 11935.
[2] S. Nath, D.K. Palit, A.V. Sapre, Chem. Phys. Lett. 330 (2000) 255.
[3] V.S. Lee, P. Nimmanpipug, et al., J. Mol. Graph. and Mod. 26 (2007) 558.
[4] M. Alfe, B. Apicella, R. Barbarella, et al., Chem. Phys. Lett. 405 (2005) 193.
[5] V.L. Aksenov, M.V. Avdeev, T.V. Tropin, et al., Physica B 385-386 (2006) 795.
[6] A. Mrzel, A. Mertelj, A. Omerzu, et al., J. Phys. Chem. 103 (1999) 11256.
[7] N.P. Yevlampieva, Yu.F. Biryulin, E.Yu. Melenevskaja, et al., Coll. and Surf. A 209 (2002) 167.
[8] A.L. Smith, J. Phys. B 29 (1996) 4975.
[9] O.A. Kyzyma, L.A. Bulavin, V.L. Aksenov, et al., Fullerenes, Nanotubes and Carbon Nanostructures 16 (2008) 610.
[10] V.L. Aksenov, M.V. Avdeev, O.A. Kyzyma, et al., Cryst. Rep. 52 (2007) 479.

IS SOLVATOCHROMISM RELATED TO FULLERENE CLUSTER FORMATION IN C_{60}/N-METHYL-2-PYRROLIDONE?

O.A.Kyzyma[a,b], M.V.Avdeev[a], V.I.Petrenko[a,b], V.L.Aksenov[c,a,d], L.A.Bulavin[b], M.V.Korobov[d], V.M.Garamus[e]

[a]*Frank Laboratory of Neutron Physics, Joint Institute for Nuclear Research, Dubna, Russia*

[b]*Taras Shevchenko Kyiv National University, Kyiv, Ukraine*

[c]*Russian Research Center "Kurchatov Institute", Moscow, Russia*

[d]*Moscow State University, Moscow, Russia*

[e]*GKSS Research Centre, Geesthacht, Germany*

The solutions of fullerene C_{60} in nitrogen-containing solvents (pyridine, N-methyl-2-pyrrolidone (NMP), benzonitrile and acetonitrile) are characterized [1-3] by the time solvatochromism, which is the time evolution of photoluminescence, Raman and UV-Vis spectra. Often, this effect is accompanied by the formation of fullerene clusters (size up to 500 nm) in the solutions [1,2], so one can assume [2] that the reason of the solvatochromism is directly determined by the cluster growth. This implies that new bonds between fullerene molecules in the clusters appear, which change the mentioned kinds of spectra. On the other hand, the solvatochromism can be related to the formation of some complexes between fullerene and solvent molecules, such as donor-acceptor complexes between fullerene and nitrogen (oxygen) in the solvent (NMP) molecules [4]. In the given work we consider these two possibilities from the viewpoint of the cluster reorganization after dissolution of the system. In particular, such reorganization is observed [5-7] for C_{60}/NMP solutions (above 40% of water in the final mixture) as a comparatively sharp increase in the small-angle neutron scattering (SANS). This points out the fact that the large clusters destroy at some extent and clusters with characteristic sizes between 10 and 100 nm appear. It is interesting that some sharp solvatochromism takes place at the water dilution as well. It was shown [6] that water addition leads to the decomposition of fullerene clusters in the solution, which is a result of the detachment of monomers from the clusters. Here, we repeat the dissolution of the cluster solution C_{60}/NMP using pure NMP. As it will be shown below, this also results in some changes of UV-Vis spectra, while the SANS signal, which is reflecting the formation of the new clusters of the previous case, does not increase.

Fullerene (Fullerenovye Tekhnologii, purity > 99.5%) was dissolved in NMP (Merck, purity > 99.5%) to obtain the C_{60}/NMP system. Then the solution was stirred for one hour at room temperature. UV-Vis absorption spectra were obtained using Helios UV-Visible Spectrophotometer (wavelength range of 200-1000 nm, quartz cells with 2 mm light pass). The spectra were obtained right after the solution preparation, several days after preparation and one month later. The new solution (several days after preparation) was dissolved with pure NMP. The volume fraction of added NMP was varied from 20 to 70 vol. % with respect to the final solutions. SANS experiments were carried out on the SANS-1 instrument at the FRG-1 steady-state reactor of the GKSS Research Center, Geesthacht, Germany. The scattering intensity (differential cross-section per sample volume) was obtained according to the standard procedure on the solutions in quartz plane cells with 1 mm neutron flight pass. The small scattering signal above the background allowed us to estimate only the integral scattering intensity over the q-interval of 0.1-1 nm^{-1}.

The time smoothing of the characteristic peak of fullerene C_{60} at 330 nm wave length in the UV-Vis spectrum of C_{60}/NMP (fig.1) repeats well the solvatochromic changes reported earlier [5,6]. The level of the SANS intensity from the old solution is extremely low (about 0.01 cm^{-1}). It is the same as it was observed previously [5] and corresponds to quite large (size more than 150 nm) fullerene clusters. The dissolution of C_{60}/NMP system with pure NMP results in solvatochromism

(fig.2), which is similar to that observed after the system is dissolved with water. One can see (fig. 2) that the characteristic peak is almost smoothed for C_{60}/NMP solution with several days later after preparation. It is interesting that, as follows from fig. 2, even slight dissolution (about 30%) of above mentioned C_{60}/NMP system leads to a solvatochromic effect (growth of the characteristic peak of fullerene C_{60} at 330 nm wave length in the UV-Vis spectrum). In contrast to the dissolution with water, in the given case the SANS intensity does not show any increase for all dissolution rates. Vice verse, it decreases in according with the dissolution rate, thus proving that the detected signal is the tale of the scattering curve from large fullerene clusters. This means that fullerene clusters do not change their structure after the dissolution of the system with NMP.

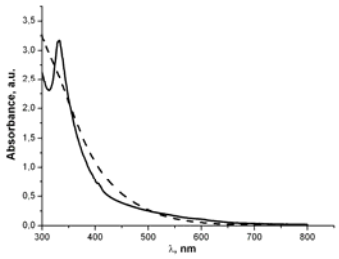

Fig. 1. Change in the UV-Vis spectrum of the C_{60}/NMP solution with time: solid line corresponds to fresh C_{60}/NMP and dashed line is the solution one month later after preparation.

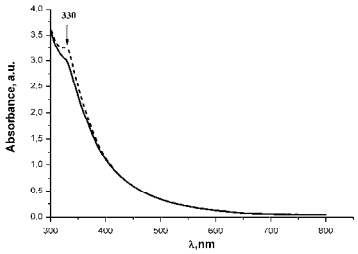

Fig. 2. Absorption spectra of the C_{60}/NMP system (several days after preparation) before (solid line) and after (dashed line) dissolution with NMP. Absorption spectra are normalized to the fullerene C_{60} concentration.

Thus, we observe the solvatochromism without any reorganization of the clusters. This experiment proves that the reason of the solvatochromic effects in the system C_{60}/NMP does not relate to the cluster formation, but rather to formation of some complexes between fullerene and solvent molecules (e.g. donor-acceptor complexes). Addition of water and NMP changes the solvent organization at the interface with the cluster surface, which varied in time after the preparation of the solution. Despite the similarity of the effects for the two solvents there are some significant differences. It seems that the effect of water is much stronger. Water molecules destroy the donor-acceptor bonds NMP-C_{60} and form their own complexes. This is confirmed by two new bands in the UV-Vis spectra at 440 and 660 nm [2]. Also, the detachment of single fullerene molecules from the clusters [6] after the addition of water suggests the formation of such complexes whose chemical potential is smaller in the solution as compared to pure fullerene molecules showing the tendency towards aggregation after they are placed in NMP.

References

[1] S. Nath, H. Pal, A.V. Sapre. (2002) Chem. Phys. Lett., 360: 422−428.
A. Mrzel, A. Mertelj, A. Omerzu, M. Copia, D. Mihailovic. (1999) J. Phys. Chem., 103: 11256−11260.
[2] M. Baibarac, L. Mihut, N. Preda, I. Baltog, J.Y. Mevellec, S. Lefrant. (2005) Carbon, 43: 1−9.
[3] N.P. Yevlampieva, Yu.F. Biryulin, E.Yu. Melenevskaja, V.N. Zgonnik, E.I. Rjumtsev. (2002) Coll. and Surf. A, 209: 167−171.
[4] V.L. Aksenov, M.V. Avdeev, T.V. Tropin, M.V. Korobov, N.V. Kozhemyakina, N.V. Avramenko, L. Rosta. (2006) Physica B, 385-386: 795-797.
[5] O.A. Kyzyma, L.A. Bulavin, V.L. Aksenov, M.V. Avdeev, T.V. Tropin, M.V. Korobov, S.V. Snegir, L. Rosta. (2008) Fullerenes, Nanotubes and Carbon Nanostructures, 16: 610−615.
[6] O.A. Kyzyma, L.A. Bulavin, V.L. Aksenov, M.V. Avdeev, T.V. Tropin, M.V. Korobov, S.V. Snegir, L. Rosta. (2008) Materials structure, 15: 17−20.

ELASTIC PROPERTIES OF REACTOR GRAPHITE GR-280 AND THEIR ANISOTROPY FROM NEUTRON DIFFRACTION AND ULTRASONIC MEASUREMENTS

T.Lokajicek[a], P.Lukas [b], A.N.Nikitin[c], I.V.Papushkin[c], V.V.Sumin[c], R.N.Vasin[c]

[a]*Institute of Geology, Academy of Sciences of the Czech Republic v.v.i., Prague, Czech Republic*
[b]*Institute of Nuclear Physics, Academy of Sciences of the Czech Republic v.v.i., Rzez, Czech Republic*
[c]*Joint Institute for Nuclear Research, Frank Laboratory of Neutron Physics, Dubna, Moscow Region, Russia*

In the course of operation of nuclear reactors graphite blocks of the core undergo a form change and the graphite itself acquires induced anisotropy of elastic, strength and thermal properties. The ascertainment of regularities of changes occurring as a result of influence of heat and irradiation is necessary for forecasting the terms of trouble-free operation of graphite stack. Measurements of lattice preferred orientation and ultrasonic velocities in the samples cut from the graphite block (made of GR-280 graphite) of the RBMK reactor have been carried out in order to study the anisotropy of its elastic properties and elucidate the mechanism of swelling of graphite blocks under the action of thermal fluxes and neutron irradiation.

GR-280 graphite is composed by middle grade coke particles and pyrolised pitch. The coke particles accounts for almost 80% of its weight. The formation process of the reactor block is extrusion, which in most of the cases tends to align the graphite grains in a certain direction. A graphitization process ends at a temperature of approximately 2400°C. Physical properties of GR-280 differ on 20-40% depending on the direction in the block. There exist two reasons for the anisotropy of the physical properties: lattice preferred orientations (LPO or "crystallographic texture") of graphite and preferred orientations of non-spherical pores and cracks (so-called "shape texture"). The influence of each of those factors on the anisotropy of bulk elastic properties of GR-280 graphite was studied by combined use of neutron diffraction and ultrasonic methods.

Neutron diffraction texture analysis of graphite sample GRA2 has been carried out using the SKAT spectrometer for quantitative texture analysis functioning on channel 7a of the IBR-2 reactor. The cell parameters of graphite were found to be a = 2.46852(4) Å and c = 6.73473(7) Å. The cell volume is 35.541 $Å^3$ and theoretical density 2.245 $g \cdot cm^{-3}$. The measured density of samples is 1.765 $g \cdot cm^{-3}$, which means the void volume fraction of 21.4%. There was noted no presence of the rhombohedral phase of graphite.

Recalculated orientation distribution function (ODF) of graphite grains is shown on Fig.1. The texture of graphite is weak; most of the orientations have corresponding ODF-values close to 1. Low ODF-values (< 0.6) form only 8% of the orientation intensity, occupying 18% of the orientation space. For high ODF-values (> 1.8) those numbers are correspondingly 10% and 5%.

To calculate bulk properties of the given polycrystalline material well known Voigt, Reuss, and GEO (geometric mean) models were used [1]. Single-crystalline graphite elastic constant were considered according to work [2]. Calculated longitudinal wave velocities in graphite material with measured texture are close to 10 km/s (Fig.2). High intrinsic anisotropy of graphite leads to coefficient of elastic anisotropy of 17%.

The ultrasonic method used in this study to measure bulk elastic properties of the graphite is based on the measurement of ultrasonic velocity in different directions in the spherical sample. Such a method makes it possible to estimate overall bulk elastic properties (at different pressures), including the influence of cracks and pores, and not only the contribution of crystal structure as it is for the neutron diffraction. Measurement of anisotropy of longitudinal ultrasonic velocity (Fig.2) was carried out at various values of pressure (from 0.1 MPa up to 150 MPa). Frequency of

propagating waves was 1 MHz, which means the wavelength of order ≈ 1 mm. That is sufficiently higher than the presumed size of inhomogenities in graphite.

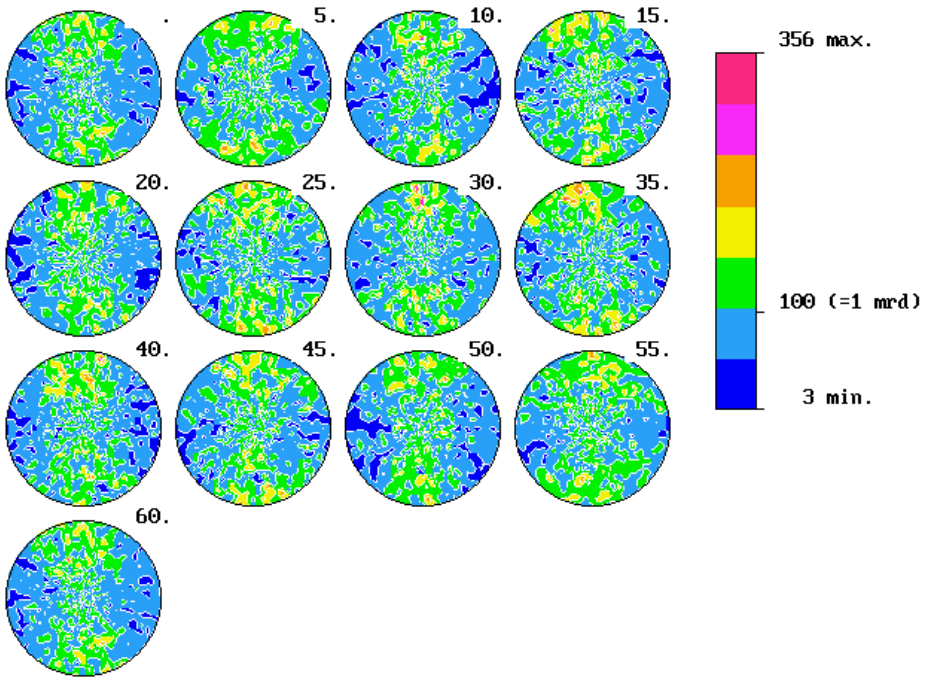

Fig.1. ODF of graphite in sample GRA2, γ-sections, linear scale contours, stereographic projection. Minimum value of ODF is f_{min} = 0.03, maximum f_{max} = 3.56, texture index F_2 = 1.19. Reference coordinate system of the sample K_A is shown, X_A axis is parallel to the extrusion direction.

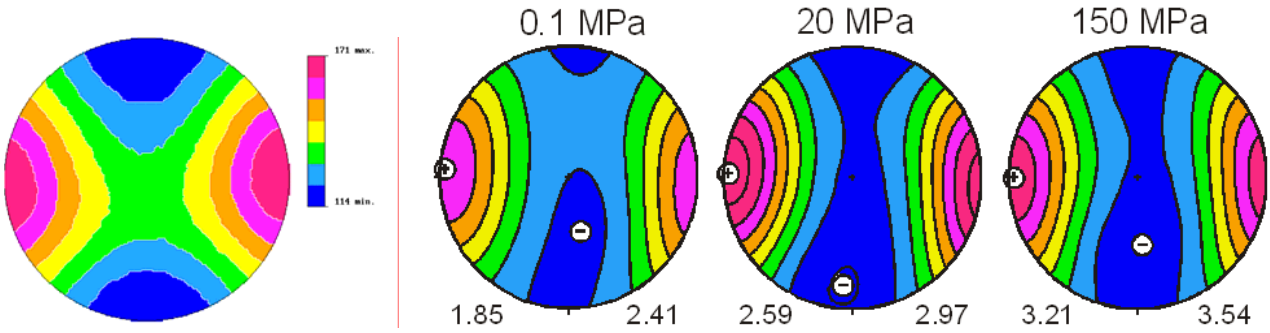

Fig.2. Longitudinal wave velocities V_P in of graphite possessing the same ODF as in the GRA2 sample calculated via geometric mean (leftmost figure, V_P values are 8.74…10.34 km/s), and measured at different pressures (0.1, 20 and 150 MPa), linear scale contours, stereographic projection.

The ultrasonic measurement coincides qualitatively with the results of texture analysis. The maximal value of the ultrasonic velocity (the "+" sign) coincides with the extrusion direction. The minimal one (the "-") lies in the plane which is perpendicular to this axis. The maximal velocity value is ≈ 30% greater than minimal at the atmosphere pressure; ≈ 15-16% greater at the pressure of 20 MPa and ≈ 10.5% greater at the pressure of 150 MPa. But quantitatively ultrasonics and neutron diffraction at this point differ greatly (V_P's at 150 MPa are 3 times lower than the calculated ones). Such behavior of the ultrasonic velocity testifies to the great contribution of pores and cracks to bulk elastic properties of graphite. The pores and basal cracks common for polycrystalline graphite are to be included into the refined model of elastic properties.

[1] S.Matthies, H.G.Priesmeyer, M.R.Daymond. On the diffractive determination of single-crystal elastic constants using polycrystalline samples. // J. Appl. Crys. 2001. V. 34. P. 585-601.
[2] A.Bosak, M.Kirsch. Elasticity of single-crystalline graphite: Inelastic x-ray scattering study. // Phys. Rev. B. 2007. V. 75. №15. 153408.

Структура гидридов $CeNi_3$ после десорбции водорода

С.А. Лушников, И.А. Бобриков*, А.М. Балагуров*, В.П. Глазков**, В.А. Соменков**

Московский государственный университет им. М.В. Ломоносова
** ЛНФ имени И.М.Франка, Объединенный институт ядерных исследований, г. Дубна*
***Российский научный центр «Курчатовский институт»*

Кристаллическую структуру интерметаллических соединений (ИМС) RT_3 (R – редкоземельный металл, T – переходный металл) принято описывать как состоящую из блоков состава RT_2 (структурный тип $MgZn_2$) и RT_5 (структурный тип $CaCu_5$), послойно наложенных вдоль оси *z*. Одним из интересных и еще не до конца понятых явлений, присущих соединениям RT_3 (с R-La, Ce, Pr, Nd), является необычно большая анизотропия расширения кристаллической решетки при их взаимодействии с водородом. С этой точки зрения особый интерес представляют гидриды на основе интерметаллида $CeNi_3$, также входящие в группу «анизотропных гидридов» [1] и отличающиеся особенно значительным расширением вдоль *z*-оси решетки ($\Delta c/c$ составляет почти 30%). Блочная структура гидридов соединений RT_3 и соответственно неравновероятное заполнение водородом позиций в блоках RT_2 и RT_5 рассматривается как одна из возможных причин анизотропного расширения решетки при последовательном увеличении концентрации водорода в структуре RT_3.

Ранее в нашей работе [1] было проведено исследование структуры гидридов $CeNi_3H_x$, полученных при абсорбции разного количества водорода, вплоть до $x = 5.2$. Было показано, что независимо от концентрации водорода, изученные гидриды имеют структуру исходного соединения с анизотропно расширенной элементарной ячейкой и несколько измененными позициями металлических атомов. Анизотропия расширения решетки максимальна при низкой концентрации водорода, а с увеличением *x* расширение становится более однородным. Не менее интересным является исследование структуры составов $CeNi_3H_x$, получающихся десорбцией водорода из гидридов с более высокой исходной концентрацией. В настоящей работе изложены результаты нейтронных дифракционных экспериментов, проведенных на изученных ранее в работе [1] образцах гидридов после частичной десорбции из них водорода.

Из исходных гидридов $CeNi_3H_{2.8}$, $CeNi_3H_{3.3}$, $CeNi_3H_{5.2}$ с помощью термодесорбции были получены составы с $x = 0.7$, 0.8, а составы с $x = 1.0$, 1.8, 3.4 и 3.8 были получены разложением на воздухе. Хотя везде для определенности говорится о гидридах, большая часть образцов была приготовлена с заменой водорода на дейтерий. Нейтронограммы измерялись на дифрактометрах ДИСК (реактор ИР-8, РНЦ КИ) и ФДВР (реактор ИБР-2, ОИЯИ). Пример измеренного и обработанного по методу Ритвельда дифракционного спектра приведен на рис. 1.

Анализ нейтронографических данных, полученных для гидридов $CeNi_3H_x$ с $x = 0.7$ и 1.0, показал, что их структура сохранила гексагональную симметрию исходного интерметаллида $CeNi_3$ ($P6_3/mmc$) с параметрами решетки практически соответствующим параметрам решетки исходного интерметаллида. В этих составах атомы водорода заполняют пустоты структурного фрагмента RT_2 и пустоты на границе между фрагментами RT_2 и RT_5. При этом в образце гидрида $CeNi_3H_{0.7}$ пустоты на границе между фрагментами RT_2 и RT_5 заполнены незначительно по сравнению с $CeNi_3H_{1.0}$. Это указывает на предпочтительное заполнение водородом пустот в структурных фрагментах

RT_2. Возможной причиной такого распределения водорода в матрице гидридов $CeNi_3H_{0.7}$ и $CeNi_3H_{1.0}$ является химическое влияние Ce, содержание которого больше в огранке пустот RT_2, и который прочнее удерживает атомы водорода в этих пустотах.

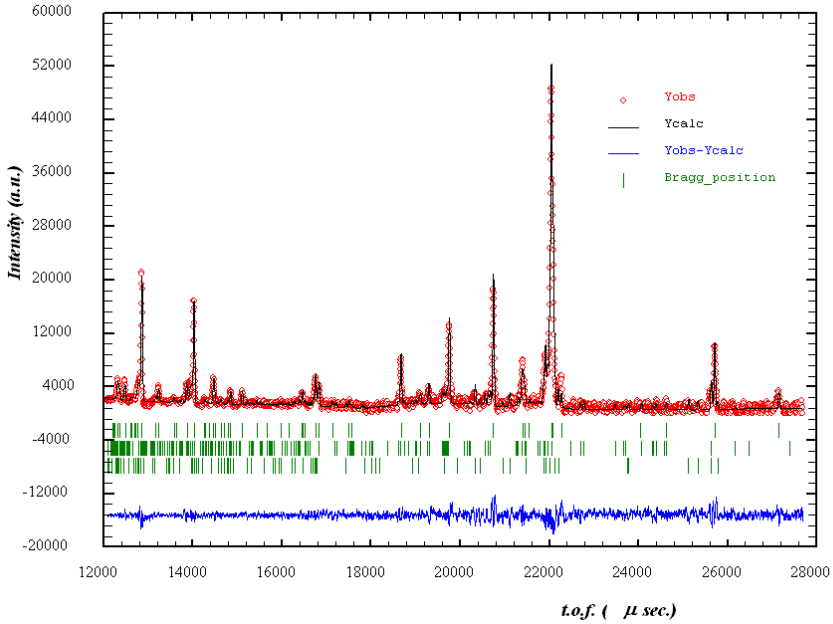

Рис. 1. Дифракционный спектр гидрида $CeNi_3H_{0.8}$, измеренный на нейтронном дифрактометре HRFD. Штрихи указывают положения пиков основной и двух дополнительных фаз (подробнее в тексте).

Результаты исследования образца гидрида $CeNi_3H_{0.8}$ показали присутствие в нем трех фаз (рис. 1). Основная фаза (около 75%) представляет собой исходный интерметаллид с гексагональным структурным типом $CeNi_3$ ($P6_3/mmc$). Вторая фаза (около 20%) имеет ромбическую структуру (Pmcn) исходного гидрида $CeNi_3H_{2.8}$. Присутствие этих двух фаз указывает на то, что гексагональная структура металлической матрицы является более устойчивой при сравнении с ромбической матрицей. Третья фаза со структурой Ce_2Ni_7 является примесной. Полученные данные по распределению водорода в основной фазе с гексагональной структурой показывают, что в большей степени водород локализован в пустотах структурного фрагмента RT_2 и в незначительном количестве на границе между фрагментами RT_2 и RT_5.

В результате нейтронографических измерений образцов гидридов $CeNi_3H_x$ с x = 1.8, 3.4, 3.8 было установлено, что структура и параметры решетки гидрида $CeNi_3H_{1.8}$ практически такие же, как у исходного интерметаллида $CeNi_3$, а гидриды $CeNi_3H_{3.4}$ и $CeNi_3H_{3.8}$ имеют анизотропно расширенную решетку с увеличенным параметром c. При десорбции водорода из гидрида $CeNi_3H_{5.2}$ до состава $CeNi_3H_{3.8}$ в его структуре освобождается октаэдрическая позиция 6h фрагмента RT_5. Остальные занятые водородом позиции в $CeNi_3H_{3.8}$ такие же, как и в гидриде $CeNi_3H_{3.3}$ [6] с различием в заселенности. При дальнейшей десорбции до состава $CeNi_3H_{3.4}$ происходит освобождение позиций $24l_2$ блока RT_5. Десорбция до состава $CeNi_3H_{1.8}$ приводит к вакантной позиции $4f_1$ блока RT_2 и снижению заселенности позиций $24l_1$ блока RT_2 и $12k_1$ на границе между блоками RT_2 и RT_5. При переходе от $CeNi_3H_{3.4}$ к $CeNi_3H_{1.8}$ происходит резкое снижение объема кристаллической решетки гидрида, сопровождающиеся уменьшением параметра c. Такое поведение при десорбции связано в первую очередь с особенностями кристаллической

структуры гидрида, имеющей блочное строение. При освобождении пустоты $4f_1$ от водорода ее расположение вдоль оси z способствует сжатию тетраэдра, и соответственно, всего фрагмента RT_2 также вдоль оси z. Деформации решетки в этом направлении не препятствуют фрагменты RT_5, которые не заполнены водородом. Снижение заселенности в позиции $24l_1$ также приводит к сжатию фрагмента структуры RT_2. Вторым важным фактором является химическое взаимодействие водорода с металлическими атомами огранки пустот. В состав огранки пустоты $4f_1$ входит три атома Ni и один атом Ce, и это способствует ее первоочередному освобождению при сравнении с пустотами $24l_1$ и $12k_1$, содержащих в огранке по два атома Ni и Ce и сильнее удерживающих водород. Однако, снижение заселенности позиций $24l_1$ и $12k_1$, содержащих больше Ce и обладающих большими объемными эффектами, соответственно приводит к большему сжатию структурного фрагмента RT_2. Таким образом, в гидридах $CeNi_3H_x$ (x = 1.8, 3.4, 3.8) по мере снижения концентрации водорода, освобождение позиций от водорода в первую очередь происходит в структурном блоке RT_5, затем на границе между блоками RT_2 и RT_5 и в позициях блока RT_2.

Сравнение объемных эффектов при гидридообразовании показывает, что в гидридах с низкой концентрацией $CeNi_3H_x$ (x=0.7, 0.8, 1.0, 1.8) они практически отсутствуют, а в гидридах с большей концентрацией $CeNi_3H_x$ (x=3.4, 3.8) изменение объема решетки примерно соответствует объемным эффектам гидридообразования $CeNi_3H_{3.3}$. Таким образом, вне зависимости от способа получения гидрида $CeNi_3H_x$ (x = 0.7, 0.8, 1.0, 1.8), при низкой концентрации водорода увеличение объема решетки при сравнении с интерметаллидом практически не происходит, несмотря на то, что водород заполняет пустоты в решетке структурного блока RT_2 с большим содержанием Ce. Это указывает на то, что находящийся в атомарном состоянии водород в междоузлиях решетки имеет небольшой положительный заряд $H^{\delta+}$.

1. Яртысь В.А. Новые аспекты структурной химии гидридов интерметаллических соединений: «изотропные» и «анизотропные» структуры. // Координац. химия. 1992, т. 18, с. 401-408.
2. Лушников С.А., Балагуров А.М., Бобриков И. А., Вербецкий В.Н., Глазков В.П., Соменков В.А. Структура и особенности химической связи в дейтеридах $CeNi_3$. // Неорг. мат., 2007. т. 43, с. 1-8.

Using Individual Spectra Simulation for Study of Pole Figures Errors

T.A. Lychagina[1], D.I. Nikolayev [1], F. Wagner[2] and C. Scheffzuek[1,3]

[1] *Frank Laboratory of Neutron Physics, Joint Institute for Nuclear Research, Dubna, Moscow region, 141980, Russia*

[2] *Letam, University of Metz, Metz, France*

[3] *Freie Universität Berlin, FB Geowissenschaften, Malteserstrasse 74-100, 12249 Berlin, Germany*

The neutron diffraction experiment is one of the methods for obtaining information about crystallographic texture. The spectrometer for quantitative texture analysis (SKAT) is successfully operated at the 7A channel of IBR-2 reactor (FLNP, JINR, Dubna) since 1997 [1]. Neutron spectra are measured at SKAT to be used for pole figures extraction. Pole figures (PFs) contain experimental information about crystallographic texture. The requirements for the accuracy of PFs are growing in correlation with the complication of the investigated problems. Thus it is very important to study sources of the PF's measurement errors to look after their minimization. It is necessary to underline that pole figures measurement errors have an integral character, i.e. they include all factors like experimental layout, neutron statistics, grain statistics, external noise etc. The local peak fit approach gives us a tool for pole figure intensity and pole figure measurement errors determination [2-3]. Pole figures measurement errors do not depend on ODF reconstruction methods and are not connected with any further computations with pole figures, so they are of "pure" experimental kind. In our previous investigations [2-3] it was established that the qualitative distribution of PF measurement errors is similar to the distribution of peak width determination errors, or in other words a determining role in the PF measurement errors plays the errors of the peak width determination. This statement is the starting point for the present work. To check this conclusion spectra simulations have been done. The purpose of such simulations is to be convinced that such behaviour of pole figure errors is a property not only of the spectrometer SKAT. It can be checked up by means of spectra simulations because the errors entered into the spectra at the simulations are not connected with a special measurement process. Investigation of pole figure measurement errors were carried out for a set of Mg+4.5%Al+1%Zn samples.

The analysis of simulated spectra allowed us to confirm the main influence of the peak width determination error on the pole figure error (see Figure)[4]. This conclusion is drawn on the basis of comparison of errors distributions. Additionally, we simulated individual spectra using model pole figures and extracted pole figures and pole figures errors from those spectra. For this case we also confirmed the same qualitative behaviour of pole figure measurement errors and peak width

determination errors. The model pole figures were calculated on the basis of normal distributions [5]. Beside, we simulated the experimental errors (noise) directly in the spectra because actually the spectra contain the primary experimental information.

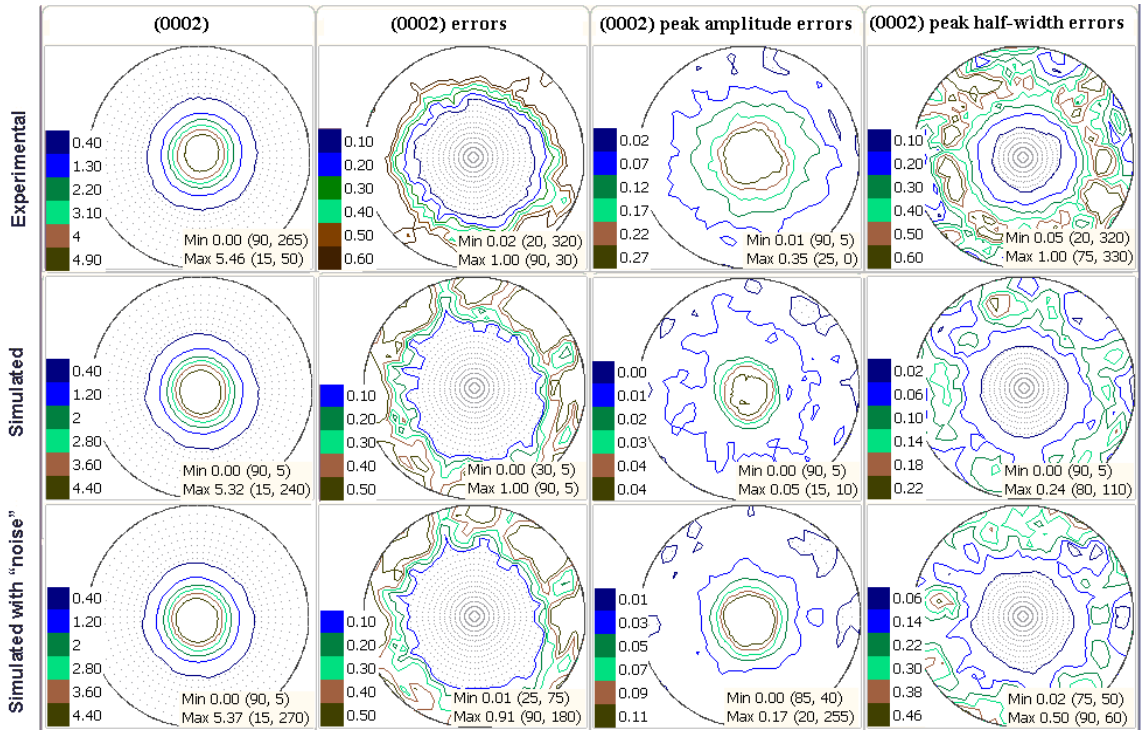

a) b) c) d)

Figure a) Pole figures (0002) for Mg+4.5%Al+1%Zn sample. The intensities are given in mrd (multiples of random distribution). b) The relative pole figure errors. c) The errors of peak amplitude. d) The errors of peak half –width.

So we can state that a decreasing of the pole figure errors can be reached by reducing of the peak width errors. One way to decrease the peak width error is to enlarge the peak width. But in this case the experimental resolution may be deteriorated. However, it can be done if the resolution in the diffraction spectrum is not so important (e.g. for texture investigations of samples with a sufficient number of isolated diffraction peaks). Similar results concerning pole figure measurement errors can be expected for data collected with X-ray measurements using position sensitive detectors.

References

[1] Ullemeyer K., Spalthoff P., Heinitz J. et al., Nucl. Instr. And Meth. A. **412**, 80 (1998)

[2] Nikolayev D.I., Lychagina T.A., Nikishin A.V., Yudin V.V., Solid State Phenomena, **105**, 77 (2005)

[3] Nikolayev D.I., Lychagina T.A., Nikishin A.V, Yudin V.V. Material Science Forum, **495-497**, 307 (2005)

[4] T. A. Lychagina, D.I. Nikolayev, F. Wagner "Using Individual Spectra Simulation for the Study of Pole Figures Errors," Texture, Stress, and Microstructure, Hindawi, vol. 2009 (2009), Article ID 237485, 10 pages, 2009. doi:10.1155/2009/237485; www.hindawi.com/journals/tsm/2009/237485.html.

[5] Savyolova T.I., Zavodskaya laboratoriya, **50,** N4, 48 (in Russian) (1984)

NEUTRON REFLECTOMETRY MODE AT MOND DIFFRACTOMETER OF IR–8 REACTOR

N.F.Miron[a], A.B.Rubtsov[b], V.A.Somenkov[a], V.I.Bodnarchuk[b], S.P.Yaradaikin[b]

[a]*Russian Research Center "Kurchatov Institute", 123182 Moscow, Kurchatov sq. 1, Russia*

[b]*Frank Laboratory of Neutron Physics, Joint Institute for Nuclear Research, 141980 Dubna, Moscow Reg., Russia*

The instrumental basis of the IR-8 reactor for condensed matter research has been succesfully operating during two last decades. However, until recently there were no instruments intended for investigations in physics of surface phenomena and layered structures. A new reflectometry mode at the acting MOND diffractometer is aimed to improve the situation.

The MOND diffractometer provides good ratio of the fast neutron flux to background (about 40) for performing reflectometry measurements. For realization of the reflectometry mode the modernization of MOND included: (1) installation of two additional collimating slits and a separate table for plain samples; (2) installation of the new detecting system (based on detector SNM-31). The scheme of the reflectometry mode at the MOND difractometer is shown in Fig.1, and its basic parametres are given in Table 1.

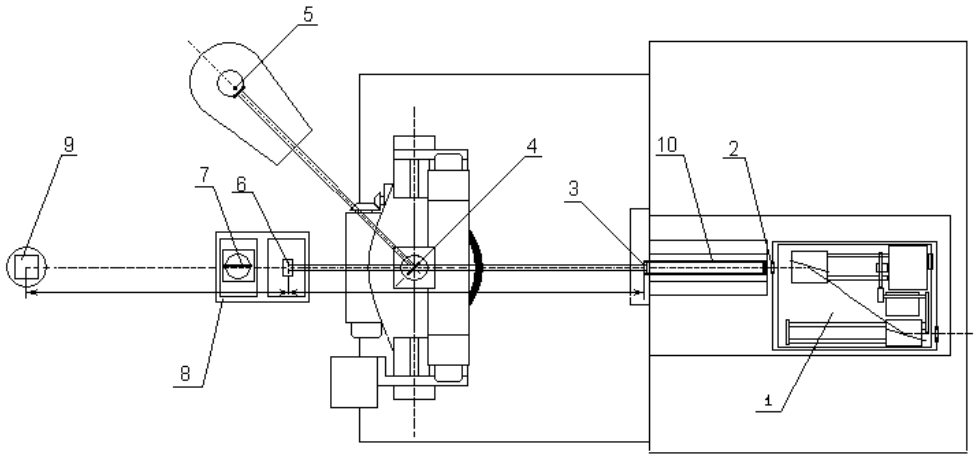

Fig.1. Scheme of reflectometry mode at MOND diffractometer (IR-8): 1 – double monochromator, 2 – first slit, 3 –monitoring detector, 4 – sample table of MOND, 5 – detector of MOND, 6 – second slit, 7 – sample position, 8 – sample table of reflecometer, 9 – detector SNM - 31, 10 –optical concentrator of neutron flux.

Table 1. Basic parameters

Wavelength range, Å	1 – 2,6
$\Delta\lambda/\lambda$, %	1
Slit size, mm	
first	0,5
second	0,3
Collimation base, mm	3500
Sample-detector distance, mm	1025

The measured experimental background curve (Fig.2) is approximated well by polynomal dependence. It was taken into account when obtaining the testing reflectivety curves given in Fig.3. They show the

reflectivty of the air/solid interfaces for the silicon substrate (Fig.3a) and curbon film with thikcness of about 200 Å (Fig.3b). As one can, the theoretical curves repeat well the experimental ones. The found value of the scattering length density (SLDs) for silicon, 2.196×10^{-6} Å^{-2} is within 5% deviation from its tabular value of 2.073×10^{-6} Å^{-2}. For carbon film, in addition to the found SLD of 7.56×10^{-6} Å^{-2} the thickness of the film is specified as 179.2 Å.

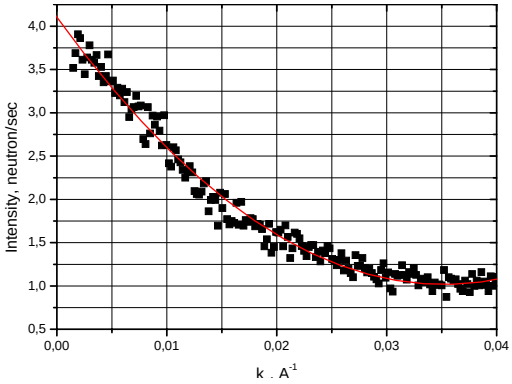

Fig.2. Background measurements.

a) b)

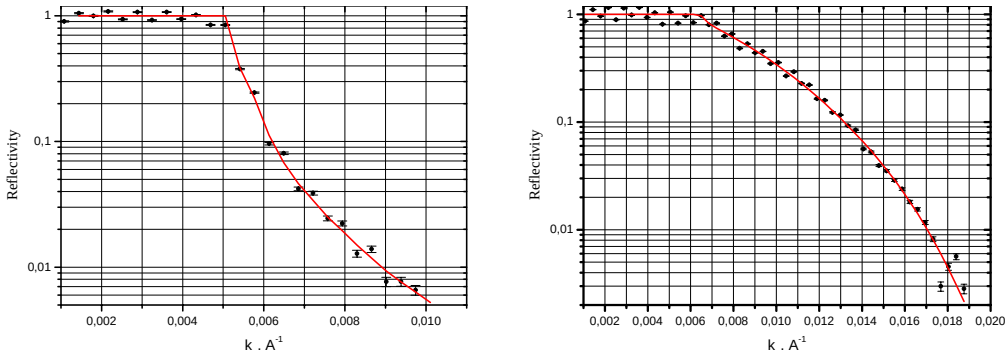

Fig.3. Testing reflectomtry curves (points) obtained at the new mode. Red lines are theoretical curves. a) silicon substrate; b) carbon film.

To summarize for the moment the reflecotmetry mode of the MOND diffractometer (IR-8) is available for testing measurments (specification of layer thicknesses and roughness in simple structures). Further steps such as an increase in the flight base for improving the signal/background ratio, and modernization of mechanical units for decreasing *k*-step are required. To expand possibilities of the instrument it is possible to install a position sensitive detector, which will allow one to study off-specular neutron scattering and also reduce the influence of mechanics on the experiment.

SMALL-ANGLE NEUTRON SCATTERING FROM VERY DILUTED MAGNETIC FLUIDS

A.V.Nagornyi[a,b], V.I.Petrenko[b,a], M.V.Avdeev[b], V.L.Aksenov[c,b,d], L.A.Bulavin[a]

[a]*Taras Shevchenko Kyiv National University, Kyiv, Ukraine*

[b]*Frank Laboratory of Neutron Physics, Joint Institute for Nuclear Research, Dubna, Russia*

[c]*Russian Research Center "Kurchatov Institute", Moscow, Russia*

[d]*Physical Faculty, Moscow State University, Moscow, Russia*

Ferrofluids (magnetic fluids) are liquid dispersions of magnetic nanoparticles covered with surfactants for preventing their coagulation in different conditions. Structure investigations of ferrofluids are of great interest from both the fundamental and application viewpoints [1,2].

The characteristic size (~10 nm) of magnetic nanoparticles in ferrofluids corresponds to a single-domain state, thus determining a superparamagnetic behavior of the magnetic fluids. One of the most discussed features of such magnetic nanoparticles is a possible non-magnetic layer on their surface, which can explain a lower, as compared to the bulk state, value of the specific magnetization of colloidal magnetic systems [3,4]. In our previous SANS experiments (both non-polarized and polarized modes) on classical ferrofluids under magnetic field it was shown [5,6] that, despite non-correlated particle locations in low concentrated samples (volume fraction of magnetic material of about 1%), still the correlation in orientation of magnetic moments of the particles take place, which results in higher (than expected) values of the apparent magnetic particle size. In the absence of the external magnetic field this causes a deviation of the experimental SANS curves from the model calculations for non-interacting particles at small q-values [7]. Taking into account the high polydispersity of the magnetic nanoparticles in the studied ferrofluids (nanomagnetite obtained by the precipitation reaction coated with a single layer of mono-carboxylic acids in non-polar organic carriers), the modeling of the structure-factor faces difficulties. In this case a decrease in the particle concentration is a natural way for eliminating the structure-factor effect.

The possibility of the small-angle neutron scattering experiment on very diluted magnetic fluids (magnetite volume fraction ~ 0.1%) for determining their structural parameters from the Guinier approximation, is considered in the present report. The accent is made on the experimental observation of a non-magnetic layer on the surface of magnetic nanoparticles dispersed in a liquid carrier. The main idea of the work is to use for this purpose very diluted magnetic fluids, where, on the one hand, the structure-factor effect is minimal because of the dipole-dipole interaction, and, from the other hand, the SANS curves can be still resolved. The relevant parameters are defined from model calculations, and the regime of the experiment on the contrast variation is selected.

An expression for the Guinier invariants (radius of gyration, R_g, and forward scattering intensity, $I(0)$) are obtained in the context of the core-shell particle model for the nuclear scattering length density profile and the model of spherical particles for the magnetic scattering density profile assuming no interaction between particles. The Guinier invariants can be written as:

$$I(0) = I_n(0) + (2/3)I_m(0) = n(\Delta\rho)^2\left[V(r) + \eta \cdot V(r+\delta)\right]^2 + (2/3)n\rho_m^2 V_m^2(r-h)\ , \tag{1}$$

$$R_g^{\,2} = \frac{3}{5}\frac{(\Delta\rho)^2\left[(r\cdot V(r) + \eta\cdot(r+\delta)\cdot V(r+\delta))^2 + (\eta\delta)^2 V(r)V(r+\delta)\right] + (2/3)\rho_m^2\cdot(r-h)^2\cdot V_m^2(r-h)}{(\Delta\rho)^2\left[V(r) + \eta\cdot V(r+\delta)\right]^2 + (2/3)\rho_m^2 V_m^2(r-h)},$$

where $\Delta\rho$ is the difference between the scattering length density of the magnetic core and surfactant layer; η and δ are the contrast and thickness of the surfactant shell; h is the thickness of a non-magnetic layer on the surface of magnetic nanoparticles; n is the concentration of magnetic nanoparticles; ρ_m is the magnetic scattering length density; $V(r)$ is the spherical volume restricted by

radius *r*. The calculations are made for magnetite-oleic acid-benzene ferrofluid which is a typical non-polar magnetic system. Figure 1 show calculated deviations of the Guinier invariants as functions of different structural parameters varied in the vicinities of typical values.

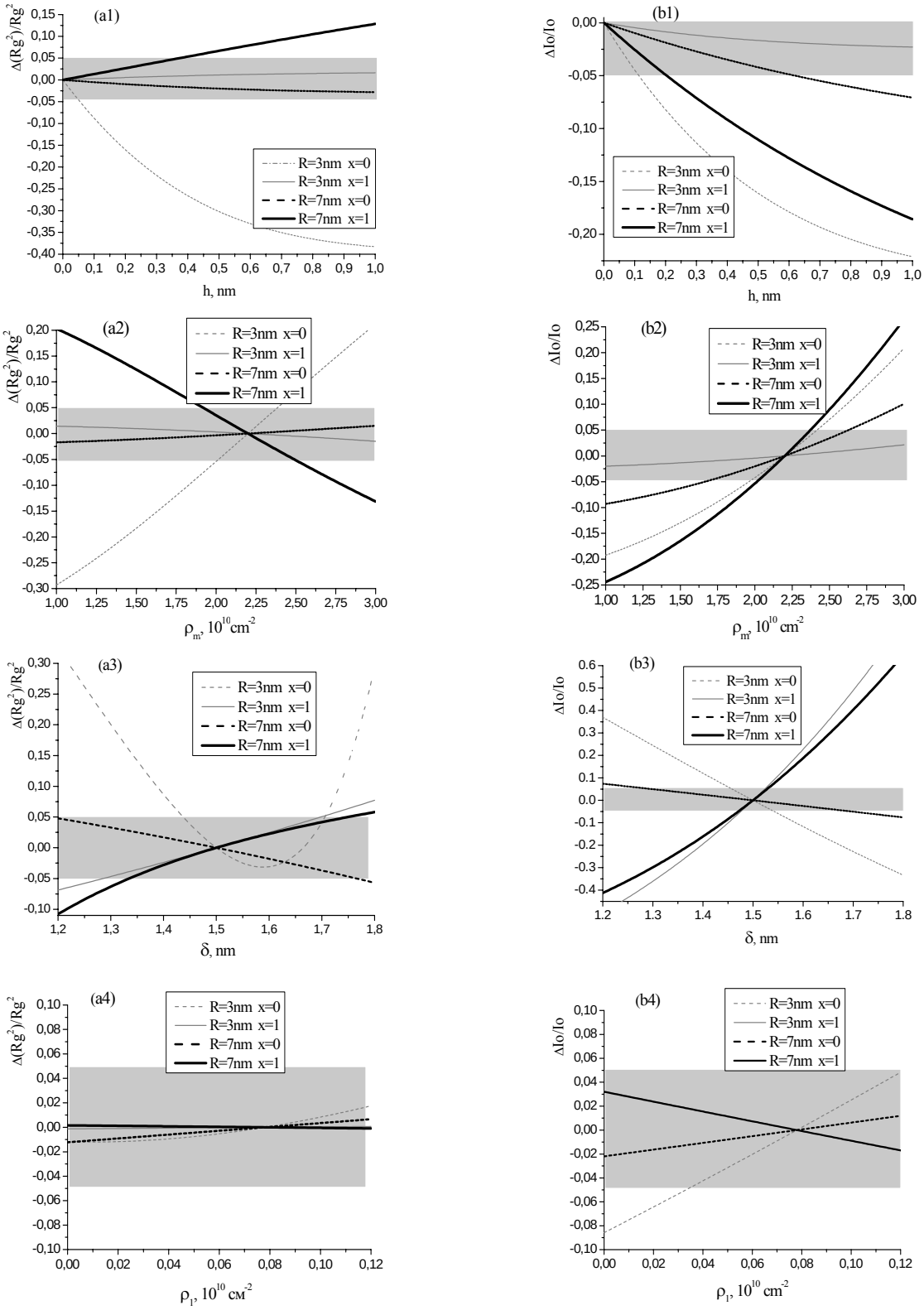

Fig.1. Dependence of relative deviation of radius of gyration (a) and forward scattering intensity (b) on variation of different structural parameters. Regions of 5% deviation are marked.

Monodisperse magnetic particles with sizes R=3 nm and R=7 nm were considered. Varying parameters are thickness of the non-magnetic layer (h), magnetic scattering length density (ρ_m), thickness (δ) and scattering length density of the surfactant shell (ρ_1). Taking into account the fact that the match point for the discussed model particles lays in an interval of 30-70% of the volume fraction of the deuterated component in the liquid carrier (depending on model parameters) the simulation is made for the cases corresponding to highest SANS signals, which are 0% (fully protonated carrier) and 100% (fully deuterated carrier). The task was to select the conditions of the SANS contrast variation experiment for determining structural features of the particles in ferrofluids with the 5% accuracy of about, which is a typical precision of the SANS experiments.

From Fig.1 we can say that the case of fully deuterated carrier with "large" magnetic particles is the most informative. Since SANS signal on very dilute ferrofluids is comparable with the incoherent background of neutron scattering on systems with high hydrogen content, it is preferred to perform the contrast variation in the x-range of 0.75 – 1.0 (75% - 100% deuterated solvent) for magnetic fluids with "large" particles (for example: the stabilization of magnetite by oleic acid in non-polar carriers). Also we can deduct that the Guinie invariants are insensitive to an uncertainty in ρ_1.

The number of experimentally required points over the contrast was evaluated from our numerical calculations. Thus, for each ferrofluid we can measure 7-10 different contrasts with the step of Δx=0.04 (4%) in the x-range of 0.75 – 1.0. The absolute values of the Guinier parameters for large particles and three values of non-magnetic layer (h = 0, 0.5 and 1.0 nm) are presented in fig.2 for the illustration of possible SANS experiment.

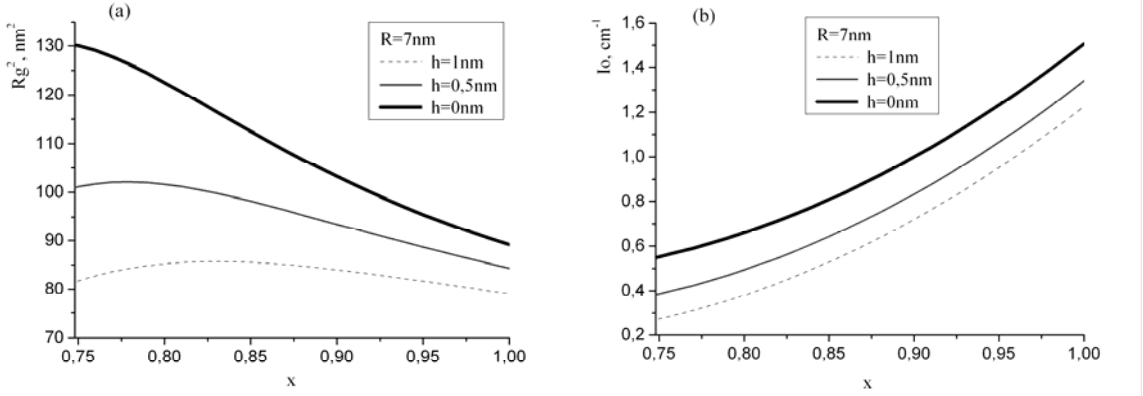

Fig.2. Expected x-dependences for the squared radius of gyration (a) and forward scattering intensity (b) in diluted sample (0.1%) of a model ferrofluid at different h-values.

The work is partially done in the frame of the project RFBR-Helmholtz (HRJRG-016).

References

[1] L.Vekas, M.V.Avdeev, D.Bica, *Magnetic Nanofluids: Synthesis and Structure, In Nanoscience and Its Applications in Biomedicine*. Ed. Donglu Shi, Springer Verlag (2009).
[2] U.Häfeli, M.Zborowski (Eds.) Proceedings of the 7th International Conference on the Scientific and Clinical Applications of Magnetic Carriers, *J. Mag. Mag. Mater.* 321 (2009).
[3] A.E.Berkowitz, J.A.Lahut, I.S.Jacobs, et al., *Phys. Rev. Lett.* 34 (1975) p.594.
[4] R.H.Kodama, A.E.Berkowitz, E.J.McNiff, et al., *Phys. Rev. Lett.* 77 (1996) p.394.
[5] V.Aksenov, M.Avdeev, M.Balasoiu, et al., *Appl. Phys. A* 74 (2002) p.943.
[6] M.V.Avdeev, *Physics Uspekhi* 50 (2007) p.1139.
[7] M.V.Avdeev, D.Bica, L.Vekas, et al., *J. Coll. Interface Sci.* 334 (2009) p.37.

SAS STUDY OF THE STRUCTURE AND PROPERTIES OF CARBOSILANE DENDRIMERS

A V Rogachev[1,2], A Yu Cherny[3], A N Ozerin[4], A M Muzafarov[4], E ATatarinova[4], V I Gordeliy[1,5,6], A I Kuklin[1,5]

[1)] Frank Laboratory of Neutron Physics, JINR, Dubna, Moscow reg., Russia
[2)] Skobeltsyn Institute of Nuclear Physics of Moscow State University, Moscow, Russia
[3)] Bogoliubov Laboratory of Theoretical Physics, JINR, Dubna, Moscow reg., Russia
[4)] Institute of Synthetic Polymeric Materials of the Russian Academy of Sciences, Moscow, Russia
[5)] Moscow Institute of Physics and Technology, Dolgoprudny , Moscow reg., Russia
[6)] IBS, Grenoble, France

Dendrimers constitute a new class of polymers with monodisperse structure, shape, and size due to a certain number of generations, resulting from well-controlled synthesis in a step-wise method [1,2].

The dendrimers has a compact structure (2-10 nm) with a large number of the functional end groups in the surface layer. The dendrimers can be considered as both macromolecules and particles simultaneously. Because of good solubility and low viscosity, the dendrimers attract substantial attention in basic and applied researches. For example, they can be used as a "laboratory" for studying the dimension size effect [3] and investigated in material science as a nanoobject with many promising application in biology, pharmacology, and chemistry.

However, direct microscopic methods yield very limited information about dendrimers' size and shape [4-6]. A more detailed information about the structure can be obtained with the help of small angle X-ray and neutron scattering. SANS experiments were performed at the YuMO instrument (JINR, Dubna, Russia) [7,8].

The mean values of the scattering length density of the dendrimers were obtained with the method of SANS contrast variation [9], see (**Fig.1**).

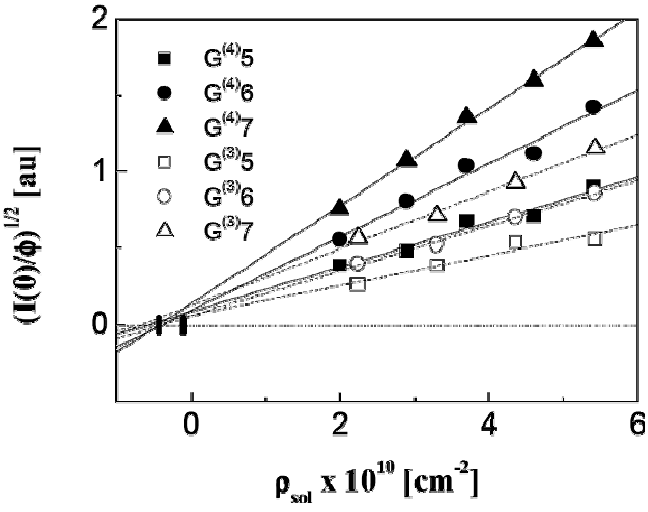

Fig.1. Normalized zero angle scattered intensity $(I(0)/f)^{1/2}$ vs. length scattering density ρ_{sol} of the solvent for $G^{(3)}5$-$G^{(3)}7$ (w = 2 wt.%) and $G^{(4)}5$-$G^{(4)}7$ (w = 1 wt.%) dendrimers. The right vertical bar corresponds to the calculated ρ_d value for $G^{(3)}5$-$G^{(3)}7$ dendrimers, the left one - for $G^{(4)}5$-$G^{(4)}7$ dendrimers.

The value of mean scattering length density for 5-7 generations is 0.4×10^{10} см$^{-2}$. Within experimental errors, this value is consistent with theoretically calculated values.

[1] rogachev@nf.jinr.ru
[1] kuklin@nf.jinr.ru

It was shown that small angle scattering curves can be fitted well by the model of homogeneous globular particles [10] **(Fig.2).**

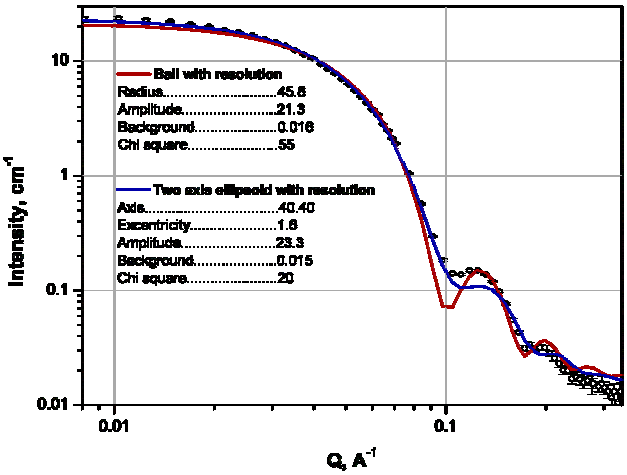

Fig. 2 SANS curve for $G^{(4)}9$ dendrimer fitted with the model scattering curves of uniform ball and uniform ellipsoid.

The volume, shape and size of several generations of dendrimers were obtained by SAS data [11-14]. It was shown that the dendrimers are monodispersive objects in size and they have anisometric shape (Fig. 3, 4).

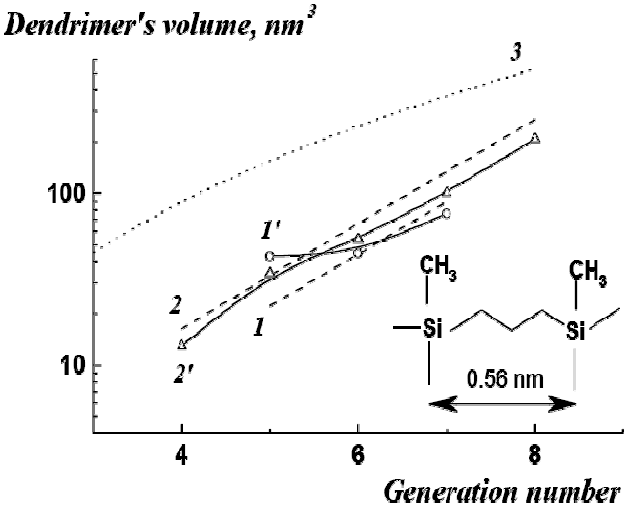

Fig.3 The molecular dendrimer volume for 4-8 generations with 3 and 4 core functionality: 1, 2 - theoretical volume from bulk density; 1', 2' - restored volume from *ab initio* method).

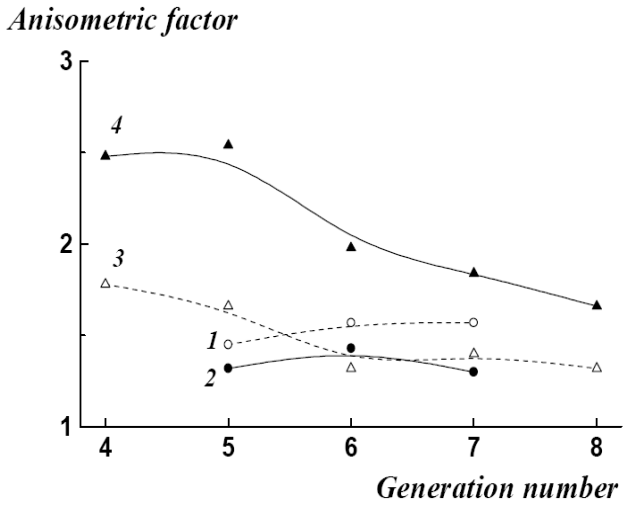

Fig. 4. The anisometric factor for 4-8 generations of dendrimers of different generations found from *Rmax*/*Rmin* (dashed lines) and *Imax*/*Imin* (solid lines) values with 3 (1, 2) and 4 (3, 4) core functionality.

The scattering length density inside the dendrimers of several generation numbers is reconstructed by using modern mathematical methods [14]. It was shown with the SANS contrast variation method that the studied dendrimers are identical in overall size and scattering length density distribution (**Fig. 5 a, b)**.

The behavior of contrast variation curves shows that all the dendrimers are chemically identical and the dendrimers in the solution are monodisperse with respect to the scattering length density inside the inner volume of dentritic macromolecule. Thus, Fig. 5*b* shows that the scattering length density is homogeneous within the experimental errors inside the dendrimer branches.

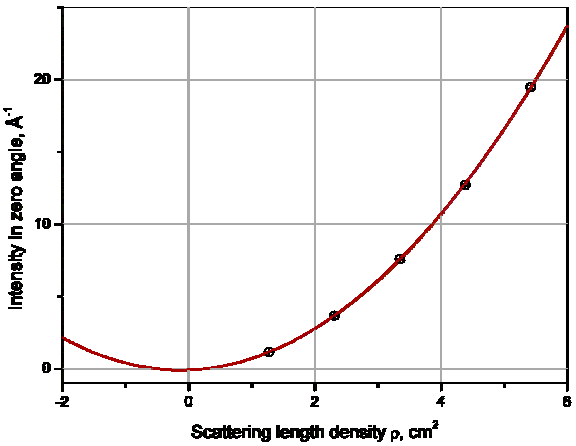

Fig. 5a). The intensity in zero angle as a function of the scattering length density of solvent.

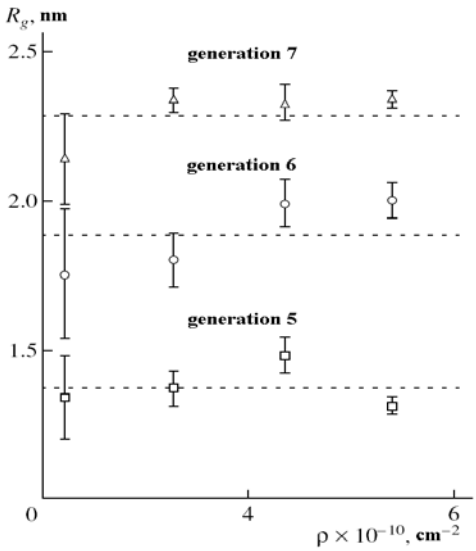

Fig.5b). The radius of gyration versus the scattering length density of solvent.

The obtained data about the detailed structure of the polycarbosilane dendrimers show that the model of linear growing and branch architecture cannot explain the anisometry and the scattering length density distribution of the macromolecules.

It was established that the high generation dendrimers share a number of traits with the low generation dendrimers, namely, globularity, monodispersity, and the shape anisometry. The inner structure of higher generation of dendrimers is more complicated than that of lower generation.

In conclusion, the spatial structure of several generations of regular hyperbranched polymers (polycarbosilane dendrimers) is studied by means of small-angle neutron and X-ray scattering. Comparative analysis of sizes, volumes, and shapes is done for all the generations from third to ninth. The mean values of the scattering length density of the dendrimers are obtained with the method of SANS contrast variation and compared with theoretically calculated values. It is shown that within experimental errors, the scattering length density is uniform inside the dendrimer branches. The permeability of the solvent inside the dendrimer is discussed [10], and the volume fraction accessible to the solvent is estimated. The structure peculiarities of the dendrimers open good prospects of exploiting dendrimer macromolecules as universal functional nanomaterials.

1. A. M. Muzafarov and E. A. Rebrov, Polymer Sci. C 42 (1), 55 (2000).
2. D. A. Tomalia, A. M. Naylov, and W. A. Goddard, Angew. Chem., Int. Ed. Engl. 29 (2), 138 (1990).
3. Rogachev A.V., Kuklin A.I., Cherny A.Yu. et al.,Preprint of the JINR, P14-2008-192 (2008).
4. T. J. Prosa, B. J. Bauer, and E. J. Amis, Macromolecules 34, 4897 (2001).
5. E. A. Tatarinova, E. A. Rebrov, V. D. Myakushev, et al., Russ. Chem. Bull., 53(11), 2591-2600, (2004).
6. B. V. Lebedev, M. V. Ryabkov, E. A. Tatarinova, et al., Russ. Chem. Bull. Int. Ed., V.52(3), 545-551, (2003).
7. Kuklin A.I., Islamov A.Kh., and Gordeliy V.I., Neutron News, vol. 16, 3, pp.16-18, (2005).
8. Kuklin A.I., Islamov A.Kh., Kovalev Yu.S. et al., Poverkhnost, №6, c.74-83, (2006).
9. Kuklin A. I., Ignat'eva G. M., Ozerina L. A., et al., Polym. Sci. A, 44, 2124–2133, (2002).
10. Rogachev A.V., Cherny A.Yu., Ozerin A.N., et al., Crystallography Reports, 52, 3, 500–504, (2007)
11. Ozerin A. N., Muzafarov A. M., Gordeliy V. I., et al., Macromol. Symp., 195, 171–178, (2003).
12. Kuklin A. I., Ozerin A. N., Islamov A. Kh., et al., J. Appl. Cryst., 36, 679–683, (2003).
13. Ozerin A. N., Muzafarov A. M., Kuklin A. I., et al., Dokl. Chem., 395, 59–62 (2004).
14. Ozerin, A. N., Svergun D.I., Volkov V.V., et al., J. Appl. Cryst. 38, 996–1003, (2005).

РЕЗУЛЬТАТЫ ПЕРВОГО СИНХРОТРОННОГО ИССЛЕДОВАНИЯ СТРУКТУРЫ МНОГОСЛОЙНЫХ ВЕЗИКУЛ СМЕСИ СФИНГОМИЕЛЕН/ФОСФОЛИПИДЫ

Н.Ю. Рябова[a], М.А. Киселёв[a], О.В. Найда[b], А.В. Забелин[b], А.М. Балагуров[a]

[a]*Объединенный институт ядерных исследований, 141980 г. Дубна, Россия*
[b]*Курчатовский центр синхротронного излучения и нанотехнологий, РНЦ «Курчатовский институт», 119991,г. Москва, Россия*

Методом рентгеновской дифракции на станции Дикси в НТК КЦСИиНТ, РНЦ «Курчатовский институт» исследованы водные растворы мультислойных везикул смеси сфингомиелен/дипальмитоилфосфатидилхолин/дипальмитоилфосфатидилэтаноламин (SM/DPPC/DPPE), входящей в их состав слизистой оболочки ротовой полости человека [1,2].

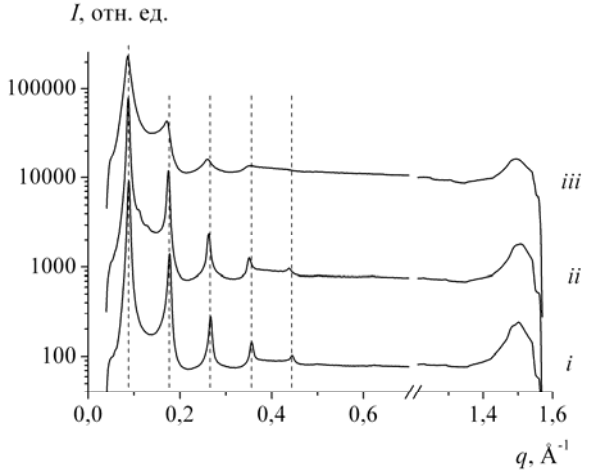

Рис. 1. Дифракционные спектры от ламеллярной ($q < 0.6$ Å^{-1}) и латеральной ($q \approx 1,5$ Å^{-1}) структуры многослойных везикул смеси фосфолипидов и сфингомиелина PL=SM/DPPC/DPPE с весовом соотношением компонент (i) PL2=1/2/1, (ii) PL1=1/2/2 и (iii) PL3=1/1/1, измеренные на спектрометре Дикси при концентрации липидов в воде 20% (для PL1 и PL2) и 10% (для PL3) при комнатной температуре. Вертикальными линиями отмечены положения дифракционных пиков смеси PL2.

На **рис. 1** представлены дифракционные спектры от структуры многослойных везикул смеси фосфолипидов и сфингомиелина PL=SM/DPPC/DPPE с разным соотношением компонент, измеренные при комнатной температуре.

Система SM/DPPC/DPPE при массовом соотношении компонентов 1/1/1, 1/2/1, 1/2/2 характеризуется ламеллярной структурой с периодом повторяемости соответственно 72,8 Å, 70,7 Å и 71,7 Å. При увеличении массовой доли DPPE до 40% (в смеси PL1=1/2/2) часть липида образует отдельную ламеллярную фазу (d ~ 56 Å) и инвертированную гексагональную фазу (a ~ 56 Å), вероятнее всего в составе с SM и DPPC, поскольку значение параметра a несколько превышает значение параметра инвертированной гексагональной фазы, образованной чистым DPPE (a ~ 52 Å).

Дифракция от углеводородных цепочек смеси 1/2/1 дает два неразрешенных пика при q = 1,48 ± 0,01 Å^{-1} и 1,50 ± 0,01 Å^{-1}, что соответствует двумерной квазигексагональной решетке с параметрами a = 4,25 Å, b = 4,19 Å. Спектр от смеси 1/2/2 также содержит неразрешенные пики при 1,49 ± 0,01 Å^{-1} и 1,51 ± 0,01 Å^{-1}, соответствующие параметрам квазигексагональной упаковки углеводородных цепочек a = 4,22 Å и b = 4,16 Å. Увеличение доли SM приводит к разупорядочиванию цепочек смеси 1/1/1, для которой характерен широкий пик в положении ~ 1,495 Å^{-1}.

Литература

[1] Squer C.A, Critical Reviews in Oral Biology and Medicine, 2(1), (1991) 13-32.
[2] Squer C.A., Cox P, Wertz P.W., Journal of Investigative Dermatology 96, No.1, (1991) 123-126.

THE UPGRADE OF PACKAGE FOR PRELIMINARY TREATMENT OF SMALL-ANGLE SCATTERING SPECTRA

A.G. Soloviev[1)], T.M. Solovieva[2)], S.A.Kutuzov[3)], A I. Kuklin[3)]

[1)] *The Laboratory of Information Technologies, JINR, Dubna, Moscow reg., Russia*
[2)] *Dzhelepov Laboratory of Nuclear Problems, JINR, Dubna, Moscow reg., Russia*
[3)] *Frank Laboratory of Neutron Physics, JINR, Dubna, Moscow reg., Russia*

A successfully operating modernized spectrometer YuMO (4-th channel of IBR-2), see [1], has been equipped with a new software package for preliminary treatment of experimental data. The basic procedures there (see Ostanevich Yu. M., Bezzabotnov V. Yu., (1992), unpublished; a short description can be found in the site [2]) were left virtually unchanged. Nevertheless, the new package has modern design and implementation, but more importantly, it has several novel features [3,4]. A significant expansion of the user base of YuMO spectrometer requires not only a user guide for its software, but also a solution of a few problems related to treatment of experimental data [5].

The modernization of this tool is not yet complete. Therefore, at present we will refrain from discussing a number of important issues. First of all, that concerns the formats of raw data, and integration of the data coming from different detectors in the two-detector version of the spectrometer [1,6]. The new package SAS was synchronized with the software of the spectrometer YuMO [7], and its development will continue with the modernization of this device.

The raw files produced by the spectrometer, contain scores from all rings of the scattering detectors (see the diagram below) grouped according to different channel numbers. A preliminary data-treatment package must convert the channel number, first, into the wavelength, and then into the neutron momentum transfer. It also must convert detector counts into the coherent scattering cross-sections.

The first task is solved by a straightforward conversion of the channel number, first, into the time of flight, and then, for known values of the moderator-detector distance, sample-detector distance, and of the radius of the corresponding ring, into the transferred momentum. The solution of the second task requires, in addition to the measurements of neutron scattering by the sample under investigation, additional experiments with standard scatterers. For that purpose, water, for instance, is placed instead of the sample in many small angle instruments.

An important feature of the spectrometer YuMO is not only its geometry (which, in fact, is axially symmetric) and the presence of a hole in the central part of the detectors for the direct beam passage, but also the presence of a standard scatterer (metal vanadium) in front of every detector. Using these scatterers, the cross-section is periodically calibrated *during* the neutron scattering experiments with the relative systematic error not exceeding 10%. It turns out, that for weakly scattering samples (scattering cross-section less than 10 cm^{-1}) an additional measurement of sample transmission, is not necessary. That gives us an opportunity to conduct a preliminary treatment of experimental data simultaneously with the measurements, directly in the absolute intensity scale.

The neutron fluxes on the samples are very significant, and the dead-times on the proportional He^3-detectors are of the order of microseconds. Therefore, one has to perform a dead-time correction.

Investigations using small angle neutron scatterings (SANS) are performed on reactors (sometimes referred to as “stationary”), and on accelerators. The pulse reactor IBR-2 combines the advantages of stationary reactors (first of all, the high neutron flux) and the periodicity of particle flow, similar to accelerators. Therefore, one can set up neutron experiments in an entirely different way than it is done on the stationary reactors, where a narrow segment around a particular wavelength is cut from the thermal neutron energy spectrum (the Maxwell distribution). The actual “cutting out” is performed either with the help of a wave selector, or with the help of a perfect crystal.

Only the time of flight method (TOF) allows one to exploit all the advantages of such a reactor. Since the velocity of thermal neutrons is not great, it is possible to analyse the neutron wavelength using its time of flight (TOF). This idea led to creation of neutron spectrometers based on time-of-flight measurements: after slowing down to thermal energies, a beam of neutrons emitted by a pulsating source is directed at a sample, where it is scattered, and is registered by detectors.

The main changes of SAS-package are:

- program for converting of raw data to format of SAS
- program for converting of raw PSD data without azimutal anysometry to format of SAS
- adapted of SAS program to this changes
- options for averaging on logarithmic or square-law scales
- advanced smoothing procedure based on spectrometer resolution [4]
- operations with histograms unified [8]
- storing parameters in configuration file unified [9]
- support for processing spectra with both 256 and 1024 channels
- support for using sas as a C++ class library
- modern visualisation [10] and cross-platform GUI

In current version SAS main window presented in figs. 1 and 2.

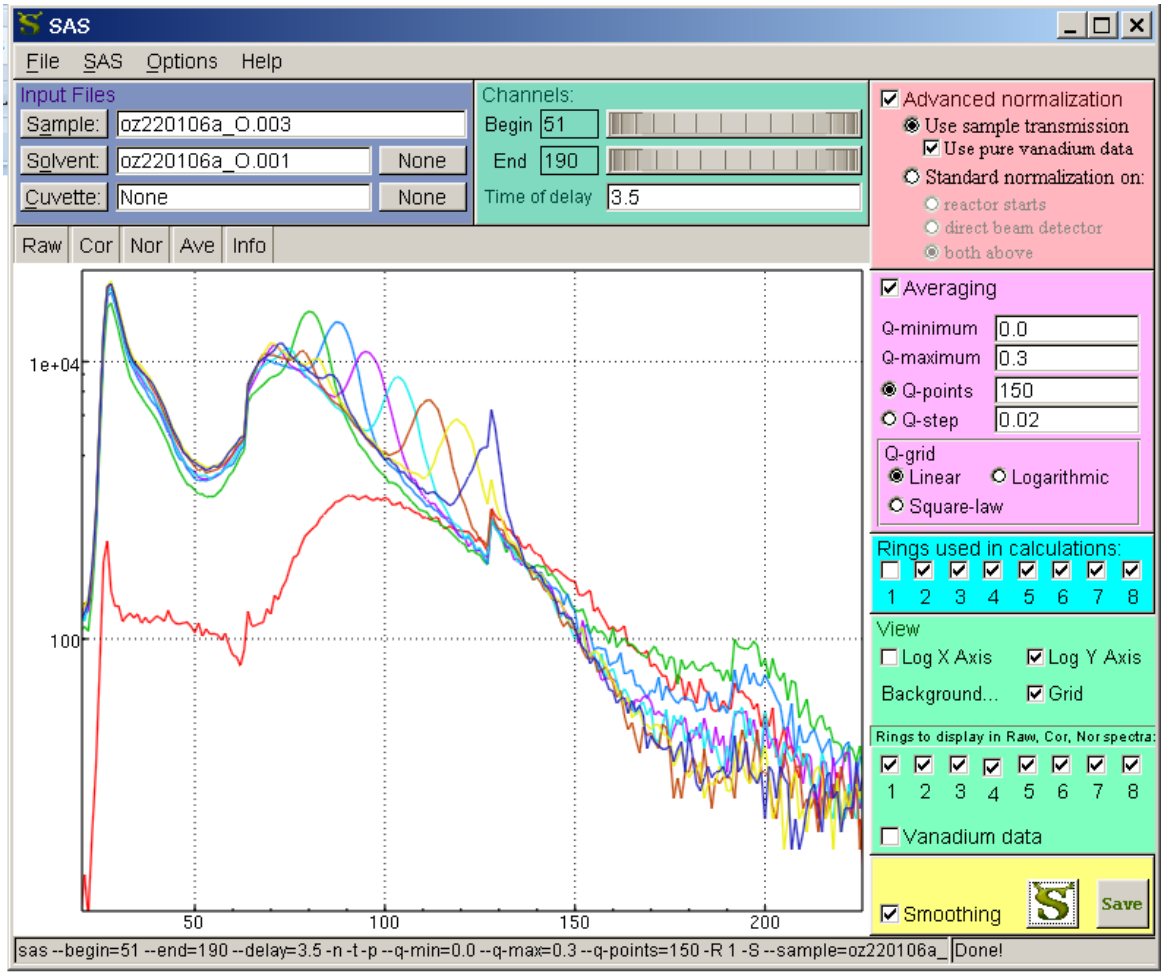

Fig.1. View of screen for "Raw" option. Dependence of count as a function of channel function.

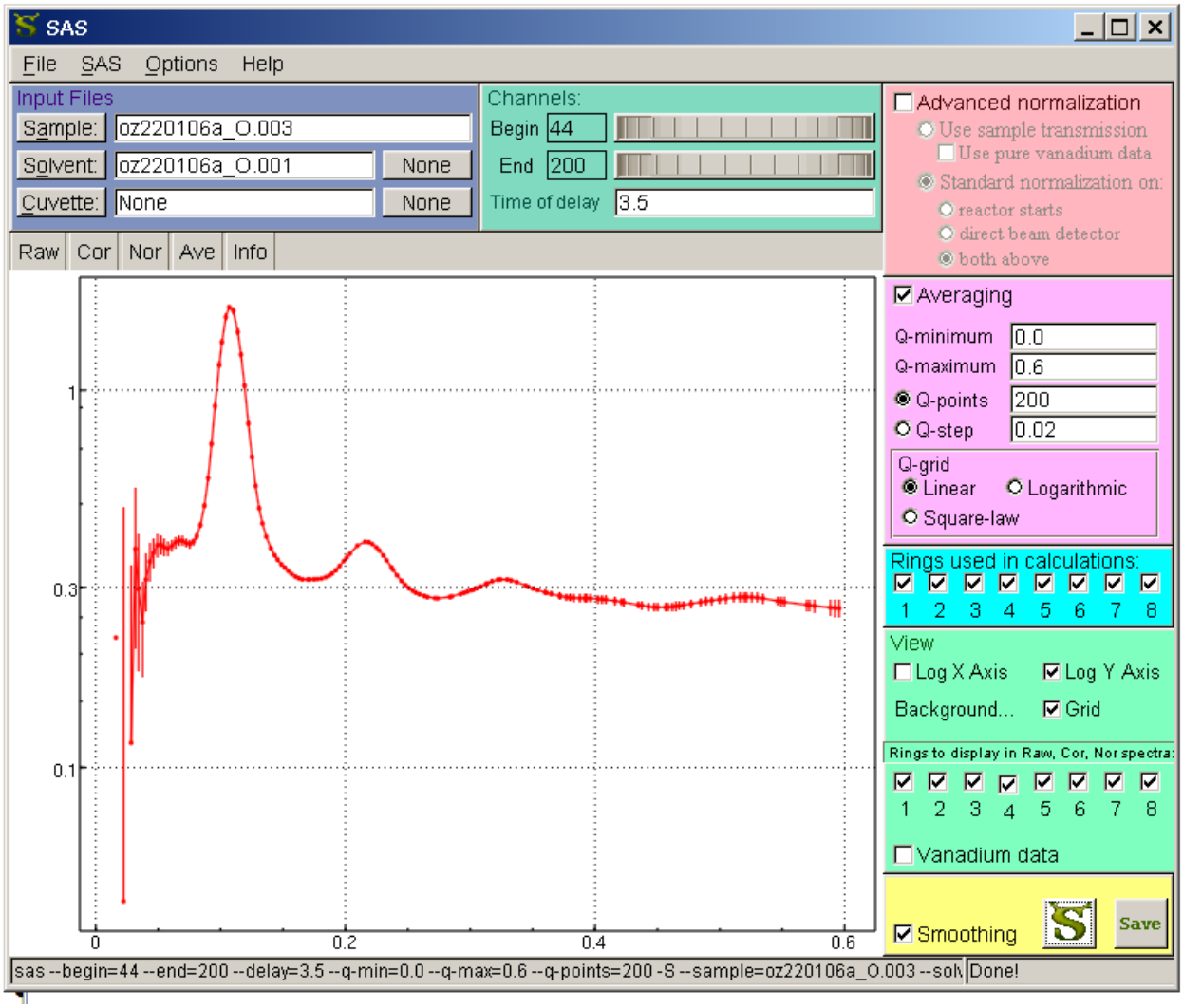

Fig.2. View of screen for "Ave" option. Dependence of scattering cross-section as as a function of module of scattering vector q.

References

[1]. Kuklin A.I., Islamov A.Kh., and Gordeliy V.I., Neutron News, vol. 16, 3, pp.16-18, (2005).
[2] http://wwwinfo.jinr.ru/programs/jinrlib/sas-1x/index.html
[3] A.G.Soloviev, T.M.Solovieva, A.V.Stadnik, A.H.Islamov and A.I.Kuklin. SAS. The Package for Small-Angle Neutron Scattering Data Treatment. Version 2.4. Long Write-Up and User's Guide. Communication of JINR P10-2003-86, Dubna, 2003.
[4] Soloviev A.G., Litvinenko E.I., Ososkov G.A., Islamov A.H. and Kuklin A.I. Application of wavelet analysis to data treatment for small-angle neutron scattering. Nuclear Inst. and Methods in Physics Research, A. 502/2-3 (2003) 498—500.
[5] http://wwwinfo.jinr.ru/programs/jinrlib/sas/index.html
[6] Kuklin A.I. et al. Optimization two-detector system small-angle neutron spectrometer YuMO for nanoobject investigation. Surface. 2006, №6, pp.74-83 (rus).
[7]. A. S. Kirilov, E. I. Litvinenko, N. V. Astakhova, S. M. Murashkevich, T. B. Petukhova, V. E. Yudin, V. I. Gordelii, A. Kh. Islamov, and A. I. Kuklin, Evolution of the SONIX Software Package for the YuMO Spectrometer at the IBR-2 Reactor, Instruments and Experimental Techniques *(Pribory i tekhnika eksperimenta)* 3, 2004, Volume 47 (6 issues), 334-336.
[8] http://wwwinfo.jinr.ru/programs/jinrlib/htl/index.htm
[9] http://wwwinfo.jinr.ru/programs/jinrlib/rc/index.html
[10] http://wwwinfo.jinr.ru/programs/jinrlib/gluplot/index.html

HEAVY METALS IN THE ENVIRONMENTAL OBJECTS OF NON-FERROUS INDUSTRIAL REGION OF MONGOLIA, THE TOWN OF ERDENET

Baljinnyam N., Gerbish Sh. , Ganbold G[1]., Lodoysamba S[1].,
Frontasyeva M.V., Pavlov S.S.

FLNP JINR, E-mail: baljan@nf.jinr.ru

[1]*Research Centre of National University of Mongolia, Ulaanbaatar*
E-mail: lodoysamba@num.edu.mn

Introduction

Long-term collaboration of the Mongolian and JINR specialists in the field of applying nuclear and related analytical techniques to the environmental studies resulted in a series of joint publications which served the purposes of monitoring heavy metals and radionuclides in different ecosystems of Mongolia. Such cities as Ulaanbaatar, Erdenet and Darkhan are experiencing the ecological stress due to insufficiently well-thought industrial activity of mining and mineral raw materials producing enterprises responsible for more than 70 % gross product in the economy of Mongolia. In 2008 a project «Development of a system of complex monitoring heavy metals and radionuclides in Mongolia based on nuclear and related analytical techniques» was approved for financing by RFBR (Russian Fund for Basic Research) – Mongolia.This project aims at the development of a system of complex monitoring heavy metals and radionuclides in Mongolia to control the state of the environment, to provide rational use of natural resources and to prevent hazardous impacts on human and animals' health of the main anthropogenic sources.

The concept of this project is based on (i) assessment of contamination of the environment with radionuclides over the territories affected by their impact; (ii) investigation of ^{137}Cs distribution in soil and terrestrial vegetation (moss, lichens), as well as of such natural radioactive elements as U, Th, and ^{40}K; (iii) assessment of contamination of the environment with heavy metals of industrially developed areas of Mongolia (Erdenet, Ulaanbaatar). The moss (*Paltegera*) was used to assess the atmospheric deposition patterns of heavy metals and other toxic elements over a large territory affected by non-ferrous industry in the town of Erdenet. Its impact on pasture animals (goats and sheep) was studied through analysis of such inner organs as lung, spleen, liver, kidney, and heart. A total of 37 elemental concentrations in these samples were determined by instrumental neutron activation analysis (INAA) using epithermal neutrons at the IBR-2 reactor, FLNP, JINR, Dubna (Ganbold G. et al., 2006). The distribution of biogenic elements and heavy metals in water samples were investigated by means of total reflection X-ray fluorescent analysis (TXRF) at Nuclear Research Centre of the National University of Mongolia, Ulaanbaatar (Gerbish Sh. et.al. 2008).

The results obtained evidence for strong accumulation of element-pollutants typical for non-ferrous industry in the town of Erdenet: Cu, Cr, Fe, Ba, *etc*. along with other trace elements and rare earths for the first time determined in these environmental objects.

Study area

Erdenet is the second largest industrial and mining city with 100 thousand populations in Mongolia. Erdenet Mining Corporation is one of the biggest ore mining and ore processing factory in Asia. Erdenet Mining Corporation (EMC or Erdenet) was established in accordance with an agreement between governments of Mongolia and Russian. It started its operation in 1978. The main mineral deposit, extracted by the Corporation was the Erdenetiin-Ovoo area which locates 400 kilometers northwest from Ulaanbaatar, 180 kilometers east from Darkhan city, 60 kilometers northern from Center of Bulgan aimag and 140 kilometers from Russian An ore-processing plant was commissioned in 1981 and Erdenet began exporting copper (30%) and

molybdenum (50%) concentrates. Today the Erdenet Mining Corporation (EMC) extracts 25.5 million tons of ores and produces 500 thousand tons of copper and 2 thousand tons of molybdenum concentrates per year. Fig.1 shows a part of the EMC map.

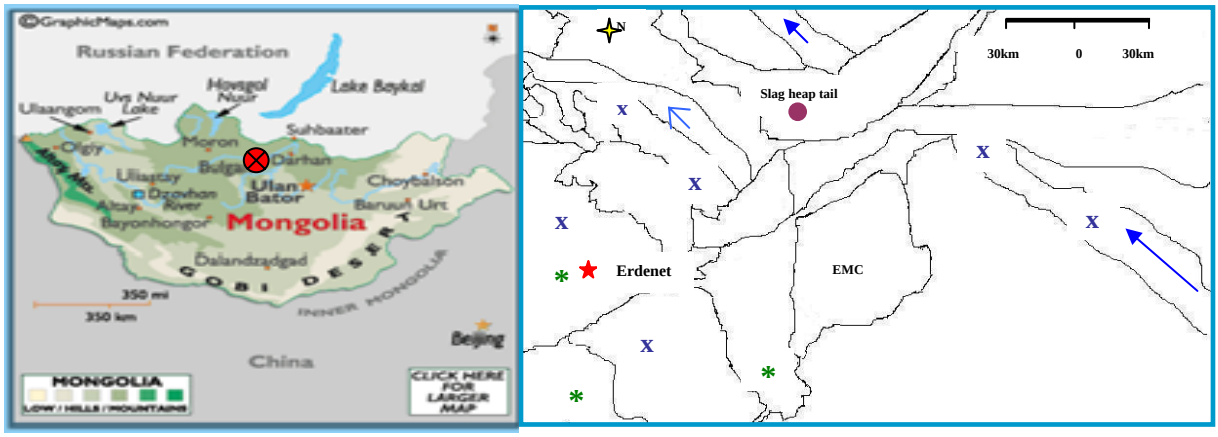

Fig.1 Sampling map in the vicinioty of Erdenet Mining corporation

★ - center of town,
\- river the Govil
\- river the Hangal
* - lichen samples
●- - inner organ samples
X - water samples

Materials and Methods

Sampling. This study is the first attempt to evaluate levels of atmospheric deposition of heavy metals and some trace elements near industrial and mining city Erdenet, using specific types of lichen biomonitors growing in the arid climate of Mongolia.

The lichens (*Parmelia separata*) were used to study the atmospheric deposition of trace elements. It was shown that the suggested types of lichens could be used as suitable biomonitors to estimate the concentration levels of heavy metals and trace elements in Erdenet atmospheric deposition. Lichen samples collected at sites located 10–15 km from the EMC. The results are compared to the data of atmospheric deposition of Morocco (Senhou A., et al. 2002) and the clear area of Mongolia (Ganbold G. et. al., 2005) (Ulaan taiga).

Monitoring studies of concentration of heavy metals and trace elements in the silts of the inflow rivers and soils are important for assessing the effect of contamination by pollutants from industrial, urban and agricultural areas. The samples of silts and soils were collected from the Hangal and Govil inflow rivers, which are mainly contaminated by anthropogenic pollutants from industrial, urban and agricultural areas of Mongolia in 2002-2003 years. The samples analysis of heavy metals, minor and trace elements must be useful to estimate sufficiently the pollution area and river's water. Water samples were collected from rivers near EMC, technological and tap water of the Power plant, the hotel, and drink water from the Shaft of the town Erdenet. Samples of inner organs of 6 pastured animals (goats and sheep) aged 2–7 years were collected from the area (around Erdenet) polluted by thin (~70 micron) white dust of the storage Slag-heap tail veterinary of the municipal units.

Analysis. *Instrumental Neutron activation analysis (INAA)*: INAA using epithermal neutrons at the IBR-2 reactor were performed at the Frank Laboratory of Neutron physics, Joint Institute for Nuclear Research, Dubna (Frontasyeva M.V. et. al., 2000).

We have determined chemical, toxic elements and some heavy metals in lichen, soil, silt and inner organs samples of around Erdenet by INAA with detection limits within the range of 0.01-10 g/g.

Total reflection X-ray fluorescent analysis (TXRF): TXRF techniques were performed at Nuclear Research Centre of the National University of Mongolia, Ulaanbaatar. We have determined contents of some heavy metals and toxic elements in water samples around Erdenet by total reflection X-Ray Fluorescence techniques (Wobrauschek P. 1998).

Results

INAA has sensitivity and accuracy for the complex monitoring measurement of heavy metals and trace elements for studying the environmental. Comparison of the results has shown that the mean content of some elements (Mg, Cl, Ca, Ti, Cr, Mn, Fe, Co, Ni, Cu, As, Sr, Zr, Mo, Ba, Cs, La, Dy, W, Au, Th) in lichen samples collected from the polluted area (Erdenet town) id higher than in lichens from the Morocco area (south-western Africa) and from the clean area (Khubsugul, Ulaan Taiga). Out of 41 determined elements biogenic or essential macroelements (Na, K, Mg, Ca, Cl) were found; biogenic or essential microelements (Fe, Cu, Zn, Mn, Cr, Se, Co, V, Ti, Ni, As); non-biogenic or other elements (Hg, Sb, Ba, Sr, Cs, Al, Rb, Zr, Nb, Au, Br, Sc, La, Tm, Hf, Ta, W, Th, U and some REE: such as Ce, Nd, Sm, Eu, Tb, Dy) were determined in samples of sediments and soils.

A total of 39 elements were determined in soil and river silt samples from polluted area and river around Erdenet town. Concentrations of some heavy toxic metals in water of river such as Ti, Cr, Mn, Fe, Ni, Cu, Zn, As, Br, Sr и Pb exceed the MPMCL accepted in Mongolia. The level of Mn content in the technological water (№ 1, 2) from the Power plant and Zn conten in tap water are higher than MPMCL accepted in Mongolia. The results of this study show that water around Erdenet town is polluted by the industrial liquid waste from the Erdenet Mining Corporation.

A total of 35 elements were determined by INAA in the samples of inner organs from goats and sheep inhabiting the area around the storage of slag heap tail in the town of Erdenet.

Acknowledgements. The authors acknowledge the financial assistance of the RFBR-Mongolia grant 08-05-90214-Mong_a.

References:

Ganbold G., Frontasyeva M. V., et al. Atmospheric Deposition of Trace Elements Around Ulanbator City Studied by Moss and Lichens Biomonitoring Technique and INAA**,** JINR Preprint E18-2005-113. Dubna 2005.

Ganbold G., Gerbish Sh., Frontasyeva M.V. et al., Assesment of Hazardous Impact on the Pastured Animals Non-Ferrous Industry in the the Town of Erdenet, Mongolia**.** JINR Commun. E18-2006–176. Dubna, 2006.

Gerbish Sh., Baljinnyam N. et al. Determination Major and Minor Elements in Sediments of the Central and Northern Mongolian some rivers using INAA. JINR, Preprint E18-2008-120. Dubna 2008.

Frontasyeva M.V., Pavlov S.S., Analytical Investigations at the IBR-2 Reactor in Dubna. JINR Preprint E14-2000-177. Dubna 2000.

Senhou A., et al. Comparison of 14 MeV-NAA, k_0-NAA and ED-XRF for Air Pollution Bio-Monitoring, // J. Radioana. Nuc. Chem. 2002. V. 253, No.2. P. 247–252.

Wobrauschek. *P.* Total Reflection X-ray Fluorescence Spectrometric Determination of Trace Elements in the Femtogram Region: a survey //J. Anal. Atomic Spectrometry, 1998, V. 13. P.333–337.

INVESTIGATION OF PERIODIC MULTILAYERS

V.Bodnarchuck, V.Ignatovich†, S.Yaradaykin,
FLNP JINR
E-mail: † ignatovi@nf.jinr.ru

L.Cser, T.Veres
KFKI, Budapest, Hungary

Introduction

Neutron supermirrors are nowadays used in many physical experiments. They are multilayer systems usually composed as a set of bilayers every one of which consists of two materials with high and low optical potentials. The supermirrors increase the angular or wave length range of total reflection comparing to mirrors consisting of a single material with high optical potential. If the single material gives total reflection for normal component k of the incident neutrons in the range $0<k<k_c$, where k_c is the limiting wave number for the given material, the supermirror can increase the interval up to nk_c. A multilayer system that gives reflectivity near 1 in the interval $0<k<nk_c$ is called Mn mirror. It became a usual practice to fabricate M2 and M3 mirrors. However there are also attempts to produce mirrors with higher n. The last record belongs to Japanese [1] who prepared mirror M6.7. Last time all the mirrors were prepared in aperiodical fashion,which means that thicknesses of layers in bilayers vary with the bilayer number. F. Mezei and P.A. Dagleish performed the first experimental study of such supermirror in 1977 [2]. The algorithm for thickness variation was proposed by J.B. Hayter and H.A. Mook in 1989 [3]. According to this algorithm the change of thicknesses of neighboring bilayers is very small and does not match interatomic distance. It leads to creation of unavoidable roughnesses on layers interface. There exists also another algorithm proposed in [4], according to which the supermirror is to be produced as a set of periodic chains with some number N of identical bilayers. The variation of thicknesses of neighboring chains in this case is larger, which may help to improve the quality of interfaces and therefore of the whole supermirror.

The goal of the given work is to investigate how well we can control the thickness and quality of periodic multilayer systems prepared by Mirrotron Ltd, Budapest. In other words we want to see how well the neutron reflectivity of produced systems match theoretical expectations, how large is diffuse scattering because of technological imperfectness and whether we can explain and control them.

Below we present results of measurements of reflectivities of fabricated multilayers and compare them to theoretical ones [5].

Methods and materials

Three samples of periodic multilayers with 2, 4 and 8 bilayers of Ni and Ti evaporated on boron float glass were prepared by the company Mirrotron Ltd, The thickness of Ni layers was 84 and Ti – 70 $\mathring{A}$. Reflectivities of these samples and of pure float glass were measured at a neutron reflectometer of KFKI of Budapest Neutron Center. The scheme of the experiment is shown in Fig. 1.

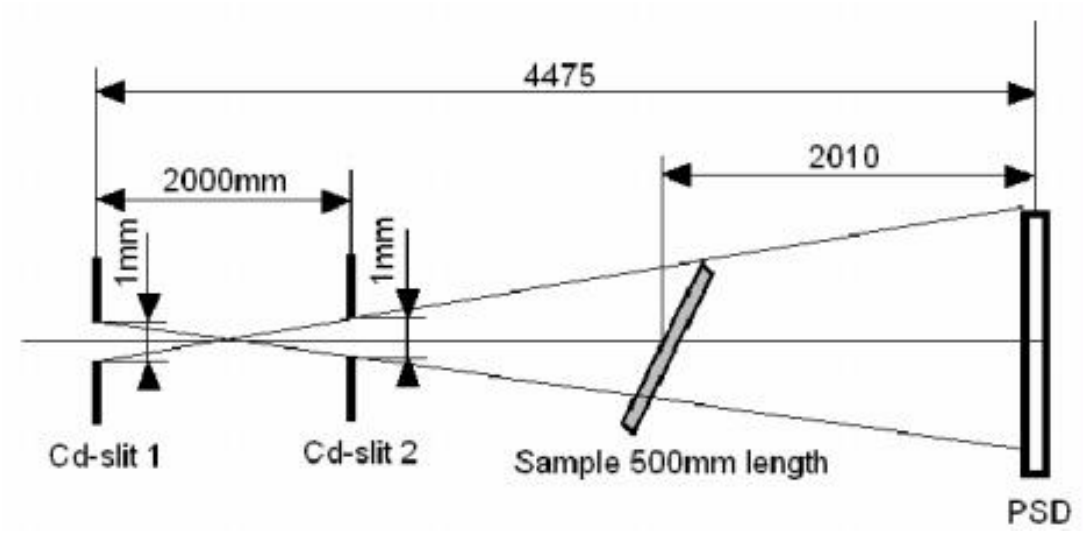

Fig.1. The scheme of the neutron reflectometer at KFKI. The sample mirror can be rotated around an axis perpendicular to the plane of the Fig. The position sensitive detector os stationary and sufficiently large to register all the reflected neutrons, when grazing angle is sufficiently small according to experimental requirements. Collimation angle was 0.5 mrad and the neutron beam was monochromatic with wave length 4.28 Angstrem and presumable resolution 3%.

Results and discussions

Fitting of the data was performed with 7 parameters. They were real parts of Ni (u'_b), Ti (u'_w) and glass (u'_s) potentials in units of the Ni one, the thickness of the Ni (l_b) and Ti (l_w) layers (in units of critical wavelength of Ni), relative momentum resolution (δ) and background (n_b). Imaginary parts of potentials were fixed to theoretical ones.

The result of fitting is shown in Fig.2 and fitted parameters are presented in Tabl. 1

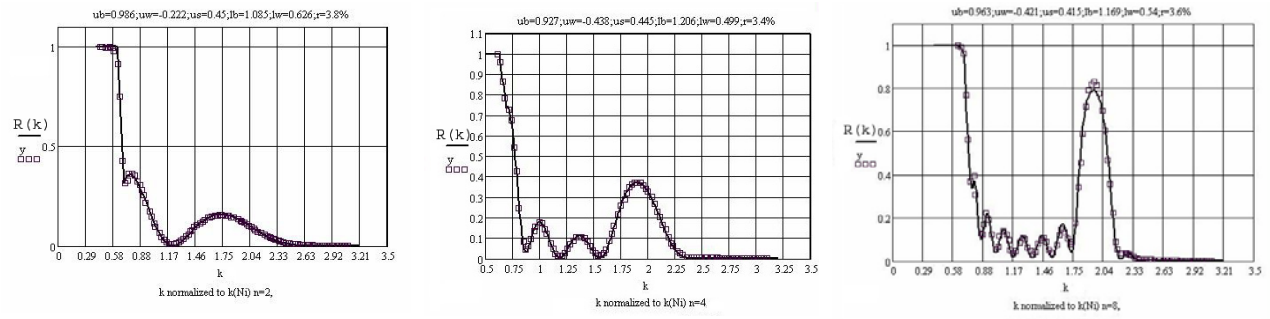

Fig.2. Linear scale fitting with 7 parameters of reflectivities of samples with 2-, 4-, and 8-bilayers Ni-Ti evaporated upon boron float glass

Table 1. Fitted values of real parts of potentials u' for Ni (b-barrier), Ti (w-well) and substrate (s), their thickness l, Resolution δ, background n_b and χ^2 for periodic chains with N=2,4,8 bilayers. Imaginary parts u'' of the potentials were fixed. The results are given in dimensionless units. The unit of energy is equal to real part of Ni theoretical optical potential $0.245\,\mu\mathrm{eV}$ and unit of length is the reduced critical wavelength $\lambda_c/2\pi = 92$ Angstrom for Ni. The parameters at the 4-th line were obtained for zero background, and parameters of 5-th line were obtained for predetermined background n_b=0.003. It is interesting to see that the fitting with smaller number parameters (6 instead of 7) gave smaller χ^2.

N	u'_b	u'_w	u'_s	u''_b	u''_w	u''_s	l_b	l_w	δ	n_b	χ^2
2	0.964	-0.258	0.452	0.00014	0.00012	0.0001	1.121	0.59	0.036	0.003	25
4	0.934	-0.388	0.446	0.00014	0.00012	0.0001	1.182	0.525	0.033	0.003	114
8	0.993	-0.242	0.398	0.00014	0.00012	0.0001	1.061	0.649	0.035	0.0089	349
8	0.963	-0.421	0.415	0.00014	0.00012	0.0001	1.169	0.54	0.036	0	209
8	0.972	-0.349	0.408	0.00014	0.00012	0.0001	1.13	0.579	0.036	0.003	151

Since the χ^2 in fitting was too high we decided to measure separately reflectivity of the empty glass mirror. Fitting of the glass mirror reflectivity with 4 parameters: real and imaginary part of glass potential, resolution and background, -- led to the result: u=0.408-0.003i, $\delta = 0.04$ and $n_b = 0.0024$. However $\chi^2 = 31$ was too high.

To improve fitting we decided to include into consideration roughness of the glass surface which is introduced via Gaussian smoothing of the glass interface, and we took into consideration randomness of atomic distribution in the glass matter and correlation of atomic positions. In total with background and resolution with the fixed complex optical potential found from previous fitting we obtained $\chi^2 = 8.5$. This value is also high, however it is considerably lower than previous 31. The result of fitting is shown in Fig. 3.

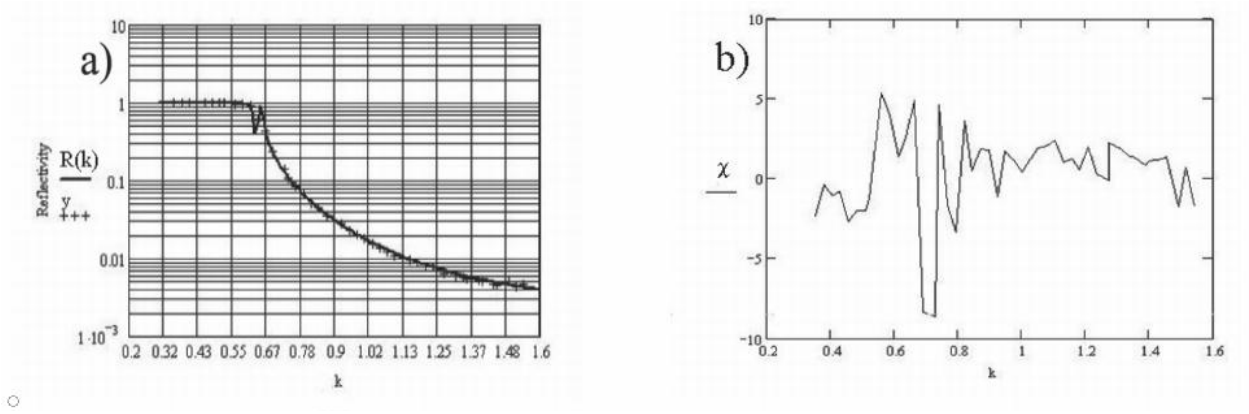

Fig. 2. a) Result of fitting in logarithmic scale of reflectivity from boron glass with function χ^2. The glass potential u=0.408-0.003i was fixed. We see some structure near the potential edge. b) χ^2 distribution for such fitting. We see some fluctuations near the edge. Without introduction of roughness and disorder this fluctuation is much higher.

Conclusions

Cooperation of theoreticians and experimentalists in research of multilayer systems is found to be very fruitful [5]. We see that technology of preparation of such systems by Mirrotron Ltd, Budapest is good, but it can be further improved after analysis of surface imperfection and their correlation with parameters of producing systems. This analysis can be performed with new experiments aimed at investigation of diffuse scattering and angular distribution of reflected neutron with better angular resolution.

References:

[1] Maruyama R, Yamazaki D, T. Ebisawa T, M. Hino M, Soyama K. Development of neutron supermirror with large critical angle. Thin solid films 2007;515:5704-6.
[2] Mezei F, and Dagleish PA. Comm. Phys. 1977;2:41.
[3] Hayter JB, Mook HA. Discrete Thin-Film Multilayer Design for X-ray and Neutron Supermirrors. J.Appl.Cryst. 1989;22:35-41.
[4] Carron I., Ignatovich VK. Algorithm for preparation of multilayer systems with high critical angle of total reflection Phys.Rev. 2003;A67:043610.
[5]V. Bodnarchuck, L. Cser, V. Ignatovich, T. Veres, S. Yaradaykin. INVESTIGATION OF PERIODIC MULTILAYERS. *Communication of JINR,* JINR E14-2009-127, (2009) Dubna, JINR.

INAA FOR STUDYING Hg (II) ACCUMULATION BY *ARTHROBACTER GLOBIFORMIS*

M.V. Frontasyeva, S.S. Pavlov, I.I. Zinicovscaia

FLNP JINR, e-mail: marina@nf.jinr.ru

N. Tsibakhahsvili[1,2], L. Mosulishvili[1], E. Kirkesali[1], I. Murusidze[2]

[1]*Andronikashvili Institute of Physics, Tbilisi 0177, Georgia*
[2]*Chavchavadze State University, Tbilisi 0179, Georgia*

P. Bode, and Th.G.van Meerten

Delft University of Technology, 2629JB Delft, The Netherlands

Introduction

Mercury is one of the most toxic metals in the environment because it binds to and inactivates essential thiols that are part of enzymes and proteins (Zeroual et al. 2001). To detoxify mercury in the environment bacteria can be used (Bruins et al. 2000). Both Gram-positive (*S. aureus, Bacillus* sp.) and Gram-negative bacteria (*E. coli, P. aeruginosa, Servatia marcescens* and *Thiobacillus ferroxidans*) demonstrate resistance to Hg(II) (Zeroual et al.2001, Bruins et al 2000). The following mechanisms are postulated to explain their resistance to metals: (1) exclusion by permeability barrier; (2) intra- and extra-cellular sequestration; (3) active transport efflux pumps; (4) enzymatic detoxification; and (5) reduction of cellular targets sensitivity to metal ions (Bruins et al. 2000). It was established recently that some strains of basalt-inhabiting Gram-positive bacteria of *Arthrobacter* genera can reduce and detoxify of Cr(VI) with high efficiency (Tsibakhashvili et al. 2009, Tsibakhashvili et al. 2008). Instrumental neutron activation analysis (INAA) was used to test the capability of one of these bacterial strains – *Arthrobacter globiformis* – to detoxify Hg(II), by (1) accumulation of Cr(VI) in *A. globiformis* in the presence of Hg(II); (2) accumulation of Hg(II) in bacterial cells; and (3) effects of Hg (II) and its mixture with Cr(VI) on the elemental composition of bacteria.

Materials and Methods

*Sample cultivation and preparation for analysis***.** The bacteria were grown in the following nutrient medium: 10 g of peptone, 1 g of yeat extract, 2 g of caseic acid hydrolysate, 5 g of NaCl, and 1 liter of distilled water**.** Cr(VI) as [K_2CrO_4] and Hg(II) as [$Hg(NO_3)_2 \cdot H_2O$] were added to the bacterial cell cultures at an early stationary phase of their growth. Our batch experiments were conducted with various initial concentrations of Cr(VI|) and Hg(II) to obtain the accumulation curves. Specifically, two sets of experiments were performed. In the first set the concentration of Hg(II) varied within the range of 50–5000 µg/l. In the second set a 500 µg/l concentration of Hg(II) was added to the bacterial cells at each given concentration of Cr(VI) within the range of 50–1000 mg/l. After being cultivated for 5 days the cells were harvested by centrifuging (10,000 rpm, 15 min, 4^0 C), rinsed twice in a 20 mM phosphate buffer and analyzed by INAA method. To prepare bacterial samples for NAA, wet biomass was placed in an adsorption-condensation lyophilizer, dried, and pelletized to 5 mm pieces (~0.5 g) by means of a titanium press form.

Instrumental neutron activation analysis (INAA). The samples were irradiated using the facilities of the 2 MW nuclear research reactor "Hoger Onderwijs Reactor" of the Reactor Institute Delft, Delft University of Technology. Two irradiations and three measurements were performed for the multielement determinations. First, elements based on short half-life

radionuclides were determined by irradiation for 30 s in the fast rabbit system, under a thermal neutron flux of approximately 1.6×10^{13} cm s^{-1}. Metallic zinc foils irradiated together with the samples allowed determination of the neutron flux; the activity of the foil was measured after the measurement of the sample. For the determination of elements based on radionuclides with "medium" and long half lives, samples were irradiated 4 h under a neutron flux of approximately 5×10^{12} cm $^{2}s^{-1}$. The neutron flux was again estimated using Zn monitors. The elemental quantification was based on the single comparator method. More details on the operation and quality assurance in this laboratory can be found elsewhere (Bode 2000, Bode et al. 1997).

Results and discussions

In our previous study (Tsibakhashvili et al. 2009) it was shown that for *A. globiformis* the accumulation of chromium, pronounced in the concentration range of 50–500 mg/l of Cr(VI) loadings, is followed by a less intense uptake, and is described by the Langmuir-Freundlich model. According to the present INAA results, the dose-dependent character of Cr(VI) accumulation by *A globiformis* is not significantly affected by the presence of 500 µg/l of Hg(II). INAA measurements revealed that the accumulation of Hg(II), similarly to the Cr(VI) accumulation, also satisfies the Langmuir-Freundlich model (Fig. 1). The strong accumulation of mercury by bacteria suggests that this undesirable element might be removed from the environment by bacterial trapping and sequestration. As it is known, the cell curface of bacteria consists of polysaccharides, proteins, teichoic acids, and lipids, which provide the amino, carboxilic, sulfydryl, phosphate, and thiol groups that can bind metals (Salzman et al. 2002).

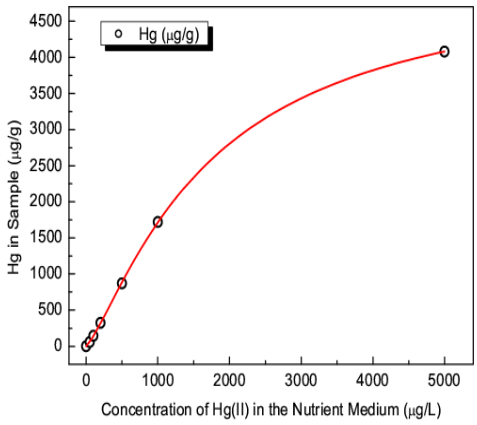

Fig.1. Accumulation of mercury by *A. globiformis*

Model: Langmuir-Freundlich

$$q = q_m \frac{(bc)^{1/n}}{1+(bc)^{1/n}}$$

q_m= 5161.41093 ± 61.39692
b = 0.00057 ± 0.00002
n = 0.79353 ± 0.01212
R^2 = 0.99996

Here c is the concentration of metal ions; q_{max} represents the maximum metal accumulation; b is the affinity parameter of the isotherm reflecting the high affinity of the biosorbent for the sorbate, and n is the empirical parameter that varies with the degree of heterogeneity

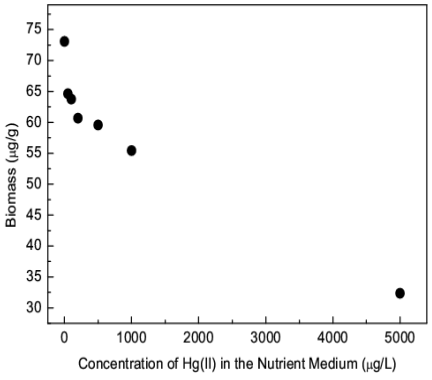

Fig.2. Effect of Hg(II) on the biomass of *A. globiformis*

Fig.2 illustrates that the production of bacterial biomass was decreased by increasing of Hg(II) concentration in the nutrient medium. The content of different elements in bacterial samples also varied depending of the Hg(II) concentration (Fig.3). The data presented in Figs. 2 and 3 illustrate that the concentration of 5000 µg/L of Hg(II) is critical for *A. globiformis.* At this concentration of Hg(II) the contents of both essential (Na, Al, Fe) and non-essential elements (La) changed drastically along with decrease of the biomass of bacteria by factor a of 2. One may assume that under this concentration loading of Hg(II) the structure of the bacterial cell wall was destroyed

Besides, INAA measurements showed an increased content of Fe in bacteria under Hg and Cr action (Fig.3), suggesting that Fe-containing biomolecules play a decisive role in detoxifying of metals such as Hg by *A. globiformis*

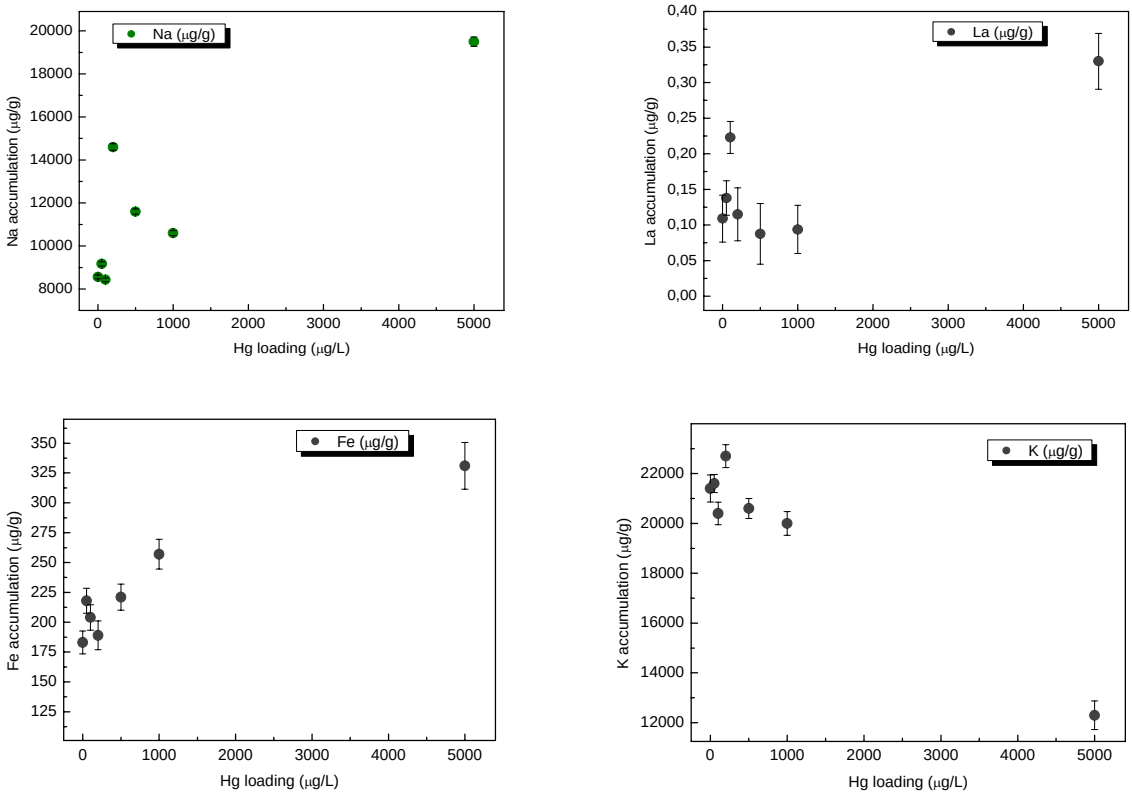

Fig.3 Effect of Hg (II) on the elemental composition of *A. globoformis*

Conclusions

INAA measurements revealed that the Gram-positive bacterial strain *Arthrobacter globiformis* isolated from polluted basalts of Georgia possesses mechanisms by which Hg(II) can be taken up and accumulated from their environment. Such uptake mechanisms can reduce mercury toxicity in environment.The mercury accumulation process fits well with the Langmuir-Freundlich model. A concentration of 5000 μg/L of Hg(II) was found to be critical for *A. globiformis.* At this concentration level of Hg(II) the structure of the bacterial cell wall was destroyed.

References

Bode P. J. Radioanal. Nucl. Chem., Vol. 245, 2000, p. 127-132.

Bode P., van Dijk C.P. J. Radioanal. Nucl. Chem., Vol. 215, 1997, p. 87-94.

Bruins M. R., Kapil S. Oehme F. Ecotox. Env. Safety., Vol. 45, 2000, p. 198-207.

Tsibakhashvili N., Kalabegishvili T., Rcheulishvili A., Murusidze I., Kerkenjia S., Rcheulishvili O., Holman H.-Y. Microbial Ecology, Vol. 57, No. 2, 2009, p. 360-366.

Tsibakhashvili N., Mosulishvili L., Kalabegishvili T., Kirkesali E., Murusidze I., Kerkenjia S., Frontasyeva M., Holman H.-Y. J. Radioanal. Nucl. Chem., Vol. 278 No. 3, 2008, 565-570.

Salzman G., Holz O. The Bacterial Cell Wall, fourth ed., Springer-Veringer, Berlin Heidelberg, New York. 2002, pp.211-217.

Zeroual Y., Moutaouakki A., Blaghen M. Current Microbiology, Vol. 43, 2001, p. 322-327.

CROSS SECTION MEASUREMENT FOR THE ^{95}Mo(n, α)^{92}Zr REACTION AT 4.0, 5.0 AND 6.0 MEV

Zhang Guohui, Zhang Jiaguo, Wu Hao, Liu Jiaming, and Chen Jinxiang
State Key Laboratory of Nuclear Physics and Technology, Institute of Heavy Ion Physics, Peking University, Beijing 100871, China
Gledenov Yu. M., Sedysheva M. V.
Frank Laboratory of Neutron Physics, JINR
Khuukhenkhuu G.
Nuclear research Centre, National University of Mongolia, Ulaanbaatar, Mongolia
Koehler P. E.
Physics Division, Oak Ridge National Laboratory, Oak Ridge, Tennessee 37831, USA
Szalanski P. J.
University of Lodz, Faculty of Physics and Applied Informatics, Lodz, Poland

Cross section data for fast neutron induced charged particle emission reactions are important in the research of nuclear reaction mechanisms, in the determination of parameters of optical model potentials and in the application of nuclear engineering. The Q value of the ^{95}Mo(n, α)^{92}Zr reaction is 6.39 MeV. Several measurements have been performed for this reaction cross section [1-4], but almost all measurements exist in the thermal and resonance energy regions. In the MeV neutron energy region, however, there is only one experimental point at E_n = 3.0 MeV with large uncertainty [5]. As a result, there are very large deviations among different evaluated nuclear data libraries such as ENDF/B-VII, JEFF3.1, JEFF3.1/A and JENDL3.3.

Cross sections as well as the forward/backward ratios of the ^{95}Mo(n, α)^{92}Zr reaction in the laboratory system were measured at E_n = 4.0, 5.0 and 6.0 MeV. Experiments were performed at the 4.5 MV Van de Graaff of Peking University, China. The setup of the present experiment is shown in Fig.1.

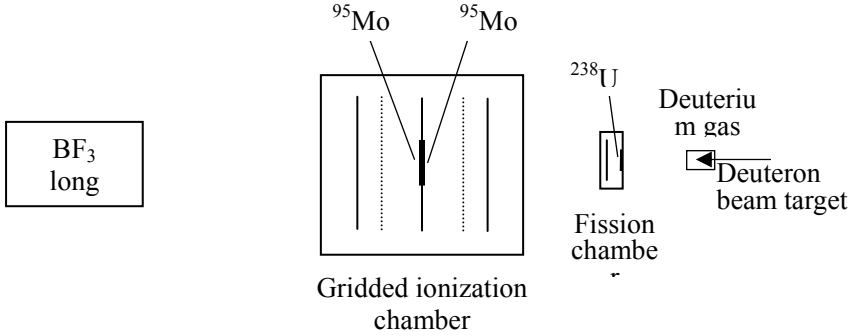

Fig. 1. Setup of the experiment.

A twin gridded ionization chamber (**GIC**) was used as alpha particle detector with the nearly 100% detection efficiency and 4π solid angle. It was constructed at the Frank Laboratory of Neutron Physics. A mixture of Kr + 2.89% CO_2 was used as working gas of the ionization chamber (pressure 1.37×10^5 Pa).

Neutrons were produced through the D(d, n)^{3}He reaction by using a cylindrical deuterium gas target (∅0.9 cm, length 2.0 cm, gas pressure 3.14–2.94 × 10^5 Pa).

The sample material is metallic molybdenum enriched in ^{95}Mo to 96.8%

(thickness 5.0 mg/cm^2 ∅11.0 cm, the backing - aluminum foil 0.127mm in thickness). The two samples are back-to-back attached to the common cathode of the **GIC**.

Two removable compound alpha sources were used for energy calibration, adjustment and checking of the electronic system.

The absolute neutron flux was determined by a small ^{238}U parallel plate fission chamber. The mass and diameter of the ^{238}U sample are (547.2 ± 7.1) μg and 2.0 cm, respectively. The abundance of the ^{238}U isotope in the sample is better than 99.997%. The working gas of the fission chamber was flowing Ar + 2.85%CO_2 gas slightly higher than atmospheric pressure. A BF_3 long counter with moderator was also employed as neutron flux monitor during the measurement.

Events in forward direction (0-90°) and backward direction (90-180°) from the back-to-back samples were measured simultaneously, and cathode-anode two dimensional spectra of alpha events for both directions were obtained. The anode spectra of the ^{238}U fission chamber were also recorded to obtain the number of the fission fragments.

Then the molybdenum samples were replaced by 0.127 mm aluminum foil and the backgrounds were measured. The position and the condition of the gridded ionization chamber, ^{238}U fission chamber, neutron source as well as the electronics remained the same as for the foreground measurement.

The following equation was adopted for cross section calculation:

$$\sigma_\alpha = K\sigma_f \frac{N_\alpha}{N_f}\frac{N_{238U}}{N_{95Mo}} \qquad (1)$$

where σ_α is the cross section to be measured; σ_f is the standard ^{238}U(n, f) cross section taken from ENDF/B-VII.0 library at the relevant neutron energy point; N_α and N_f are the number of alpha events from the ^{95}Mo(n, α)^{92}Zr reaction and the number of fission counts from the ^{238}U(n, f) reaction, respectively; N_{238U} and N_{95Mo} are the numbers of atoms of ^{238}U and ^{95}Mo in the samples, respectively. K is the neutron flux density ratio on ^{238}U and ^{95}Mo samples which can be calculated numerically according to the dimensions and positions of the samples with respect to the gas target as well as the angular distribution of the D(d, n)^{3}He reaction.

The expression of K is as follows:

$$K = \frac{\int_{-l/2}^{l/2}\int_0^{tg^{-1}\frac{d_1+x}{r_1}} 2\pi \sin\theta f(\theta) d\theta dx}{\int_{-l/2}^{l/2}\int_0^{tg^{-1}\frac{d_2+x}{r_2}} 2\pi \sin\theta f(\theta) d\theta dx} \cdot \frac{\pi r_2^2}{\pi r_1^2} \qquad (2)$$

where l is the length of the gas cell of the deuterium target; r_1 and r_2 are the radius of the ^{238}U and ^{95}Mo samples, respectively; d_1 and d_2 are the distances from the center of the deuterium gas cell to the ^{238}U and to the ^{95}Mo samples, respectively; and $f(\theta)$ is the angular distribution of neutrons from the D(d, n)^{3}He reaction.

Fig.2 shows the forward direction cathode-anode two-dimensional spectrum at E_n = 6.0 MeV. As shown in Fig. 3, after background subtraction the measured number of alpha events from the ^{95}Mo(n,α)^{92}Zr reaction was obtained.

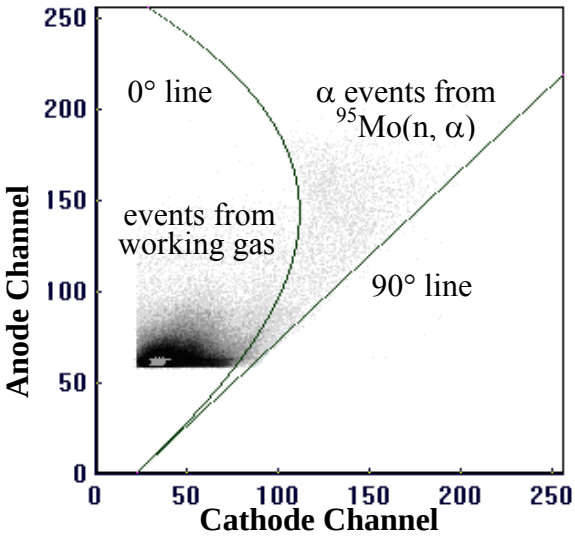

Fig. 2. Cathode-anode two-dimensional spectrum of forward events at E_n = 6.0 MeV.

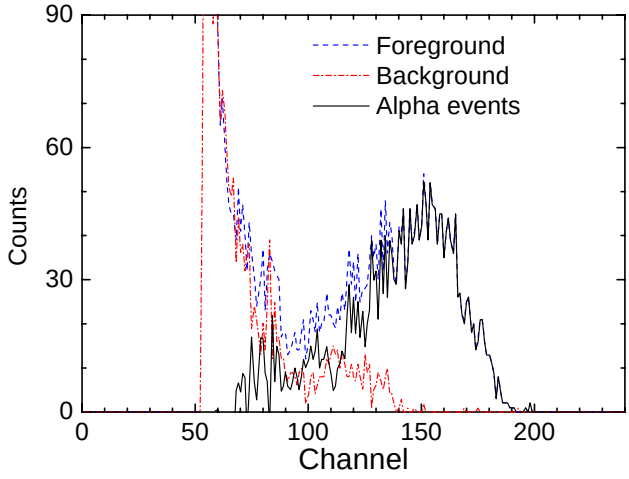

Fig. 3. Anode spectrum of forward events at E_n = 6.0 MeV between 0° and 90° lines.

The results of our measurements are represented on the Fig. 4 and Table 1.

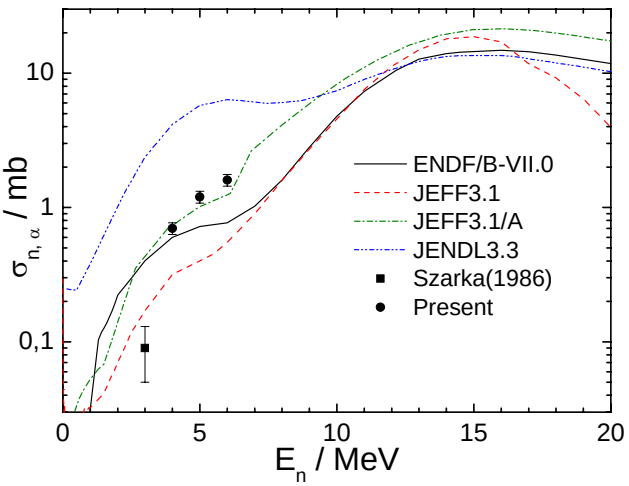

Fig. 6. Present cross sections compared with existing evaluations and measurements.

Table 1. Cross section data and forward/backward ratios in the laboratory reference system for the ^{95}Mo(n, α)^{92}Zr reaction.

E_n (MeV)	$\sigma_{n,\alpha}$ (mb)	Forward/back-ward ratio
4.0±0.23	0.70±0.07	1.07 ± 0.14
5.0±0.16	1.22±0.12	1.25 ± 0.14
6.0±0.12	1.70±0.17	1.35 ± 0.14

1. Antonov, A., Balabanov, N., Gledenov, Y.M., Pak Hong Chol, Popov, Y.P., Semyonov, V.G., Florek, M.F., 1976. Reaction (n, alpha) at resonance energies on Mo, Zn, Ru, Pd, Sm, Yb isotopes. JINR-P3-9815.

2. Antonov, A., Balabanov, N., Gledenov, Y. M., Pak Hong Chol, Popov, Y.P., 1978. Study of the (n,α) reaction and new range of α decay of compound states of nuclei. Yad. Phys. 27, 18-28.

3. Gledenov, Y.M., Balabanov N.P., 1980. Estimation of the cross sections of (n, α) reactions for a number of reactor materials in the neutron energy range up to 1 MeV. Symposium on the 5th all union conference on neutron physics, Kiev, 15-19, Sep. 1980, Vol.3, 306-310.

4. Rapp, W., Koehler, P.E., Kappeler, F., Raman, S., 2003. ^{95}Mo(n, α) cross section from 1 eV to 500 keV: A test of the α+nucleus optical potential used in calculating reaction rates for explosive nucleosynthesis. Phys. Rev. C 68, 015802.

5. Szarka, I., Florek, M., Jahn, U., 1986. Gas proportional telescope used to investigate rare reactions induced by 3 MeV neutrons. Nucl. Instrum. Meth. B 17, 472–474.

Level density, radiative strength functions from the $(n_{th},2\gamma)$ reaction and main properties of the ^{96}Mo nucleus

V.A. Khitrov, A.M. Sukhovoj

Joint Institute for Nuclear Research, Dubna, Russia

The first data on level density ρ and radiative strength functions k of ^{96}Mo nucleus were obtained by Oslo group from reaction $(^3He,\alpha)$ and inelastic scattering ^3He [1]. Unfortunately, reliability of the obtained by them unknown up to now strongest enhancement of k (at extrapolation of E_γ^{prim} to zero) was not grounded by analysis of experimental errors. Although the method for modeling the total γ-spectra without random fluctuations was suggested in [2]. Its use showed that the mentioned effect can be explained even by insignificant systematical underestimation of the total γ-spectra intensities which increases as decreases energy of decaying levels of ^{96}Mo [3].

Results [1] were alternatively tested in [4] using experimental intensities of two-step cascades to 12 final levels of this nucleus. The experiment was performed on thermal neutron beam in Rez. Unfortunately, the authors of the analysis did not take into account three points being very important for obtaining reliable data on ρ and k for primary γ-transitions from γ-decay of compound-nuclei with high level density.

1. Each experimental spectrum consists of two symmetrical parts containing both primary and secondary cascade γ-transitions. This makes difficult to compare experimental data with calculation within given sets of dependences of ρ and k at given energy of their primary (or secondary) transitions. At present the only possibility to solve this problem is known: the methods of nuclear spectroscopy for determination of the most probable dependence of cascade intensity in function of the primary transition energy [5].

2. The summed intensity of cascades and transition to ground-state always equals 100%. Therefore, any deviation in intensity distribution of cascades terminating at arbitrary final level shifts all or unknown portion of the rest of the data. This means that the regularly observed in region $0.5B_n$ very significant enhancement of strength functions of the secondary γ-transitions [6] distorts the ρ value obtained from cascade intensity.

3. Intensities of the two-step cascades can be reproduced with equal and minimal values of χ^2 by infinite set of ρ and k. Due to nonlinearity of equations their probable values are limited. Moreover, this region does not include, in practice for all the studied nuclei [7], the values predicted by the Fermi-gas model (for instance, in variant [8]). Therefore, any test of any sets of models (like that performed in [4] of level density and strength functions must include the proof that the minimum of χ^2 corresponds to them.

General conclusion from analysis of the two-step cascade intensities [6] and [7]: all generally accepted ideas of level density $\rho_\lambda = D_\lambda^{-1}$ and radiative strength functions $k = \Gamma/(E_\gamma^3 D_\lambda A^{2/3})$ as of monotonous dependences on γ-transition energy E_γ and excitation E_λ cannot reproduce the measured intensities of two-step cascades within precision of experiment.

Practically expected systematical error at the use of methods [5] and [6] in accordance with results of analysis [9] can change values of found ρ and k with respect to desired values as a maximum by 2-3 times if error in normalization of intensity varies in limits -25% to +25%. Moreover, corresponding errors change magnitude and sign as changing energy of gamma-transition and excitation of nucleus.

By now information on ρ and k for even-even spherical nuclei was obtained only for ^{74}Ge, ^{114}Cd and ^{124}Te [10]. All the mentioned above stipulated to perform independent analysis of the

data published in [4]. Unfortunately, the method of decomposition [5] of experimental intensity into components for which cascade transition with energy E_γ is the primary or secondary one and for determination of cascade population $P - i_1 = (i_1 i_2)/i_{\gamma\gamma} - i_1$ up to excitation energy ≈ 5 MeV [6] requires experimental spectra. Therefore, below is performed analysis only for the data presented in [4] in Fig. 9.

For selection of sets of ρ with different parity and k of *E1*- and *M1*-transitions which provide the best approximation there was used a variant of the Monte-Carlo method for solution of systems on non-linear equations used earlier in [6] and [7]. Naturally, determination of limits of intervals of desired parameters in this case cannot be precise - it is well known that the Monte-Carlo method is ineffective at determination of low-probable events.

The obtained limits of intervals for values of random functions $\rho = \psi(E_{ex})$ and $k = \phi(E_1)$ reproducing all 11 experimental spectra with practically the same minimal χ^2 are considerably wider than it can be achieved using method [5]. The width of intervals for values of parameters is strongly increased by involving in approximation of cascade intensities to levels $E_f > 1.5$ MeV.

In practice, the found width of interval for possible values of ρ and k is overestimated by order of magnitude relatively to potential possibilities of experiment. This conclusion follows from comparison between results obtained by means of methods [6] and [7] for the same nuclei with accounting for different quality of information accumulated in experiment in Rez and earlier (with worse equipment) in Dubna and Riga. There is not observed clearly expressed very considerable [1] or noticeably less [4] enhancement of strength functions at decreasing of primary γ-transition energy in parameters obtained by us. Their some increase, observed in approximately one quarter of cases, can be connected, most probably, with overestimation of calculated cascade intensity with the primary γ-transitions energy not less than 2 MeV and, correspondingly, with underestimation of intensity of secondary γ-transitions with the same energy. A proof of presence or absence of this strengthening cannot be obtained without the use of method [5]. One can suppose that indirectly, by considerably bigger derivative from strength functions for energy of primary transitions being by 3 MeV higher than in [1], the first possibility is more probable.

At approximation, density of levels in ^{96}Mo with different parity in region of B_n was taken equal and fixed to the data on neutron resonances. Densities below B_n could have different value, but their sum at E_{ex}=2.6 MeV was compared to known density of discrete levels. Variation of capture cross-sections ratio of thermal neutrons for two spin channels showed that $\approx$ 33% of captures in state J=2 provides for maximal quick decrease in parameter χ^2 in iterative process and simultaneously - acceptable reproduction of experimental intensities of cascades to levels $E_f \geq 2.4$ MeV and ground state of this nucleus.

Experimental intensities of cascades to different final levels do not allow independent determination of ratio between thermal neutron capture cross sections [11] for both spin channels. So, almost equal total intensity of cascades to levels E_f=2426 and 2438 keV ($J^\pi = 2^+$ and 5^+) cannot be reproduced in calculation at any ratio of cross sections without the assumptions on strong difference of level spin dependence from generally adopted law. If one does not take into account possibility of mistaken determination of spins for these levels then the hypothesis of dependence of the secondary γ-transition intensities on structure of excited level seems to be more probable. The effect is observed in calculation, for example, in the frameworks of quasiparticle-phonon nuclear model [12]. Comparison between forms of the best approximating calculated intensities to the final (phonon-less) state and the fist excited level (quadrupole phonon) shows their principal difference. It appears itself as clearly expressed bump in centre of intensity distribution of cascades to level E_f=778 keV. Such dependence on wave function structure of cascade final level is essentially averaged at determination of $\rho = \psi(E_{ex})$ and $k = \phi(E_1)$ in the frameworks of methods [6] and

[7]. The threshold for approximation of the data in our analysis was taken equal to 0.9 by analogy with [4]. The lowest level of negative parity is E_f =2225 keV, therefore strength function of the $E1$-transitions can be reliably determined only for 0.9< E_1 <7 MeV. The sets of functions $\rho = \psi(E_{ex})$ and $k = \phi(E_1)$ obtained for different initial data are presented in figures 1 and 2. These functions provide the least practically achievable value of χ^2 for all 11 experimental spectra.

The described process more effectively uses the experimental data like those presented in [4], first of all, for both throwing away any mistaken model ideas of level density and strength functions and for revealing of considerable systematical errors in corresponding data of the other experiments. The use of any assumed functions $\rho = \psi(E_{ex})$ and $k = \phi(E_1)$ as the initial data for iterative process allows one to search for arbitrary random solutions and to compare the values of χ^2 / f for them.

The values obtained for given nucleus in iterative process allow one undoubtedly to reject, for example, ideas of Fermi-gas model for level density as not corresponding with experiment. Analogous conclusion follows and for "low-energy tail" of radiative strength functions [1]. In spite of considerable and inevitable uncertainty of their obtained values, the data presented in Figs. 1 and 2 are high-informative and reliable enough in order to get conclusions on properties of nucleus ^{96}Mo which appear themselves in process of cascade gamma-decay of its compound state.

REFERENCES

1. A.Schiller et al., Phys.Rev. C. V.73, P.034311 (2006).
2. V.A. Khitrov, A.M. Sukhovoj et al., JINR preprint E3-2003-7, Dubna, 2003.
   V.A. Khitrov, A.M. Sukhovoj et al., Proc. of the XI International Seminar on Interaction of Neutrons with Nuclei, Dubna, 22-25 May 2003, JINR E3-2004-9, (Dubna, 2004) p. 107.
   V.A. Khitrov, A.M. Sukhovoj et al., nucl-ex/0305006.
3. V.A. Khitrov, A.M. Sukhovoj, Proc. of the XVI International Seminar on Interaction of Neutrons with Nuclei, Dubna, June 2008, JINR E3-2008-47, (Dubna, 2008) p. 46.
4. M.Krticka et al., Phys.Rev. C. V.77, p.054319 (2008).
5. S.T. Boneva, V.A. Khitrov, A.M. Sukhovoj, Nucl. Phys. A.V. 589 P.293, 1995.
6. A.M. Sukhovoj, V.A. Khitrov, Phys. Part. Nucl. V.36, No.4, P.359, 2005.
7. E.V. Vasilieva, A.M. Sukhovoj, V.A. Khitrov, Phys. At. Nucl. V.64(2), 2001. P.153;nucl-ex/011017.
8. W.~Dilg et al., Nucl. Phys. A, V.217, P.269, 1973.
9. V.A. Khitrov, Li Chol, and A.M. Sukhovoj, Proc. of the XI International Seminar on Interaction of Neutrons with Nuclei, Dubna, May 2003, E3-2004-9 (Dubna, 2004), p.98; nucl-ex/0404028.
10. A.M. Sukhovoj, V.A. Khitrov, JINR communication E3-2007-22, Dubna, 2007.
11. S.F. Mughabghab, Neutron Cross Sections BNL-325. V. Part A, Ed. by S.F. Mughabhab, M.~Divideenam, and N.E. Holden, Academic Press, New York, 1984.
12. L.A. Malov, F.M. Meliev, V.G. Soloviev, Z. Phys. A, Bd.320, P.521, 1985.
13. V.M. Strutinsky, Proc. of Int. Conf. Nucl. Phys., Paris, P.617, 1958.
14. http://www.nndc.bnl.gov/nndc/ensdf.
15. A.M. Sukhovoj, W.I. Furman, V.A. Khitrov, Phys. At. Nucl. V.71, No.6, 2008.
16. S.G. Kadmenskij, V.P. Markushev, W.I. Furman, Sov. J. Nucl. Phys. V.37. P.165, 1983.

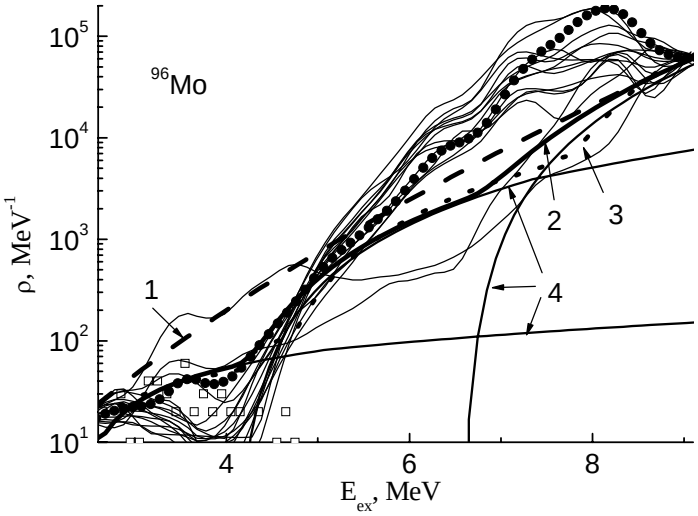

Fig. 1. Line 1 - model values [10] thin curves - the best random functions of the density of intermediate cascade levels, reproducing $I_{\gamma\gamma}$ with practically the same least values χ^2. Points - their mean value. Line 2 - approximation by model [13] with parameter g, depending on shell inhomogeneties of one-particle spectrum, line 3 - the same for g =const. Lines 4 - partial densities of two-, four- and six-quasiparticle levels. Squares - density of known levels from evaluated decay scheme [14].

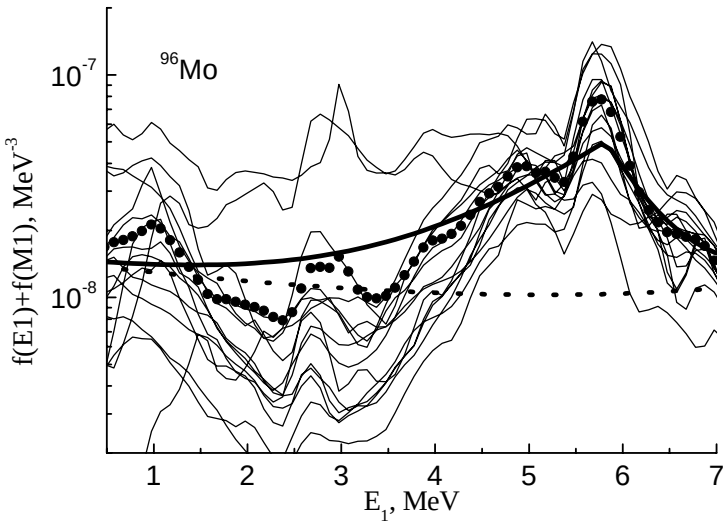

Fig. 2. Thin curves - the best random functions reproducing $I_{\gamma\gamma_\gamma}$ with practically the same smallest values χ^2. Points - their mean value. Solid curve - the best approximation by model [15], dotted curve - contribution in strength function of model [16].

INVESTIGATION OF LIGHT ELEMENT CONTENTS IN SUBSURFACE LAYERS OF SILICON

A.P. Kobzev †
Frank Laboratory of Neutron Physics, JINR, 141980 Dubna, Russia
J. Huran
Institute of Electrical Engineering, Slovak Academy of Sciences, Dúbravská cesta 9, 841 04 Bratislava, Slovak Republic
D. Maczka
Institute for Atomic Energy, Swierk-Warsaw, Poland
M.Turek
Institute of Physics, Maria Curie-Sklodowska University, pl. M. Curie-Sklodowskiej 1, 20-031 Lublin, Poland
E-mail: † *kobzev@lnf.jinr.ru.*

Introduction

Demands of higher power, radiation hardness, operating frequency, temperature and speed are potentially met by silicon carbide. This material has also additional attractive properties such as wide band gap, high breakdown field, high electron saturation velocity. SiC can be used as a thin buffer layer for the growth of diamond films on silicon substrates. The significance of this material results from the fact that its electrical and optical properties can be controlled by varying the carbon, silicon and hydrogen composition in the films. Plasma enhanced chemical vapour deposition (PECVD) offers an attractive opportunity to fabricate amorphous hydrogenated SiC films at intermediate substrate temperatures and it provides high quality films with good adhesion, good coverage of complicated substrate shapes and high deposition rate. Recently, Si-rich a-SiC_x:H films have attracted new attention in the photovoltaic community, since this material has shown an excellent electronic surface passivation of c-Si comparable with thermal SiO_2 and low temperature amorphous silicon nitride (a-SiN_x) passivation [1].

Amorphous hydrogenated carbon (a-C:H) films are frequently deposited by PECVD. It was recently shown that such layers have various optical and electrical properties [2]. PECVD with an ionic density of $10^9/cm^3$ deals with hydrogenated carbon films while arc current discharge provides ta-C films, i.e. tetrahedral carbon with highly fourfold coordinated carbon (high sp^3 content). Introduction of hydrogen can be interesting when negative effects such as a decrease of the level of sp^3 or a decrease of the hardness can be circumvented. The advantage of bonded hydrogen is that it can diminish strain and stress during film deposition and increase the deposited film thickness.

Experimental

A n-type silicon wafer with resistivity 2-7 Ω cm and (111) orientation was used as the substrate for the a-C:H and a-SiC:H films. Prior to the deposition, standard cleaning was used to remove impurities from the silicon surface, and 5% hydrofluoric acid was used to remove the native oxide on the wafer surface.

The elastic recoil detection (ERD) method is the best way for the investigation of layers prepared in this way because ERD characteristics, like depth resolution, sensitivity, limiting measured thickness, are the most appropriate for this task. The ERD method is based on the measurement of the recoiled proton spectrum. Protons are emitted from target bombarded by a helium ion beam. The scattered helium ions are absorbed in a special filter and recoiled protons loss a part of their energy and then are registered by a surface barrier detector. A helium ion beam provided by a Van de Graaff accelerator is usually employed in the ERD method [3].

Results and discussion

PECVD silicon carbide films of different thicknesses were analyzed using two RBS and ERD analytical method simultaneously. For data processing is used the SIMRA computer code [4]. Fig.1 shows a typical RBS spectrum for a sample containing carbon and hydrogen atoms in surface layer with a thickness of 1.35×10^{18} at/cm^2. In this figure one can see a part of the spectrum of helium ions scattered by silicon atoms in the substrate (100 % silicon).

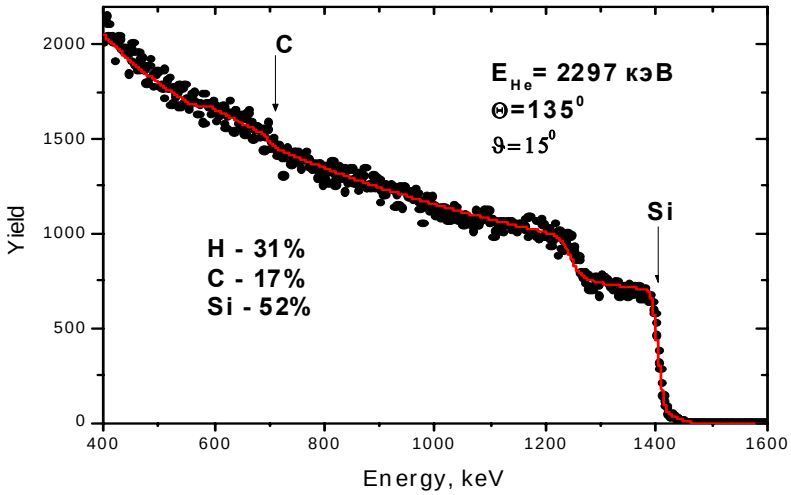

Fig.1. Experimental (points) and calculated (line) spectra of helium ions backscattered by a sample with a thick subsurface layer containing light elements.

The calculated spectrum was normalized to the experimental one by selection the number of helium ions coming to the sample during the analysis. Thus, the number of helium ions A_i, registered in one channel of the multi channel analyzer, having an energy width of ΔE, can be calculated [5]:

$$A_i = Q\sigma(E,\theta)\Delta\Omega N\tau/\cos\theta_1 \qquad (1)$$

where Q is the total number of helium ions coming to the sample during the analysis; $\sigma(E,\theta)$ is the differential cross-section of the recoiling process; $\Delta\Omega$ – the solid angle of the detector; θ_1 is the angle between the direction of the beam and the normal to the surface of the sample; $N\tau/\cos\theta_1$ is the thickness of the layer, corresponding to an energy width ΔE of a single channel of the analyzer. Moreover, the ion energy loss depends on the energy loss factor $[S]$ and of the thickness x of the layer:

$$\Delta E = [S]x \qquad (2)$$

If there is only one element in the layer, the ion energy loss may directly be calculated using eq. (2). Because only one quantity, Q, from equation (1) is unknown, we can determine it after normalization of the experimental spectrum to the calculated one in the region where helium ions were scattered by the silicon atoms of the substrate. This also allows to exclude the systematic error of the measurement the solid angle of the detector as well as the systematic error of the determination the number of incident particles coming to the target during the analysis. In order to calculate the ion energy loss in the layer consisting of two elements, the Bragg's rule is used. Hence, the stopping cross-section of a compound $\varepsilon^{A_m B_n}$ consisting from A and B atoms with the corresponding concentrations m and n is given by:

$$\varepsilon^{A_m B_n} = m\varepsilon^A + n\varepsilon^B \qquad (3)$$

The part of the RBS spectrum corresponding to the surface layer containing hydrogen is characterized by a lower yield of helium ions scattered on silicon atoms, because the atomic concentration of Si atoms, C_{Si}, is lower in this layer. In such case there is a possibility to determine atomic concentration of hydrogen atoms C_H from the RBS spectrum taking into account an additional condition:

$$C_H = 1 - C_{Si} \qquad (4)$$

If this layer contains hydrogen and silicon atoms, there is a possibility to measure the ERD spectrum only and to determine the depth distribution of H atoms. In this case one can obtain the stopping power and determine the hydrogen concentration in the H and Si containing layer using the same additional condition (4). When there are more then two elements in the layer, the task of determination of the hydrogen content (using the ERD spectrum only) can not be done correctly, because the stopping power of helium ions and the stopping power of recoiled protons in this layer are changed due to the presence of the third element.

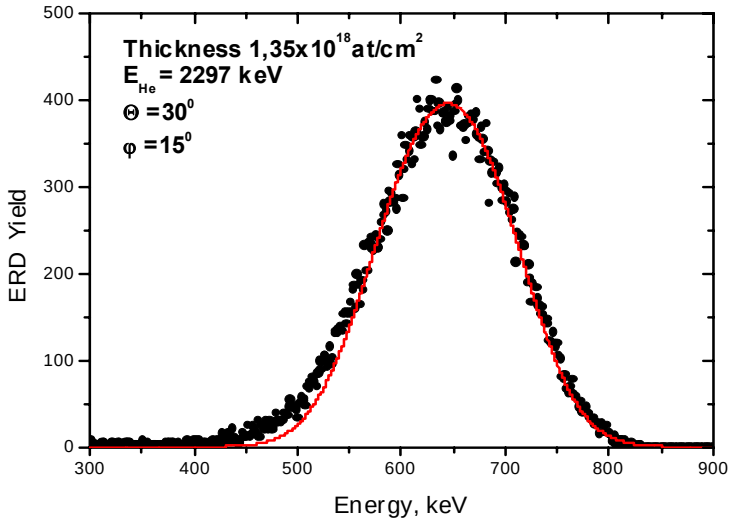

Fig.2. ERD spectrum for the same sample.

In that case the task of determination of the element concentrations may be carried out by computations taking into account the RBS spectrum together with the ERD one. Fig. 2 shows the ERD spectrum measured simultaneously with the RBS spectrum presented in Fig.1. The yield of recoiled protons in this spectrum is sufficient to determine the hydrogen concentration with a good precision. In the RBS spectrum measured under an angle of 135^o (see Fig. 1) there is rather intensive yield of helium ions, scattered on Si atoms. Thus, combining both the ERD and RBS spectra together and making use of equation (4), one can determine the concentrations of the three elements in the layer with a satisfactory precision. The thickness of the surface layer was also determined in the same experiment. It is equal to $1.35x10^{18}$ at./cm^2 with a precision of $5x10^{16}$ at/cm^2.

Conclusion

A special methodology for the determination of the concentration of light elements in the subsurface layer of solids by the ERD method using a helium ion beam is discussed in this paper. A SiC_x:H sample was analyzed by the combination of the ERD and RBS methods. Such way there is a possibility to improve the precision for the determination of the element content and of the thickness for subsurface layers of silicon samples doped with light elements such as hydrogen and carbon. The precision of the measurement of the element concentration for each of the three elements (hydrogen, carbon and silicon) is close to 1 atomic percent.

References

1. Vetter M., Voz C., Ferre R., Martin I., Orpella A., et al. Thin Solid Films 2006, 290, 511-512.
2. Grill A., Thin Solid Films 1999, 189, 355-356.
3. Kobzev A.P. Nucleonica, 1999, vol. 44, N2, 309-316.
4. Mayer M. SIMNRA http://www.rzg.mpg.de/~mam/
5. Wei-Kan Chu, Mayer J.W., Nicolet M.A., Backscattering spectrometry. Academic Press, New York, San Francisco, London ,1978.

Extraction of the neutron-electron scattering length from the neutron diffraction data measured on noble gases.

L,V.Mitsyna[1], V.G.Nikolenko[1], S.S.Parzhitski[1], A.B.Popov[1], G.S.Samosvat[1]

Frank Laborotory of Neutron Physics, JINR, 141980 Dubna, Moscow region, Russian Federation

Investigations of the n,e-interaction for the purpose of extracting the neutron-electron scattering length b_{ne}, which is directly connected with the fundamental physical value of neutron mean squared charge radius, continued for a long time. There is a dozen of the most precise experimental b_{ne} values with errors $< 0.05 \cdot 10^{-3}$ fm by now, which were obtained by different methods. However, in spite of their existence there were doubts about the validity of their declared accuracy, as they differ by ~5 standard deviations. In all methods there are principal troubles connected with the necessity of introducing large corrections in size of order of the investigated effect. Thus, further investigations of this problem with the aim to adjust b_{ne} value are desired and required as before. Besides there is intrigue in the fact that all known experimental b_{ne} values were scattered around the so-called Foldy scattering length in the interval about ±10%

$$b_F = -\frac{\mu e^2}{Mc^2} = -1.468 \cdot 10^{-3} \text{ fm.}$$

More accurate definition of the b_{ne} value takes on special significance, because the coincidence of b_{ne} and b_F values would be surprising for actual theoretical concept. Possible equality of these two values signifies a non-trivial phenomenon, namely the charge distribution of a neutron scattered on the outside charge becomes apparent through neutron magnetic moment only.

From the point of view of comprehension of all introduced corrections the simplest experiment to obtain b_{ne} value is the slow neutron scattering by noble gas. Nevertheless, in these experiments it is impossible to ignore the thermal motion of gas atoms and the diffraction on nuclei of neighboring atoms even at low gas densities. The new method to obtain b_{ne} value proposed in Dubna permits to use much more dense gases and get rid of difficulties connected with distorting effect of diffraction, while measuring the n,e-effect the diffraction can be taken into account with satisfactory accuracy. Our method is based on two facts:

1) diffraction and n,e-interaction contributions to scattering cross section have very different dependences on the momentum transfer $\hbar q$ (oscillating and monotonous);
2) diffraction contribution to the scattering is proportional to a gas density n (or even has a term with n^2), but the nuclear and n,e-scatterings do not depend on n.

Investigations of the neutron diffraction in monatomic gases in quest of interatomic interaction potentials are progressing in the last decades. As for gas densities, the pressures up to hundreds atmospheres are used in these experiments. So, the effect of n,e-scattering in them is essentially more than in the researches like.

According to conceptions accepted in literature we describe the neutron scattering intensity per one target atom and unity neutron flux with the accuracy enough for our purposes by the following expression

$$\frac{dI(q)}{d\Omega} = \alpha \frac{\sigma_s}{4\pi} \left\{ F_s(V_0, q, A)(1+B) + \frac{nC(q)}{1-nC(q)} F_s(V_0, q, 2A) \left(\frac{\sigma_{coh}}{\sigma_s} + B \right) \right\}, \quad (1)$$

where α is normalizing constant, $B = \frac{8\pi a_{coh} b_{ne} Z f(q)}{\sigma_s}$, q is the wave number of momentum transfer, σ_s and σ_{coh} are the total and coherent nuclear scattering cross sections, a_{coh} is the length of coherent nuclear scattering, Z is the number of electrons in atom, $f(q) = \left[1 + 3(q/q_0)^2\right]^{-1/2}$ is the electron form factor of an atom, q_0 is the Hartree-Fock's constant, which characterizes atomic properties. For taking into account the influence of the atoms thermal motion on the neutron scattering distribution in expression (1) we used kinematics description. The thermal motion effect is described by function F_s

$$F_s(V_0, \theta, A) = \frac{(A+1)^2}{A^2 \sqrt{\pi} V_0 U_0} \int_0^\infty \frac{V^2}{\sqrt{V_0^2 + V^2 - 2V_0 V \cos\theta}} \times$$

$$\times \exp\left\{ - \frac{(V^2 - V_0^2 \frac{A-1}{A+1} - \frac{2V_0 V \cos\theta}{A+1})^2}{4(\frac{A}{A+1})^2 U_0^2 (V_0^2 + V^2 - 2V_0 V \cos\theta)} \right\} dV. \quad (2)$$

In expression (2) θ is the scattering angle of neutron in the laboratory reference frame, V_0 is the initial neutron velocity, V is its velocity after scattering, A is the atom mass number, $U_0 = \sqrt{\frac{2kT}{mA}} = 128.9\sqrt{\frac{T}{A}}$ [m/s], T is the gas temperature in K.

Function $C(q)$ is connected with the structure factor $S(q)$ by formula

$$S(q) - 1 = \frac{nC(q)}{1-nC(q)}. \quad (3)$$

Here n is the gas density and $C(q)$ is the correlation function.

The problem of b_{ne} value determination comes to accurate separating the n,e-contribution from the diffraction waves with taking into account the thermal motion of atoms, which is the main correction for experiments with gases.

Unfortunately, for diffraction description there is no strict theory yet, so in our analysis we used different phenomenological expressions for convergent oscillations of the correlation function $C(q)$, such as

$$C(q) = (A_1 - A_2 n) \exp(-A_3 q) \sin(\frac{2\pi q}{A_4} + A_5), \quad (4)$$

where one or two of parameters $A_1 - A_5$ were sometimes fixed.

Testing the different phenomenological formulas for $C(q)$ description including hard-core model approach adjudicated that all considered variants with the exception of the last one fit to the experimental data satisfactorily (with $\chi^2 \sim 1$ per points).

In order to test the proposed method of the b_{ne} value determination we used the literature experimental data, where the structure factors $S(q)$ were obtained for gaseous Kr, isotope ^{36}Ar and for liquid Kr.

The fits the experimental structure factors for 17 gas densities n = (0.26–6.19)·10^{21} cm^{-3} and 78 values of q up to 4 $Å^{-1}$ for gaseous Kr with the accuracy $3 \cdot 10^{-3}$ for all q and all n simultaneously were carried out with ten parameters: normalizing multiplier α, B and eight parameters A_i for describing functions C_0 and C_1 by formula (4) (assuming that A_2=0) were done. If α parameter was fixed the statistical error of b_{ne} became to 3%. The more realistic result obtained with free parameter α is placed in the first line of Table.

As ^{36}Ar has an anomalously large scattering cross section $\sigma_s \approx 78$ b, and n,e-effect for it must be ~10 times less than for natural Ar, so extracting b_{ne} value from the ^{36}Ar diffraction data allowed us to make a check of our method sensitivity. We used $S(q)$ data obtained in the Institute Laue-Langevin in Grenoble for $q = (0.24 - 10.1)\,Å^{-1}$ at four densities of gaseous isotope ^{36}Ar with the accuracy from 0.06% up to 0.2%. We could describe these experimental data satisfactorily at $q \geq 3$ $Å^{-1}$ only. Moreover, all the data for the lowest density of argon were rejected because of large χ^2 criterion. The weighted average result for the other three densities is shown in Table (line 2) with the statistical and systematic errors.

The b_{ne} value was also obtained from the diffraction data of structure functions $S(q)$ measured in Grenoble for seven close densities of liquid Kr in the interval of q ~ (0.4 – 17) $Å^{-1}$. In this case we made an attempt to apply our new method to liquid, in spite of there is a problem of adequate consideration of thermal motion for atoms of liquid. Our analysis of the data is based on assumption that authors have properly made corrections on the thermal motion atoms. The wide range of q and a lot of experimental information (~5000 experimental data points) allows us to verify different variants of b_{ne} value extracting.

Having no possibility to describe diffraction for liquid correctly in the whole interval of q we tried to escape safely a correlation between α and b_{ne} in a variety of ways. In particular, we made an attempt to reduce the normalization parameter in the fittings dividing the working q interval into six visible periods of the diffraction. In each of them we summed up the experimental structure factors and separating n,e-contribution obtained three independent b_{ne} values from the three ratios of these sums. However, we did not get acceptable error of b_{ne} value in this case too.

We performed also the fit with one parameter B and seven parameters $\alpha_1 \div \alpha_7$ to all data $S^{\exp}(n,q)$ simultaneously at fixed A_i fitted before for each sample. This led to a very good result with the error size of the order of 3 % (3-rd line of Table). Unfortunately, this result can not be accepted as significant one because it depends on varying the limits of the working q-interval. It can be evidently explained by insufficiently satisfactory description of neutron diffraction in liquid state of Kr. Nevertheless, this example demonstrates future prospects of obtaining b_{ne} value with the good accuracy by means of performing similar measurements with gaseous samples.

A problem of the extracted neutron-electron scattering length precision in the proposed method depends not only on the statistical accuracy of the measured angle distributions of neutrons scattered by gas but also on an extent of diffractometer isotropy – the constancy of the product of detector efficiency and the solid angle at all angles. The exclusion of the dependency of neutron probability registration by the detectors on a scattering angle is fundamentally important task. In this problem was solved by normalizing the angle distribution of neutrons scattered by gaseous krypton on such distribution of neutrons scattered by vanadium. However, the order of vanadium isotropy is not known with

the accuracy, which would be sufficient for our purposes. To obtain b_{ne} value with the accuracy ~ 2% the facility anisotropy must be less than $\sim 3 \cdot 10^{-4}$, that is practically impossible condition.

The only possibility to avoid this trouble is to perform relative measurements of two noble gases with strongly different n,e-contributions to scattering cross sections, for example Ar and ^{36}Ar, which have n,e-contributions 1.7% and 0.2%, or Xe and Kr, whose ones are 2.1% and 1.2%, correspondingly.

High sensitivity of the new method to the n,e-scattering length extracting was also shown in the work with ^{36}Ar, where n,e-effect is 10 times less than for natural argon and krypton.

Different versions of the b_{ne} value determination by new method were applied in the wide range of q and a lot of experimental data for liquid Kr. It was shown that realization of similar measurements with gaseous samples would permit to obtain the b_{ne} value with the accuracy ~ 3 %.

Furthermore, a principal possibility to obtain b_{ne} value with the accuracy ~ 2 % in relative experiment was shown and discussed.

We had also the aim to draw attention of the neutron scientific community to use proposal method on beams of ILL reactor.

Table

Target	Fittings	$<b_{ne}> \cdot 10^3$, fm
Kr	for all q and all n simultaneously	–1,53±0,24
^{36}Ar	averaged value of simultaneous fits for each n	1,33±0,28±0,57
Liquid Kr	simultaneous fit for all $S(n,q)$ with individual fixed A_i and varied different α_i for each sample	–1,35±0,03
	simultaneous fit for all $S(n,q)$ with varied common A_i and single α	–1,39±0,12

AN INFLUENCE OF HYPOTHETICAL EXTRA-SHORT-RANGE INTERACTION ON THE SCATTERING ANISOTROPY OF COLD NEUTRONS BY NOBLE GASES.

A.B.Popov

Frank Laborotory of Neutron Physics, JINR, 141980 Dubna, Moscow region, Russian Federation

A possibility of obtaining a better constraint on the hypothetical new interaction is discussed in [1] and compared with those usually quoted in the literature. The authors of this paper also argue that one could avoid the influence of the n,e-interaction in the scattering of neutrons by atoms by using very slow neutrons. In fact, the authors of [1] erroneously assume that the n,e-scattering contribution is absent at the transferred momentum $q = 0$. On the contrary the contribution of the n,e-scattering to the total amplitude is maximal actually at small q. However, in this case it does not depend on the scattering angle and in reality it does not prevent from searching for other effects which introduce an anisotropy to the scattering of very slow neutrons by atoms. We carried out calculations with the purpose to specify behavior of the forward – backward scattering anisotropy of neutrons depending on the velocity of neutrons after scattering taking into account parameters of the extra-short-range interaction.

Here we are talking about the description of scattering of mono-energetic neutrons on one-atom gas in view of thermal motion of atoms. In this case, let us remind the distribution of scattered neutrons is described by the expression:

$$f_{Tur}(V_0, V, \theta, A) = \frac{(A+1)^2}{A^2\sqrt{\pi}V_0 B_0}\frac{V^2}{\sqrt{V_0^2 + V^2 - 2V_0 V\cos\theta}}\times$$

$$\exp\left\{-\frac{(V^2 - V_0^2\frac{A-1}{A+1} - \frac{2V_0 V\cos\theta}{A+1})^2}{4(\frac{A}{A+1})^2 B_0^2 (V_0^2 + V^2 - 2V_0 V\cos\theta)}\right\} \qquad (1)$$

where

V_0 is the initial velocity of a neutron,

V is the velocity of a neutron after scattering,

θ is the scattering angle,

A is the atomic weight (number).

$$B_0 = \sqrt{\frac{2kT}{mA}} = 128.9\sqrt{\frac{T}{A}}\ \text{[m/s]}.$$

Without going into a detailed discussion on the origin of the extra-short-range interaction we take advantage of the expression for the amplitude of this interaction given in [1]:

$$f_V(\theta) = -A\frac{g^2}{4\pi}\hbar c\frac{2m\lambda^2/\hbar^2}{1+(q\lambda)^2}, \qquad (2)$$

$$q = 2k\sin(\theta/2),$$

which can be rewritten as

$$f_V(\theta) = -A\frac{g^2}{2\pi\hbar c}\frac{mc^2\lambda^2}{\{1+[2k\sin(\theta/2)\lambda]^2\}} \Rightarrow -\frac{A}{2\pi}\frac{939.6\ MeV}{197.3\ MeV\ fm}\frac{(g\lambda)^2}{\{1+[2k\sin(\theta/2)\lambda]^2\}}, \qquad (3)$$

where g is a dimensionless constant, and λ is the size of the interaction region.

The differential cross section of neutron scattering taking into account smallness of a hypothetical interaction and neglecting the n,e-interaction and Schwinger's scattering contributions will be proportional to the expression

$$d\sigma \sim f_N^2 + 2 f_N f_V , \qquad (4)$$

and taking into account the thermal motion of gas atoms

$$d\sigma(V_0, V, \theta, A) \sim (f_N^2 + 2 f_N f_V) f_{Tur}(V_0, V, \theta, A) . \qquad (5)$$

We are interested in the scattering anisotropy of neutrons depending on the initial velocity and the velocity after scattering. The calculations of the following ratio

$$R(V_0, V) = \frac{d\sigma(V_0, V, 45^0)}{d\sigma(V_0, V, 135^0)} \qquad (6)$$

were carried out analytically and using the Monte-Carlo method for argon gas at room temperature and normal pressure.

The question on the relative signs of amplitudes f_N and f_V is not clear to us. It has an important effect on the distribution of scattered neutrons. From figure 6 of paper [1] one can conclude that the authors assumed the opposite signs for these amplitudes (curves with the f_V taken into account pass below those obtained in the absence of additional interaction). Following this assumption we performed analytical calculations of scattering anisotropy of neutrons by argon at the specified angles using the formula (6) for parameters in a range $g = 0.3 \cdot 10^{-7} - 0.3 \cdot 10^{-6}$ and $\lambda = 1 - 100\ nm$, and also without taking into account additional interaction ($g = 0$).

The results of these calculations are presented in Fig. 1, which shows that the anisotropy curves for the specified values of g only weakly depend on λ and this dependence practically disappears with reduction of the constant g down to $g = 0.3 \cdot 10^{-7}$.

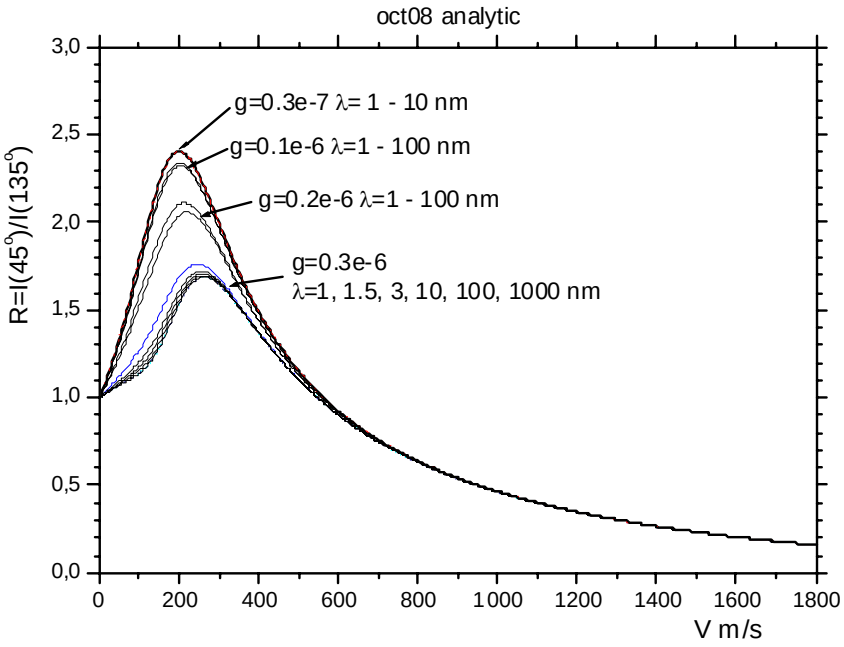

Fig.1. Anisotropy of neutrons (scattered by argon atoms) with initial velocity $V_0 = 200\ m/s$ depending on their final velocity for the parameters specified in the figure.

The calculations by the Monte-Carlo method were performed for different sets of values g и λ and for initial velocities $V_0 = 20$ and $200\ m/s$. To exclude the contribution from the hypothetical interaction the constant g was set to zero. In figure 2 some results of calculations of the scattering anisotropy of neutrons and their comparison with analytical ones are given. We can conclude that the results of Monte-Carlo calculations are in good agreement with the analytical ones. Monte-Carlo calculations for different sets of g and λ also confirm that at $g \le 0.1 \cdot 10^{-6}$ it is hardly possible to find a dependence of the anisotropy on the λ value. At the same time obtained as a result of the Monte-Carlo calculations of distribution of scattered neutrons for final velocities and angles have allowed to extract angular distributions of scattered neutrons for the chosen intervals of final velocities. Results of calculations for initial velocity of neutrons $V_0 = 20\,m/s$ are shown in figure 3 .

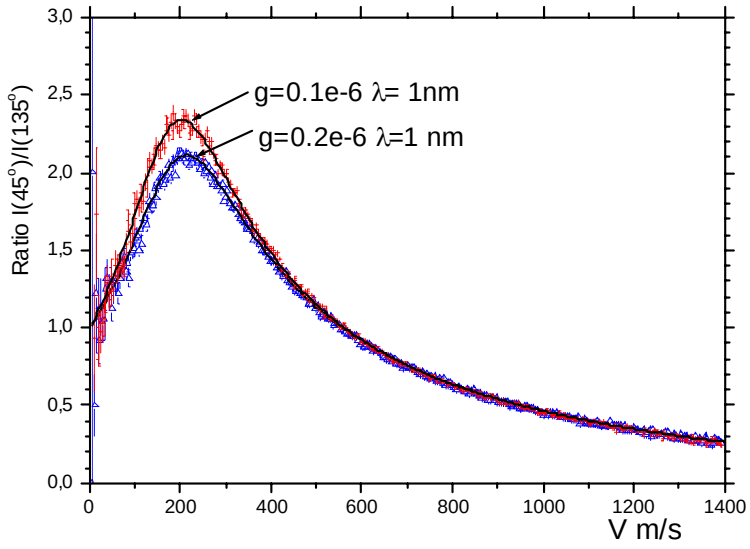

Fig.2. Comparison of some analytical anisotropy (curves) and Monte-Carlo results (points) for argon, $V_0 = 200\ m/s$.

Figure 3 shows that contrary to the dependence of neutron scattering anisotropy from the final velocity, the effects due to the presence of the extra-short-range interaction are more apparent in the angular distributions. Thus it is favorable to carry out measurements with even colder neutrons. The proposed technique of calculations of angular distributions allows to estimate expected experimental effects depending on the initial velocity of neutrons and chosen interval of final velocities. Naturally, if a realization of such an experiment becomes possible it is necessary to search for an optimum of V_0 and ΔV to achieve necessary statistics.

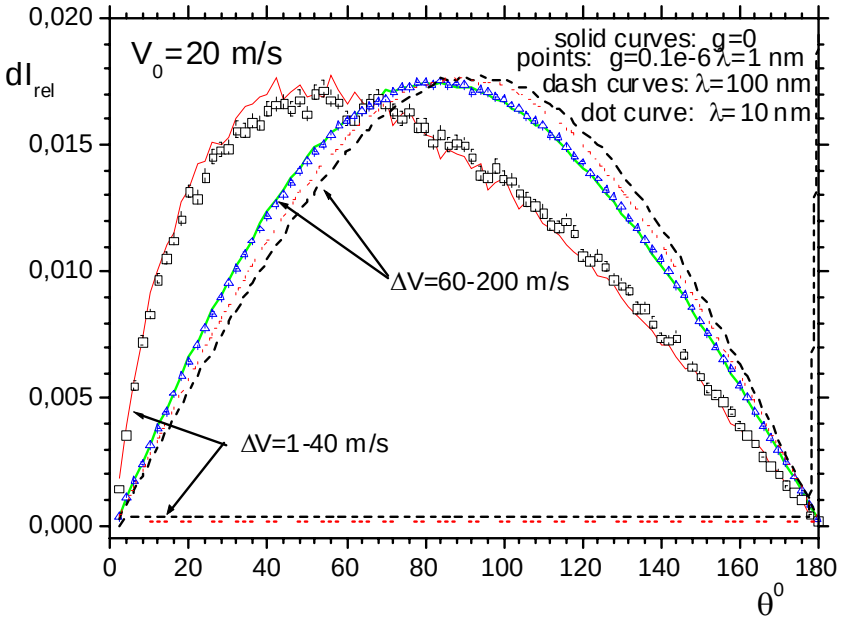

Fig. 3. Angular distributions (Monte-Carlo calculations) for neutrons with initial velocity $V_0 = 20\ m/s$ for $g = 0$ (solid curves), $g = 0.1 \cdot 10^{-6}$, $\lambda = 1\ nm$ (points), $\lambda = 10\ nm$ (dotted curves), $\lambda = 100\ nm$ (dashed curves) for the chosen intervals of final velocities $\Delta V = 1 - 40\ m/s$ and $\Delta V = 80 - 200\ m/s$.

References

1. V. V. Nesvizhevsky, G. Pignol, K. V. Protasov, "Neutron scattering and extra-shortrange interaction", Phys. Rev**. D77**, 034020 (2008).

Measurement of neutron total cross-section and resonance parameters of xenon [1]

Skoy V.R. †
FLNP JINR
E-mail: † skoy@nf.jinr.ru

Wang T.F., Kim G.N.
Departament of Physics, Kyuongpook National University, Daegu, 702-701, Republic of Korea

Oh Y.D., Cho M.H., Ko I.S., Namkung W.
Department of Physics, Pohang University of Science and technology, Pohang 790-784, Republic of Korea

Neutron total cross-sections and resonance parameters are basic quantities of nuclear data, which play an important role in the development and application of the nuclear science and technologies. Precise measurements of neutron cross-sections are of great importance for the safe design of nuclear reactors and for the evaluation of the neutron flux density and the energy spectrum around a reactor. Resonance parameters of isotopic nuclei, which undergo a complex process of evaluation and analysis based on experimental data of transmission measurement or capture measurement, are finding an increasingly important role in practical applications that are concerned with computations of reactor temperature coefficients, neutron reaction yields, self-protection effects and related matters. Neutron resonance parameters also can provide reliable information for a number of other fields, including fundamental science and medical application. Recent progress in optical polarization technique of noble gases opens a wide range of their application in applied and fundamental research. The ^{129}Xe isotope is good for magnetic resonance imaging of human blood system. The ^{131}Xe isotope can be a good candidate of a polarized target for the test of time reversal invariance.

Xenon isotopes ^{129}Xe and ^{131}Xe have strong s-wave low-lying resonances at 9.5 and 14.4 eV, respectively. The resonance at 14.4 eV is extremely strong and its peak cross-section achieves about 70 000 barns. It means that even a small distortion of a resonance shape owing to the Doppler broadening provides a systematic error for the polarization determination. This problem may be solved if one performs a measurement of total cross-section σ_0 at room temperature. Then, one needs to extract the resonance parameters taking into account a particular model of Doppler broadening. After that one can recalculate the resonance shape for any desired temperature and use it as a model of σ_0. Therefore, the measurements of nuclear data for the xenon gas are required because of their insufficient accuracy.

A few measurements of the neutron total cross-sections and resonance parameters for xenon gas are reported. In the present work, the total cross-sections of natural Xe have been measured in the energy range between 0.1 and 40 eV by the neutron TOF method at the Pohang neutron facility (PNF) [2]. The PNF consists of an electron linac, a water-cooled Ta target and a 12 m long TOF path. The resonance parameters for Xe isotopes were determined from the fitting of transmission rate by using the Multilevel R-Matrix code SAMMY [3] and compared with those of Mann et al. [4], Mughabghab [5] and Landolt-Börnstein [6]. Target cell for Xe We have performed an experiment with two specially manufactured target cells. Both target cells are identical in material and geometry, but one of them had a fill-in pipe with valve and a manometer as shown in Fig. 1. The target cell, a stainless steel cylinder with an inner diameter of 5.45 cm and a height of 13.0 cm, was filled with natural xenon gas at 14.1 psi pressure at 22^{o}C. The 0.5-mm thick Al plate was used for the window of the target cell. The thickness of xenon gas in target cell was 6.335×10^4 atom/barn. The empty cell was filled with air.

The SAMMY code uses the Bayes' theorem (generalized least squares) to fit the transmission data to obtain resonance parameters. For the Doppler broadening and resolution analysis, the MULTI method was applied: the free gas model was applied to the Doppler

broadening, and the convolution of Gaussian and exponential function was applied to the resolution. We fitted the transmission of the natural Xe gas sample with the SAMMY code to obtain the resonance parameters of each resonance peak in the neutron energy region from 3 to 30 eV, as shown in the Fig. 2. The present data were fitted with the spin definition in ENDF/B-VII.0. The resonance parameters were listed in Table 1 compared with those of Mughabghab, Landolt-Börnstein and Mann et al., and the evaluated values based on ENDF/B-VII.0 and JENDL-3.3. We get the neutron width Γ_n from the fitting but we listed calculated value of $g\Gamma_n$ in Table 1 to compare with other measurements and with the evaluated values. The overall resonance parameters are generally in good agreement with other measurements and the evaluated data from both JENDL-3.3 and ENDF/B-VII.0.

References:

1. V.R. Skoy at al., Nucl. Inst. Meth. B267 (2009) 2351.
2. V.R. Skoy at al., J. Korean Phys. Soc. 41 (2002) 314.
3. N.M. Larson, RSICC Peripheral Shielding Routine collection SAMMY-M2a: A Code System for Multilevel R-Matrix Fits to Neutron Data Using Bayes' Equations (PSR-158, SAMMY-M2a), Oak Ridge National Laboratory, 1999.
4. D.P. Mann, at al., Phys. Rev. 116 (1959) 1516.
5. S.F. Mughabghab, Editor, *Atlas of Neutron Resonances: Resonance Parameters and Thermal Cross sections Z = 1 − 100* (fifth ed.), Elsevier, Amsterdam (2006).
6. Landolt-Börnstein In: H. Schopper, Editor, *Low Energy Neutron Physics*, Springer, Berlin (1998).
7. K. Shibata et al., JENDL-3.3, J. Nucl. Sci. Technol. 39 (2002) 1125.
8. M.B. Chadwick et al., Nucl. Data Sheets 107 (2006) 2931.

Table 1 Resonance parameters of Xe isotopes.

Isotope	J	l	Represent	E_{res} (eV)	Γ_γ (meV)	$g\Gamma_n$ (meV)
^{124}Xe	0.5	0	Present [1]	5.09±0.06	89.50±8.95	12.92±1.26
			Mann et al. [4]	5.16±0.06	-	7.6±0.8
			Mughabghab [5]	5.16±0.01	100	13.3±1.8
			Landolt-Börnstein [6]	5.16±0.09	-	12.4±0.18
			JENDL-3.3 [7]	5.16	90.0	12.4
			ENDF/B-VII.0 [8]	5.16	100.0	13.3
^{129}Xe	1.0	0	Present	9.66±0.01	143.66±10.38	5.82±0.17
			Mann et al.	9.47±0.20	-	8.25±0.75
			Mughabghab	9.570±0.008	140±30	2.4±1.7
			Landolt-Börnstein	9.5±0.2	110±10	4.5±0.2
			JENDL-3.3	9.5	110.0	4.5
			ENDF/B-VII.0	9.57	109.0	4.62
^{124}Xe	0.5	0	Present	10.12±0.09	90.47±9.04	53.97±5.29
			Mann et al.	-	-	-
			Mughabghab	9.88±0.01	100	42.3±6.0
			Landolt-Börnstein	9.88±0.20	-	39.5±0.6
			JENDL-3.3	9.88	90.4	39.6
			ENDF/B-VII.0	9.88	100.0	42.3
^{131}Xe	2.0	0	Present	14.47±0.01	93.00±8.87	150.83±2.54
			Mann et al.	14.1±0.4	-	175±25
			Mughabghab	14.410±0.014	93±16	131.5±5.0
			Landolt-Börnstein	14.4±0.3	94±17	135±5
			JENDL-3.3	14.41	95.54	135.12
			ENDF/B-VII.0	14.41	94.0	131.5

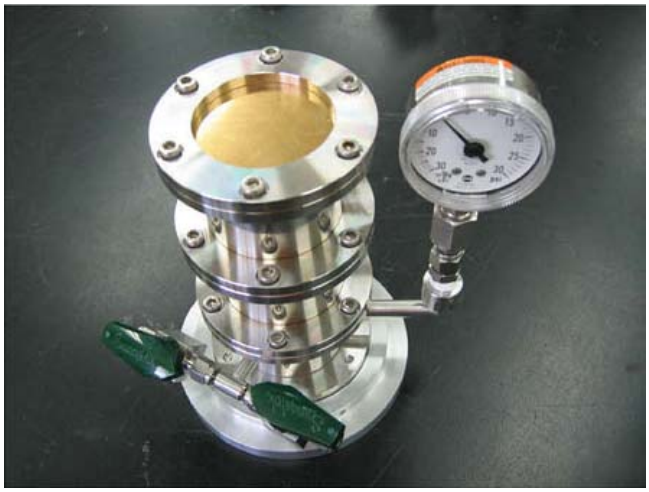

Fig. 1. Vessel with natural Xe.

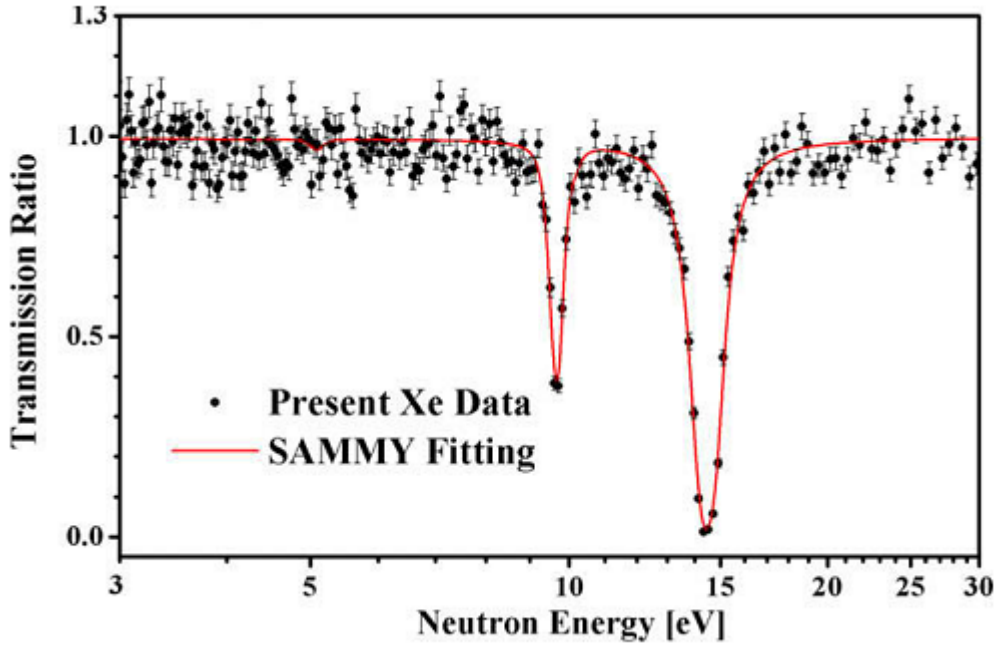

Fig. 2. Measured transmission ratio of Xe with a fitting result from the SAMMY code.

Multicrystal Scintillation Detector for Investigation of Angular Correlations in (n,γ) Reactions

Vadim R. Skoy[a], Guinyun Kim[b], Manwoo Lee[b], and Kyung Sook Kim[b]

[a]*Frank Laboratory of Neutron Physics, Joint Institute for Nuclear Research, Dubna, 41986, Russia*

[b]*Department of Physics, Kyuongpook National University, , Daegu, 702-701, Republic of Korea*

***Abstract*—An improvement of method for the study of time reversal (T) violation is described. It consists of measurement of the forward-backward asymmetry in direct γ-ray transitions after unpolarized neutron capture in p-wave resonances. The γ-detector consists of 12 BGO crystals were tested equipped with new high performance DAQ system based on flash ADC modules.**

I. Introduction

Violation of *T* (time reversal) invariance was observed in the decays and oscillation of K- and B-mesons only. No evidence of *T*-violation in hadrons or nuclear reactions has been found. The experimental check-up of *T*-invariance in these reactions basically requires polarized beams and polarized or aligned targets. This technique is complicate and quite expensive, so no full-scale experiments were performed yet.

However, it was shown [1] that measurements of angular correlations in individual γ-quanta transitions from unpolarized neutron capture might give important information about certain sort of *T*-violating interaction in nuclei. The feasibility of experimental result presented in [1] was limited by capabilities of those days technique. The efficiency of two NaI detectors to detect 9 MeV γ-quanta was relatively low, and the data acquisition system did not observe direct γ-ray transitions in the vicinity of neutron p-wave resonance with desired precision. Nevertheless, the measurements reported in [1] set the upper limit of *T*-violation interaction in neutron reactions.

The progress in experimental technique during last 20 years encourages us for significant improvement of results.

II. Models of T-violation in Nuclear Reactions

There are many models, which introduce time reversal violating interaction in nuclear reactions [2]. All of them are divided in two sorts. First sort unites the models of *T*-violation with simultaneous breaking of space parity (P). Second sort contains the models, which break *T*-invariance but hold space parity. The interaction, which might show itself in neutron capture, belongs to the second sort. If one uses S-matrix scattering formalism, then the experimental effect related to *T*-violating, *P*-conserving interaction is connected with quantity

$$\delta S_J \approx S_J\left(1\tfrac{1}{2} \to 1\tfrac{3}{2}\right) - S_J\left(1\tfrac{3}{2} \to 1\tfrac{1}{2}\right) \neq 0. \qquad (1)$$

Here, $S_J\left(lj \to l'j'\right)$ is the scattering matrix element, which corresponds to the transition of p-wave neutrons ($l = l' = 1$) in a resonance with spin J from a channel $j = \frac{1}{2}$ to a channel $j' = \frac{3}{2}$ and vice versa. Equation (1) means that *T*-violating might leads to the difference of probabilities of transitions between two p-wave states of compound nuclei. Let us consider two neighboring p-wave resonances with amplitudes of neutron widths $\sqrt{\Gamma_{n1}(lj)}$, and $\sqrt{\Gamma_{n2}(lj)}$ respectively. *T*-violating interaction may mix these resonances in a way [4]:

$$\sqrt{\Gamma_{n1}(lj)} \to \sqrt{\Gamma_{n1}(lj)} + \frac{iv_T}{D}\sqrt{\Gamma_{n2}(lj)}. \qquad (2)$$

where, iv_T is the purely imaginary matrix element which characterize the strength of *T*-violating interaction, and *D* is spacing between two p-wave resonances.

Evaluation of (1) gives the result [1], [5]

$$\delta S_J \approx \mathrm{Im}\left(\sqrt{\Gamma_{n1}\left(1\tfrac{1}{2}\right)} \cdot \sqrt{\Gamma_{n1}\left(1\tfrac{3}{2}\right)}^{*}\right) \neq 0. \qquad (3)$$

This equation satisfied when the amplitude of neutron width is a complex quantity as it follows from (2).

From other hands, (3) describes the interference between two resonances. However, the angular correlations of γ-quanta after neutron capture arise owing the interference between neutron resonances too (most often s- and p-waves) [6]. The methods and technique are developed for investigations of these correlations is a good opportunity to test the above model of *T*-violation.

III. Experimental Strategy

The simplest way to understand the angular correlation of γ-quanta produced by neutron capture reaction is to measure a forward-backward asymmetry. The sketch of basic experimental arrangement is shown on Fig. 1.

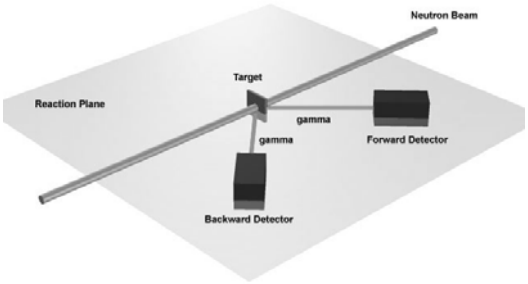

Fig. 1. Basic experimental arrangement for the forward-backward asymmetry measurement.

Le us denotes the numbers of γ-quanta have been absorbed by forward and backward detectors as $N_F = N(\theta)$ and $N_B = N(\pi - \theta)$ respectively, where θ is polar angle between the neutron beam and axis of the forward detector. The forward-backward asymmetry ε_{FB} is expressed as:

$$\varepsilon_{FB} = \frac{N_F - N_B}{N_F + N_B} \ . \qquad (4)$$

We have mentioned that this correlation arises from the interference between s- and p-wave resonances. Usually the measurement is provided in vicinity of p-wave resonance, which sits on a top of s-wave resonance wing. The dependence of ε_{FB} on neutron energy *E* in the vicinity of p-wave resonance is characterized by a term

$$\varepsilon_{FB}(E) \sim \frac{E - E_p}{\Gamma_p}, \qquad (5)$$

where E_p and Γ_p are the energy and total width of p-wave resonance, respectively. We see, that the forward-backward asymmetry $\varepsilon_{FB}(E)$ crosses zero at $E = E_p$. If one assumes the presence of *T*-violating, *P*-conserving interaction and take into account Eq. (2), then the energy behavior of Eq. (5) will become

$$\varepsilon_{FB} \sim \frac{E - E_p + \Delta E_T}{\Gamma_p}, \quad \Delta E_T \approx \frac{\Gamma_p}{D} \cdot v_T \, . \qquad (6)$$

Thus, *T*-violating, *P*-conserving interaction shifts the zero-crossing point of the curve $\varepsilon_{FB}(E)$.

However, to extract the shift ΔE_T in Eq. (6) one needs to define energy E_p by an independent way. Fortunately that is possible. Indeed, the theoretical expression for $N_F + N_B$ does not depend on ΔE_T [1]. Thus, if we have two sets of experimental data N_F and N_B, we take their sum and extract all necessary resonance parameters: E_p, Γ_p, $\sqrt{\Gamma_n(lj)}$, etc. with fitting procedure. Then, we take the difference $N_F - N_B$ and fit it assuming only one free parameter ΔE_T. All other parameters are fixed by the previous fit. Thus, all we need is to extract ΔE_T from the same experimental data. This approach is free from systematic errors which are connected with other parameters, since we use *exactly same* data sets.

IV. CONFIGURATION OF GAMMA DETECTOR

The best condition for investigating the angular correlations is to measure direct γ-transitions with the energy of about 10 MeV (for heavy nuclei). The theoretical analysis for direct γ-transition is much more simple than that for cascades. However, the γ-transition detector must be efficient for high-energy γ-quanta. For this purpose the Monte Carlo simulation was performed with the same size of CsI and BGO crystal. The simulation has been done for 10-MeV γ-rays generated at 10 cm apart from detector and randomly distributed in direction. Fig. 2 shows the simulated pulse-height spectra for CsI (5×5×15 cm^3), and BGO (5×5×7.5 cm^3) crystals with 200,000 γ-ray events. The numbers are the spectra areas above 8 MeV. We see that for the given dimensions BGO crystal is about 2 times more efficient than CsI.

Figure 1 is the NaI detector configuration used in Barabanov *et al.* [1]. Since the asymmetry (ε_{FB}) does not depend on an azimuthal angle (around beam axis), one can apply more detectors to increase solid angle. We have employed a γ-ray detection system for measuring the angular correlations with 12 scintillation detector elements, each made of a BGO crystal (Shanghai SICCAS High Technology Co.) with 5 cm ×5 cm active area and 7.5 cm length, coupled to a Hamamatsu H7195 photomultiplier tube, which is shown in Fig. 3. Eight (blue) detectors are used for the measurement of asymmetry itself. Four (yellow) detectors perpendicular to the neutron beam direction will be used as the reference detector, for monitoring additional spectroscopic information, and investigation of other angular correlations [6].

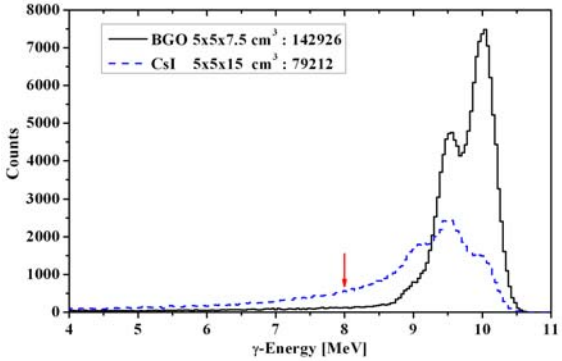

Fig. 2. The simulated pulse-height spectra for CsI and BGO crystals. The numbers are the spectra areas above 8 MeV.

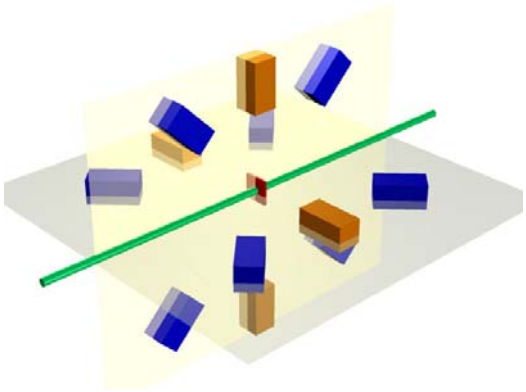

Fig. 3. Twelve-detector set for the measurement of forward-backward asymmetry.

V. Detector Performance

The BGO crystals were wrapped several layers of Teflon tape and were covered by white paper and black tape. One open side of the BGO crystals was coupled with silicone optical grease directly to the entrance window of a 2 inch photomultiplier type Hamamatsu H7195.

We measured the light yield dependence of our BGO crystals on temperature within a range from 16° to 26° C. We have developed the crystal temperature compensation module based on DS1820 sensor [7].

After correcting the temperature dependence of the light yield, a good linearity of light response for γ-ray sources was obtained as shown in Fig. 4.

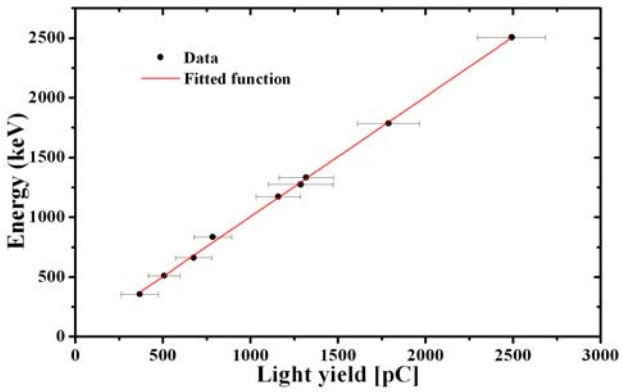

Fig. 4. Linearity of light yield in BGO crystals.

The energy resolution of BGO detector was obtained by using the several γ-sources as shown in Fig. 5 (about 12 % for 1 MeV γ-rays).

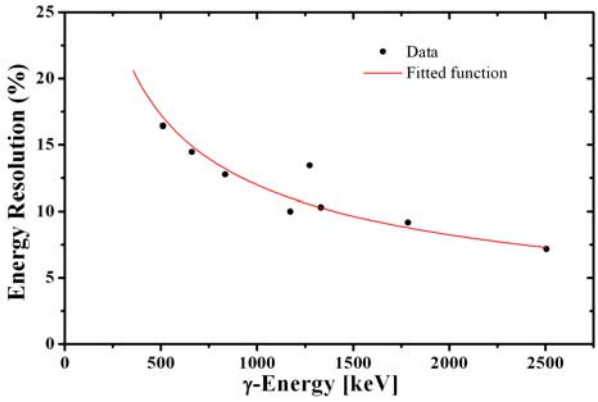

Fig. 5. Energy resolution of BGO crystals.

VI. Data Acquisition System

The 100 MHz flash-ADC-based data taking system has been designed. The pulse signal generated when electron hit the Ta-target is used as a start signal for 100 MHz flash-ADC. Output signals from the BGO γ-detectors are fed into two 8-channel flash-ADC (NFADC100) produced by Notice Korea. The TOF data are stored in a data acquisition (DAQ) system. The flash-ADC measures and stores both the arrival time and the pulse shape of the prompt γ-quanta from neutron capture reactions and background signals. The arrival time of the prompt γ-quanta will give the information of the neutron energy and the pulse shape that of the γ-quanta energy.

Fig. 6 demonstrates the energy resolution has been obtained with ^{60}Co source for our detectors attached to flash-ADC. We could separate 1173.2 keV and 1332.5 keV peaks from ^{60}Co.

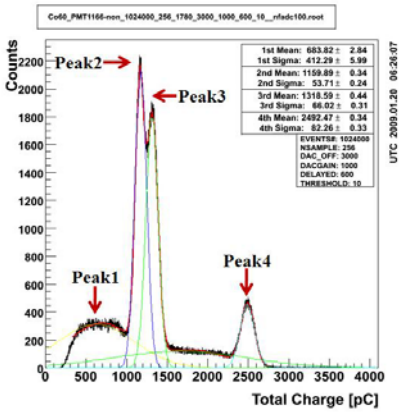

Fig. 6. Pulse height spectrum of ^{60}Co source with BGO detectors attached to 100 MHz flash-ADC.

References

[1] A. L. Barabanov *et al.*, "Testing T-odd, P-Even Interactions with γ rays from Neutron p-Wave Resonances," *Phys. Rev. Lett.*, vol. 70, no. 9, pp. 1216-1219, 1993.

[2] V. P. Gudkov, "Symmetry Violation in Heavy Nuclei," in *Proc. Fundamental Physics with Pulsed Neutron Beams*, Research Triangle Park, NC, USA, 2000 pp. 117–126.

[3] R.S. Conti, I.B. Khriplovich, "New limits on T-odd, P-even interactions," *Phys. Rev. Lett.*, vol. 63, no. 22, pp. 3262-3265, 1992.

[4] V. E. Bunakov, “Enhancement Effects of the P-Conserving T-Invariance Violation in Neutron Transmission,” *Phys. Rev. Lett.*, vol. 60, no. 22, pp. 2250-2253, 1988.
[5] A. M. Lane, R. G. Thomas, “R-Matrix Theory of Nuclear Reactions,” *Revs. Mod. Phys.*, vol. 30, no. 2, pp. 257-353, 1958.
[6] V. V. Flambaum, O. P. Sushkov, “Angular and Polarization Correlations in the (n,γ) Reaction,” *Nucl. Phys. A*, vol. 435, no. 2, pp. 352-380, 1985.
[7] See at http://martybugs.net/electronics/tempsensor/hardware.cgi for serial sensor, http://datasheets.maxim-ic.com/en/ds/DS18S20.pdf for Dallas sensor, and http://www.digitemp.com for software of digital temperature sensor.
[8] G. N. Kim *et al*., “Nuclear Data Production Facility Based on the Electron Linac,” *J. Korean Phys. Soc.*, vol. 43, no. 4, pp. 479-486, 2003.

NEUTRON ACTIVATION ANALYSIS FOR AIR POLLUTION STUDY IN CROATIA

Spiric Z.[1], Frontasyeva M.V., Pavlov S.S., Gundorina S.F., Ostrovnaya T.M.

Frank Laboratory of Neutron Physics, Joint Institute for Nuclear Research
E-mail: marina@nf.jinr.ru
[1]Oikon Ltd – Institute for Applied Ecology, Zagreb, Croatia
E-mail: zspiric@oikon.hr

Introduction

Since the first joint European moss survey in 1995 (Rühling et al, 1996), a gradually increasing number of countries have joined this program. In the subsequent survey in 2000 (Harmens et al., 2004) 28 countries participated including Hungary, Slovenia, and Austria, all neighboring countries to Croatia. Prior to the third joint European moss survey in 2005/2006 it was therefore decided to include Croatia among the participating countries. The purpose of this report is a presentation and discussion of the results obtained for mosses collected in Croatia in 2006. To the knowledge of the authors this is the first application in Croatia of biomonitoring atmospheric deposition of metals, except for a local study of mercury and some other elements from the petroleum industry undertaken in 1996–2004 using lichens (Hovart et al., 2000).

Materials and Methods

The following moss genera, *Hylocomium splendens, Hypnum cupressiforme, Brachythecium rutabulum* and *Homalothecium* were found suitable for assessing atmospheric deposition of key heavy metals and other elements in Croatia. This combination of species has also already been used for biomonitoring purposes in some other European countries where other recommended species were not available. Interspecies comparisons showed that *Brachythecium rutabulum* and *Homalothecium* could be used along with *Hylocomium splendens, Pleurozium schreberi,* and *Hypnum cupressiforme.*

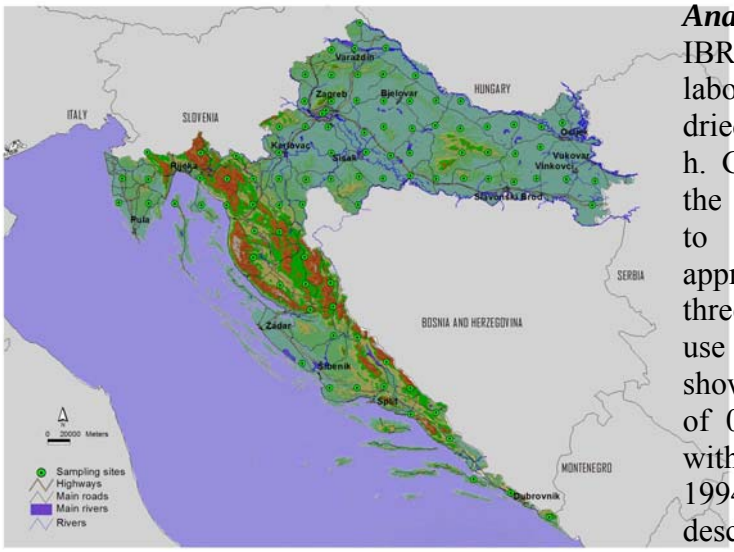

Fig. 1. Sampling sites

Sampling. The sampling sites are shown on the map in Fig. 1. Sampling was carried out during the period July – August 2006. A total of 94 moss samples were evenly collected over the territory of Croatia.

Analysis. NAA was performed at the reactor IBR-2 at the FLNP, JINR, Dubna. In the laboratory the samples were cleaned and air-dried to constant weight at 30–40 ^{o}C for 48 h. Green–brown moss shoots repre-senting the last three years´ growth were subjected to analysis, as they correspond approximately to the deposition over the last three years. Previous experience from the use of NAA in moss biomonitoring has shown that *Hylocomium splendens* samples of 0.3 g are sufficiently large to be used without homogenization (Steinnes et al., 1994). Details of gamma-spectrometry are described elsewhere (Steinnes et al., 1995). The Quality control of NAA results was ensured by simultaneous analysis of the examined samples and reference materials (RM) Lichen–336 IAEA and NORD DK-GIS-INTEGRO software package with raster and vector graphics was used to construct raster-based contour maps.

Results and discussion

Multivariate statistical analysis (factor analysis) was used to identify and characterize different pollution sources and to point out the most polluted areas. The six factors are interpreted as follows:

Factor 1 has particularly high values of Na(0.89), Mg(0.82), Al(0.95), Sc(0.95), Ti(0.97), V(0.89), Cr(0.92), Fe(0.93), Co(094), Ni(0.87), Cs(0.86), Ba(0.72), Hf(0.96), Ta(0.93), Th(0.98), U(0.96), and REE (rare-earth elements). Most of these elements are typical of crustal material.

Factor 2 is a typical pollution component associated with a point source: Zn(0.83), As(0.60), and Cd(0.82) (Fig. 2).

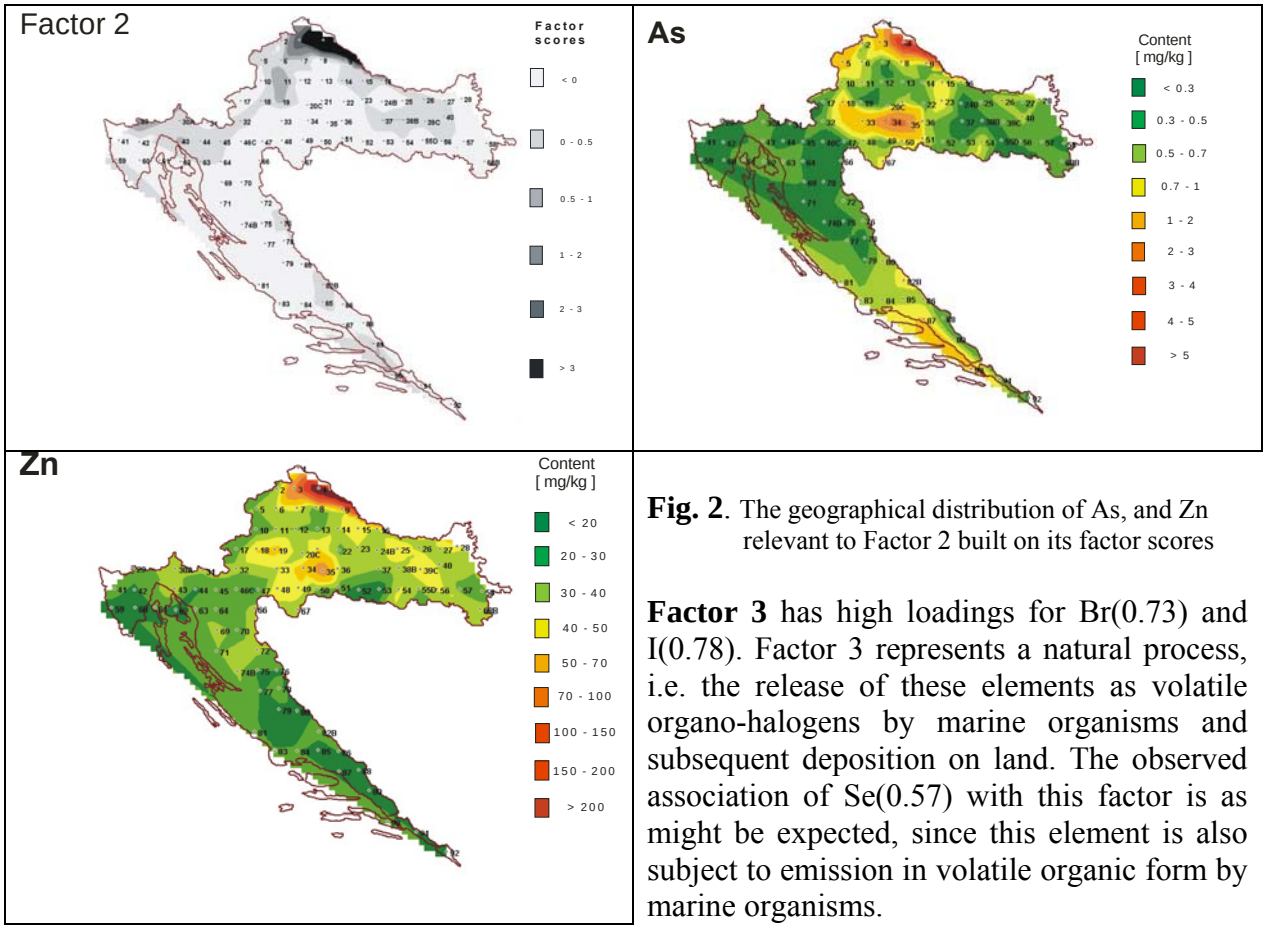

Fig. 2. The geographical distribution of As, and Zn relevant to Factor 2 built on its factor scores

Factor 3 has high loadings for Br(0.73) and I(0.78). Factor 3 represents a natural process, i.e. the release of these elements as volatile organo-halogens by marine organisms and subsequent deposition on land. The observed association of Se(0.57) with this factor is as might be expected, since this element is also subject to emission in volatile organic form by marine organisms.

Factor 4, with high factor loadings for Cl(0.85) and K(0.85), and **Factor 5**, with high loadings for Mn(0.84), are probably not pollution-related, but connected to the normal nutrient uptake of the moss.

Factor 6, with high loadings for Cu(0.64), Sb(0.52), and Hg(0.62), appears like a typical pollution factor. The geographical distribution of Factor 6 is shown in Fig. 3, along with distribution maps for Cu and Sb. The highest factor score is observed at site 93B located in the center of Zagreb, but moderate to high values are also observed at sites 5, 9, 30A, 34, and 48. Cu and Sb are known to be emitted from automobile traffic.

Factor 7, with relatively high positive loading for Pb, is strongly dominated by a high Pb value at site 21 located east of the center of Zagreb, the source of which is not known.

As evident from the results obtained, it is clear that Croatia is considerably polluted compared to many other countries in Europe. Still the situation in Croatia with respect to metal deposition is markedly better than in some of its neighboring countries, in particular with relation

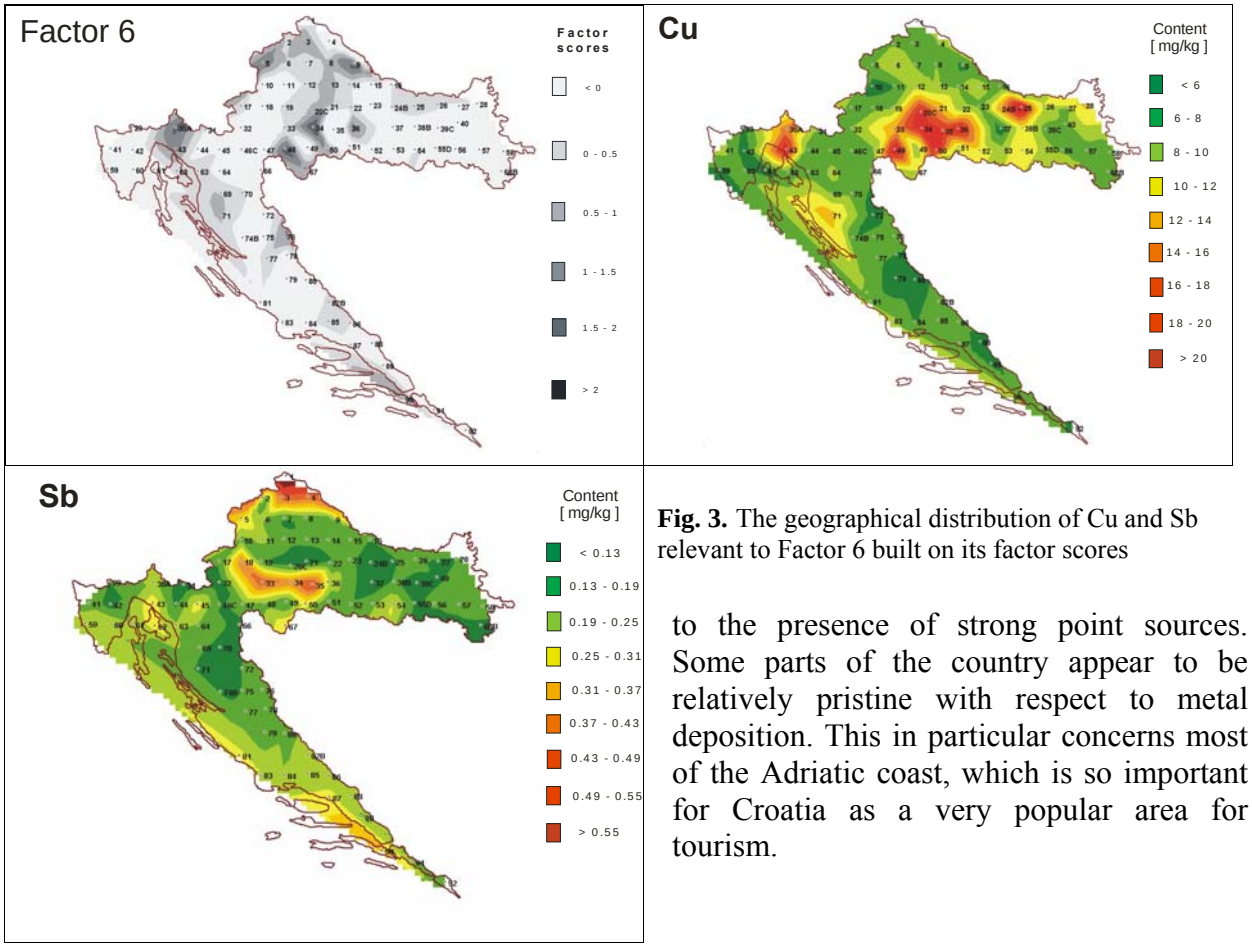

Fig. 3. The geographical distribution of Cu and Sb relevant to Factor 6 built on its factor scores

to the presence of strong point sources. Some parts of the country appear to be relatively pristine with respect to metal deposition. This in particular concerns most of the Adriatic coast, which is so important for Croatia as a very popular area for tourism.

Acknowledgements. The authors express their gratitude to L. Barandovski and Z. Mesić for collaboration and help in collecting of moss samples, and E. Povtoreyko for preparation of GIS maps.

References:

Harmens H., Buse A., Büker P., Norris D., Mills G., Williams B., Reynolds B., Ashenden T.W., Rühling Å., Steinnes E.. Heavy metal concentrations in European mosses: 2000/2001 survey. Journal of Atmospheric Chemistry, Vol. 49. 2004, p. 425-436.

Horvat M., Jeran Z., Spiric Z., Jacimovic R., Miklavcic V. Mercury and other elements in lichens at INA-Naftaplin gas treatment plant, Molve, Croatia. Journal of Environmental Monitoring, Vol. 2, 2000, p. 139-144.

Rühling Å., Steinnes E., Berg T. Atmospheric Heavy Metal Deposition in northern Europe 1995, Nord 1996:37, Nordic Council of Ministers, Copenhagen 1996, 46 pp.

Steinnes E., Hanssen J.E., Rambæk J.P., Vogt N. B. Atmospheric deposition of trace elements in Norway: temporal and spatial trends studied by moss analysis. Water, Air, and Soil Pollution. Viol. 74, 1994, p. 121-140.

Steinnes E.,. Frontasyeva M.V. Epithermal analysis of mosses used to monitor heavy metal deposition around an iron smelter complex. The Analyst. Vol. 120, 1995, p. 1437-1440.

NEUTRON EMISSION IN FISSION OF ^{252}Cf(SF)

Sh. Zeynalov[a,b]
[a])*FLNR-JINR*
E-mail: zeinal@zeinal.nf.jinr.ru

F.-J. Hambsch[b], S. Oberstedt[b], I. Fabry[b]
[b])*EC-JRC-Institute for Reference Materials and Measurements, Belgium*

Introduction

The digital signal processing (DSP) along with a twin Frisch grid ionization chamber (TGIC) was used to measure the kinetic energy-, mass- and angular distributions of fission fragments in correlation with prompt fission neutrons emitted in spontaneous fission of ^{252}Cf. The experiment was basically adopted from Ref. [1] with some improvements in instrumentation and data analysis, which allowed a significant quality improvement of the results. The anode current caused by a fission fragment (FF) in the TGIC was amplified by a current amplifier and sampled with a 10 bit, 80 Ms/sec waveform digitizer (WFD). The prompt fission neutron (PFN) time-of-flight (TOF) spectroscopy was done using an analogue TDC after pulse shape discrimination using charge-to-digital (QDC) conversion. The measurement of the FF characteristics both in coincidence and non-coincidence with the PFN emission was done in the same measurement without readjusting the apparatus. A Cf-sample, on a 100 μg/cm^2 thick Ni foil backing with an activity of ~500 FF/sec, was mounted on the common cathode of the TGIC, which operated under normal conditions with as working gas P-10 at a constant flow of ~(50-100) ml/min. About 12*10^6 coincidences between FF and PFN were acquired in the measurement, which is more than the double compared to Ref [1].

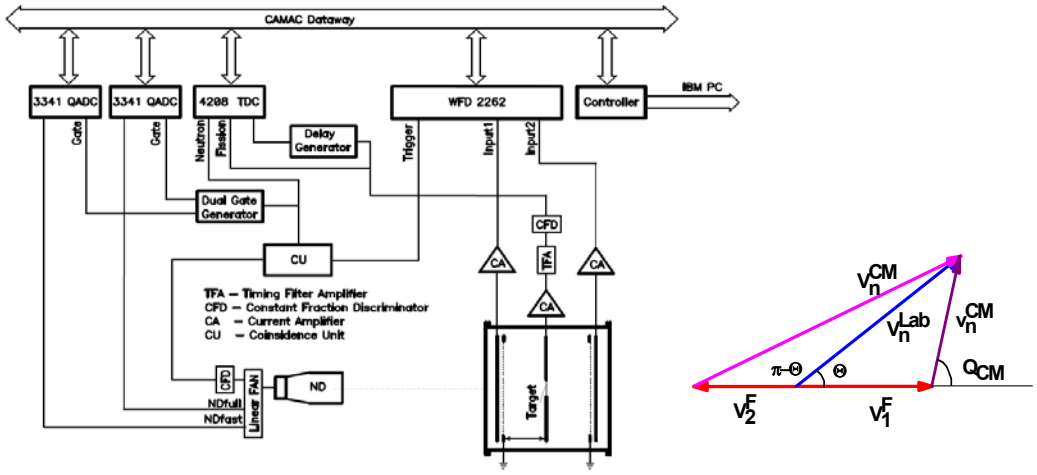

FIGURE 1. Experimental setup (left), graph depicting PFN emission kinematics (right).

Experimental Analysis and results

The FF kinetic energy and the angle between a FF and the TGIC axis was analysed using DSP algorithms described in Ref. [3]. The waveforms $P_{1,2}[L]$ of 512 samples each, first pass a differentiating filter to subtract the baseline. Then $P_1[L]$ and $P_2[L]$ were digitally integrated in a L=100 channel (~1.2 μs) window to obtain the total charge released by the corresponding FF during deceleration in the TGIC using the formula $P_i[L] = \sum_{k=Tg}^{Tg+L} A_i[k]$. To measure the angle Θ_i between the FF and the TGIC's axis the drift time method, utilizing the drift time dependence on

Θ_i of electrons released by the FF, was implemented: $T_i[L] = \frac{\sum_{k=Tg}^{Tg+L} k * A_i[k]}{\sum_{k=Tg}^{Tg+L} A_i[k]} - T_g$, where Tg is the trigger signal sample position. The trigger signal was obtained from the common cathode pulse

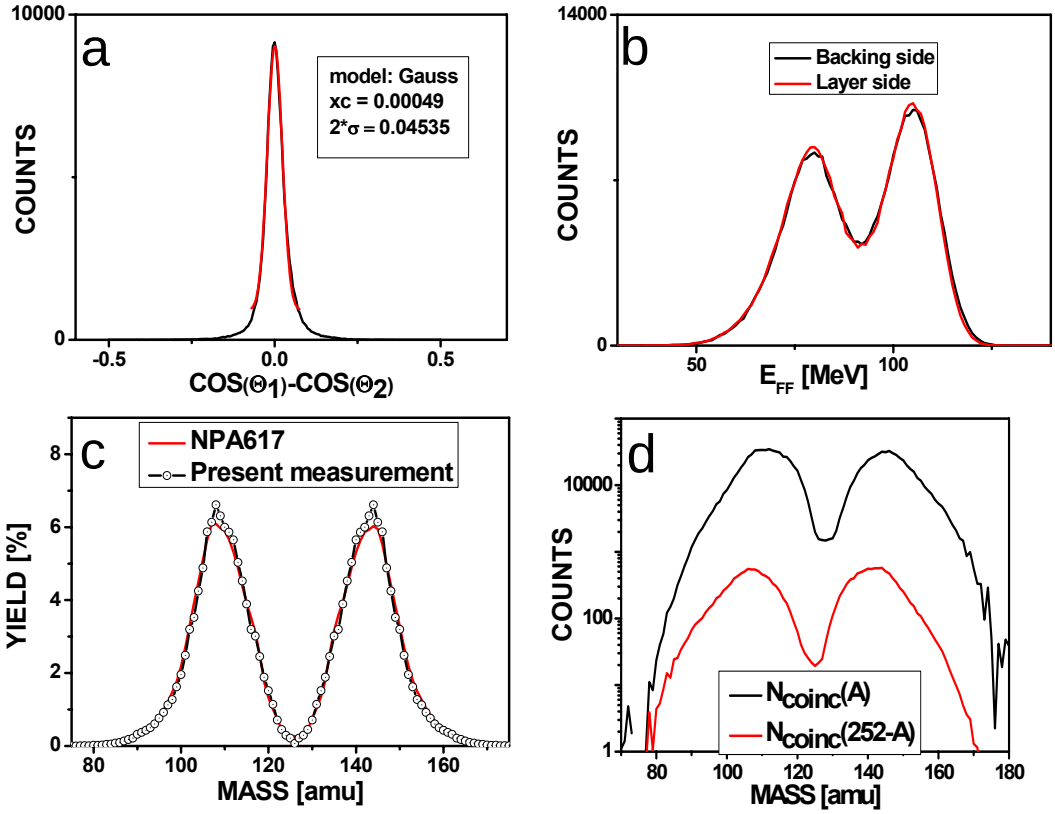

Fig 2. a) Precision of FF angle measurement; b) FF kinetic energy distributions; c) FF mass distribution; d) Mass distribution measured in coincidence with PFN for FF emitted toward the ND in comparison with mass distribution for FF emitted in opposite direction (red line).

and referred to as the time instant of the fission event. The dependence of $\cos(\Theta_i)$ on the drift time can be found using the following formulae:

$T_{90} = \frac{D + 0.5 * d}{W}$, $T_{90} - T(E) = (T_{90} - T_0(\mathrm{E})) * \cos(\Theta)$, $P^C = \frac{P^O * T_{90}}{T_{90} + \sigma * T}$, where D, d are the cathode-grid and grid-anode distances, respectively, W is the free electron drift velocity, T_0, T_{90} are the drift times for FF having Θ_i equal to 0^o and 90^o, respectively, σ is the grid inefficiency, P^C, P^O are the grid inefficiency corrected and uncorrected total charges collected on the anodes, T is the drift time for the considered FF. The above formulae were obtained considering the drift of electrons in the electrostatic fields created between the cathode-grid and grid–anode spaces of the TGIC. The PFN kinetic energy was analyzed from the TOF measurement using the prompt fission gamma (PFG) peak position as a reference point. The PFG peak position and its width broadening dependence on PFG pulse height were measured and parameterized. Then the PFN TOF distribution was considered as a distribution, satisfying to the following integral equation:

$$f_s(t) = \int_0^\infty F(\tau) h(t-\tau) d\tau, \quad \int_0^\infty h(t-\tau) d\tau = 1 \ ,$$

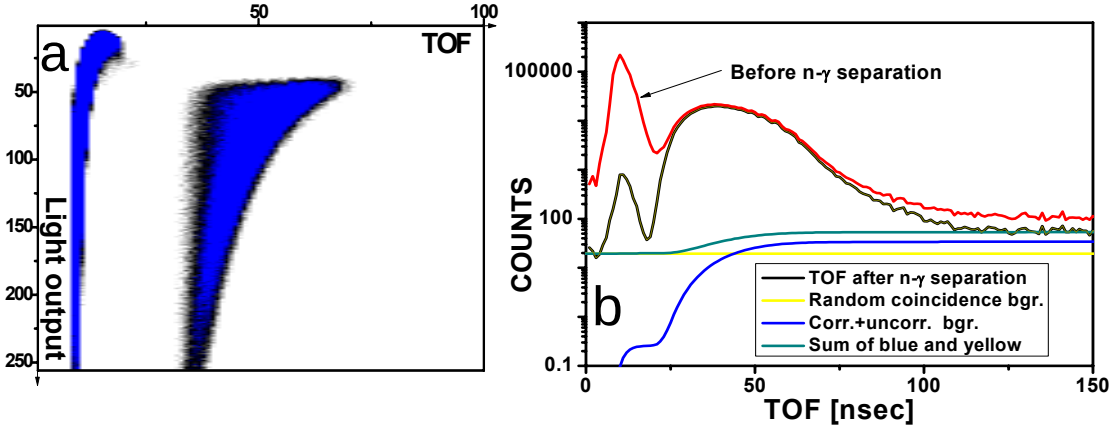

Fig 3. a) PFN TOF versus total light output plot demonstrates reference shift and broadening; b) PFN TOF distribution illustrating the n-γ separation and background subtraction.

where $f_s(t)$ is the measured TOF distribution after background subtraction. F(τ) is the original TOF distribution and h(t-τ, λ, η) is the resolution function (RF). The RF depends on the total light output (λ) and on the flight path fluctuation due to the finite thickness of the neutron detector (ND) (η). For each FF in coincidence with the ND the following values were recorded: two FF kinetic energies FF_1, FF_2, PFN TOF value, total light output λ and pulse shape information. The pulse shape information was used to separate PFN from PFG and allowed to suppress the PFG radiation by ~240 times. The remaining background was considered consisting of two parts: random coincidences between the TGIC and delayed neutrons from the target and the radioactivity of the surrounding materials which is a time independent background and coincidences correlated with the fission events (when a fission event was detected by the TGIC, but a PFN hitting the ND after being scattered by air or other surrounding material) and uncorrelated coincidence (a fission event triggered the apparatus, but a PFN is detected from the next fission occurring during the dead time of the apparatus). The random coincidence rate was analysed using the following formula: $R = N_1 * N_2 * \Delta$, where N_1, N_2 are the TGIC and the ND counting rates, respectively and Δ is the resolution time of the coincidence unit. Correlated and uncorrelated background can be calculated using the following formulae: $N_{un}(t) \approx N_1 \int_0^{\Delta} \tau(f(t-\tau)-R)d\tau$, $N_c \approx N_1 \int_0^{\infty} \tau(f(\alpha(t-\tau))-R)d\tau$, where α>1 is a fitting parameter. After these background contributions were subtracted the PFN TOF distribution was converted to the PFN energy spectrum divided by $\sqrt{E_{PFN}}$ and compared to a Maxwell distribution $N * \exp(-E_{PFN}/1.42)$, $N = \int_0^{\infty} f(t)dt$ to find the ND efficiency dependence on the PFN energy.

The results of the present measurement of PFN multiplicity distributions are in very good agreement with those of Ref. [1]. The isotropic angular distribution of the PFN in the FF center-of-mass reference system is confirmed (see left part of Fig. 4). For the first time, however, no reduction of the neutron multiplicity at low TKE was observed (see middle part of Fig. 4). This is expected from energy balance considerations. Also the PFN multiplicity as a function of FF mass (see right part of Fig. 4) is in reasonable good agreement with Ref. [1].

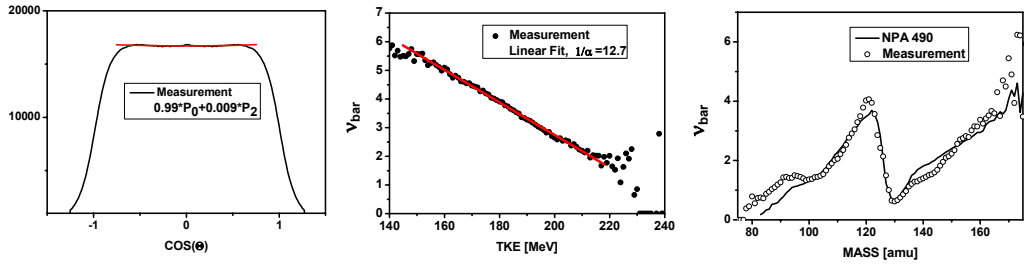

FIG 4. a) Center-of-mass angular distribution; b) PFN multiplicity as a function of TKE; c) PFN multiplicity as a function of FF mass..

References

1. C. Budtz-Jorgensen and H.-H. Knitter, Nucl. Phys. A490 (1988) 307.
2. F.-J. Hambsch, S. Oberstedt, Nucl. Phys. A617 (1997) 347.
3. O.V. Zeynalova, Sh.S. Zeynalov, F.-J. Hambsch, S. Oberstedt, Bulletin of the Russian Academy of Sciences: Physics, 2009, Vol. 73, No. 4, pp. 506–511. © Allerton Press, Inc., 2009.

DSP algorithms for fission fragment and prompt fission neutron spectroscopy

O. Zeynalova[a], Sh. Zeynalov[a,b]
[a]) LIT-JINR, FLNP-JINR
E-mail: zeinal@ nf.jinr.ru

F.-J. Hambsch[b], S. Oberstedt[b], I. Fabry[b]
[b])EC-JRC-Institute for Reference Materials and Measurements, Belgium

Introduction

In recent decades the DSP technology gained dominance in respect to the traditional analogue signal processing technique in experimental nuclear physics due to the higher flexibility and an obvious economical reason. Hardware modules provided diversity of signal analysis possibilities by modification of the signal processing software only. In this work we present algorithms developed for investigation of correlations between prompt neutron emission and the FF mass and energy distributions. The ^{252}Cf target was mounted in the centre of the common cathode of a twin Frisch-grid ionization chamber (GTIC) in such a way that each of the FF is stopped in the corresponding half of the GTIC. Anodes pulses caused by FF were used to obtain mass-, kinetic energy and the emission angle of the FF with respect to the cathode-plane normal. The anode current pulse after being integrated with a charge-sensitive pre-amplifier (CSA) was converted to the step-like pulse with the height proportional to the FF kinetic energy released during its deceleration in the TGIC working gas mixture. Since a portion of the FF kinetic energy is absorbed inside the target layer and the target backing, the angle between cathode normal and FF (Θ-angle) was needed for the correction of the measured FF kinetic energy. The GTIC cathode pulse was used as the time reference both for the neutron time-of-flight (TOF) measurement and for the Θ-angle measurement. The correlated anode pulses along with the corresponding cathode pulse and the neutron detector (ND) signal were sampled with four 100 MHz WFD having 12 bit amplitude resolution. The waveforms were analysed to obtain the following information about every fission event: kinetic energy values for both FF, their Θ-angles, prompt fission neutron (PFN) pulse shape and pulse height information along with the corresponding TOF value. These data eventually are converted to FF masses and kinetic energies, to PFN kinetic energy and the Ψ-angle between neutron and the FF.

Experimental setup

The TGIC was mounted inside a stainless steel cylindrical vessel having a diameter of 285 mm and a height of 200 mm. As counting gas a mixture made of 90%Ar+10%CH_4 (P-10) was used in the TGIC at a pressure of 1.05 bar. The continuous regeneration of the counting gas was kept at a constant flow rate of 30-50 ml/min. The cathode was made of stainless steel having the diameter of 178 mm and a thickness of 2 mm. The circular hole in the cathode centre was used to mount the ^{252}Cf target with a source strength of about 500 fissions/s. Anodes were made from an aluminium foil (0.1 mm thickness) glued onto the stainless steel ring with an external diameter of 178 mm, a width of 20 mm and a thickness of 1 mm. Grids were made of stainless steel wires with a diameter of 0.1 mm and a pitch of 2 mm stretched over the stainless steel disks, similar to those used for the anodes. The spot of the ^{252}Cf target of ~10 mm is made by depositing ^{252}Cf nuclei on a nickel foil with a thickness of 100 μg/cm^2 and a diameter of 50 mm. A simplified block diagram of the TGIC and the data acquisition system consisting of four WFD is presented in Fig. 1. Sampling of the detector pulses was performed with 12 bit pulse height resolution and 100 MHz sampling frequency. Sampling was triggered when the common cathode pulse passes the selection criteria of the CFD. Four simultaneously sampled waveforms were acquired for each fission event in the local random access memory of the PC. Each of the waveforms consisted of L samples taken before and of M samples taken after the triggering. The L and M values were programmatically configured before the data acquisition is started. Union of L+M samples composed the sampled pulse of the corresponding detector output. Sequential unions were combined in blocks containing 10000 fission events that were recorded to the PC hard disk.

Fission fragment analysis

Main data analysis was performed off-line by retrieving waveforms from the hard disk. Each fission event was fully represented by the set of four waveforms A_1, A_2, K and N. The K-waveform was used as a time reference. The FF fragment kinetic energy consumed during the ionization of the working gas of TGIC was proportional to the height of the corresponding A_1-, A_2- waveform. Determination of the height of the step-like pulse performed using the following signal processing described in more detail in ref. [1]. Anode pulse (*V(t)*-continuous form, *V(kΔ)* –

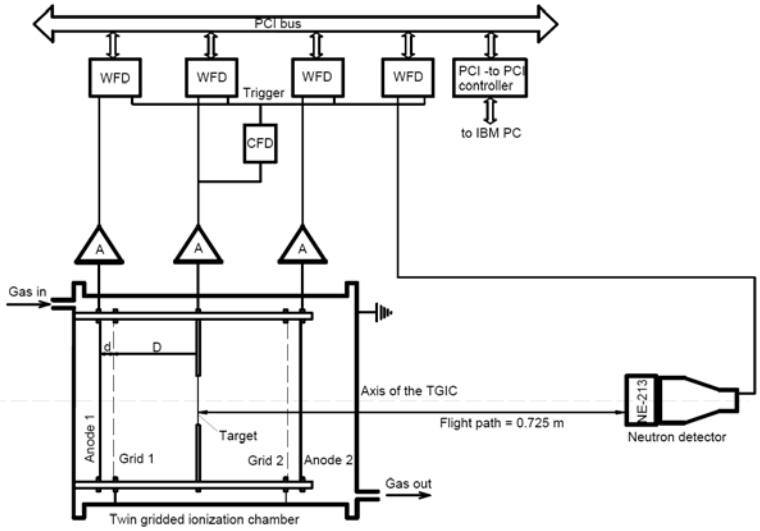

Fig 1. Simplified block diagram of the xperimental setup(D =30 mm, d=6 mm).

sampled form) passed through the following differentiating filter:

$$Q(t) = V(t)W(0) - \int_0^t V(t)\frac{dW(t-\tau)}{d\tau}d\tau \Rightarrow \text{for } W(t) = \exp(-\lambda t)$$
$$Q(k\Delta) = V(k\Delta) - \frac{1}{\lambda}\sum_{i=0}^{k} V(i\Delta)\exp(-\frac{\Delta(k-i)}{\lambda}) \quad (1)$$

The main aims of the differentiating filter were: 1) subtract the non-zero basement from the waveforms; 2) to localise the peak value of the pulse. Then the pulse *Q(kΔ)* was integrated in order to improve the signal-to-noise ratio. In this work the following simple integration formula was implemented:

$$P_i = \sum_{j=Tg}^{Tg+100} Q(k\Delta) \quad (2),$$

where Tg is time reference of fission event and P_i stand for two (i=1,2) anode pulse height values. Determination of the Θ_1- and Θ_2-angles as schematically illustrated in Fig. 2 was done using anode waveforms *V(kΔ)*. Free electrons drifting towards the corresponding anodes with the constant velocity *W* approached the anodes at different time depending on the FF angle. Time *T* between the fission

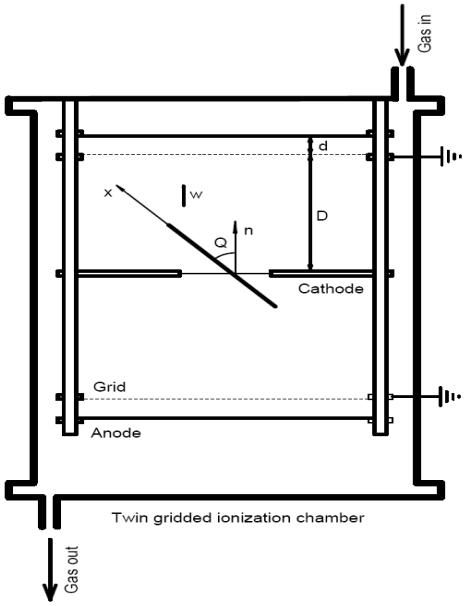

Fig 2. Illustration of the fission-fragment angle determination: free electrons are drifting towards the anode on electrostatic field created between cathode-grid-anode

reference Tg and the time instant, when the anode pulse raised to the half of its full height could be found using the following formula:

$$T_{90} - T = (T_{90} - T_0(\mathrm{E})) * \cos(\Theta) \qquad (3),$$

where $T = \sum_{k=Tg}^{Tg+100} k\Delta I_i[k\Delta] - Tg$, $T_{90} = \frac{D + 0.5 * d}{W}$. *D and d* – are the cathode-grid and grid-anode distances respectively and $I_i(k\Delta)$, $i=1,2$ were the current waveforms obtained from the corresponding waveforms $V_i(k\Delta)$ as was explained in ref. [1] Function $T_0(E)$ can be determined experimentally in calibration measurement by preselecting the FF emitted with angle $\Theta=0$. The measured FF pulse height first was corrected taking into account grid inefficiency factor, characterizing incompleteness of anode shielding by the grid from the current, created by moving charges in the cathode-grid space of the TGIC:

$$P^C = \frac{P^O * T_{90}}{T_{90} + \sigma * T} \qquad (4),$$

where P^C, P^O - are corrected and measured pulse height values respectively and σ-is a grid inefficiency factor as defined in ref. [2]. Two dimensional function $R(P^C, T)$ was constructed using the pairs of P^C, T values are presented in Fig. 3. Considering $R(P^C = const, T)$ as function of argument *T* one got equation (1) with the fixed value of P^C, which provided the possibility to evaluate the values *T*, corresponding to $\cos(\Theta) = 1$. The procedure was repeated for different values of P^C in order to obtain pairs of (P^C,*T*), represented the samples of function $T_0(P^C)$. These samples were fitted with parabola, represented analytically the $T_0(P^C)$ - function. After the described calibration procedure was implemented the equation (1) was used to determine the $\cos(\Theta)$ using the measured value of *T*. For each fission event the two cosine values were determined in each chamber and a distribution function $n(\cos(\Theta_1), \cos(\Theta_2))$ was plotted as shown on the left hand side of Fig. 4. The right side graph of Fig. 4 illustrates the precision of cosine measurement in the range 0.5<cos(Θ)<1.0 obtained as the differences distribution of n(cos(Θ$_1$)-cos(Θ$_2$)). The cosine value used in the data analysis was evaluated as:

$$\cos(\Theta) = 0.5 * (\cos(\Theta_1) + \cos(\Theta_2) \qquad (5)$$

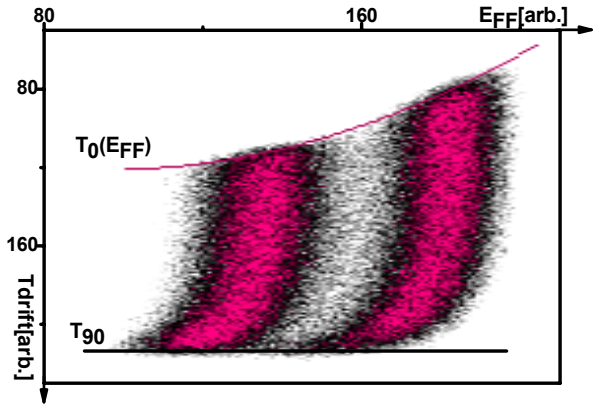

Fig 3. Illustration of the cos(Q) determination

The cosine value used for correction of the FF pulse height due to the energy lose in the target and the backing layers using the procedure developed in refs [3,4]. Final pulse height and mass distribution were plotted in fig. 5.

Prompt fission neutron time-of-flight spectroscopy

The flight path for PFN chosen to be 0.725m and the signals K and N were used for the TOF measurement. The time marks were obtained using constant fraction time marking algorithm (CFTM), which widely used in commercially available nuclear electronics module – constant fraction discriminator (CFD). This algorithm produced accurate time mark independent on the signal pulse height provided the signal rise time did not depend on the signal pulse height. In programmatic realization of the CFTM method one needed the signal interpolation between sampling points. The Shannon interpolation polynomial is the natural interpolation approach in this case, providing most accurate result.

In practical implementations Shannon interpolation suffered from sampling noise due to the finite resolution of the sampling ADC, therefore, linear, parabola or cubic interpolation schemes are frequently used instead due MORE

sampling noises immunity. To improve the sampling noises influence the waveforms passed through the low pass the finite impulse response (FIR) - 4-th order CR-RC^4 -filter:

$$B_4(t,\tau) = \frac{1}{\tau * 3!}\left(\frac{t}{\tau}\right)^3 * \exp(-\frac{t}{\tau}) \text{ or in the sampled form}$$

$$V[i] = a_0U[i] + b_1U[i-1] + b_2U[i-2] + b_3U[i-3] + b_4U[i-4] + b_5U[i-5]$$

$$x = \exp(-1/\tau),\ a_0 = (1-x)^4 \qquad (6),$$

$$b_1 = 5x,\ b_2 = -10x^2,\ b3 = 10x^3,\ b_4 = -5x^4,\ b_5 = x^5$$

where V[i] is the filter output, U[i] is input waveform and τ is the shaping parameter. It should be noticed that filtering improved significantly the differential nonlinearity of the pulse height measurement, making it even better than one of the analogue signal processing module. The PFN spectroscopy was done using parabola interpolation formula. Below the formulas for different interpolation polynomials are presented:

$f(t_k + \Delta) = f(t_k) + \Delta * (f(t_{k+1}) - f(t_k))$ - linear interpolation

$$f(t_k + \Delta) = a(t_k + \Delta)^2 + b(t_k + \Delta) + c$$

$$a = \frac{f(t_{k+2}) - 2f(t_k) + f(t_k)}{2},$$

- parabola

$$b = f(t_{k+1}) - f(t_k) - a(2k+1),$$

$$c = f(t_k) - bk - ak^2.$$

$$f(t_k + \Delta) = a(t_k + \Delta)^3 + b(t_k + \Delta)^2 + c(t_k + \Delta) + d$$

$$a = \frac{f(t_{k+2}) - 3f(t_{k+1}) + 3f(t_k) - f(t_{k-1})}{(k+2)^3 - 3(k+1)^3 + 3k^3 + (k-1)^3},$$

$$b = \frac{f(t_{k+2}) - 2f(t_{k+1}) + f(t_k) - a((k+1)^3 - 2(k+1)^3 + k^3)}{2},$$ -cubic parabola

$$c = f(t_{k+2}) - f(t_{k+1}) - b(2k+3) - a((k+2)^3 - (k+1)^3),$$

$$d = f(t_{k+2}) - c(k+2) - b(k+2)^2 - a(k+2)^3.$$

Because of high sensitivity of ND to the prompt fission gamma radiation a pulse shape discrimination procedure was implemented to suppress the gamma background. The pulse shape discrimination method utilised a difference between the falling edges of the pulses caused by neutrons and photons. One of the popular analogue method performed the integration of the ND pulse inside two intervals - the narrow window of ~25 nsec width and the wide window of ~250 nsec width refs. [5,6]. The beginning of both windows were adjusted to the beginning of the ND pulse. In the present report we implemented the similar method and the pulse shape separation is illustrated in Fig. 6a where for each pulse two dimensional distribution was plotted in coordinates x and y calculated using the following calculation:

$$x = \int_0^T I(t)dt,\quad y = \int_0^{10*T} I(t)dt,\ \text{where } I(t) \text{ - is interpolated signal} \qquad (7)$$

After the photons were suppressed by pulse shape analysis in the range of pulse heights from 0.05 to 5.0 V the TOF distribution was created and plotted in fig. 6b. The reference shift and the width of the reference distribution broadening are shown in Fig. 7. A similar effect was observed and reported in ref [7].

Conclusions

Digital signal processing (DSP) algorithms for FF and PFN spectroscopy were developed in our work. The algorithms were implemented in the measurement of the ^{252}Cf(SF) reaction using a complete digitization approach with four 12 bit/100 MHz WFD. DSP algorithms were developed as recursive procedures performing signal processing similar to those available in various analogue nuclear electronics modules such as CFD, pulse shape discriminator (PSD), peak-sensitive analogue-to-digital converter (pADC), pulse shaping amplifier (PSA) or timing filter amplifier (TFA). To measure the angle between FF and the cathode plane normal of the TGIC a new algorithm was developed having advantage over the traditional analogue pulse processing schemes. Algorithms were tested by comparing our results of DSP data analysis of the ^{252}Cf(SF) reaction with data available from literature [9] demonstrating the better quality of DSP over traditional analogue signal processing.

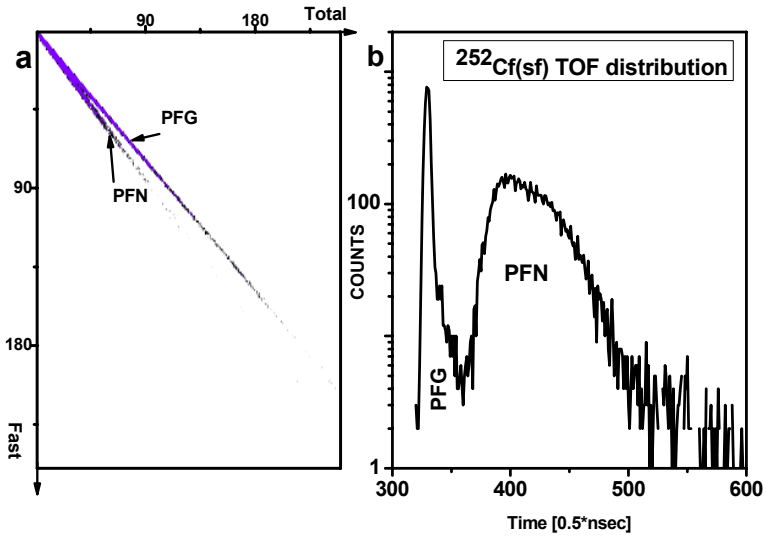

Fig. 4. a) PFN from PFG pulse shape separation principle illustrated in a two dimensional representation of total light output versus fast component light output b)TOF distribution acquired in ^{252}Cf(SF) after pulse shape separation was applied.

References:

[1] O.V. Zeynalova, Sh.S. Zeynalov, F.-J. Hambsch, S. Oberstedt, Bulletin of the Russian Academy of Sciences: Physics, 2009, Vol. 73, No. 4, pp. 506–511. © Allerton Press, Inc., 2009.

[2] O.Bunemann, T.E.Granshaw and J.A.Harvey, Can.Jour.Res. A27 (1949) 19

[3] Budz-Jørgenson C., Knitter H.-H., Streade Ch., Hambsch F.-J., and Vogt R Nucl. Instr. and Meth. A258 (1987) 209.

[4] Sh.S. Zeinalov, M. Florek, W.I. Furman, V.A. Kriatchkov, Yu.S. Zamyatnin, Proc. VII Int. Seminar on Interaction of Neutrons with Nuclei (ISINN-7), Dubna, Russia, May 25-28, 1999, p.258. Nucl. Instr. and Meth. A 274 (1989) 217

[5]. M. Moszynski, G.J. Costa, G. Guillaume, B. Heusch, A. Huck and S. Mouatassim
Nucl. Instr. and Meth. A 350 (1994) 226

[6]. G.F . Knoll, Radiation detection and measurements (Wiley, New York, 2000).

[7]. J. Cub, E. Finckh, K. Gebhardt, K. Geissdorfer, R. Lin, J. Strate and H. Klein

[8]. R. Bottger, H. Klein, A. Chalupka, Strohmaier, Nuclear Science and Engineering 106 (1990) 377.

[9] F.-J. Hambsch, S. Oberstedt, Nucl. Phys. A617 (1997) 347.

5. PUBLICATIONS

CONDENSED MATTER PHYSICS

1. Atomic and magnetic structures (diffraction)

1. Cornei N., Craus M.-L., Lozovan M., Mita C., **Journal of Optoelectronics and Advanced Materials-SYMPOSIA**, Vol. 1, No. 2, 2009, p. 174 – 177;
2. Craus Mihail-Liviu, Lozovan Mihai, Cornei Nicoleta, Dobrea Viorel, Chiriac Horia, **Sensor Letters**, Volume 7, Number 3, June 2009 , pp. 247-250(4)
3. Craus M. – L., Cornei N., Lozovan M. and Balasoiu M., **Solid State Phenomena** Vol. 152-153 (2009) pp 85-88
4. Craus M.-L., Cornei N., Lozovan M., **Journal of Optoelectronics and Advanced Materials-SYMPOSIA**, Vol. 1, No. 2, 2009, p. 169 – 173.
5. Craus M.-L., Cornei N., Lozovan M., Balasoiu M., **Solid State Phenomena**, Vol.152-153 (2009) 85-88.
6. Golosova N.O., Kozlenko D.P., Dubrovinsky L.S., Drozhzhin O.A., Istomin S.Ya., and Savenko B.N., **Phys. Rev. B**, v. 79, pp. 104431-1-5 (2009).
7. Kichanov S.E., Kozlenko D.P., Wasicki J., Dubrovinsky L.S., Czarnecki P., Nawrocik W., Savenko B.N., Pogoreliy D.K., Podurets K.M., **Journal of Molecular Structure**, v. 921, pp. 68-71 (2009).
8. Kozlenko D.P., Jirak Z., Golosova N.O.and Savenko B.N., **Eur. Phys. J. B**, v. 70. pp. 327-334 (2009).
9. Lashkarev G. V., Sichkovskyi V. I., Radchenko M. V., Aleshkevych P., Kovalyuk Z. D., Dmitriev O. I., Butorin P. E., Yakiela R., Nedelko N., Slawska-Waniewska A., Lytvyn P. M., Balagurov A.M., Beskrovnyy A. I., Szymczak R., Dobrowolski W., **Physica B** (submitted).
10. Luca D., Craus M.L., Cornei N., Fosalau C., Mita C., Lozovan M., „The La0.54Sm0.11Ca0.35MnO3 perovskites doped with Cu for the sensor", **Proc. of SPIE Vol. 7297, Advanced Topics in Optoelectronics, Microelectronics, and Nanotechnologies IV**, 2009, 72972J-1 - 72972J-4;
11. Luca D., Craus M.L., Mita C., Cornei N., Lozovan M., Paicu G., „Magnetic/temperature sensors and their electrical transport properties", Proc. of SPIE Vol. 7297, **Advanced Topics in Optoelectronics, Microelectronics, and Nanotechnologies IV**, 2009, 72972I-1 - 72972I-4;
12. Mirmelstein A., Clementyev E., Kerbel O., Kozlenko D., Akshentsev Yu., Voronin V., Berger I., **Journal of Nuclear Materials**, v. 385, pp. 57-59 (2009).
13. Mita C., Craus M. L., Cornei N., Lozovan M., **Journal of Optoelectronics and Advanced Materials-SYMPOSIA**, Vol. 1, No. 2, 2009, p. 190 – 193;
14. Pomjakushin V.Yu., Sheptyakov D.V., Pomjakushina E.V., Conder K., Balagurov A.M., **Phys. Rev. B**, 2009, accepted.
15. Sheptyakov D.V., Pomjakushin V.Yu., Drozhzhin O.A., Istomin S.Ya., Antipov E.V., Bobrikov I.A., Balagurov A.M., **Phys. Rev. B**, 2009, v.80(2), p. 024409 (1-9).
16. Wasicki J., Kozlenko D.P., Pankov S.E., Bilski P., Pajzderska A., Hancock B.C., Medek A., Nawrocik W., and Savenko B.N., **J. Pharm. Sci.** v. 98, pp. 1426-1437 (2009).
17. Авдеев М.А., Мартынов П.Н., Мельников В.П., Новиков А.Г., Пучков А.В., **ФТТ**, 2009, принято к печати.
18. Лушников С.А., Бобриков И.А., Балагуров А.М., Глазков В.П., Соменков В.А., **Неорг. мат.**, 2009, принято к печати.
19. Сумин В. В., Симкин В. Г., Шеверев С. Г., Леонтьева-Смирнова М.В., Чернов В.М., **ФММ**, 108 (2009) 1-6.
20. Сумин В.В., Шеверев С.Г., Wimpory R., **Физика твердого тела**, 2009, принята к печати.
21. Троянчук И.О. , Бушинский М.В. , Добрянский В.М. , Карпинский Д.В., Сиколенко В., Балагуров А.М., **Письма в ЖЭТФ**, 2009, т. 89(7), с. 375-380.
22. Дмитриев А.И., Каминский В.М., Лашкарев Г.В., Буторин П.Е., Ковалюк З.Д., Иванов В.И., Бескровный А.И., **ФТТ**, 2009, том 51, выпуск 11, 2207.

2. Soft matter (small angle scattering and diffraction)

1. Anitas E. M., Balasoiu M., Bica I., Osipov V. A., Kuklin A. I., **OAM-RC**, 3(6), pp. 621-624, 2009.
2. Anitas E. M., Kolesnikov D. V., Kuklin A. I., Balasoiu M., Osipov V. A., **Сообщения ОИЯИ** E11-2009-154, ОИЯИ, 2009.
3. Balasoiu M., Bica I., Vatzulik B., Kuklin A.I., Almasy L., Kohlbrecher J., РСНЭ-НБИК 2009, **Сборник тезисов докладов участников VII Национальной конференции «Рентгеновское, Синхротронное излучения, Нейтроны и Электроны для исследования наносистем и материалов. Нано-Био-Инфо-Когнитивные технологии» РСНЭ – НБИК 2009**, ИК РАН, РНЦ КИ, Москва, Россия, 2009. p.62,
4. Balasoiu M., Craus M. L., Anitas E.M., Bica I., Plestil J., Kuklin A. I., **Preprint JINR**. E14-2008-194.
5. Balasoiu M., Craus M. L., Plestil J., Haramus V., Erhan R., Anitas E. M., Lozovan M., Kuklin A. I., Bica I., **Preprint** JINR E14-2008-123.

6. Balasoiu M., Craus M.L., Anitas E.M., Bica I., Plestil J., Kuklin A.I.. ,Физика Твердого Тела, ISSN:0367-3294, **Изд:ФТТ им. А.Ф. Иоффе**, 2009 (принята в печать).
7. Balasoiu M., Kuklin A.I., Orelovich O.L., Kovalev Yu.S., Arzumanian G.M., Kurkin T.S., Stolyar S.V., Iskhakov R.S., Raikher Yu.L., **Preprint JINR.** P14-2008-200.
8. Balasoiu M., Stolyar S. V., Iskhakov R.S., Ishchenko L.A., Raikher Y.L., Kuklin A. I., Orelovich O. L., Kovalev Y. S., Kurkin T. S., Arzumanian G.M., **Romanian Journal of Physics**, ISSN:1221-146X, Изд:Publishing House of the Romanian Academy, 2009 (accepted).
9. Balasoiu M., Stolyar S.V., Iskhakov R.S., Ishchenko L. A., Raikher Yu.L., Kuklin A.I., Соловьёв Д.В., Kurkin T.S., Arzumanian G.M., **Сборник тезисов докладов участников VII Национальной конференции «Рентгеновское, Синхротронное излучения, Нейтроны и Электроны для исследования наносистем и материалов. Нано-Био-Инфо-Когнитивные технологии» РСНЭ – НБИК 2009**, ИК РАН, РНЦ КИ, Москва, Россия, 2009. p.61.
10. Raikher Yu. L., Stepanov V.I., Stolyar S.V., Ladygina V.P., Balaev D.A., Ishchenko L.A., Balasoiu M., **Physics of Solid State**, Vol.52, No.2 (2010)277-284
11. Raikher Yu. L., Stepanov V.I., Stolyar S.V., Ladygina V.P., Balaev D.A., Ishchenko L.A., Balasoiu M., **Preprint JINR** P19-2009-112.
12. Rajewska A., **Journal of Physical Chemistry** (submited).
13. Rajewska A., **Physical Rev E.** (submited).
14. Ryabova N.Y., Kiselev M.A., Dante S., Hauss T., Balagurov A.M., **European Biophysics Journal** (accepted).
15. Анитас Ю.М., Черный А.Ю., Балашою М., Осипов В.А., Куклин А.И., **Сборник тезисов докладов участников VII Национальной конференции «Рентгеновское, Синхротронное излучения, Нейтроны и Электроны для исследования наносистем и материалов. Нано-Био-Инфо-Когнитивные технологии» РСНЭ – НБИК 2009**, ИК РАН, РНЦ КИ, Москва, Россия, 2009. стр.464,
16. Горшкова Ю.Е., Горделий В.И., Куклин А.И., **Сборник тезисов докладов участников VII Национальной конференции «Рентгеновское, Синхротронное излучения, Нейтроны и Электроны для исследования наносистем и материалов. Нано-Био-Инфо-Когнитивные технологии» РСНЭ – НБИК 2009**, ИК РАН, РНЦ КИ, Москва, Россия, 2009., стр.69,
17. Дубровин Е.В., Муругова Т.Н., Мотовилов К.А., Ягужинский Л.С., Яминский И.В., **Российские нанотехнологии**, 4, №9-10, 2009, с. 66-68.
18. Иваньков О.И., Исламов А.Х., Куклин А.И., Булавин Л.А., **Сборник тезисов докладов участников VII Национальной конференции «Рентгеновское, Синхротронное излучения, Нейтроны и Электроны для исследования наносистем и материалов. Нано-Био-Инфо-Когнитивные технологии» РСНЭ – НБИК 2009**, ИК РАН, РНЦ КИ, Москва, Россия, 2009. стр. 80.
19. Ковалев Ю. С., Левкович Н. В., Куклин А. И., Апель П. Ю., **Коллоидный журнал**, 2009, том 71, №5,с. 616-622.
20. Киселев М.А., Ермакова Е.В., Рябова Н.Ю. и др., **Кристаллография** (в печати).
21. Киселев М.А., Ермакова Е.В., Филиппова С.Н., Сургучева Н.А., Данте С., Хаус Т., Гальченко В.Ф., **Биофизика**, 2009, т.54, в.4, с.668-674
22. Куклин А.И., Рогачев А.В., Черный А.Ю., Муругова Т.Н., Докукин Е.Б., Исламов А.Х., Иваньков О.И., Ковалев Ю.С., Соловьев Д.В., Утробин П.К., Соловьев А.Г., Горделий В.И.. **Сообщения ОИЯИ** Р14-2009-128.
23. Куклин А.И., Рогачев А.В., Черный А.Ю., Муругова Т.Н., Докукин Е.Б., Исламов А.Х., Иваньков О.И., Ковалев Ю.С., Соловьев Д.В., Утробин П.К.,.Соловьев А.Г, Горделий В.И., **Сборник тезисов докладов участников VII Национальной конференции «Рентгеновское, Синхротронное излучения, Нейтроны и Электроны для исследования наносистем и материалов. Нано-Био-Инфо-Когнитивные технологии» РСНЭ – НБИК 2009**, ИК РАН, РНЦ КИ, Москва, Россия, 2009. стр. 344.
24. Муругова Т.Н., Горделий В.И., Куклин А.И., Иваньков О.И., Солодовникова И.М., Юрков В.И., Ягужинский Л.С., **Труды XIII научной конференции молодых ученых и специалистов ОИЯИ**, 2009, с. 23-26
25. Муругова Т.Н., Кривандин А.В., Куклин А.И., Муранов К.О., Аксенов В.Л., Островский М.А., **Сборник тезисов докладов участников VII Национальной конференции «Рентгеновское, Синхротронное излучения, Нейтроны и Электроны для исследования наносистем и материалов. Нано-Био-Инфо-Когнитивные технологии» РСНЭ – НБИК 2009**, ИК РАН, РНЦ КИ, Москва, Россия, 2009. стр. 87.
26. Рогачев А. В., Куклин А. И., Черный А. Ю., Озерин А. Н., Музафаров А. М., Татаринова Е. А., Горделий В. И., **Физика Твердого Тела**, ISSN:0367-3294, Изд:ФТТ им. А.Ф. Иоффе, 2009 (принята в печать)
27. Рогачев А.В., Куклин А.И., Черный А.Ю., Озерин А.Н., Музафаров А.М., Татаринова Е.А., Горделий В.И., **Препринт ОИЯИ**, Р14-2008-192. 2008.
28. Рогачев А.В., Озерин А.Н., Черный А.Ю., Музафаров А.М., Татаринова Е.А., Исламов А.Х., Горделий В.И., Куклин А.И., **Сборник тезисов докладов участников VII Национальной конференции «Рентгеновское, Синхротронное излучения, Нейтроны и Электроны для исследования наносистем и материалов.**

Нано-Био-Инфо-Когнитивные технологии» РСНЭ – НБИК 2009, ИК РАН, РНЦ КИ, Москва, Россия, 2009. стр. 233.

29. Соловьев Д.В., Куклин А.И., Исламов А.Х., Утробин П.К., Иваньков О.И., Булавин Л.А.,.Горделий В.И., **Сборник тезисов докладов участников VII Национальной конференции «Рентгеновское, Синхротронное излучения, Нейтроны и Электроны для исследования наносистем и материалов. Нано-Био-Инфо-Когнитивные технологии» РСНЭ – НБИК 2009**, ИК РАН, РНЦ КИ, Москва, Россия, 2009. стр. 102,
30. Рябова Н.Ю., Киселев М.А., Dante S., Hauß T., Балагуров А.М., **Труды XIII-ой научной конференции молодых ученых и специалистов ОИЯИ** – тезисы докладов (г. Дубна, 2009 г.), с. 27-30.
31. Рябова Н.Ю., Киселев М.А., Балагуров А.М., **Кристаллография (**принята к печати)
32. Рябова Н.Ю., Киселев М.А., Балагуров А.М., **Биофизика** 54 № 5, с. 852-862.
33. Рябова Н.Ю., Киселев М.А., Бескровный А.И., Балагуров А.М., **Физика твердого тела** (принята к печати).
34. Филиппова С.Н., Киселев М.А., Ермакова Е.В., Сургучева Н.А., Забелин А.В., **Бюллетень Московского общества испытателей природы, отдел биологический** т. 114, вып. 2, прил. 1, Физиология и генетика микроорганизмов в природных и экспериментальных системах, М: МАКС Пресс, 2009. стр. 274-277.

3. Nanostructured materials (small-angle scattering)

1. Avdeev M.V., Bica D., Vekas L., Aksenov V.L., Feoktystov A.V., Marinica O., Rosta L., Garamus V.M., Willumeit R., **J. Colloid Interface Sci.** 334 (2009) 37–41.
2. Avdeev M.V., Bica D., Vekas L., Aksenov V.L., Feoktystov A.V., Rosta L., Garamus V.M., Willumeit R., **Solid State Phenomena**. 152-153 (2009) 182–185.
3. Avdeev M.V., Dubois E., Mériguet G., Wandersman E., Garamus V.M., Feoktystov A.V., Perzynski R., **J. Appl. Cryst.** 42 (2009) 1009-1019.
4. Avdeev M.V., Rozhkova N.N., Aksenov V.L., Garamus V.M., Willumeit R., Osawa E., **J. Phys. Chem.** C 113 (2009) 9473–9479.
5. Балашою М., Аксенов В.Л., Куклин А.И., Никитенко Ю.В., Дугинов В.Н., Мамедов Т.Н., Грабчев Б., Бика Д., Векаш Л., **Сборник тезисов докладов участников VII Национальной конференции «Рентгеновское, Синхротронное излучения, Нейтроны и Электроны для исследования наносистем и материалов. Нано-Био-Инфо-Когнитивные технологии» РСНЭ – НБИК 2009**, ИК РАН, РНЦ КИ, Москва, Россия, 2009. стр. 70.
6. Bodnarchuck V., Cser L. , Ignatovich V., Veres T. , Yaradaykin S. , Investigation of periodic multilayers, JINR Comm. E14-2009-127. JINR: 2009.
7. Feoktystov A.V., Avdeev M.V., Aksenov V.L., Petrenko V.I., Bulavin L.A., Bica D., Vekas L., Garamus V.M., Willumeit R.., **Solid State Phenomena** 152-153 (2009) 186–189.
8. Feoktystov A.V., Bulavin L.A., Avdeev M.V., Garamus V.M., Kopcansky P., Timko M., Koneracka M., Zavisova V., **Ukr. J. Phys.** 54(4) (2009) 348–354.
9. Feoktystov A.V., Bulavin L.A., Avdeev M.V., Vekas L., Garamus V.M., Willumeit R., **Ukr. J. Phys.** 54(3) (2009) 266–273.
10. Kyzyma O.A., Korobov M.V., Avdeev M.V., Garamus V.M., Petrenko V.I., Aksenov V.L., Bulavin L.A.. **Fullerenes, Nanotubes and Carbon Nanostructures**, accepted (2009).
11. Petrenko V.I., Avdeev M.V., Aksenov V.L., Bulavin L.A., Rosta L., **Solid State Phenomena** 152-153 (2009) 198–201.
12. Petrenko V.I., Avdeev M.V., Almásy L., Bulavin L.A., Aksenov V.L., Rosta L., Garamus V.M., **J. Col. Surf. A** 337 (2009) 91–95.
13. Vekas L., Avdeev M.V., Bica D., **Nanoscience and Its Applications in Biomedicine**, Ed. Donglu Shi, Springer Verlag, 2009, Chapter 25, pp. 645-704
14. Авдеев М.В., Боднарчук И.А., Петренко В.И., Холмуродов Х.Т., Ярадайкин С.П.. **Журнал Физической Химии** 83(7) (2009) 1275–1280. (Avdeev M.V., Bodnarchuk I.A., Petrenko V.I., Kholmurodov Kh.T., Yaradaikin S.P.. The determination of the limiting partial molar volume of solutions of monocarboxylic acids in benzene by molecular dynamics simulation. Russian Journal of Physical Chemistry A 83 (7) (2009) 1129–1133)
15. Аксенов В.Л., Тропин Т.В., Кизима Е.А., Авдеев М.В., Коробов М.В., Рошта Л., **Физика твердого тела**, (в печати, 2009). (Aksenov V.L., Tropin T.V., Kyzyma O.A., Avdeev M.V., Korobov M.V., Rosta L., On fullerene cluster formation in nitrogen-containing solvents, Physics of the Solid State, in press (2009).)
16. Нагорный А.В., Петренко В.И., Авдеев М.В., Булавин Л.А., Аксенов В.Л., **Поверхность. Рентгеновские, синхротронные и нейтронные исследования** (принято к публикации, 2009),. (Nagorny A.V., Petrenko V.I., Avdeev M.V., Bulavin L.A., Aksenov V.L., Journal of Surface Investigation. X-ray, Synchrotron and Neutron Techniques, accepted (2009))
17. Петренко В.И., Авдеев М.В., Аксенов В.Л., Булавин Л.А., Рошта Л., **Поверхность. Рентгеновские, синхротронные и нейтронные исследования** 2 (2009) 92–96. (Petrenko V.I., Avdeev M.V., Aksenov V.L.,

Bulavin L.A., Rosta L., Magnetic fluids with excess of a surfactant according to the data of small-angle neutron scattering, Journal of Surface Investigation. X-ray, Synchrotron and Neutron Techniques 3(1) (2009) 161–164)

18. Петренко В.И., Аксенов В.Л., Авдеев М.В., Булавин Л.А., Rosta L., Vekas L., Garamus V.M., Willumeit R.. **Физика Твердого Тела** (в печати, 2009). (Petrenko V.I., Aksenov V.L., Avdeev M.V., Bulavin L.A., Rosta L., Vekas L., Garamus V.M., Willumeit R.. Structure analysis of water-based ferrofluids by means of small-angle neutron scattering. Physics of the Solid State, in press (2009))
19. Феоктистов А.В., Авдеев М.В., Аксенов В.Л., Булавин Л.А., Бика Д., Векаш Л., Гарамус В.М., **Поверхность. Рентген., синхротрон. и нейтрон. исслед.** 1 (2009) 3–6. (Feoktystov A. V., Avdeev M. V., Aksenov V. L., Bulavin L. A., Bica D., Vekas L., Garamus V. M., Willumeit R., Small-angle neutron scattering contrast variation on magnetite-myristic acid-benzene magnetic fluid, Journal of Surface Investigation. X-ray, Synchrotron and Neutron Techniques 3(1) (2009) 1-4)

4. Thin films (reflectometry, polarized neutrons)

1. Aksenov V.L., Khaidukov Yu.N., Nikitenko Yu.V., **Journal of Physics: Conference Series** (submitted)
2. Aksenov V.L., Nikitenko Yu.V., Khaidukov Yu.N., Vdovichev S.N., Borisov M.M., Morkovin A.N., Mukhamedzhanov E.Kh., **Journal of Surface Investigation**, Vol. 3, p. 495-499 (2009)
3. Ignatovich V.K., Nikitenko Yu.V., Radu F., **NIM A**, v. 604, № 3 (2009) 653-661.
4. Ignatovich V.K., Nikitenko Yu.V., **ЖЭТФ**, т. 137, вып. 3 (2010).
5. Kozhevnikov V. F., Giuraniuc C. V., Van Bael M. J., Temst K., Van Haesendonck C., Mishonov T.M., Charlton T., Dalgliesh R.M., Khaidukov Yu.N., Nikitenko Yu.V., Aksenov V.L., Gladilin V.N., Fomin V.M., Devreese J.T., Indekeu J.O, **Physical Review B**, v. 78, 012502(1-4), 2009.
6. Nikitenko Yu.V., **Physics of Particles and Nuclei**, v.40, № 6 (2009) 890-947.
7. Игнатович В.К., Никитенко Ю.В., Фраерман А.А., **ЖЭТФ**, т. 138, вып. 1 (2010).

5. Atomic and magnetic dynamics (inelastic neutron scattering)

1. Hetmańczyk J., Migdał-Mikuli A., Mikuli E., Hołderna-Natkaniec K., Hetmaczyk Ł., Natkaniec I., **Journal of Molecular Structure**, 923 (2009) 103–109.
2. Migdał-Mikuli A., Mikuli E., Hetmańczyk J., Hetmańczyk Ł., Hołderna-Natkaniec K., Natkaniec I., **Journal of Alloys and Compounds**, 469 (2009) 73–81.
3. Smirnov L. S., Natkaniec I., Johnson M.R., Ivanov A.S., Troyanov S.I., **Crystallography Reports**, 2009, Vol. 54, No 3, pp. 477–482. (Original Russian Text published in Kristallografiya, 2009, Vol. 54, No. 3, pp. 510–516).
4. Smirnov L.S., Kolesnikov A.I., Flerov I.N., Laptash N.M., **Physics of the Solid State**, 51 (2009) 2362-2366. (Original Russian Text published in Физика Твердого Тела, 51 (2009) 2224-2228.)
5. Smirnov L.S., Natkaniec I., Belushkin A.B., Smith D., Prager M., **Journal of Surface Investigation. X-ray, Synchrotron and Neutron Techniques**, 3 (2009) 847-856. (Original Russian Text published in Поверхность, рентгеновские, синхротронные и нейтронные исследования, 2009, № 11, 3-13).
6. Puchkov A., Kalinin I., Kats E., Koza M., Tonon X., Lauter H., Lauter V., **ILL Annual Report 2008**, Grenoble, 2009, pp.58-59.
7. Агранович В.М., Дубовский О.А., **Физика твёрдого тела** 2009. Т.51. вып.8. с.1541-1546.
8. Благовещенский Н.М., Морозов В.А., Морозов В.М., Новиков А.Г., Пашнев М.А., Савостин В.В., Савостин Д.В., **Труды регионального конкурса научных проектов в области естественных наук.** Вып. 14. Калуга: Издательство АНО «Калужский научный центр», 2008, с. 470 – 477.
9. Благовещенский Н.М., Новиков А.Г., В.В.Савостин, **ФТТ**, 2009, принято к печати.
10. Благовещенский Н.М., Новиков А.Г., Осава Е., Рожкова Н.Н., **ФТТ**, 2009, принято к печати.
11. Благовещенский Н.М., Новиков А.Г., Савостин В.В., Шимкевич А.Л., **Теплофизические свойства веществ и материалов. Труды XII Российской конференции по теплофизическим свойствам веществ** 7-10 октября 2008г., Москва. М.: Интерконтакт Наука, 2009, с.143 – 150.
12. Дубовский О.А., Орлов А.В., Семенов В.А., **Труды регионального конкурса научных проектов в области естественных наук,** Издательство АНО "Калужский научный центр", Вып.14, 2009, с.110-120.
13. Дубовский О.А., Орлов А.В., **Препринт ФЭИ**-3159, 2009, 31 стр.
14. Дубовский О.А., Орлов А.В., **ФТТ**, 2009 (принято к печати).
15. Калинин И.В., Кац Е., Коза М., Лаутер В.В., Лаутер Х., Пучков А.В., **Сборник тезисов докладов на XXXV совещании по физике низких температур (НТ-35)**, Черноголовка, 29 сентября-2 октября 2009, стр.16-17.
16. Калинин И.В., Кац Е., Коза М., Лаутер В.В., Лаутер Х., Пучков А.В., **ЖЭТФ**, 2009 (направлено в печать).
17. Калинин И.В., Лаутер В.В., Пучков А.В., **Труды регионального конкурса научных проектов в области естественных наук**, Издательство АНО "Калужский научный центр", Вып.14, 2009, с.103-109.
18. Лисичкин Ю.В., Новиков А.Г., Сахарова Л.А., журнал **Известия ВУЗов**, серия «Ядерная энергетика», 2009 (принято к печати)
19. Лисичкин Ю.В., Новиков А.Г., Сахарова Л.А., **Препринт ФЭИ**-3148, Обнинск, 2009, 36с.

20. Семенов В.А., Козлов Ж.А., Крачун Л., Матееску Г., Морозов В.М., Опреа А.И., Опреа К., Пучков А.В., **ФТТ**, 2009 (принято к печати).

6. Applied studies (texture, stresses, geological materials)

1. Frischbutter, A., Walther, K. & Scheffzuek, Ch., Abstract for the **Deutsche Tagung fuer Forschung mit Synchrotronstrahlung, Neutronen und Ionenstrahlen an Großgeraeten, SNI 2010**, Berlin (Germany), February 24-26, 2010.
2. Kern H., Mengel K., Strauss K.W., Ivankina T.I., Nikitin A.N., Kukkonen I.T., **Physics of the Earth and Planetary Interiors**, 2009, vol.175, 151-166.
3. Lokajicek T., Lukas P., Nikitin A.N., Papushkin I.V., Sumin V.V., Vasin R.N., **Carbon**, 20100 (submitted).
4. Lychagina, T.A., Nikolayev, D.I. & Wagner, F., **doi:10.1155/TSM, Article ID 237485**.
5. Matthies S. and Wenk H.-R., **J. Appl. Cryst.** 2009. 42, 564-571
6. Matthies S., **Solid State Phenomena. Trans. Tech. Publications**, Switzerland, 2009 (submitted).
7. Mosch, S., Nikolayev, D., Ewiak, O. & Siegesmund, S., **Optimierte Gewinnung. Naturstein** 5, 102-103, 2009.
8. Mosch, S., Nikolayev, D., Ewiak, O. & Siegesmund, S., **Steinbruch und Sandgrube**. 5, 8-11, 2009
9. Mosch, S., Nikolayev, D., Siegesmund, S. & Ewiak, O., **Bulletin of Engineering Geology and the Environment**, 2009 (submitted)
10. Nikitin A.N., Vasin R.N., **Neutron News**. 2009 (accepted).
11. Scheffzuek, Ch., Hempel, H., Frischbutter, A. & Walther. K., Abstract at for **Deutsche Tagung fuer Forschung mit Synchrotronstrahlung, Neutronen und Ionenstrahlen an Großgeraeten, SNI 2010**, Berlin (Germany), February 24-26, 2010.
12. Walther, K., Scheffzuek, Ch. & Frischbutter, A., Abstract for the **Deutsche Tagung fuer Forschung mit Synchrotronstrahlung, Neutronen und Ionenstrahlen an Großgeraeten, SNI 2010**, Berlin (Germany), February 24-26, 2010.
13. Mosch, S. Nikolayev, O. Ewiak & S. Siegesmund, **Optimierte, Gewinnung. Naturstein** 05/09,102-103
14. Mosch, S., Nikolayev, D., O. Ewiak & S. Siegesmund, **Steinbruch und Sandgrube**, 5, 8-11, 2009.
15. Mosch, S.Nikolayev, D., Siegesmund, S. & O. Ewiak., **Bulletin of Engineering Geology and the Environment** (submitted)
16. Базалеев Н.И., Бандурян Б.Б., Иванкина Т.И., Клепиков В.Ф., Литвиненко В.В., Лонин Ю.Ф., Никитин А.Н., **Письма в ЭЧАЯ**, 2009, т.6, № 5(154), с.684-693.
17. Никитин А.Н., Васин Р.Н., Круглов А.А., **Физика Земли**. 2009 (сдано в печать).
18. Никитин А.Н., Васин Р.Н., Родкин М.В., **Физика Земли**, 2009, № 4, с.67-75.
19. Никитин А.Н., Иванкина Т.И., Игнатович В.К., **Физика Земли**, 2009, № 5, с.57-69.
20. Никитин А.Н., Почепцова О.А., Маттис З., **Кристаллография**, 2009 (принята в печать).
21. Родкин М.В., Никитин А.Н., Васин Р.Н. **Сейсмотектонические эффекты твердотельных превращений в геоматериалах.** М.: Геос, 2009, 220 с. (монография)
22. Сумин В.В., Васин Р.Н., Папушкин И.В., Балагуров А.М., Ведерников П.А., Свириденко Ю.В., Шнайдер Р., Вимпори Р., **Атомная энергия**. 2009 (сдано в печать).

7. Instruments and Methods

1. Avdeev M.V. , Bodnarchuk V.I. , Lauter-Pasyuk V.V. , Lauter H., Rubtsov A.B. , Aksenov V.L. , Yaradaikin S.P. , Ul'yanov V.A. , Trounov V.A. , Kalinin S.I. , **Journal of Physics: Conference Series**, 2009 (accepted).
2. Manoshin, S.A., Belushkin, A.V., Kulikov, S.A., Shabalin, E.P., Walther, K., Scheffzuek, C. & Zhuravlev, V.V. **Nuclear Instruments and Methods in Physics** *A:* **608** (3), 447-453.
3. Кожевников С.В. , Отт Ф., **Физика Твёрдого Тела** 2010 (в печати).
4. Кутузов С.А., Богдзель А.А., Балагуров Д.А., Миронова Г.М., **Сообщение ОИЯИ**, Р13-2009-140, Дубна, 2009.
5. Миронова Г.М., Кутузов С.А., Богдзель А.А., Балагуров Д.А., **Тезисы VII Национальная конференция «Рентгеновское, Синхротронное излучения, Нейтроны и Электроны для исследования наносистем и материалов. Нано-Био-Инфо-Когнитивные технологии (РСНЭ-НБИК 2009)** Москва, ИК РАН - РНЦ КИ, 16-21 ноября, 2009, с.596.
6. Калинин И.В., Куликов С.А., Морозов В.М., Новиков А.Г., Пучков А.В., Черников А.Н., Шабалин Е.П.. **Письма в ЭЧАЯ**, 2009 (в печати).
7. Лохматов В.И., Новиков А.Г., Пучков А.В., Сиротин А.П., **ФТТ,** 2009 (принято к печати).
8. Куклин А.И., Исламов А.Х., Ковалев Ю.С., Утробин П.К. , Кутузов С.А., Иваньков О.И., Муругова Т.Н., Рогачев А.В., Горделий В.И., **Сообщения ОИЯИ**, Р13-2009-68.
9. Куклин А.И., Исламов А.Х., Рогов А.Д., Горшкова Ю.Е., Утробин П.К., Ковалев Ю.С., Рогачев А.В., Иваньков О.И., Кутузов С.А., Соловьев Д.В. и Горделий В.И. **Сообщение ОИЯИ** Р3-2009-114. Дубна, 2009.

10. Куклин А.И., Муругова Т.Н., Горшкова Ю.Е., Балашою М., Исламов А.Х., Ковалев Ю.С., Кутузов С.А., Рогачев А.В., Утробин П.К., Иваньков О.И., Горделий В.И., **Сборник тезисов докладов участников Второго Международного форума по нанотехнологиям**, 2009 стр. 239-241.
11. Khaidukov Yu.N., Nikitenko Yu.V., **NIM A**, 2009 (submitted).
12. Kozhevnikov S.V., Ott F., **Solid States Physics** (2010) (in press).
13. Kozhevnikov S.V., Ott F., Paul A., Rosta L., **European Journal of Physics Special Topics** 168 (2009) 87-92.
14. Трунов В.А., Балагуров А.М., Бескровный А.И., Голосовский И.В., Зобкало И.А., Курбаков А.И., Рыбаков В.Б., Смирнов О.П., Соколов А.Е., Ульянов В.А., Черненков Ю.П.,Чернышев В.В., **Тезисы VII Национальная конференция «Рентгеновское, Синхротронное излучения, Нейтроны и Электроны для исследования наносистем и материалов. Нано-Био-Инфо-Когнитивные технологии (РСНЭ-НБИК 2009)** Москва, ИК РАН - РНЦ КИ, 16-21 ноября, 2009, с. 432.

Patents

1. В.Л. Аксёнов, Ю.В. Никитенко, патент на изобретение “Способ определения пространственного распределения магнитного момента в нанослое, № 2360234 от 27.06.09.

Reports at Schools and Conferences

1. Aksenov V.L., Peculiarities of magnetic states in Ferromagnet/Superconductor" heterostructures due to proximity effects, Polarized Neutrons and Synchrotron X-rays for Magnetism, 2-5 August 2009, Bonn, Germany.
2. Avdeev M.V., Neutron scattering in diagnostics of carbon nanostructures, 9th Biennial International Workshop Fullerenes and Atomic Clusters, IWFAC’09. School for young scientists, 6-10 July, St.-Petersburg, Russia
3. Avdeev M.V., New developments in applications of SANS contrast variation for structure research of magnetic fluids, SAS-09. 13-18 Sept. Oxford, United Kingdom
4. Avdeev M.V., On structural features of fullerene C60 dissolved in carbon disulfide: complementary study by small-angle neutron scattering and molecular dynamic simulations, 9th Biennial International Workshop Fullerenes and Atomic Clusters, IWFAC’09. 6-10 July, St.-Petersburg, Russia
5. Avdeev M.V., Small-angle neutron scattering analysis of a water-based magnetic fluid with charged stabilization: contrast variation and scattering of polarized neutrons, SAS-09. 13-18 Sept. Oxford, United Kingdom
6. Avdeev M.V., Small-angle neutron scattering study of the structure of water-based ferrofluids for brain cancer treatment, SAS-09. 13-18 Sept. Oxford, United Kingdom.
7. Avdeev M.V., Structure analysis of water-based ferrofluids for brain cancer treatment, Workshop «Smart Fluids and Complex Flows» 5-6 June 2009, Timisoara, Romania.
8. Balagurov A.M. “Advanced neutron diffraction at pulsed sources: new ideas, new technique, new science” Seminar LNS (PSI), 10.11.2009.
9. Balagurov A.M. Present day high-intensity and high-resolution neutron diffraction and neutron scattering under high pressure, International School of Crystallography, 41st Course: High-Pressure Crystallography, Erice, Italy, 4 – 14 June 2009, v.1, pp.31 – 41.
10. Blagoveshchenskii N.M., Novikov A.G., Rozhkova N.N., Osava T., Diffusion ccharacteristics of water in the vicinity of single – nano buckydiamond as revealed by quasielastic neutron scattering, report on Int.conf. “Fullerenes and Clusters, IWAC’2009” (С. Петербург, 6 – 10 июля 2009 г.)
11. Blagoveshchenskii N.M., Novikov A.G., Investigation of liquid lithium relaxation time by means of the memory function formalism, Report on the 9-th International Conference on QENS, PSI, Switzerland, 9 -13 Feb. 2009.
12. Bodnarchuk V.I., Project of the new multifunctional reflectometer GRAINS with horizontal sample plane at the IBR-2M pulsed reactor in Dubna, International Conference on Neutron Scattering ICNS-2009, May 3 - 7, 2009, Knoxville, USA
13. Bodnarchuk V.I., Project of the new multifunctional reflectometer GRAINS with horizontal sample plane at the IBR-2M pulsed reactor in Dubna, Modelling and data analysis for grazing incidence and off-specular scattering OffSpec2009, 27-29 September, 2009, Muenchen-Feldafing, Germany, poster.
14. Bodnarchuk V.I., Small-angle neutron scattering study of the structure of water-based ferrofluids for brain cancer treatment, International Conference on Neutron Scattering ICNS-2009, May 3 - 7, 2009, Knoxville, USA
15. Ivankina T.I., Kern H., Nikitin A.N., Lokajicek T., The effect of crystallographic and shape preferred orientation on the bulk elastic anisotropy of a foliated biotite gneiss at high pressures, Десятая международная конференция "Физико-химические и петрофизические исследования в науках о Земле" памяти проф. Ю.С. Геншафта. 26 - 29 октября 2009 года. Москва. ГЕОХИ РАН, ИГЕМ РАН, ИФЗ РАН, ГО «Борок» ИФЗ РАН.
16. Kern H., Ivankina T.I., Nikitin A.N., Lokajicek T., The contribution of crystallographic and shape preferred orientation to the bulk elastic anisotropy of a foliated biotite gneiss, Abstracts of the 3rd International Conference on Texture and Anisotropy of Polycrystals (ITAP-3), 23-25 September 2009, Göttingen, Germany.
17. Kozlenko D.P., High pressure induced spin liquid phase and spin fluctuations in multiferroics RMnO3 (R=Y, Lu), International Conference on Magnetism, 26-31 July 2009, Karlsruhe, Germany

18. Kozlenko D.P., Physical phenomena in strongly correlated magnetic oxides: lessons from neutron diffraction at High pressures, International School of Crystallography, 41th Corse: High Pressure Crystallography, 4-14 June 2009, Erice, Italy
19. Kozlenko D.P., "Spin fluctuations and structural modifications in frustrated multiferroics RMnO3 (R = Y, Lu) at high pressure", International Workshop on Advanced Crystallography at High Pressurem 19-22 July 2009, Harbin, China
20. Panitkova I.V., Kozlenko D.P., Lukin E.V., Tucker M.G., Park J.-G., Savenko B.N. "High pressure effects on the crystal structure of multiferroic YMnO3 in the vicinity of para-ferroelectric phase transition", 14th International Seminar on Neutron Scattering Investigations in Condensed Matter
21. Kozhevnikov S.V. Modelling and Data Analysis for Grazing Incidence and Off-Specular Scattering, 27-29 September 2009, Feldafing (Germany). Data representation in off-specular neutron scattering
22. Kyzyma O.A., Cluster formation and solvatochromism in fullerene C60 solutions based on nitrogen-containing solvents, 9th Biennial International Workshop Fullerenes and Atomic Clusters, IWFAC'09. 6-10 July, St.-Petersburg, Russia
23. Kyzyma O.A., Small-angle neutron scattering studies of the influence of solvent polarity on cluster reorganization in C60/N-methyl-2-pyrrolidone solutions, XIV International Conference on Small-angle scattering, SAS-09. 13-18 Sept. Oxford, United Kingdom
24. Matthies S. On the combination of self-consistent and geometric mean elements for the calculation of the elastic properties of textured multi-phase samples. Abstracts of the 3rd International Conference on Texture and Anisotropy of Polycrystals (ITAP-3), 23-25 September 2009, Göttingen, Germany.
25. Natkaniec I., Hołderna-Natkaniec K., "INS and DFT investigations of low frequency dynamics of hexanol isomers".9th International Conference on Quasielastic Neutron Scattering, QENS2009, 10-13 February, 2009, PSI, Switzerland
26. Natkaniec I., Hołderna-Natkaniec K., "INS and DFT investigations of low frequency dynamics of hexane and hexanol molecules in solid state". 14th International Seminar on Neutron Scattering Investigations in Condensed Matter, UAM, Poznań, 14 -16 May 2009.
27. Natkaniec I., Hołderna-Natkaniec K., "Neutron Spectroscopy and ab-initio Modeling Dynamics of Hexanol Isomers". VI Ogólnopolska Konferencja Rozpraszania Neutronów i Metod Komplementarnych w Badaniach Fazy Skondensowanej, DPT Reymontówka, k. Siedlec, 14-18 June, 2009.
28. Petrenko V.I., Nematic-isotropic phase transition in the solutions of saturated mono-carboxylic acids in non-polar solvents studied by SANS. XIV International Conference on Small-angle scattering, SAS-09. 13-18 Sept. Oxford, United Kingdom
29. Rajewska A., Aggregation in water micellar dilutes solutions of three nonionic classic surfactants: C10E7 and C12E7 and C14E7 study by SANS method, International Conference on Neutron & X-ray Scattering, Kuala Lumpur (Malaysia), 29 June – 1 July, 2009.
30. Rajewska A., SANS study of gemini nonionic surfactant in mixed micellar solutions, XIV International Conference on Small – Angle Scattering, Oxford (UK) 13-18 September 2009.
31. Rajewska A., Aggregation of mixed surfactant system by SANS method study of aggregation in mixed micellar solutions of nonionic. 2nd FRM II User Meeting, Garching (Germany), 24 May 2009
32. S.E. Kichanov, D.P. Kozlenko, V.I. Voronin, B.N. Savenko, V.P. Glazkov, Pressure Induced Кичанов С.Е. Chenges in magnetic structure of manganite La0.75Ca0.25MnO3, European School on Magnetism 2009, September 1-10th 2009, Timisoara, Romania
33. Scheffzuek, Ch., Walther, K. & Frischbutter, A. (2009), Texture and residual as well as applied strain evaluation on dolomite-anhydrite rock samples by in situ neutron time-of-flight diffraction, Abstract at the 3rd Int. Conf. on Texture and Anisotropy of Polycrystals (ITAP 3), Goettingen (Germany), September 23-25, 2009, p. 69.
34. Smirnov L.S., Natkaniec I., Ollivier J., Prager M., The QENS study of ammonium ion dynamics in Me1-x(NH4)xY (Me=K, Rb; Y=Cl, Br, I, SCN) mixed crystals, International Conference on Neutron Scattering, ICNS2009, Knoxville, May 3-7, 2009.
35. Taran Yu.V., TOF ND stress analysis of fatigue degradation and martensitic transformation of austenitic steel AISI 321 under uni- and biaxial cycling loading, The ISIS seminar of 23 June 2009, Rutherford Appleton Laboratory, Didcot, UK
36. Tropin T.V., Application of the nucleation theory for describing kinetics of cluster formation and growth in solutions of fullerene C60, VIII Research Workshop «Nucleation Theory and Applications», 1-30 April 2009, BLTP, JINR, Dubna, Russia
37. Tropin T.V., Application of the nucleation theory for describing kinetics of cluster formation and growth in solutions of fullerene C60, International Bogolyubov Conference "Problems of theoretical and mathematical physics", 21-27 August, 2009, Moscow-Dubna, Russia
38. Tropin T.V., Kinetics of fullerene cluster growth in nitrogen-containing solvents, 9th Biennial International Workshop Fullerenes and Atomic Clusters, IWFAC'09. 6-10 July, St.-Petersburg, Russia

39. Vasin R.N., Crystallographic preferred orientation and properties of quartz: a neutron diffraction study of Earth's crust rocks, PAC for Condensed Matter Physics 30th meeting, 25-26 June 2009.
40. Vasin R.N., Lokajicek T., Nikitin A.N., Sumin V.V., Bulk elastic anisotropy of reactor graphite after exploitation from neutron diffraction and ultrasonic measurements, Abstracts of the 3rd International Conference on Texture and Anisotropy of Polycrystals (ITAP-3), 23-25 September 2009, Göttingen, Germany.
41. Vasin R.N., Nikitin A.N., Ivankina T.I., Ullemeyer K., Classification of quartz textures in crustal rocks derived from time-of-flight neutron diffraction data, Abstracts of the 3rd International Conference on Texture and Anisotropy of Polycrystals (ITAP-3), 23-25 September 2009, Göttingen, Germany.
42. Авдеев М.В., Магнитные наночастицы в растворах для медикобиологических применений, II Высшие курсы стран СНГ для молодых ученых, аспирантов и студентов старших курсов по современным методам исследований наносистем и материалов, Синхротронные и нейтронные исследования наносистем СИН-НАНО 2009, 28 июня - 13 июля 2009, Москва – Дубна, Россия,
43. Авдеев М.В., Малоугловое рассеяние нейтронов в диагностике магнитных наночастиц для медикобиологических применений, VII Национальная конференция "Рентгеновское, Синхротронное излучения, Нейтроны и Электроны для исследования наносистем и материалов. Нано-Био-Инфо-Когнитивные технологии" РСНЭ-НБИК 2009. Москва, Россия, 16-20 ноября
44. Авдеев М.В., Малоугловое рассеяние нейтронов, Всероссийская научная школа для молодежи «Современная нейтронография: междисциплинарные исследования наносистем и материалов», 12 - 20 октября 2009, Дубна
45. Авдеев М.В., Нейтронная нанодиагностика магнитных частиц в растворах для медикобиологических применений, Роснанофорум 2009, 6-8 октября 2009, Москва, Россия
46. Аксенов В.Л., Изменения магнитного состояния слоистой гетероструктуры ферромагнетик/сверхпроводник под влиянием сверхпроводящего перехода, 35Совещание по физике низкихтемператур (НТ-35), 29сентября - 2 октября, Черноголовка,
47. Балагуров А.М., Нейтронные спектрометры на реакторе ИБР-2М: статус и перспективы, РСНЭ-НБИК 2009, 16-21 ноября 2009 г., Москва.
48. Бардушкин В.В., Никитин А.Н., Чекасина И.И., Яковлев В.Б. Анизотропия эффективных физико-механических характеристик неоднородных материалов типа кварцевая матрица-боиотит. Третья международная конференции «Деформация и разрушение материалов и наноматериалов» DFMN-09, Москва, ИМЕТ им. А.А. Байкова РАН, 12-15 октября 2009.
49. Боднарчук В.И., Проект нового многофункционального рефлектометра GRAINS с горизонтальным расположением плоскости образца на импульсном реакторе ИБР-2М в Дубне, VII Национальная конференция "Рентгеновское, Синхротронное излучения, Нейтроны и Электроны для исследования наносистем и материалов. Нано-Био_Инфо-Когнитивные технологии", 16-21 ноября 2009, Москва, Россия
50. Бокучава Г.Д., Балагуров А.М., Сумин В.В., Папушкин И.В. “Нейтронный фурье-дифрактометр ФСД для исследования остаточных напряжений в материалах и промышленных изделиях” РСНЭ-НБИК 2009, 16-21 ноября 2009 г., Москва.
51. Васин Р.Н. Геофизические исследования с использованием нейтронографии. Всероссийская научная школа для молодежи «Современная нейтронография: междисциплинарные исследования наносистем и материалов. 2-20 октября 2009.
52. Дубовик В.М., Кривицкий В.А., Круглов А.А., Давление как динамический фактор стимулирования ядерных реакций в нано, микро и макромире, Сборник статей. Система "Планета Земля": 15 лет междисциплинарному научному семинару. 1994—2009. М.: ЛЕНАНД, 2009. с.153-158.
53. Ермакова Е.В., XIII Научная конференция Объединения молодых ученых и специалистов (ОМУС) ОИЯИ, Дубна, 16-21 февраля 2009
54. Калинин И.В., Кац Е., Коза М., Лаутер В.В., Лаутер Х., Пучков А.В., Сосуществование сверхтекучего и твердого гелия в аэрогеле, XXXV Совещание по физике низких температур (НТ-35), Черноголовка, 29 сентября-2 октября 2009, стр.16-17
55. Кизима Е.А., Особенности кластерообразования фуллерена С60 в полярных растворителях, VII Национальная конференция "Рентгеновское, Синхротронное излучения, Нейтроны и Электроны для исследования наносистем и материалов. Нано-Био-Инфо-Когнитивные технологии" РСНЭ-НБИК 2009, 16-21 ноября 2009, Москва, Россия
56. Кичанов С.Е., Исследование кристаллической структуры и структурных аспектов кластерообразования в ксерогелях GeO2-Eu2O3-Ag, РСНЭ-НБИК-2009, 16 - 21 ноября 2009, г. Москва
57. Лукин Е.В, Исследование кристаллической структуры перхлората пиридина PyHClO4 при высоком давлении и температуре, РСНЭ-НБИК-2009, 16 - 21 ноября 2009, г. Москва
58. Муругова Т.Н., Структурные изменения во внутренней мембране митохондрий, индуцированные системой объемной регуляции., 2009 Институт теоретической и экспериментальной биофизики РАН, г. Пущино, 2009
59. Нагорный А.В., Моделирование малоуглового рассеяния нейтронов на магнитных жидкостях с неполярными основами. VII Национальная конференция "Рентгеновское, Синхротронное излучения,

Нейтроны и Электроны для исследования наносистем и материалов. Нано-Био-Инфо-Когнитивные технологии" РСНЭ-НБИК 2009, 16-21 ноября 2009, Москва, Россия

60. Никитенко Ю.В., Возможности нейтронных исследований характеристик магнитного слоя в осциллирующем магнитном поле, нанофизика и наноэлектроника, XIII Международный симпозиум, 16-20 марта 2009, Нижний Новгород
61. Никитин А.Н., Маттис З., Юрченко О.А., Тепловые и транспортные особенности галоидных горных пород, возникающие вблизи размещенного в них радиоактивного источника. Тематический семинар «Структура и свойства кристаллов». Институт кристаллографии им.А.В.Шубникова РАН. Москва. 23 июня 2009.
62. Петренко В.И., Переход нематик–изотропная жидкость в растворах насыщенных монокарбоновых кислот по данным малоуглового рассеяния нейтронов. VII Национальная конференция "Рентгеновское, Синхротронное излучения, Нейтроны и Электроны для исследования наносистем и материалов. Нано-Био-Инфо-Когнитивные технологии" РСНЭ-НБИК 2009, 16-21 ноября 2009, Москва, Россия,
63. Рубцов А.Б., Создание нейтронного рефлектометра на тепловых нейтронах, VII Национальная конференция "Рентгеновское, Синхротронное излучения, Нейтроны и Электроны для исследования наносистем и материалов. Нано-Био-Инфо-Когнитивные технологии" РСНЭ-НБИК 2009, 16-21 ноября 2009, Москва, Россия
64. Рябова Н.Ю., Joint RID-ICTP-IAEA Advanced Workshop on Neutron probing for compositional and structural characterisation of materials and biological samples, Нидерланды, Дельфт, 10-17 мая, 2009г.
65. Савенко Б.Н., Исследование полиморфного фазового перехода в резорциноле при высоком давлении» РСНЭ-НБИК-2009, 16 - 21 ноября 2009, г. Москва
66. Тропин Т.В., Кинетика роста кластеров С60 в растворах в азот-содержащих растворителях, XIII научная конференция молодых ученых и специалистов ОИЯИ, ОМУС-2009, 16-21 февраля, ОИЯИ, Дубна, Россия
67. Тропин Т.В., Кинетическая теория кластерообразования в растворах фуллеренов: новые подходы и сравнение с экспериментом, VII Национальная конференция "Рентгеновское, Синхротронное излучения, Нейтроны и Электроны для исследования наносистем и материалов. Нано-Био-Инфо-Когнитивные технологии" РСНЭ-НБИК 2009, 16-21 ноября 2009, Москва, Россия
68. Тропин Т.В., Модели кластеров в растворах фуллеренов, Всероссийская конференция с элементами научной школы для молодых ученых "Структура и динамика молекулярных систем", 5-8 октября 2009, КГУ, Казань, Россия, стендовый доклад.
69. Феоктистов А.В., Малоугловое рассеяние нейтронов на биосовместимых магнитных жидкостях для терапии рака мозга, VII Национальная конференция "Рентгеновское, Синхротронное излучения, Нейтроны и Электроны для исследования наносистем и материалов. Нано-Био-Инфо-Когнитивные технологии" РСНЭ-НБИК 2009, 16-21 ноября 2009, Москва, Россия
70. Хайдуков Ю.Н., Neutron waveguide regime to study proximity effects at superconductor/ferromagnet interface, РСНЭ 2009, Москва, 16-21 ноября 2009
71. Хайдуков Ю.Н., STRUCTURE AND ADSORPTION ABILITIES OF NANOPOROUS Ti,V-(N, He) COATINGS Седьмая международная конференция “Ядерная и радиационная физика”, Алматы, 8-11 сентября 2009
72. Хайдуков Ю.Н., Эффекты близости в слоистых сверхпроводяще-ферромагнитных системах. Возможности рефлектометрии поляризованных нейтронов."XIII научная конференция “ОМУС-2009”, Дубна, 16-21 февраля 2009 года
73. Хайдуков Ю.Н., Neutron waveguide regime to study proximity effects at superconductor/ferromagnet interface, Modelling and Data Analysis for Grazing Incidence and Off-Specular Scattering (OffSpec 2009), Мюнхен, 27-29 сентября 2009г

NEUTRON NUCLEAR PHYSICS

1. Experimental investigations

1. Atchison F. et al., **Nucl. Instr. Meth.**, A611 (2009) 252.
2. Bodnarchuck, Cser L., Ignatovich V., Veres T., Yaradaykin S., **Сообщение ОИЯИ**, E14-2009-127, (2009) Дубна, ОИЯИ.
3. Gericke M., Page S., Ramsay D., Alarcon R., Balascuta S., Barron L., Bowman J.D., Carlini R.D., Chen W., Chupp T.E., Crawford C., Cowrig S., Dabaghyan M., Freedman S.J., Gentile T.R., Gillis R.C., Greene G.L., Hersman F.W., Ino T., Jones G.L., Lauss B., Leuschner M., Losowski B., Mahurin R., Masuda Y., Mei J., Mitchell G.S., Muto S., Nann H., Penttila S.I., Salas-Bacci A., Santra S., Seo P.-N., Sharapov E.I., Sharma M., Smith T., Snow W.M., Wilburn W.S., and Yuan V., **Nucl. Instrum. Methods in Phys. Res. A**, v.611 p.239, 2009.
4. Gledenov Yu.M., Sedyshyeva M.V., Stolupin V.A., Guohui Zhang, Jiaguo Zhang, Hao Wu, Jiaming Liu, Jinxiang Chen, G.Hkuukhenkhuu, Koehler P.E., Szalanski P.J., **Physical Review C** 80, 044602 (2009)
5. Guohui Zhang, Jiaguo Zhang, Li’an Guo, Hao Wu, Jinxiang Chen, Guoyou Tang, Gledenov Yu.M., Sedysheva M.V., Khuukhenkhuu G., Szalanski P.J., **Applied Radiation and Isotopes** 67 (2009) 46−49

6. Guohui Zhang, Hao Wu, Jiaguo Zhang, Jiaming Liu, Yuxiang Yin, Jinxiang Chen, Gledenov Yu.M., Sedysheva M.V., Khuukhenkhuu G., Koehler P.E., Szalanski P.J., **Applied Radiation and Isotopes** 68 (2010) 180−183
7. Guohui Zhang, Hao Wu, Jiaguo Zhang, Jiaming Liu, Jinxiang Chen, Gledenov Yu.M., Sedysheva M.V., Khuukhenkhuu G., and Szalanski P.J., **Eur. Phys. J. A** (2009) DOI 10.1140/epja/i2009-10886-2
8. Kamanin D.V., Pyatkov Yu.V., Kopach Yu.N., Krasznahorkay A., Tyukavkin A.N., Alexandrov A.A., Alexandrova I.A., Borzakov S.B., Zhuchko V.E., Kondratiev N.A., Kuznetsova E.A., Panteleev Ts., **Сообщения ОИЯИ** 4/ 9/2009
9. Lychagin E.V., Muzychka A.Yu., Nekhaev G.V., Nesvizhevsky V.V., Pignol G., Protasov K.V., Strelkov A.V. **Physics Letters B** 679 (2009) 186–190
10. Mutterera M., Trzaska W.H., Kopatch Yu.N., Sillanpäa M., von Kalben J., Khlebnikov S.V., Schrieder G., and Tyurin G.P., **Nuclear Instruments & Methods in Physics Research A.** Vol.608, No.2. - p.275-286
11. Pokotilovski Yu. N., Novopoltsev M. I., Geltenbort P., Eur. Phys. Journ. AP 45 (2009) 21202.
12. Sheets S.A., Agvaanluvsan U., Becker J.A., Bechvar F., Bredeweg T.A., Haight R.C., Jandel M., Krticka M., Mitchell G.E., O'Donnell J.M., Parker W., Reifarth R., Rundberg R.S., Sharapov E.I., Ullmann J.L., Vieira D.J., Wilhelmy J.B., Wouters J.M., and Wu C.Y., **Phys. Rev. C**, v.79 p.024301, 2009.
13. Skoy V.R., Wang T.F., Kim G.N., Oh Y.D., Cho M.H., Ko I.S., Namkung W., **Nuclear Instruments and Methods in Physics Research Section B: Beam Interactions with Materials and Atoms**, 267, 14, (2009), 2351-2356.
14. Skoy V.R., Guinyun Kim, Manwoo Lee, and Kyung Sook Kim., **IEEE Transactions on Nuclear Science** (submitted).
15. Sukhovoj A.M., Bondarenko V.A., Honzatko J., Khitrov V.A. and Tomandl I., **Fizika** (Zagreb), 2008, B17(4), 463-480.
16. Utsuro M, Ignatovich V. K. **NEUTRON OPTICS**. Japanese edition, 2009.
17. Vesna V.A., Gledenov Yu.M., Nesvizhevsky V.V., Petukhov A.K., Sedyshev P.V., Soldner T., Shulgina E.V., **Nuclear Physics A** 827 (2009) 425c−427c
18. Vesna V.A., Gledenov Yu.M., Nesvizhevsky V.V., Petukhov A.K., Sedyshev P.V., Shulgina E.V., **Nuclear Instruments and Methods in Physics Research A** 611 (2009) 244–247
19. Zeynalov Sh., Hambsch F.-J., Oberstedt S., Fabry I., 4th International Workshop on Nuclear Fission and Fission Product Spectroscopy, May 13-16, 2009, **AIP Conference proceedings**, V1175. pp. 359-362
20. Zeynalova O.V., Zeynalov Sh.S., Hambsch F.-J., Oberstedt S., **Bulletin of the Russian Academy of Sciences: Physics**, 2009, Vol. 73, No. 4, pp. 506–511. © Allerton Press, Inc., 2009.
21. Зейналова О. В., Зейналов Ш., Хамбш Ф.-Й., Оберстедт Ш., Фабри И., **AIP Conf. Proc.** -- October 29, 2009 -- Volume 1186, pp. 430-439 1st International conference on applications of mathematics in technical and natural sciences;
22. Суховой А.М., Хитров В.А., **ЯФ**, 2009, 72(9), 1480-1488.
    Sukhovoj A.M., Khitrov. V.A., **Physics of atomic nucleus**, 2009, 72(9), 1426-1434.
23. Суховой А.М., Хитров В.А., Фурман В.И., **ЯФ**, 2009, 72(10) 1817-1824.
    Sukhovoj A.M., Khitrov V.A., Furman W.I., **Physics of atomic nucleus,** 2009, 72(10), 1759-1766.
24. Тюкавкин А.Н., Пятков Ю.В., Каманин Д.В., Копач Ю.Н., Александров А.А., Александрова И.А., Борзаков С.Б., Воронов Ю.Н., Денисов С.В., Ефимов Г.Л., Жучко В.Е., Кондратьев Н.А., Кузнецова Е.А., Лаврова Ю.Е., Митрофанов С.В., Пантелеев Ц., Саламатин В.С.и Цурин И.П., **Приборы и техника эксперимента**, No.4. (2009), с.66-76

2. Theoretical investigations

1. Ignatovich V. K., **Ядерная Физика**, 72 (2009) 47-52.
2. Ignatovich V.K., Pokotilovski Yu.N., **The European Physical Journal** C 64 (2009) 19-23.
3. Ignatovich V. K. and Phan. L.T.N., **American Journal of Physics**, 77 (2009) 1093-1117.
4. Ignatovich V.K., Nikitenko Yu.V. and Radu F., **Nuclear Instruments and Methods in Physics Research. Section** A. 604 (2009) 653-661.
5. Lyuboshitz V.L., Lyuboshitz V.V., **Ядерная физика**, 2009, т.72 (2) , сс. 340-347
   Lyuboshitz V.L., Lyuboshitz V.V., **Physics of Atomic Nuclei** , 2009, v.72 (2), pp. 311-318] .
6. Lyuboshitz V.L., Lyuboshitz V.V., **JINR Preprint** E2-2009-42 , Dubna, 2009
7. Lyuboshitz V.L., Lyuboshitz V.V., **Ядерная физика** (2010) (принято к печати).
8. Lyuboshitz V.L., Lyuboshitz V.V., Proceedings of the International Conference “Strong and ElectroWeak Matter 2008” – SEWM-2008 (Amsterdam, the Netherlands), **Nuclear Physics A**, 2009, v. 820 , pp. 311c-314c.
9. Игнатович В.К., **Кристаллография** 54 (2009) 122-128.
   K. Ignatovich, **Crystallography Reports** (Kristallografiya), 54 (2009) 118-121.
11. Игнатович В.К., Фан Л.Т.Н., **Сообщение ОИЯИ**, Р4-2009-39 (2009) Дубна, ОИЯИ
10. Франк И., **Ядерная физика**, 2009, т. 72,№11, с. 1878–1882.
    Frank A.I., **Physics of Atomic Nuclei**, 2009, Vol. 72, No. 11, pp. 1818–1822/

3. Applied research

1. Alekseenok Yu.V., Frontasyeva M.V., Korokin A.Zh., **Proceedings of The "5th International Summer School on Nuclear Physics Methods and Accelerators in Biology and Medicine"**, 6-15 July, 2009, Bratislava, Slovakia, American Institute of Physics, 2009, pp. 2.
2. Aničić M., Tasić M., Frontasyeva M.V., Tomašević M., Rajšić S., Mijić Z., Popović A., **Environmental Pollution**, Vol. 157, 2009**,** p. 673-679, http://doi:10.1016/j.envpol.2008.08.003
3. Aničić M., Tomašević M., Tasić M., Rajšić S., Popović A., Frontasyeva M.V.; Lierhagen S., Steinnes E., **Journal of Hazardous Materials**, Elsevier, March, 2009, http://doi:10.1016/j.hazmat.2009.05.112
4. Cristache C. I., Duliu O. G., Culicov O. A., Frontasyeva M. V., Ricman C., Toma M., **Applied Radiation and Isotopes**, Vol. 67, 2009, p. 901-906.
5. Cristache C., Simion C.A., Margineanu R.M., Culicov O.A., Frontasyeva M.V., Matei M., Duliu O.G., **Radiochimica Acta**, Vol. 97, 2009**,** p. 333-337.
6. Cristache C., Culicov O., Gmeling K., Toma M., Frontasyeva M., Duliu O.G., **Journal of Radioanalytical and Nuclear Chemistry**, 2009**,** Vol. 279, No. 1, p. 7-12, http://dx.doi.org/10.1007/s10967-007-7214-z
7. Cristache C., Culicov O., Toma M., Frontasyeva M., Duliu O.G., Oaie G., **Marine Pollution Bulletin**, Vol. 58, 2009**,** p. 827-831, http://doi:10.1016/j.marpolbul.2009.01.021
8. Culicov O.A., Frontasyeva M.V., Daraban L., Ghiurca V., **Studia Universitatis Babes-Bolyai, Physica**, Liv. 2, 2009, p. 41-50.
9. Dimovska S., Stafilov T., Šajn R., Frontasyeva M.V., **Radiation Protection Dosimetry**, 2009. http://www.rpd.oupjournals.org
10. Duliu O.G., Cristache C.I., Culicov O.A., Frontasyeva M.V., Szobotca S.A., Toma M., **Applied Radiation and Isotopes**, Vol. 67, 2009, p. 939-943.
11. Duliu O.G., Cristache C.I., Oaie G., Culicov O.A., Frontasyeva M.V., Toma M., Constantinescu E., **Journal Geo-Marine Letters** (submitted).
12. Duliu O.G., Cristache C.I., Oaie G., Ricman C., Culicov O.A., Frontasyeva M.V. **American Institute of Physics Proceedings Series**. 2009 (submitted)
13. Dutov A.G., Komar V.A., Shipilo N.V., Azarko I.I., Frontasyeva M.V., Pavlov S.S., Synthesis of fine crystalline diamonds. In book "**Diamond and Related Materials**". Editor Frank Columbus, Nova Science Publishers, Inc., USA, 2009 **(**in print**).**
14. Kobzev A.P., Huran J., Maczka D., Turek M., **VACUUM**, vol. 83, supplement 1, pages S124 – S126, (2009).
15. Frank A.I., Geltenbort P., Jentschel M., Kulin G.V., Kustov D.V., Nosov V.G., Strepetov A.N., **Nuclear Instruments and Methods in Physics Research A** 611 (2009) 314–317
16. Frank A.I., and Kozlov A.V., **Physica B. Condensed Matter**, 404 (2009) 2550-2552.
17. Frontasyeva M.V., **Proceedings of The "5th International Summer School on Nuclear Physics Methods and Accelerators in Biology and Medicine**", 6-15 July, 2009, Bratislava, Slovakia, American Institute of Physics, 2009, pp.8.
18. Frontasyeva M.V., **Ovidius University Annals of Chemistry**, Vol. 20, No. 1, 2009, p. 11-18. ISSN-1223-7221.
19. Frontasyeva M.V., Pavlov S.S., Mosulishvili L.M., Kirkesali E.I., Ginturi E., Kuchava N., **Ecological Chemistry and Engeneering.** Vol. 16, No. S3, 2009, p. 277-285.
20. Frontasyeva M.V., Meresova J., Holy K., Sykora I., **Acta Physica Universitatis Comenianae**, Vol. L.LI, Number 1and 2, 2010, p. 155-161.
21. Harmens H., Norris D. A., Steinnes E., Kubin E., Piispanen J., Alber R., Aleksiayenak Y., Blum O., Coşkun M., Dam M., De Temmerman L., Fernández Escribano J. A., Frolova M., Frontasyeva M., Gonzalez Miqueo L., Grodzińska K., Jeran Z., Korzekwa S., Krmar M., Kvietkus K., Leblond S., Liiv S., Magnússon S., Maňkovská B., Pesch R., Rühling Å., Santamaria J., Schröder W., Spiric Z., Suchara I., Thöni L., Urumov V., Yurukova L., Zechmeister H. G., **Environmental Pollution**, 2009 (submitted)
22. Kreuz M., Nesvizhevsky V.V., Schmidt-Wellenburg P., Soldner T., Thomas M., Börner H.G., Naraghi F., Pignol G., Protasov K.V., Rebreyend D., Vezzu F., Flaminio R., Michel C., Morgado N., Pinard L., Baeßler S., Gagarski A.M., Grigorieva L.A., Kuzmina T.M., Meyerovich A.E., Mezhov-Deglin L.P., Petrov G.A.,.Strelkov A.V, Voronin A.Yu.,**Nuclear Instruments and Methods in Physics Research A** 611 (2009) 326–330
23. Krmar M., Radnović D., Frontasyeva M.V., Pavlov S.S., and Pankratova Y.S., Atmospheric deposition of heavy metals and airborne radionuclides studied by the moss biomonitoring technique. In book: **Advances in Environmental Modelling and Measurements**, (Eds.) D.T. Mihailović and B. Lalić, Nova Science Publishers, Inc., New York, 2009. ISBN: 978-1-60876-599-7.
24. Nguyen Viet H., Frontasyeva M.V., Trinh Thi T.M., Gilbert D., Bernard N., **Environmental Science and Pollution Research**, http://doi: 10.1007/s11356-009-0258-6, 2009.
25. Marinova S., Yurukova L., Frontasyeva M.V., Strelkova L.P., Marinov A., Karadzhinova A.G., **Ecological Chemistry and Engineering**, (submitted)
26. Marinova S., Yurukova L., Frontasyeva M.V., Strelkova L.P., Marinov A., Karadzhinova A.G., **JINR Preprint**, E18-2009-53, Dubna, 2009, pp. 19.

27. Meresova J., Florek M., Holy K., Ješkovský M., Sýkora I., Burda C., Melicherová T., Mankovska B., Oszlanyi J., Frontasyeva M.V., Pavlov S.S., **JINR Preprint**, E18-2009-27, Dubna, **2009**, pp. 18.
28. Oprea C., Szalanski P. J., Gustova M. V., Oprea I. A., Buzguta V., **Applied Radiation and Isotopes**, ISSN:0969-8043, Elsevier Science Ltd, 67, 12, 2142-2145, 2009.
29. Oprea C., Szalanski P.J., Gustova M.V., Oprea I.A., Buzguta V., **VACUUM**, ISSN:0042-207X, Elsevier, 83, Suppl. 1, S166-S168, 2009.
30. Oprea C., Maslov O.D., Gustova M.V., Belov A.G., Szalanski P.J., Oprea I.A., **VACUUM**, ISSN:0042-207X, Elsevier, 83, Suppl. 1, S162-S165, 2009.
31. Oprea A. I, Oprea C., Gledenov Yu.M., Sedyshev P.V., Pirvutoiu C., Vladoiu D., **Romanian Reports in Physics**, ISSN:1221-1451, Romanian Academy of Science, 2009 (in press).
32. Oprea A. I., Oprea C., Pirvutoiu C., Vladoiu D., **Romanian Reports in Physics**, ISSN:1221-1451, Romanian Academy of Science, 2009 (in press).
33. Oprea C., Maslov O. D., Gustova M. V., Oprea I.A., Belov A. G., Szalanski P. J., **Romanian Reports in Physics**, ISSN:1221-1451, Romanian Academy of Science, 2009 (in press).
34. Oprea C., Mateescu G., Oprea I.A., Kozlov Zh.A., Semenov V.A., Craciun L., Puchkov A.V., **Romanian Reports in Physics,** ISSN:1221-1451, Romanian Academy of Science, 2009 (in press).
35. Popovic D., Bozic T., Stevanovic J., Frontasyeva M.V., Todorovic D., Ajtic J., Spasic Jokic V., **Environmental Science and Pollution Research,** 2009**.** http://DOI: 10.1007/s11356-009-0274-6 (accepted)
36. Spiric Z., Frontasyeva M.V., Steinnes E., Stafilov T**., Journal of Hazardous Materials**, 2009 (submitted)
37. Spiric Z., Frontasyeva M.V., Stafilov T., Steinnes E., Bukovec D., Gundorina S.F.,. Ostrovnaya T.M, Enimiteva V., **JINR Preprint**, E18-2009-149, Dubna, **2009**, pp. 28.
38. Stafilov T., Šajn R., Pančevski Z., Boev B., Frontasyeva M.V., Strelkova L.P., **Journal of Hazardous Materials**, Elsevier, August, 2009, http://doi:10.1016/j.jhazmat.2009.10.094
39. Tsibakhashvili N.Ya., Mosulishvili L., Kirkesali E., Kalabegishvili T., Kerkenjia S., Frontasyeva M.V., Zinicovscaia I., **Chemistry** (Journal of Moldova) General, Industrial and Ecological Chemistry, 2009 (submitted)
40. Афонин Н.Н., Логачева В.А., Шраменко Ю.С., Ховив А.М., Вахтель В.М., Кобзев А.П., **Конденсированные среды и межфазные границы**, том 11, №1, стр. 21 – 30, (2009).
    Afonin N.N., Logacheva V.A.,. Shramenko Yu.S, Hoviv A.M., Vachtel V.M., Kobzev A.P., **Condenced mediums and interphasic borders**. V. 11, №1, pp. 21 – 30, (2009).
41. Балжиням Н., Ганболд Г., Гэрбиш Ш., Лодойсамба С., Фронтасьева М.В., Павлов С.С., **Препринт ОИЯИ**, Р18-2009- 90, Дубна, **2009**.
42. Быстрицкий В.М., Герасимов В.В., Замятин Н.И., Зубарев Е.В., Кадышевский В.Г., Кобзев А.П., Крылов А.Р., Ноздрин А.А., Рапацкий В.Л., Рогов Ю.Н., Садовский А.Б., Саламатин А.В., Сапожников М.Г., Сисакян А.Н., Слепнев В.М., **Письма в ЭЧАЯ**. Том 6, №6(155), стр. 831 – 840, (2009).
    Bystritsky V.M., Gerasimov V.V., Zamjatin N.I., Subarev E.V., Kadyshevsky V.G., Kobzev A.P., Krylov A.R., Nozdrin A.A., Rapatsky V.L., Rogov Yu.N., Sadovsky A.B., Salamatin A.V., Sapozhnikov M.G., Sissakian A.N.,. Slepnev V.M., **Physics of Particles and Nuclei Letters**. Vol. 6, N6(155), pp. 831 – 840, (2009).
43. Вергель К.Н., Фронтасьева М.В., Каманина И.З., Павлов С.С., **Экология урбанизированных территорий**, вып. 3, 2009, с. 88-95.
    Vergel' K.N., Frontasyeva M.V., Kamanina I.Z., Pavlov S.S., **Ecology of Urbinized Terrotories** (RF), Vol. 3, 2009, p. 88-95 (in Russian).
44. Гэрбиш Ш., Ганболд Г., Балжиням Н., **Физик** (Монголия), Том 309, № 15, 2009, с/ 47-50.
    Gerbish Sh., Ganbold G., Baljannyam N., **Physic** (Mongolia), Vol. 309, No. 15, 2009, p. 47-50 (in Russian).
45. Горбунов А.В., Ляпунов С.М., Окина О.И., Фронтасьева М.В., Павлов С.С., **Препринт ОИЯИ**, D-18-2009-17, Дубна, 2009.
46. Горелова С.В., Песцов Г.В., Гинс М.С., Кононков П.Ф., Фронтасьева М.В., Ермакова Е.В., Ляпунов С.М., Горбунов А.В., Окина О.И., **Агрохимия**, № 9, 2009, с. 76–87.
    Gorelova S.V., Pestsov G.V., Gins M.S., Kononkov P. F., Frontasyeva M.V., Ermakova E.V., Lyapunov S. M., Gorbunov A.V., and Okina O.I., **Agrochemistry**, No. 9, 2009**,** p. 76-82 (in Russian).
47. Грабовський В., Дзендзелюк О., Трофімук А., Фронтасьєва М., Сватюк Н., Маслюк В., Направлена в **ДАН Украины** (Направлена в печать)
    Grabovsky V., Dzendzelyuk O., Trofimuk A., Frontasyeva M., Svatyuk N., Maslyuk V., **Communication of the Academy of Sciences of Ukraine**, 2009 (submitted)
48. Ильченко И.Н., Былова Н.А., Фронтасьева М.В., Ляпунов С.М., Окина О.И., Горбунов А.В., Павлов С.С., Куликова О., Арутюнов Г.П., **Общественное здоровье и профилактика заболеваний**. 2009, № 2, стр. 8-11.
    Ilchenko I.N., Bylova N.A., Frontasyeva M.V., Lyapunov S.M., Pavlov S.S., Culicov O.A., Okina O.I., Gorbunov A.V., Aroutiounov G.P., **Public Health and Disease Prevention**, No. 2, 2009, p. 8-11 (in Russian).
49. Никитин А.Н., Иванкина Т.И., Игнатович В.К., **Физика Земли**, 45 (2009) 57-69.
    Nikitin A.N., Ivankina T.I. and Ignatovich V.K, **Izvestiya, Physics of the Solid Earth** 45 (2009) 424–436.

50. Панкратова Ю.С., Зельниченко Н.И., Фронтасьева М.В., Павлов С.С., **Общественно-научный журнал «Проблемы региональной экологии»**, № 1, 2009**,** с. 57-63.
    Pankratova Yu. S., Frontasyeva M.V., Pavlov S.S., Zelnitchenko N.I., **Problems of Regional Ecology**, No.1, 2009, p.57-63.
51. Реутов В.Ф., Залужный А.Г., Кобзев А.П., Сохацкий А.С., **Журнал технической физики**, том 79, вып. 9, с. 63 – 70, (2009).
    Reutov V.F., Saluznyj A.G., Kobzev A.P., Sochatskij A.S, **Journal of Technical Physics**. V.79, supplement 9, pp.63 -70, (2009).
52. Судницын И.И., Крупенина И.И., Фронтасьева М.В., Павлов С.С., **Агрохимия**, № 7, Июль **2009**, с. 66-70.http://www.maikonline.com/maik/showArticle.do?auid=VAFWSTFZTN
    Sudnitsyn I.I., I.I. Krupenina, M.V. Frontasyeva, S.S. Pavlov., **Agrochemistry,** No. 7, July **2009**, p. 66-70.
44. Франк А.И.**. Успехи физических наук**, (2009) т. 179, №4, с. 424-434.
    Frank A.I. **Physics-Uspekhi**. **v.52,** No. 4, 397-406
53. Фронтасьева М.В., Павлов С.С., Аксенова Н.Г., Мосулишвили Л.М., Белокобыльский А.И., Киркесали Е.И., Гинтури Э.Н., Кучава Н.Е., **Журнал аналитической химии**, Том 64, № 7, 2009**,** с. 776-789. УДК 543.522
    Frontasyeva M.V., Pavlov S.S., Aksenova N.G., Mosulishvili L.M., Belokobylsky A.I., Kirkesali E.I., Ginturi, E.N. Kuchava Y.E., **Journal of Analytical Chemistry**, Vol. 64, No. 7, 2009, p. 776-789 (in Russian). УДК 543.522
54. Фронтасьева М.В., **Методическое пособие. УНЦ**-2009-38, Дубна, 2009.

Reports at Schools and Conferences

1. Aleksiayenak Yu., Frontasyeva M.V., Vermaercke P., Korokin A., Trace element atmospheric deposition study in Belarus based on moss analysis. ISINN-17, 27-30 May, 2009, Dubna, p.16; Book of Abstracts BioMAP-5.
2. Baljinnyam N., Gerbish Sh., Ganbold G., Lodoysamba S., Frontasyeva M.V., Heavy metals in the environmental objects of non-ferrous industrial region of Mongolia, the town of Erdenet. The 2nd International Conference on X-Ray Analysis, Proceeding of Conference, p. 185-193, Ulaanbaatar, Mongolia, 2009.
3. Baljinnyam N., Gerbish Sh., Ganbold G., Lodoysamba S., Frontasyeva M.V., Pavlov S.S., Heavy metals in the environmental objects of non-ferrous industrial region of Mongolia, the town of Erdenet. ISINN-17, 27-30 May, 2009, Dubna; p. 70.
4. Coskun M., Frontasyeva M.V., Gorelova S., Pantelica A., Saitanis K., Tomasevic M., Yurukova L., Biomonitoring of air quality using plants. ISINN-17, 27-30 May, **2009**, Dubna; Book of Abstracts BioMAP-5, p. 21, 20-24 September 2009, Bienos Aires, Argentina.
5. Duliu O.G., Cristache C.I., Oaie G., Ricman C., Culicov O.A., Frontasyeva M.V., Epithermal Neutron Activation Analysis of Some Geological Samples of Different Origin. Proceedings of The 7th General Conference of BPU (Alexandroupolis, Greece, 9-13 September 2009, http://bpu7.phys.uoa.gr/).
6. Duliu O.G., Cristache C., Oaie G., Culicov O.A., and Frontasyeva M.V., Cs-137 geochronology, epithermal neutron activation analysis, and principal component analysis of heavy metals pollution of the Black Sea anoxic continental shelf sediments. Geophysical Research Abstracts, Vol. 11, EGU2009-4992, European Geosciences Union General General Assembly, EGU 2009, Vienna, Austria, 18-24 April 2009.
7. Duliu O.G., Cristache C., Oaie G., Culicov O.A., Frontasyeva M.V., Toma M., On the distribution of major and trace elements as determined by epithermal neutron activation analysis in unconsolidated sediments of the anoxic continental platform of the Black Sea. Book of Abstracts, ISINN-17, 27-30 May, 2009, Dubna, p. 25.
8. Florek M., Merešová J., Holý K., Ješkovský M., Sýkora I., Burda C., Melicherová, T. Frontasyeva M.V., Pavlov S.S., Comparison of Elemental Concentrations in the Atmosphere in Bratislava with other Slovakian and European Sites. ISINN-17, 27-30 May, 2009, Dubna, p. 28.
9. Frontasyeva M.V., Radioanalytical investigations at FLNP JINR for Life Sciences. Book of Abstracts, Int. Conf. on Radiochemistry. Marianske Lazne, Czech Rep., 18-21 April, 2010.
10. Frontasyeva M.V., Aleksiayenak Yu.V., Steinnes E., Florek M., Sykora I., Jeskovsky M., Ramatlhape I., Faanhof A., Moss biomonitoring of long-lived radionuclides in Belarus: 20 years after Chernobyl. Book of Abstracts of The 22nd Task Force Meeting UNECE ICP Vegetation (February 2-5, 2009, Braunschweig, Germany).
11. Frontasyeva M.V., Aleksiayenak Yu.V., Steinnes E., Florek M., Holy K., Jeskovsky M., Sykora I., Ramatlhape I., Faanhof A., Atmospheric deposition of radionuclides in Belurus and Slovakia: 20 years after Chernobyl. Book of Abstracts, ISINN-17, 27-30 May, 2009, p. 29; Dubna; Book of Abstracts BioMAP-5, 20-24 September 2009, Bienos Aires, Argentina.
12. Furman W.I., Muzichka A.Yu., Crawford B.E., Howell C.R., Kandiev Ya., Levakov B.G., Litvin V.I., Lychagin E.V., Lyzhin A.E., Mitchell G.E., Nekhaev G.V., Sharapov E.I., Shvetsov V.N., Stephenson S.L., Strelkov A.V., Tchernukhin Yu.I., and Tornow W., Current status of the experiment on direct measurement of neutron-neutron scattering length at the reactor YAGUAR, Proceedings of the First Ulaanbaatar Conference on Nuclear Physics and Applications, AIP Conf. Proc., v.1109, p.53, 2009.
13. Gagarski A., Petrov G., Guseva I., Zavarukhina T., Gonnenwein F., Mutterer M., von Kalben J., Trzaska W., Sillanpaa M., Kopatch Yu., Tiourine G., Soldner T., Nesvizhevsky V., Detailed study of the effects following from

rotation of the scissioning nuclei in ternary fission of 235U by cold polarized neutrons ("ROT" and "TRI" effects), Proceedings of 16th International Seminar on Interaction of Neutrons with Nuclei. Dubna, June 11-14, 2008. Dubna 2009., p. 356
14. Gledenov Yu.M., Sedysheva M.V., Stolupin V.A., Khuukhenkhuu G., Szalanski P.J., Jiaguo Zhang, Lian Guo, Hao Wu, Jinxiang Chen, Guoyou Tang, Guohui Zhang, Cross Section Measurement for the 147Sm(n,α)144Nd Reaction at 5.00 and 6.00 MeV. In: Proc. of the 16 International Seminar on Interaction of Neutron with Nuclei (ISINN-16), Dubna, 2009,) E3-2009-33, p. 248-254.
15. Goryaynova Z.I., Frontasyeva M.V., Pavlov S.S., Pavlov D.F., Heavy metals and REE in bottom sediments and dreissenids of the Rybinsk reservoir. Proceedings of ISINN-16 (11-14 June, 2008, Dubna), pp. 5, 2009.
16. Ignatovich V.K., Analytical calculation of the neutron spectrum for direct measurement of nn scattering at pulsed reactor yaguar, Proceeding of XVI ISINN p. 61-68, JINR Dubna 2009.
17. Khitrov V.A., Sukhovoj A.M., Maslov V.M., Level density and radiative strength functions of the {^{237}$U nucleus from the (n,γ) reaction, XVI International Seminar on Interaction of Neutrons with Nuclei, Dubna, June 2008, E3-2009-33, Dubna, 2009, pp. 164-181.
18. Khuukhenkhuu G., Gledenov Yu.M., Sedysheva M.V., and Odsuren M., The Systematic Study of (n,p) Cross Sections for 18 and 20 MeV. In: Proc. of the 16 International Seminar on Interaction of Neutron with Nuclei (ISINN-16), (Dubna: JINR, 2009) E3-2009-33, p. 255-260.
19. Korokin A., Frontasyeva M.V., Assessment of air pollution levels in urban areas by using bioindication. ISINN-17, 27-30 May , 2009, Dubna; p. 41.
20. Lyuboshitz V.L., Lyuboshitz V.V., The medium with polarized nuclei and effects of low-energy neutron refraction and reflection, Proceedings of the XVII International Seminar on Interaction of Neutrons with Nuclei -- ISINN-17 (Dubna, May 27 -30, 2009)
21. Lyuboshitz V.L., Lyuboshitz V.V., Low-energy scattering of a polarized neutron on a polarized proton, Proceedings of XVI International Seminar on Interaction of Neutrons with Nuclei -- ISINN-16, JINR E3-2009-33, Dubna, 2009, pp. 342-349.
22. Lyuboshitz V.L., Lyuboshitz V.V., Angular correlations in the decays of $\Lambda\Lambda$ and $\Lambda\overline{\Lambda}$ pairs produced in relativistic heavy ion collisions, Proceedings of the XIII International Conference on Selected Problems of Modern Physics, dedicated to the 100-th anniversary of the birth of D.I.Blokhintsev, JINR E1,2-2009-36 , Dubna, 2009, pp. 192-195.
23. Lyuboshitz V.L., Lyuboshitz V.V., Spin correlations of the electron and positron in the two-photon process $\gamma\gamma \rightarrow e^+e^-$ // Proceedings of the XIII Advanced Research Workshop on High Energy Spin Physics – DSPIN-09 (Dubna, September 1 - 5, 2009) (in press)
24. Lyuboshitz V.L., Lyuboshitz V.V., Spin correlations in the $\Lambda\Lambda$ and $\Lambda\overline{\Lambda}$ systems generated in relativistic heavy ion collisions // Proceedings of the XIII International Conference on Elastic and Diffractive Scattering – EDS-09 (Geneva, Switzerland, June 29 – July 3, 2009) (in press).
25. Mazurkevich A.N., Piotrovsky Yu.Yu., Frontasyeva M.V., Strelkova L.P., Neutron activation analysis of ceramics dated from neolithic age. Book of Abstracts, ISINN-17, 27-30 May, 2009, Dubna, p. 72.
26. Oprea C., Oprea A.I., Sedyshev P.V., Gledenov Yu.M., Stepanenko V.A., Spectra processing in asymmetry (n,p) reactions, 2009 17th International Seminar on Interaction of Neutrons with Nuclei (ISINN17), FLNP - JINR, Dubna, Russia (in press).
27. Oprea C., Gustova M.V., Maslov O.D., Belov A.G., Niculescu M., Oprea I.A., Mihul A., Nuclear and atomic methods applied for researches concerning trace element content of medicinal plants, 2009 17th International Seminar on Interaction of Neutrons with Nuclei (ISINN17), FLNP - JINR, Dubna, Russia (in press).
28. Oprea C., Velichkov A., Oprea I.A., Filosofov D.V., The method of perturbation of the □□ angular correlations and HFI used for essential oil researches, authors, , 2009 17th International Seminar on Interaction of Neutrons with Nuclei (ISINN17), FLNP - JINR, Dubna, Russia (in press).
29. Oprea C., Gustova M.V., Oprea I.A., A FA neural network –based approach for human exposure analysis in urban areas, 2009, 17th International Seminar on Interaction of Neutrons with Nuclei (ISINN17), FLNP - JINR, Dubna, Russia (in press).
30. Oprea C., Maslov O.D., Gustova M.V., Belov A.G., Oprea I.A., Ciofu R., Mihul A., Studies concerning the influence of inorganic pollutants on the quality of agricultural soils, 17th International Seminar on Interaction of Neutrons with Nuclei (ISINN17), FLNP - JINR, Dubna, Russia (in press).
31. Oprea A.I., Pirvutoiu C., Vladoiu D.N., Oprea C., Sedyshev P.V., Gledenov Yu.M., Sedysheva M.V., On the forward - backward effect in the (n,p) reaction on 35Cl and 14N, , 2009, 17th International Seminar on Interaction of Neutrons with Nuclei (ISINN17), FLNP - JINR, Dubna, Russia (in press).
32. Oprea A.I., Pirvutoiu C., Vladoiu D., Oprea C.D., Sedyshev P.V., Gledenov Yu.M., Sedysheva M.V., Evaluation of the (n,alpha) cross section using the Hauser – Feshbach approach for 64Zn and 147Sm nuclei with incident neutron energy up to some MeV, 17th International Seminar on Interaction of Neutrons with Nuclei (ISINN17), FLNP - JINR, Dubna, Russia (in press).

33. Pantelica A., Culicov O., Frontasyeva M.V., Badita C.R., Călinescu I.C., Elemental concentrations in vegetable species from industrial zones in Romania determined by INAA. Book of Abstracts, Int. Conf. on Radiochemistry. Marianske Lazne, Czech Rep., 18-21 April, 2010.
34. Pantelica A., Frontasyeva M.V., Georgescu J.I., Pincovschi E., Trace element concentrations in vascular plants (tree leaves) around a fertilizer plant in Romania determined by INAA. Book of Abstracts, ISINN-17, 27-30 May, 2009, Dubna, p. 53.
35. Popescu I.V., Frontasyeva M.V., Ene A., Stihi C., Gheboianu A., Culicov O., Vlaicu Dh., Comparative studies on heavy metal content of mosses used in environmental biomonitoring. International symposium on applied physics materials science, environment and health, Dunarea de Jos University of Galati, Romania, November 28-29, 2009.
23. Saitanis K., Frontasyeva M.V., Ostrovnaya T.M., Gundorina S.F., Tzamgiozis L., Ambient air monitoring with moss bag technique in the Thriassion Plain, Attika, Greece. Book of Abstracts of The 22nd Task Force Meeting UNECE ICP Vegetation (February 2-5, 2009, Braunschweig, Germany).
24. Saitanis K., Frontasyeva M.V., Steinnes E., Trace elements monitoring with moss bags in Greece. Book of Abstracts, ISINN-17, 27-30 May, 2009, Dubna, p. 56; Book of Abstracts BioMAP-5, 20-24 September 2009, Bienos Aires, Argentina.
25. Shvetsov V.N., Sharapov E.I., Stephenson S.L., and Crawford B.E., Comparison of calculated and measured yields of medical isotopes produced by electron bremsstrahlung, Proceedings of the XVII International Seminar on Interaction of Neutrons with Nuclei: ISINN-17, Dubna, May 27-30,2009 (in press).
36. Spiric Z., Frontasyeva M., Stafilov T., Enimiteva V.,. Bukovec D., Mercury biomonitoring in Croatia, 9th International Conference on Mercury as a Global Pollutant (9 ICMGP), Guiyang, China; June 7-12, 2009. www.mercury2009.org/introduction.htm - 13k
37. Steinnes E., Frontasyeva M.V., Barandovski L., Coskun M., Krmar M., Marinova S., Pavlov S.S., Spiric Z., Stafilov T., Urumov V. and Yurukova L., Assessment of trace metal air pollution in some Balkan countries based on large-scale application of moss miomonitoring. Book of Abstracts of BioMAP-5, 20-24 September 2009, Bienos Aires, Argentina.
38. Stephenson S.L., Crawford B.E., Yager-Elorriaga D.A., Pagan C.F., Sharapov E.I., Showalter-Bucher R.A., Muzichka A.Yu., Furman W.I., Lychagin E.V., Krylov A. R., Nekhaev G.V., Shvetsov V.N., and Strelkov A .V., On the gas desorption problem in the nn-experiment at the YAGUAR reactor, XVII International Seminar on Interaction of Neutrons with Nuclei, ISINN-17 Abstracts, E3-2009-50, Joint Institute for Nuclear Research, Dubna, p. 59, 2009.
39. Sukhovoj A.M., Furman W.I., Khitrov V.A., Status and problems of experimental study of excited nucleus superfluidity. In: XVI International Seminar on interaction of Neutrons with Nuclei, Dubna, June 2008, E3-2009-33, Dubna, 2009, pp. 181-192.
40. Sukhovoj A.M., Khitrov V.A., Parameters of distribution of the primary gamma-transition intensities following resonance neutron capture and some properties of compound nuclei ^{157,159}Gd, XVI International Seminar on Interaction of Neutrons with Nuclei, Dubna, June 2008, E3-2009-33, Dubna, 2009, pp. 192-203.
41. Sukhovoj A.M., Khitrov V.A.. Possibility of experimental determination of reliable parameters of the compound-state gamma-decay and some errors of analysis: ^{96}Mo as an example. XVI International Seminar on Interaction of Neutrons with Nuclei, Dubna, June 2008, E3-2009-33, Dubna, 2009, pp. 203-220.
18. Sukhovoj A.M., Khitrov V.A., Radiative capture of thermal and resonance neutrons, main parameters of the gamma-decay process and properties of the ^{174}Yb Nucleus, XVI International Seminar on Interaction of Neutrons with Nuclei, Dubna, June 2008, E3-2009-33, Dubna, 2009, pp. 220-230.
19. Sukhovoj A.M., Khitrov V.A., Parameters of cascade gamma-decay of compound-nuclei ^{146}Nd, ^{156}Gd, ^{172}Yb, ^{182}Ta, ^{184}W, ^{191}Os, ^{231,233}Th, ^{239}U, ^{240}Pu from experimental data of reaction (n,γ). In: XVI International Seminar on Interaction of Neutrons with Nuclei, Dubna, June 2008, E3-2009-33, Dubna, 2009, pp. 230-237.
20. Sukhovoj A.M., Khitrov V.A., About nucleus "superfluid-normal" state transition dynamics, Proceedings of the 2-nd international conference "Current problems in nuclear physics and atomic energy", Part 2, Kyiv, 2009, pp. 511-515.
21. Sukhovoj A.M., Khitrov V.A., Radiative capture of resonance and thermal neutrons, main parameters of the gamma-decay process and the properties of nucleus ^{174}Yb. Proceedings of the 2-nd international conference "Current problems in nuclear physics and atomic energy", Part 2, Kyiv, 2009, pp. 560-566.
42. Sukhovoj A.M., Furman W.I., Khitrov V.A., Precise approximation of sums of experimental radiative strength functions of dipole gamma-transition, Proceedings of the 2-nd international conference "Current problems in nuclear physics and atomic energy", Part 2, Kyiv, 2009, pp. 552-559.
43. Vesna V.A., Gledenov Yu.M., Nesvizhevsky V.V., Petukhov A.K., Sedyshev P.V., Soldner T.,. Shul'gina E. V, Zimmer O., Measurement of the P-odd asymmetry of γ-quanta from ^{10}B(n,α)^{7}Li*→Li(g.st.) reaction at Heightened Frequency of Neutron Polarization Switching. ISINN-16. Neutron Spectroscopy, Nuclear Structure, Related Topics. (Dubna: JINR, 2009) E3-2009-33, 83-90

44. Tsibakhahsvili N., Mosulishvili L., Kirkesali E., Kerkenjia S., Frontasyeva M.V., Pavlov S.S., Zinicovscaia I.I., Bode P., and.van Meerten Th.G., NAA for studying detoxification of Cr and Hg by Arthrobacter globiformis. Book of Abstracts, Int. Conf. on Radiochemistry. Marianske Lazne, Czech Rep., 18-21 April, 2010.
45. Tsibakhahsvili N., Mosulishvili L., Kirkesali E., Kerkenjia S., Frontasyeva M.V., Pavlov S.S., Zinicovscaia I.I., Bode P., and.van Meerten Th.G., NAA for studying effects of potentially toxic metals (Cr, Hg) on Arthrobacter globiformis. III International Conference on Environmental, Industrial and Applied Microbiology (Fostering cross-disciplinary applied research in microbiology and microbial biotechnology). BioMicroWorld 2009 (2-4 December, 2009, Lisbon, Portugal).
46. Tsibakhashvili N., Mosulishvili L., Kirkesali E., Kalabegishvili T., Kerkenjia S., Frontasyeva M.V., Zinicovscaia I., Holman H-Y., Application of epithermal neutron activation analysis to study heavy metal interactions with indigenous bacteria. Book of Abstracts of The 12th Annual Meeting of the Israel Analytical Chemistry Society, ISRANALYTICA-12 (Tel Aviv, Izrael, 20-21 January, 2009).
47. Tsibakhashvili N., Mosulishvili L., Rcheulishvili A., Kalabegishvili T., Rcheulishvili O., Frontasyeva M.V., Kirkesali E., Zinicovscaia I., Effects of heavy metals on the chromium detoxification by Arthrobacter species. Book of Abstracts, ISINN-17, 27-30 May, 2009, Dubna, p. 65.
48. Tsibakhashvili N., Mosulishvili L., Kirkesali T., Kalabegishvili T., Kerkenjia S., Frontasyeva M.V., Zinicovscaia I., Elemental content of indigenous bacteria under different chromium loadings. ISINN-17, 27-30 May, 2009, Dubna; p. 64.
49. Tyakavkin A.N., Pyatkov Yu.V., Kamanin D.V., Kopatch Yu.N., Alexandrov A.A., Alexandrova I.A., Borzakov S.B., Voronov Yu.N., Denisov S.V., Efimov G.L., Zhuchko V.E., Kondratyev N.A., Kuznetsova E.A., Lavrova Yu.E., Mitrofanov S.V., Panteleev Ts., Salamatin V.S., Tsurin I.P., *Measuring of the fragments nuclear charges at the MINI-FOBOS spectrometer,* Proceedings of 16th International Seminar on Interaction of Neutrons with Nuclei: "Neutron Spectroscopy, Nuclear Structure, Related Topics". Dubna, June 11-14, 2008. Dubna 2009., p. 393-401,
50. Zeynalov Sh., Zeynalova O.V., Hambsch F.-J., Oberstedt S., Fabry I., DSP algorithms for fission fragment and prompt fission neutron spectroscopy, Scientific Workshop on Neutron Measurements, Theory and Applications, 28-30 April 2009 IRMM, Geel, Belgium.
51. Zeynalov Sh., Hambsch F.-J., Oberstedt S., Fabry I., Neutron emission in fission of ^{252}Cf(sf). 4th International Workshop on Nuclear Fission and Fission Product Spectroscopy, May 13-16, 2009, CEA Cadarache, France
52. Быстрицкий В.М., Герасимов В.В., Ильгузин Д.А., Кобзев А.П., Крылов А.Р., Паржицкий С.С., Ананьин П.С., Дудкин Г.Н., Каминский В.Л., Нечаев Б.А., Падалко В.Н., Петров А.В., Быстрицкий Вит.М., Возняк Я., Филиппович М., Тулеушев Ю.Ж., Гази С.,. Гуран Й. Экспериментальное определение фактора усиления реакции d(d,n)3He в ZrD2 и TiD2 в области астрофизичсеких энергий, 7 Международная конференция «Ядерная и радиационная физика» (Алматы, 8 – 11 сентября 2009г.)
53. Зейналова О.В., Зейналов Ш., Хамбш Ф.-Й.,. Оберстедт Ш, Фабри И., Спектроскопия продуктов деления 252cf(sf) с применением цифровой обработки сигналов, Международной конференция ЯДРО-2009, Чебоксары, 15-19 июня 2009 г.
26. Зейналова О.В., Зейналов Ш., Хамбш Ф.-Й., Оберстедт Ш., Фабри И., DSP Algorithms for Fission Fragment and Prompt Fission Neutron Spectroscopy 1st International conference on applications of mathematics in technical and natural sciences, Sozopol, Bulgaria, 22-27 June, 2009

DEVELOPMENT AND CONSTRUCTION OF ELEMENTS OF NEUTRON SPECTROMETERS FOR CONDENSED MATTER INVESTIGATIONS

1. Kulagin E.N., Kulikov S.A., Shabalin E.P., **Nuclear Instruments and Methods in Physics Research Section A: Accelerators, Spectrometers, Detectors and Associated Equipment**, v.606, No 3, p.p.637-644, 2009
2. Kulikov S., Shabalin E., **Romanian Journal of Physics**, Publishing House of the Romanian Academy, v.54, No 3-4, p.p.361-367, 2009
3. Manoshin S.A., Belushkin A.V. et al., **Nuclear Instruments and Methods in Physics Research** (Section A), V., 608, 3, 447-453, 2009.
4. Булавин М.В., Кулагин Е.Н., Куликов С.А., Мухин К.А., Шабалин Д.Е., Шабалин Е.П., **Сообщение ОИЯИ** Р13-2009-72, Дубна, 2009 г.

Reports at Schools and Conferences

1. Bruckel T., Voigt J., Ioffe A., Manoshin S., Diffractometer for non-equilibrium states of condensed matter. International Conference on Neutron Scattering, May 5-7, 2009, Knoxville, USA, Book of abstracts.
2. Kirilov A.S., Murashkevich S.M., Okulov R.Yu., Petukhova T.B., Development of the remote control of the spectrometers on the IBR-2M reactor, XXII International Symposium on Nuclear Electronics & Computing, Sept. 7-14, Varna, Bulgaria, Book of abstracts, p.34.

3. Kirilov A.S., Murashkevich S.M., Okulov R.Yu., Petukhova T.B., An Arrangement of the Remote Control of Spectrometers on the IBR-2M Reactor, Instruments and Experimental Techniques, v.52, No. 1, pp. 37–42.
4. Manoshin S., Kulikov S., Belushkin A., Zhuravlev V., Ioffe A., Vitess software package: simulations of neutron instruments, XXII International Symposium on Nuclear Electronics & Computing, Sept. 7-14, Varna, Bulgaria, Book of abstracts, p.25.
5. Nikul'nikov A.V., Sirotin A.P., Zhuravlev V.V., Control systems of neutron beam choppers at the physical instruments of the IBR-2 reactor, XXII International Symposium on Nuclear Electronics & Computing, Sept. 7-14, Varna, Bulgaria, Book of abstracts, p.47.
6. Черников А.Н., Буздавин А.П., Журавлев В.В., Рем Кван Чол, Глазков В.П., Шахтный криостат для охлаждения камер высокого давления с алмазными и сапфировыми наковальнями. VII Национальная конференция "Рентгеновское, Синхротронное излучение, Нейтроны и Электроны для исследования наносистем и материалов" РСНЭ_НБИК 2009,16-21 ноября, Тезисы Докладов, ИК РАН, РНЦ КИ, Москва, стр. 619 (будет опубликовано в журнале "Поверхность").

6. PRIZES

State Prize of the Government of the Republic of Macedonia
M.V.Frontasyeva, L.P.Strelkova, Geochemical Atlas of Veles and Environs

Annual European High Pressure Research Group Award
D. Kozlenko, Pressure-induced phenomena in complex manganese and cobalt oxides: tuning of magnetic, charge, orbital ordering and spin states

JINR 2009 prizes

Experimental physics research:

II prize
D.P.Kozlenko, B.N.Savenko, S.E.Kichanov, E.V.Lukin
Magnetic, charge and orbital ordering in complex manganese oxides R1-xAxMnO3-d at high pressures

Scientific and technical applied research:

II prizes
M.V.Rodkin, A.N.Nikitin, R.N.Vasin
Seismotectonic effects of solid state transformations in geomaterials

E.V. Lychagin, A.Y.Muzychka, V.V.Nesvizhevsky, G.V.Nekhaev, G.Pignol, K.V.Protasov, A.V.Strelkov
Investigation of coherent scattering of slow neutrons on the nano-particles and the creation of a neutron bottle for cold neutrons

Encouraging prizes
M.V.Frontasyeva, S.S.Pavlov, O.A.Culicov, O.Duliu, C.Cristache, M.Toma
Neutron activation analysis for geological studies in Romania

7. SEMINARS

Date	Authors	Title
10.03.2009	***E.G.Batyrbekov*** (National Nuclear Centre of the Republic of Kazakhstan)	In-reactor nuclear-excited sources of coherent and non-coherent optical radiation with direct and combined pumping
03.04.2009	***Acad. V.M.Buznik*** Innovation Technology Center, RAS «Chernogolovka»)	Fluoropolymer nanomaterials
24.12.2009	***M.I.Mokrousov*** (researcher, Space Research Institute, RAS)	Development of scientific equipment for nuclear-physical space experiments
	A.A.Vostrukhin **(**engineer, Space Research Institute, RAS)	Methods of design and development of software of equipment for scientific space experiments in nuclear planetology
	A.V.Malakhov **(**engineer, Space Research Institute, RAS)	Ground-based complex for nuclear-physical space experiments

8. ORGANIZATION AND USER INTERACTION

8.1. STRUCTURE OF LABORATORY AND SCIENTIFIC DEPARTMENTS

Directorate:
Director:
A.V.Belushkin
Deputy Director:
V.N.Shvetsov
Deputy Director:
Deleg Sangaa
Scientific Secretary:
O.A.Culicov

Reactor and Technical Departments
Chief engineer: A.V.Vinogradov
IBR-2 reactor
Chief engineer: A.V.Dolgikh
Department of IREN
Head: V.G.Pyataev
Mechanical maintenance division
Head: A.A.Belyakov
Electrical engineering department
Head: V.A.Trepalin
Design bureau
Head: A.A.Kustov
Experimental workshops
Head: A.N.Kuznetsov

Scientific Departments and Sectors
Condensed matter department
Head: D.P.Kozlenko
Nuclear physics department
Head: Yu.N.Kopatch
Department of IBR-2 spectrometers complex
Head: S.A.Kulikov

Administrative Services
Deputy Director: S.V.Kozenkov
Secretariat
Finances
Personnel

Scientific Secretary Group
Translation
Graphics
Artwork

NEUTRON SCATTERING STUDIES OF CONDENSED MATTER

Sub-Division	Title	Head
Sector 1: Neutron Diffraction. Head: A.M. Balagurov		
Group No.1	HRFD	A.M.Balagurov
Group No.2	DN-2	A.I.Beskrovnyi
Group No.3	DN-12	B.N.Savenko
Group No.4	Geomaterials	A.N.Nikitin
Group No.5	SCAT	Ch.Scheffzük
Sector 2: Neutron Optics. Head: M.V. Avdeev		
Group No.1	Surfaces	Yu.V.Nikitenko
Group No.2	Nanostructures	M.V.Avdeev
Small angle scattering group.		**Head: A.I. Kuklin**
Inelastic scattering group.		**Head: I.Natkaniec**

NUCLEAR PHYSICS DEPARTMENT

Sub-Division	Title	Head
Sector 1. Correlation γ-spectroscopy and development of experimental installations.		**Head: N.A.Gundorin**
Sector 2. Investigation of neutron properties		**Head: Ye.V. Lychagin**
Sector 3. Neutron activation analysis.		**Head: M.V.Frontasyeva**
Group No.1	Analytical	M.V.Frontasyeva
Group No.2	Experimental	S.S.Pavlov
Group No.4	**Fission**	**Yu.N.Kopatch**
Group No.5	**Proton and α-decay**	**Yu.M.Gledenov**
Group No.6	**Polarized neutrons and nuclei**	**V. P. Skoy**

DEPARTMENT OF IBR-2 SPECTROMETERS COMPLEX

Sub-Division	Title	Head
Group No.1	Detectors	A.V. Churakov
Group No.2	Electronics	A.A. Bogdzel
Group No.3	Information technologies	A.S. Kirilov
Group No.4	Sample environment and choppers	A.P. Sirotin
Group No.5	Cryogenic investigations	A.N. Chernikov
Group No.6	Methodical developments	-
Group No.7	Cold moderators	S.A. Kulikov

8.2. MEETINGS AND CONFERENCES

In 2009, FLNP organized the following meetings:

1. *XVII International Seminar on Interaction of Neutrons with Nuclei: «Fundamental Interactions & Neutrons, Nuclear Structure, Ultra cold Neutrons, Related Topics» (ISINN-17), Dubna, May 25-29.*
2. *II Advanced Courses of CIS Countries for young researchers, Ph.D. students and graduate students on modern methods in investigations of nanosystems and materials Synchrotron and Neutron Investigation of Nanosystems (SYN NANO), Moscow – Dubna, June 28 – July 13.*
3. *All-Russian Neutron School for Young Scientists and Students "Modern Neutron Diffraction Studies: Interdisciplinary Research of Nanosystems and Materials", Dubna, October 12-20.*

In the year 2010, FLNP will organize the following meetings:

1. *XVIII International Seminar on Interaction of Neutrons with Nuclei: «Fundamental Interactions & Neutrons, Nuclear Structure, Ultra cold Neutrons, Related Topics» (ISINN-18), Dubna, May 19-22.*
2. *III Higher Courses of CIS for young scientists, post-graduate and graduate students on advanced methods of research in nanosystems and materials "Synchrotron and Neutron Investigations of Nanosystems (SYN-nano-2010).*
3. *All-Russian Scientific School for Young Scientists and Students "Modern Neutron Diffraction Studies: Interdisciplinary Research of Nanosystems and Materials" (if a grant of the Russian Ministry of education and science will be available).*
4. *Anniversary workshop "50 years from the IBR-1 reactor's start-up".*

8.3. EDUCATION

The objective of the FLNP educational program is the training of specialists in the field of neutron methods for condensed matter and nuclear physics research. The students of the Neutron Diffraction Department of MSU, of the Interfaculty Center «Structure of Matter and New Materials» and of the Electronics and Automatics Department of MIREA (Moscow State Institute of Radioengineering, Electronics and Automatics) perform their term and diploma works in FLNP.

At the JINR University Centre the students from Tula State University, Tver State University and other universities of Russia and JINR Member States (Czech Republic, Slovakia, Romania, Poland) and Associated countries (Egypt, South Africa) write their term papers and do summer practical work in FLNP.

Two scientific schools for advanced training of young scientists were organized in the Frank Laboratory of Neutron Physics in 2009: the II Advanced Courses of CIS Countries for young researchers, Ph.D. students and graduate students on modern methods in investigations of nanosystems and materials "Synchrotron and Neutron Investigation of Nanosystems" (SYN-NANO-2009) (June 28 – July 13, 2009, Moscow – Dubna) and the all-Russian Neutron School for Young Scientists and Students "Modern Neutron Diffraction Studies: Interdisciplinary Research of Nanosystems and Materials" (October 12-20, 2009, Dubna). Participants the Schools had ample opportunity to establish new scientific contacts with other researchers to enrich their experimental ideas with new research methods. During the guided excursion to the IBR-2 high-flux pulsed reactor, the participants became familiar with this unique facility and the variety of neutron-scattering investigations carried out at FLNP. The Schools were not confined only to the lectures and practical laboratory work. The participants were encouraged to present their own investigations in poster sessions, being held every working day of the Schools.

These Schools continued the tradition of the FLNP Schools for young scientists devoted to the fundamental and applied aspects of neutron research in the fields of condensed-matter physics, materials science and related topics.

8.4. COOPERATION

List of Visitors from Non-Member States of JINR in 2009

Name	Country	Dates
Hans Johen Lauter	France	23.01.-31.01
Valeriya Lauter	USA	23.01.-31.01
Klaus Ullemaer	Germany	01.02-14.02
Kristina Holderna-Natkanec	Poland	03.02-22.02
Matei Florek	Slovakia	06.02-17.02
Klaus Ullemaier	Germany	08.02-14.02
Deleg Sangaa	Mongolia	15.02-22.02
Aleksandr Frishbutter	Germany	17.02-27.02
Kurt Valter	Germany	17.02-27.02
Batjargal Bombor	Mongolia	15.03-20.03
Klaus Ullemaier	Germany	15.04-25.04
Aleksandru Dobrin	Sweden	04.05-07.05
Yurgen Schraiber	Germany	22.05-25.05
Gohuei Chjan	China	25.05-06.06
Aleksandr Ponomarev	Ukraine	28.05-30.05
Tomas Vilpert	Germany	03.06-11.06
Eiliv Staines	Norway	11.06-18.06
Sergei Korneev	Byelorussia	15.06-28.06
Andrei Potapenko	Byelorussia	15.06-28.06
Anastasiya Safronova	Byelorussia	15.06-28.06
Igor Zhuk	Byelorussia	15.06-28.06
Karol Ondriash	Slovakia	23.06-30.06
Ihab Abdel-Latif El Saied	Egypt	24.06-30.06
Sergei Snegir	Ukraine	28.06-05.07
Miroslav Kulik	Poland	07.07-22.07
Pavel Shalanski	Poland	11.07-23.08
Kristina Holderna-Natkanec	Poland	03.08-23.08
Klaus Ullemaier	Germany	12.08-22.08
Holger Titze-Yensch	Germany	13.08-16.08
Angel Angelov	Bulgaria	02.09-03.09
Eji Yanik	Poland	13.09-20.09
Kurt Valter	Germany	14.09-19.09
Aleksandr Frishbutter	Germany	14.09-19.09
Klaus Ullemaier	Germany	11.10-17.10
Oktavian George Duliu	Romania	02.11-25.11
Yuzef Andjeevski	Poland	08.11-15.11
Marian Kuruya	Romania	23.11-25.11
Shandor Takach	Hungary	29.11-12.12
Zoltan Syuch	Hungary	29.11-12.12
David Yansen	SAR	29.11-12.12
Gergi Rashschevski	Bulgaria	30.11-06.12
Dariush Monchka	Poland	30.11-12.12
Shagdarin Chadraabal	Mongolia	06.12-13.12
Anka Irina Geboianu	Romania	07.12-14.12
Ioana Daniela Dulama	Romania	07.12-14.12
Dumitru Gabriel Dima	Romania	07.12-14.12
Antoaneta Ene	Romania	07.12-14.12
Klaus Ullemaier	Germany	12.01.10-22.01.10
Stanislav Vratislav	Czech Rep.	14.01.10-22.01.10
Maiya Dlouga	Czech Rep.	14.01.10-22.01.10

8.5. PERSONNEL

Distribution of the Personnel per Department as of 31.12.2009

Theme	Departments	Main staff
-1036-	Nuclear Physics Department	42
-1031-	Condensed Matter Physics Department	37,75
-1052-	IBR-2 Spectrometers Complex Department	37,55
-0993-	IREN Department	12
-0851-	IBR-2 Department	48
	Mechanical and Technical Department	45
	Electric and Technical Department	29
	Central Experimental Workshops	38
	Nuclear Safety Group	2,7
	Design Bureau	5
	FLNP infrastructure:	
	Directorate	8.5
	Services and Management Department	26,5
	Scientific Secretary Group	3,5
	Supplies Group	4,5
Total		**340**

Personnel of the Directorate as of 31.12.2009

Country	People
Armenia	1
Bulgaria	2
Moldova	1
Germany	2
Georgia	2
KPDR	7
Azerbaijan	2
Mongolia	4
Poland	4
Romania	6
Russia	21
China	1
Ukraine	8
TOTAL	**61**

8.6. FINANCE

Financing of the FLNP Scientific Research Plan in 2009 (th. USD)

No.	Theme	Financing plan, $ th.	Expenditures For 12 months, $ th.	In % of FLNP Budget
I	**Condensed matter physics**	7671,9	6207,1	80,9
	-1069-	1906,5	1733,0	90,9
	-0851-	4617,2	3609,2	78,2
	-1075-	1148,2	864,9	75,3
II	**Neutron nuclear physics**			
	-1036-	2045,9	1783,4	87,2
	TOTAL:	**9717,8**	**7990,5**	**82,2**